technische universität
dortmund

Dissertation
zur Erlangung des akademischen Grades
Dr. rer. nat. im Fach Physik

Rare radiative charm decays in and beyond the standard model

Nico Adolph
geboren in Osnabrück

2022

Lehrstuhl für Theoretische Physik IV
Fakultät Physik
Technische Universität Dortmund

Erstgutachterin:	Prof. Dr. Gudrun Hiller
Zweitgutachter:	Jun.-Prof. Dr. Emmanuel Stamou
Vorsitzender der Prüfungskommission:	Prof. Dr. Mirko Cinchetti
Mitglied der Prüfungskommission:	Dr. Chris Malena Delitzsch
Datum der Abgabe:	27. Mai 2022
Datum der mündlichen Prüfung:	26. Oktober 2022

Kurzfassung

Diese Dissertation beinhaltet eine Studie über seltene radiative $|\Delta c| = |\Delta u| = 1$ Übergänge innerhalb und jenseits des Standardmodells. Für die 18 Dreikörperzerfälle $D \to P_1 P_2 \gamma$ mit $P = \pi, K$ werden die Zerfallsamplituden mittels Lows Theorem, QCD Faktorisierung und HHχPT berechnet. Es werden Standardmodellvorhersagen für Verzweigungsverhältnisse, CP-Asymmetrien sowie Vorwärts-Rückwärts-Asymmetrien bestimmt. Effekte neuer Physik in den Koeffizienten der elektromagnetischen Dipoloperatoren werden unter Einhaltung der aktuellen Einschränkungen untersucht. Die Photonpolarisation in $D_s \to K_1(\to K\pi\pi)\gamma$ Zerfällen wird im Hinblick auf Effekte neuer Physik in den Dipolkoeffizienten ausgewertet. Innerhalb des Standardmodells stimmt der Polarisationsparameter mit dem standardmodellartigen Partnerzerfall $D^+ \to K_1^+(\to K\pi\pi)\gamma$ bis auf U-spin brechende Korrekturen überein. Die Existenz von Partnerzerfällen ermöglicht die Konstruktion eines Null-Tests, welcher keine genaue Kenntnis des hadronischen $K_1 \to K\pi\pi$ Zerfalls benötigt. Abschließend werden verschiedene Möglichkeiten, das Standardmodell mit seltenen radiativen Zerfällen von charm Baryonen zu testen, diskutiert. Basierend auf der approximativen $SU(3)_F$ Symmetrie der QCD sowie ihrer Untergruppen werden Relationen zwischen Partnerzerfällen ausgearbeitet. Verzweigungsverhältnisse, CP-Asymmetrien sowie die Photonpolarisationen werden als Observablen betrachtet und die potentiellen Effekte neuer Physik abgeschätzt. Methoden zur Extraktion der Photonpolarisation aus den Zweikörperzerfällen $B_c \to B\gamma$ polarisierter charm Baryonen sowie aus den Zerfallsketten $B_c \to B(\to B'P)\gamma$ mit selbst-analysierenden Hyperonen B werden vorgestellt.

Abstract

This thesis comprises a study of rare radiative $|\Delta c| = |\Delta u| = 1$ transitions within and beyond the standard model of particle physics. For the 18 three-body decays $D \to P_1 P_2 \gamma$ with $P = \pi, K$, decay amplitudes are derived using Low's theorem, QCD factorization and heavy hadron chiral perturbation theory. Standard model predictions for branching ratios, CP asymmetries as well as forward-backward asymmetries are determined. Moreover, the effects of new physics in the coefficients of the electromagnetic dipole operators are investigated respecting the current constraints. The photon polarization in $D_s \to K_1^+(\to K\pi\pi)\gamma$ decays is studied with respect to new physics effects in the dipole coefficients. Within the standard model, the polarization parameter agrees with the SM-like partner decay $D^+ \to K_1(\to K\pi\pi)\gamma$ up to U-spin breaking corrections. The existence of partner decays allows to construct a null test which does not require precise knowledge of the hadronic $K_1 \to K\pi\pi$ decay. Finally, different ways to test the standard model with rare radiative decays of charm baryons are discussed. Based on the approximate $SU(3)_F$ symmetry of QCD as well as its subgroups, relations between partner decays are worked out. Branching ratios, CP asymmetries as well as the photon polarizations are considered as observables and the potential of new physics effects is estimated. Methods for the extraction of the photon polarization from two-body decays $B_c \to B\gamma$ of polarized charm baryons as well as from decay chains $B_c \to B(\to B'P)\gamma$ with self-analyzing hyperons B are presented.

Acknowledgements

First of all, I would like to thank my advisor, Gudrun Hiller, for giving me the opportunity to work as a PhD student at the high-energy physics department in Dortmund. Throughout the years as a bachelor student, master student and finally PhD student, she has encouraged me to work independently on my research projects and to pursue my own way of working and researching, while always providing help and guidance when I needed it. I would also like to thank Emmanuel Stamou for agreeing to be the second referee of this thesis.

Furthermore, I am grateful to the German Academic Exchange Service for my scholarship, which enabled me to work on a research project at the University of Cincinnati. I also have to thank Joachim Brod, who mentored me during my time in Cincinnati and provided me with valuable tips regarding physics and living in Cincinnati.

I would like to thank all current and former members of the department for the positive, comfortable, supporting and motivating work environment. I have really enjoyed the last few years at the department.

I really appreciate that Gerwin, Tim H., Stefan, Dominik, Tim B. and Lara have agreed to proofread the manuscript. Your comments really helped a lot to improve my thesis.

I am very grateful to Christian, Felix, Gerwin, Jasmin, Tim and Vanessa for the time we spent together during our studies and for the many great moments outside of university. I would also like to thank Steffen and Ramona for their friendship and support. A special thanks to Mary, who has always been there for me over the last few years. I could not have asked for a better friend.

Finally, I would like to thank my family. In particular, I would like to thank my aunt Petra, who supported me throughout my studies. My biggest thanks go to my parents and my sister. I am grateful for the unconditional support I have received my entire life. Without you, this work would not have been possible.

Publications

This thesis is based on the following publications by the author, Refs. [1–4]:

- Nico Adolph, Gudrun Hiller and Andrey Tayduganov,
  "Testing the standard model with $D_{(s)} \to K_1(\to K\pi\pi)\gamma$ decays",
  In: Phys. Rev. D **99.7** (2019), 075023,
  DOI:10.1103/PhysRevD.99.075023,
  eprint: arXiv:1812.04679 [hep-ph].

- Nico Adolph, Joachim Brod and Gudrun Hiller,
  "Radiative three-body D-meson decays in and beyond the standard model",
  In: Eur. Phys. J. C **81.1** (2021), 45,
  DOI:10.1140/epjc/s10052-021-08832-3,
  eprint: arXiv:2009.14212 [hep-ph].

- Nico Adolph and Gudrun Hiller,
  "Probing QCD dynamics and the standard model with $D^+_{(s)} \to P_1^+ P_2^0 \gamma$ decay",
  In: JHEP **06** (2021), 155,
  DOI:10.1007/JHEP06(2021)155,
  eprint: arXiv:2104.08287 [hep-ph].

- Nico Adolph and Gudrun Hiller,
  "Rare radiative decays of charm baryons",
  In: Phys. Rev. D **105.11** (2022), 116001,
  DOI:10.1103/PhysRevD.105.116001,
  eprint: arXiv:2203.14982 [hep-ph].

Contents

1 Introduction

At the fundamental level, physics is based on two central theories. On the one hand, the theory of general relativity (GR) describes the relation between mass, energy, momentum and the curvature of the four-dimensional space-time and interprets gravity as a geometrical property of the space-time curvature. So far, the predictions of GR have been mostly in agreement with observations and experiments. As the last major discovery, the prediction of gravitational waves was confirmed by the LIGO experiment in 2015 [5]. On the other hand, the standard model of particle physics (SM) describes the properties of the microscopic building blocks of nature as well as their interactions. This includes the strong, weak and electromagnetic interaction, thus the other three known forces of nature. When the Higgs boson [6–8] was directly detected by the ATLAS and CMS experiments [9, 10] at the Large Hadron Collider (LHC) in 2012, the last missing piece of the the SM was discovered and thus the SM was completed.

Despite the enormous success of the SM, there are some observations which cannot be explained. A known deficiency are the missing neutrino masses, which are necessary to explain the observed neutrino oscillations [11, 12]. In addition, the amount of visible matter in the universe cannot be explained by the violation of charge parity (CP) symmetry in the SM [13]. Moreover, it is known that visible matter accounts for only $\sim 5\%$ of the total energy content of the universe. About five times as much is present in form of dark matter, for which, however, there is no explanation within the SM [14]. Besides experimental observations, there are also theoretical shortcomings. First of all, there is no quantum theory of gravity, which would be desirable in view of a unified theory of all forces of nature. Furthermore, perturbation theory does not work for arbitrarily high energy scales within the SM. Moreover, the Standard Model contains 18 parameters whose values are not based on theoretical arguments but must be determined by experiments. It is conspicuous that ten of the parameters originate from the quark sector of the SM (six quark masses, three mixing angles and one phase) and show strong hierarchical structures. Both the large number and its unsubstantiated structure are unsatisfactory from a theoretical point of view.

So far, there is no evidence of direct detection of particles beyond the standard model (BSM). Since direct searches require that the collider experiments provide enough energy to create the BSM particles mass, new physics is likely to exist at an energy scale that cannot be reached with current collider setups. Indirect searches, on the other hand, provide an opportunity to test much higher energy scales. If theoretical and experimental precision reach a sufficient level, loop induced virtual contributions of new physics (NP) can lead to measurable deviations from SM predictions in low-energy observables.

In recent years, several indirect searches have drawn attention. Measurements of the anomalous magnetic moments of the charged leptons are one of them. For muons, there are currently deviations of up to $4.1\,\sigma$, depending on the theory prediction [15–17]. Similarly,

although not quite as significant, the measured anomalous magnetic moments of electrons deviate from the SM predictions by $2.4\,\sigma$ [18, 19]. Furthermore, there are numerous discrepancies in semileptonic decays of B mesons, both in charged current $b \to c l^- \bar{\nu}_l$ and flavor changing neutral current (FCNC) $b \to s l^+ l^-$ transitions. Branching ratios of $b \to s\mu^+\mu^-$ transitions [20–24] as well as $B \to K^*\mu^+\mu^-$ angular observables [25–29] deviate from the SM. Of particular interest are the null tests of lepton flavor universality with the ratio type observables $R_{K^{(*)}}$ [30–35] and $R_{D^{(*)}}$ [36–54], which have the advantage of small theoretical uncertainties. The deviations of the b anomalies are mostly in the range of $2-3\sigma$. However, the last measurement of $R_{D^{(*)}}$ by Belle is compatible with the SM within 1.2 standard deviations [52].

Complementary to K and B physics, charm physics offers the possibility to search for NP in the up-type sector of the standard model of particle physics. $D^0 - \bar{D}^0$ mixing, hadronic decays [55–64] as well as (semi)leptonic decays [65–76] provide suitable options. The latter also offer the possibility to test the hint for violation of lepton flavor universality. Moreover, radiative charm decays complement those studies. Radiative $|\Delta c| = |\Delta u| = 1$ decays have branching ratios of order $\mathcal{O}(10^{-7} - 10^{-3})$ and are therefore rare enough to be sensitive to BSM processes, but also accessible to precision studies at current and future experiments such as LHCb [77], Belle II [78], BES III [79], Super charm-tau factory [80] and FCC [81].

This thesis, which is based on [1–4], discusses multiple different opportunities to test the SM with $c \to u\gamma$ transitions and is organized as follows:

- In chapter 2 and 3 the standard model of particle physics and the framework of weak effective theory (WET) for $c \to u\gamma$ transition are briefly summarized.
- In chapter 4 all 18 $D \to PP\gamma$ decay modes with $P = \pi, K$, which are induced by dimension six operators, are discussed. SM predictions as well as different BSM benchmarks for (differential) branching rations, forward-backward asymmetries and CP asymmetries are provided.
- In chapter 5 the photon polarization in $D^+_{(s)} \to K_1^+(\to K\pi\pi)\gamma$ decays is extracted using an up-down asymmetry in the $K\pi\pi$ system. We take advantage of partner decays in charm physics, one of which is SM-like and one BSM sensitive, to construct a null test. We estimate the hadronic proportionality factor in the asymmetry to estimate the experimental sensitivity.
- In chapter 6 the weak radiative decays of charmed anti-triplett (Λ_c, Ξ_c^+, Ξ_c^0) and sextet (Σ_c^{++}, Σ_c^+, Σ_c^0, $\Xi_c'^+$, $\Xi_c'^0$, Ω_c) baryons are discussed. We use the approximate $SU(3)_F$ flavor symmetry to relate decay amplitudes and extract the SM amplitudes from SM-like decays. Due to missing experimental data, we use benchmarks motivated by data on $D^0 \to \overline{K}^{*0}\gamma$. We estimate the potential impact of NP in branching ratios, CP asymmetries and the photon polarization. We discuss both a method to determine the photon polarization in two-body decays of polarized charm baryons and via self-analyzing decay chains.
- A conclusion is given in chapter 7 and additional information on parameters, form factors, helicity amplitudes and flavor relations are provided in five appendices A-E.

2 The standard model of particle physics

The standard model of particle physics unifies our present generally accepted knowledge of all known forces of nature, except gravity. It describes interactions on the fundamental level by the exchange of different mediators. The SM is formulated in terms of quantum fields, where each field is associated with a particle. Their interactions arise from the local gauge symmetry

$$SU(3)_C \times SU(2)_L \times U(1)_Y, \tag{2.1}$$

where quantum chromodynamics (QCD), the strong interaction, emerge from the $SU(3)_C$ gauge group [82–85]. The remaining $SU(2)_L \times U(1)_Y$ gauge group defines the electroweak interaction before electroweak symmetry breaking [86–88]

The matter content of the SM can be divided into two different categories, fermions and bosons. Overall, the SM contains 12 fermions (and their antiparticles) with spin-1/2, whose charges under the gauge groups specify how they interact. The fermions can further be divided into quarks and leptons. There are three charged leptons namely the e^-, the μ^- and the τ^- with electric charge $Q = -1$. The charged leptons differ only by their masses. Analogously, there are three electrically neutral neutrinos ν_e, ν_μ and ν_τ, which are massless in the SM. A charged lepton and the corresponding neutrino form a so-called generation of leptons. The first generation consists of e^- and ν_e, the second of μ^- and ν_μ and the third of τ^- and ν_τ. Neglecting the masses of the charged leptons, the three generations are exact copies of each other. All leptons interact via the weak force, but they do not interact strongly.

Furthermore, the fermions include the quarks, which exist in 6 different flavors: up u, down d, charm c, strange s, top t and bottom b. Analogously to the leptons, the quarks also form three generations. The first consists of u and d, the second of c and s and the third of t and b. As in the case of the leptons, the quarks of the three generations differ only in their masses. Additionally, the quarks can be categorized by their electric charge. The up-type quarks u, c and t have an electric charge of $Q = 2/3$, while the down-type quarks d, s, b have $Q = -1/3$. All quarks interact via the weak nuclear force. Moreover, they are charged under the $SU(3)_C$ and, therefore, interact via the strong interaction. All SM fermions as well as their representations and charges under the gauge symmetries are listed in Table 2.1.

Besides the fermions, the SM contains 12 gauge bosons with spin-1, which act as force carriers of the strong, weak and electromagnetic interaction: The massless gluons mediate the strong interactions between particles with color charge. There are eight versions of gluons, which differ in the combination of color and anticolor charge. Therefore, gluons couple not only to quarks, but also among themselves. The massive $W^\pm$ and Z bosons are the mediators of the weak interaction. They couple to left-handed fermions and right-handed antifermions and, in case of the $W^\pm$, change the fermions flavor in the interaction. Finally, the massless photon mediates the electromagnetic force. It couples to

Particle	$SU(3)_C$	$SU(2)_L$	Y	T_3	Q
$\begin{pmatrix} u \\ d \end{pmatrix}_L, \begin{pmatrix} c \\ s \end{pmatrix}_L, \begin{pmatrix} t \\ b \end{pmatrix}_L$	3	2	$-1/6$	$1/2$ $-1/2$	$2/3$ $-1/3$
$\begin{pmatrix} \nu_e \\ e^- \end{pmatrix}_L, \begin{pmatrix} \nu_\mu \\ \mu^- \end{pmatrix}_L, \begin{pmatrix} \nu_\tau \\ \tau^- \end{pmatrix}_L$	1	2	$-1/2$	$1/2$ $-1/2$	0 -1
u_R, c_R, t_R	3	1	$2/3$	-	$2/3$
d_R, s_R, b_R	3	1	$-1/3$	-	$-1/3$
e^-_R, μ^-_R, τ^-_R	1	1	-1	-	-1

Table 2.1: Group representations and charges of the SM fermions. Y is the weak hypercharge, T_3 ist the third component of the weak isospin and $Q = Y + T_3$ is the electric charge. The subscript L/R denote the left/right handed fields, respectively.

all particles which carry an electric charge. The last particle of the standard model is the Higgs boson, which is a spin-0 boson. Its non-trivial vacuum expectation value gives rise to the SM masses of all particles.

2.1 Quantum chromodynamics

The local gauge symmetries define the allowed interactions of the SM fermions. The Lagrangian is restricted to expressions that are invariant under these symmetries. To construct the QCD Lagrangian, we consider the transformation behavior of the quark fields under $SU(3)_C$, the gauge symmetry of QCD. In contrast to the leptons, quarks carry a color charge and thus transform non-trivially as a triplet

$$q_i \to q_i' = U q_i = \exp\left(i T^a \theta_a(x)\right) q_i \,, \tag{2.2}$$

where we sum over repeated indices ($a = 1, ..., 8$). The index $i = \{u, d, s, c, b, t\}$ denotes the flavor of the quark field. θ_a are real parameters which depend on space and time. The T^a are the generators of the $SU(3)_C$ and obey the Lie algebra

$$\left[T^a, T^b\right] = i f_c{}^{ab} T^c \,, \tag{2.3}$$

where the real and totally antisymmetric parameters $f_c{}^{ab}$ are called structure constants. In the fundamental representation, the generators are given by the Gell-Mann matrices $T^a = \lambda^a/2$ and are normalized as $\mathrm{Tr}(T^a T^b) = \delta^{ab}/2$. The structure constants are given by

$$f_c{}^{ab} = \frac{-i}{2} \mathrm{Tr}\left(\left[T^a, T^b\right] T_c\right) \,. \tag{2.4}$$

The starting point for the construction of the QCD Lagrangian is the free Lagrangian of fermion fields

$$\mathcal{L}_0 = \bar{q}_i^\alpha (i \partial\!\!\!/ - m_i) q_i^\alpha \,, \tag{2.5}$$

where $\alpha = \{r, g, b\}$ denotes the color index, which we will suppress in the following. We use the notation $a\!\!\!/ = a_\mu \gamma^\mu$ with the Dirac matrices γ_μ. Furthermore, we define the field $\bar{\psi}$

as $\bar{\psi} = \psi^\dagger \gamma_0$. By performing the gauge transformation (2.2) on the free Lagrangian, it can be shown that $\mathcal{L}_0$ is not gauge invariant

$$\mathcal{L}_0 \to \mathcal{L}_0 + i\bar{q}_i U^\dagger (\partial_\mu U) q_i \,. \tag{2.6}$$

To obtain a Lagrangian that is invariant under the local symmetry transformation (2.2), an additional field G_a^μ has to be introduced. The new Lagrangian

$$\mathcal{L} = \mathcal{L}_0 - g_s \bar{q}_i \gamma_\mu T^a G_a^\mu q_i \tag{2.7}$$

introduces interactions between quark fields q_i and the gauge field G_a^μ, where the strength of the coupling is described by the strong coupling constant g_s. The new gauge fields, which are called gluons, are also color charged. However, they do not transform under the fundamental representation of the symmetry group like the quark fields, but under the adjoint representation. Moreover, the gluons are vector bosons, as the fields have a Lorentz index. The transformation behavior of the gluon field is given by

$$T^a G_a^\mu \to U T^a G_a^\mu U^\dagger + \frac{i}{g_s} (\partial_\mu U) U^\dagger \,, \tag{2.8}$$

eliminating the additional term in (2.6). Thus, an infinitesimal transformation is given by

$$G_a^\mu \to G_a^\mu - \partial^\mu \theta_a - \theta_b f_a{}^{bc} G_c^\mu \,, \tag{2.9}$$

from which we can see that a mass term $\propto G_a^\mu G_{a\mu}$ would violate gauge invariance. Therefore, gauge bosons have to be massless. Since gauge bosons are supposed to be dynamical degrees of freedom, which can propagate through space and time, a kinetic term is required. The kinematic term $\propto G_a^{\mu\nu} G_{a\mu\nu}$ has to be defined in terms of the field strength tensor

$$G_a^{\mu\nu} = \partial^\mu G_a^\nu - \partial^\nu G_a^\mu + g_s f_a{}^{bc} G_b^\mu G_c^\nu \tag{2.10}$$

in order to obtain a Lorentz- and gauge invariant expression. Due to the non-abelian gauge group of QCD, the field strength tensor (2.10) contains a term which is quadratic in the gluon field. Therefore, the kinetic term gives rise to self interactions of gluons with triple and quartic vertices. Overall, the QCD Lagrangian can thus be written as

$$\mathcal{L} = \bar{q}_i (i \not{D} - m_i) q_i - \frac{1}{4} G_a^{\mu\nu} G_{a\mu\nu} \,, \tag{2.11}$$

where $D_\mu = \partial_\mu + i g_s T^a G_a^\mu$ denotes the covariant derivative. In general, the gauge invariance of QCD allows an additional interaction [89]

$$\mathcal{L} = -\theta_{\mathrm{QCD}} \frac{g_s^2}{64\pi^2} \epsilon_{\alpha\beta\gamma\delta} G_a^{\alpha\beta} G_a^{\gamma\delta} \,, \tag{2.12}$$

which would introduce a CP violating strong phase θ_{QCD}. A consequence of this interaction would be a non-vanishing electric dipole moment (EDM) of neutrons. Current measurements of the neutron EDM yield an upper limit of $d_n \lesssim 10^{-26}\, e\,\mathrm{cm}$, which translates into a tiny CP violating phase $\theta_{\mathrm{QCD}} \lesssim 10^{-10}$ [90, 91]. However, the SM does not provide an explanation for this extremely small value. This fine tuning problem, which is referred to as strong CP problem, is one of the unsolved issues of the SM.

2.2 The electroweak interaction

To define the representations and transformation properties of quarks and leptons under the electroweak symmetry group $SU(2)_L \times U(1)_Y$, we have to introduce left- and right-handed fields

$$\psi_{L/R} = P_{L/R}\psi = \frac{1 \mp \gamma_5}{2}\psi\,, \tag{2.13}$$

where $\gamma_5 = i\gamma_0\gamma_1\gamma_2\gamma_3$. While the transformation properties of the left- and right-handed fields only differ by the charges (see table 2.1) for the $U(1)_Y$, there are different representations in the case of $SU(2)_L$. The ψ_L (with $\psi = q, l$) are doublets which transform under the fundamental representation. A $SU(2)_L$-doublet is composed of an up- and down-type quark or a neutrino and a charged lepton

$$q_L = \begin{pmatrix} u_L \\ d_L \end{pmatrix}\,, \quad l_L = \begin{pmatrix} \nu_L \\ e_L \end{pmatrix}\,. \tag{2.14}$$

Analogously, there are doublets for the second and third generations of quarks and leptons. The right-handed fields u_R, d_R and e_R for up-type quarks, down-type quarks and charged leptons, respectively, transform trivially as singlets. Therefore, the gauge transformations read

$$\begin{aligned} \psi_L &\to \psi'_L = U_L U_Y \psi_L = \exp(i\tau^I \theta_I(x)) \exp(iY\theta(x))\psi_L\,, \\ \psi_R &\to \psi'_R = U_Y \psi_R = \exp(iY\theta(x))\psi_R\,. \end{aligned} \tag{2.15}$$

Here, Y denotes the hypercharge and τ^I with $I = 1, 2, 3$ are the generators of the $SU(2)_L$ which obey the Lie algebra

$$[\tau^I, \tau^J] = i\epsilon^{IJK}\tau^K\,, \tag{2.16}$$

where ϵ^{IJK} is the Levi-Civita tensor. In the fundamental representation the generators are given by the Pauli matrices $\tau^I = \sigma^I/2$. Analogously to QCD, we have to introduce gauge fields W_I^μ and B^μ to make the Lagrangian gauge invariant. They transform as

$$\begin{aligned} \tau^I W_I^\mu &\to U_L \tau^I W_I^\mu U_L^\dagger + \frac{i}{g}(\partial^\mu U_L) U_L^\dagger\,, \\ B^\mu &\to B^\mu - \frac{1}{g'}\partial^\mu\theta\,, \end{aligned} \tag{2.17}$$

where g and g' are the gauge couplings of $SU(2)_L$ and $U(1)_Y$, respectively. The corresponding field strength tensors read

$$\begin{aligned} W_I^{\mu\nu} &= \partial^\mu W_I^\nu - \partial^\nu W_I^\mu - g\epsilon^{IJK} W_J^\mu W_K^\nu\,, \\ B^{\mu\nu} &= \partial^\mu B^\nu - \partial^\nu B^\mu\,. \end{aligned} \tag{2.18}$$

The gauge invariant Lagrangian, containing the kinetic terms for fermions and gauge bosons as well as their interactions, is given by

$$\begin{aligned} \mathcal{L}_{\text{EW}} = {} & i\bar{q}_L^i \not{D} q_L^i + i\bar{l}_L^i \not{D} l_L^i + i\bar{u}_R^i \not{D} u_R^i + i\bar{d}_R^i \not{D} d_R^i + i\bar{e}_R^i \not{D} e_R^i \\ & - \frac{1}{4} W_{\mu\nu}^I W^{I\mu\nu} - \frac{1}{4} B_{\mu\nu} B^{\mu\nu}\,. \end{aligned} \tag{2.19}$$

The index i represents the different generations of quarks and leptons, respectively. The covariant derivatives for left- and right-handed fields are defined as

$$\begin{aligned} D^\mu \psi_L &= (\partial_\mu + ig\tau^I W_I^\mu + ig' Y B^\mu)\psi_L \,, \\ D^\mu \psi_R &= (\partial_\mu + ig' Y B^\mu)\psi_R \,. \end{aligned} \tag{2.20}$$

The Lagrangian (2.19) yields two properties that are not consistent with experimental observations. On the one hand, the gauge bosons are massless, since gauge invariance would be broke otherwise. However, it is known from experiments that the gauge bosons of the weak interaction have a mass. On the other hand, fermions have to be massless as well, as their left- and right-handed parts transform differently. Therefore, fermionic mass terms

$$m\bar{\psi}\psi = m\bar{\psi}_L\psi_R + m\bar{\psi}_R\psi_L \tag{2.21}$$

would violate the $SU(2)_L$ gauge symmetry.

2.3 Electroweak symmetry breaking and the Yukawa sector

To obtain a mass for the gauge bosons of the weak interaction, we have to introduce the concept of spontaneous symmetry breaking (SSB). For this purpose, a scalar complex field ϕ is introduced which transforms as a doublet under $SU(2)_L$ and has a hypercharge of $Y = 1/2$. The transformation properties are thus described by

$$\phi \to \phi' = U_L U_Y \phi = \exp(i\tau^i \alpha_i)\exp(-\beta/2)\phi \,. \tag{2.22}$$

The kinetic terms of ϕ and the interactions with the electroweak gauge bosons are encoded in the covatiant derivative. Furthermore, field ϕ has a symmetric and quartic potential [6–8]

$$\begin{aligned} \mathcal{L}_\phi &= (D_\mu\phi)^\dagger (D^\mu\phi) + \mu^2\phi^\dagger\phi - \frac{\lambda}{2}(\phi^\dagger\phi)^2 \,, \\ D^\mu\phi &= \left(\partial^\mu - ig\tau^i W_i^\mu + i\frac{g'}{2}B^\mu\right)\phi \,. \end{aligned} \tag{2.23}$$

For positive parameters μ^2 and λ, the quartic potential potential has an infinite number of minima, which satisfy $|\phi|^2 = \phi^\dagger\phi = \mu^2/\lambda = v^2$. Here, v is referred to as the vacuum expectation value (VEV) of the field ϕ. In general, a complex doublet is described by four real fields. Since the ϕ transforms as a doublet, it is possible to use a special gauge, the unitary gauge, where three of the four fields vanish. This technique is called gauge-fixing. Therefore, expanding ϕ around its VEV, we can write the scalar field as

$$\phi = \frac{1}{\sqrt{2}}\begin{pmatrix} 0 \\ v + h(x) \end{pmatrix} \,. \tag{2.24}$$

where h is known as the Higgs field. Although the Lagrangian was gauge invariant at the beginning, the vacuum state no longer preserves the symmetry as a whole. Gauge

transformations with $\alpha_1 = \alpha_2 = 0$ and $\alpha_3 = \beta$ leave the vacuum state invariant. Thus, the electroweak symmetry is not completely broken, instead

$$SU(2)_L \times U(1)_Y \xrightarrow{\text{SSB}} U(1)_{\text{EM}} \,. \tag{2.25}$$

The remaining symmetry ensures that the theory contains a massless gauge boson which will be identified with the photon. By inserting (2.24) in (2.23), we find that three mass terms $\propto v^2$ for three massive gauge bosons are generated

$$\mathcal{L}_\phi \supset \frac{1}{2}\frac{v^2}{4}\left[g^2(W_1^\mu)^2 + g^2(W_2^\mu)^2 + (-gW_3^\mu + g'B^\mu)^2\right] . \tag{2.26}$$

The three massive vector bosons $W^\pm$, Z as well as the massless photon A arise as linear combinations of the original gauge fields

$$\begin{aligned}
W^{\pm\mu} &= \frac{1}{\sqrt{2}}(W_1^\mu \mp iW_2^\mu) && \text{with mass} && m_W = \frac{gv}{2} \,, \\
Z^\mu &= \frac{1}{\sqrt{g^2+g'^2}}(gW_3^\mu - g'B^\mu) && \text{with mass} && m_Z = \frac{v}{2}\sqrt{g^2+g'^2} \,, \\
A^\mu &= \frac{1}{\sqrt{g^2+g'^2}}(gW_3^\mu + g'B^\mu) && \text{with mass} && m_A = 0 \,.
\end{aligned} \tag{2.27}$$

The change of basis from (W_3, B) to (Z, A) can be describes by a rotation matrix

$$\begin{pmatrix} Z \\ A \end{pmatrix} = \begin{pmatrix} \cos(\theta_w) & -\sin(\theta_w) \\ \sin(\theta_w) & \cos(\theta_w) \end{pmatrix} \begin{pmatrix} W_3 \\ B \end{pmatrix} , \tag{2.28}$$

where θ_w is the weak mixing angle, also known as Weinberg angle. The Weinberg angle can be expressed by the electroweak coupling constants

$$\cos(\theta_w) = \frac{g}{\sqrt{g^2+g'^2}} \,, \qquad \sin(\theta_w) = \frac{g'}{\sqrt{g^2+g'^2}} \,. \tag{2.29}$$

In addition, there is also a connection to the electromagnetic coupling constant $e = g\sin(\theta_w) = g'\cos(\theta_w)$. Furthermore, the masses of the $W^\pm$ bosons and the Z boson are linked via $m_W = m_Z\cos(\theta_w)$. Finally, we can rewrite the interactions of quarks with electroweak gauge bosons (2.19) in terms of the gauge bosons' mass eigenstate fields

$$\mathcal{L}_{\text{EW}} \supset eA^\mu J_\mu^{\text{EM}} + \frac{e}{\sin(\theta_w)} Z^\mu J_\mu^Z + \frac{g}{\sqrt{2}}\left(\bar{u}_L^i W^{+\mu}\gamma_\mu d_L^i + \bar{\nu}_L^i W^{+\mu}\gamma_\mu e_L^i + \text{h.c.}\right) , \tag{2.30}$$

where the electromagnetic current J_μ^{EM} and the neutral Z current J_μ^Z are given by

$$\begin{aligned}
J_\mu^{\text{EM}} &= Q_i\left(\bar{\psi}_L^i\gamma_\mu\psi_L^i + \bar{\psi}_R^i\gamma_\mu\psi_R^i\right) , \\
J_\mu^Z &= \frac{1}{\cos(\theta_w)}\left(\bar{\psi}_L^i\gamma_\mu\tau^3\psi_L^i - \sin^2(\theta_w)J_\mu^{\text{EM}}\right) .
\end{aligned} \tag{2.31}$$

$Q_i = T_3 + Y$ denotes the electric charge quantum number of the fermions. Here, we can see that all interactions are flavor diagonal, i.e., only fermions within a generation interact

with each other.
The generation of fermion masses works according to the same principle. We construct interactions between fermions and the field ϕ, which satisfy the gauge symmetries

$$\mathcal{L}_{\text{Yuk}} = -Y^u_{ij}\bar{q}^i_L\tilde{\phi}u^i_R - Y^d_{ij}\bar{q}^i_L\phi d^i_R - Y^e_{ij}\bar{l}^i_L\phi e^i_R + \text{h.c.}\,, \tag{2.32}$$

where Y^u, Y^d and Y^e are the Yukawa matrices for up-type quarks, down-type quarks and charged leptons, respectively. i and j denote generation indices and $\tilde{\phi} = i\sigma^2\phi^*$. Note that right-handed neutrinos are not included in the SM because they have never been observed in experiments. Thus, neutrinos remain massless in the SM, although it is known that they must have tiny masses $\lesssim \mathcal{O}(\text{eV})$ [11, 12]. After SSB, we obtain mass terms $\propto v$ from the fermion Yukawa couplings

$$\mathcal{L}_{\text{mass}} = -\frac{v}{\sqrt{2}}\left(Y^u_{ij}\bar{u}^i_L u^i_R + Y^d_{ij}\bar{d}^i_L d^i_R + Y^e_{ij}\bar{e}^i_L e^i_R\right) + \text{h.c.}\,. \tag{2.33}$$

In general, the Yukawa matrices are not diagonal and therefore the mass matrices M^ψ are not diagonal either. Thus, the so-called flavor basis, which has been used so far, is not equivalent to the physical mass basis. The transformation between flavor basis (u, d) and mass basis (u', d') is given in terms of unitary matrices, which diagonalize the mass matrices

$$\psi_{L/R} = U^\psi_{L/R}\psi'_{L/R}\,, \qquad M^\psi = \frac{v}{\sqrt{2}}U^{\psi\dagger}_L Y^\psi U^\psi_R\,. \tag{2.34}$$

The change from flavor to mass basis has neither an effect on the neutral currents in (2.30), nor on the interactions of quarks with gluons, since they always link a fermion antifermion pair with the same chirality. However, this is not the case for the charged current interaction. Due to the interaction of up- and down-type quarks, the charged quark current occurs to be non diagonal [92]

$$\mathcal{L}_{\text{CC}} = \frac{g}{\sqrt{2}}\left(\bar{u}'^i_L\gamma_\mu V_{ij}d'^i_L + \bar{\nu}'^i_L\gamma_\mu e'^i_L\right)W^{+\mu} + \text{h.c.}\,. \tag{2.35}$$

However, the rotation to the mass basis doesn't change the lepton current. This is due to the fact that neutrinos are left-handed in the SM. This allows to choose a rotation for neutrinos that cancels the rotation of the charged lepton fields. The combination of rotations of up- and down-type quarks $V = U^{u\dagger}_L U^d_L$ is called Cabibbo-Kobayashi-Maskawa (CKM) matrix [93, 94]. The CKM matrix is strictly unitary. The CKM matrix has four degrees of freedom, which consist of three angles and one CP-violating phase [95]. A common representation of the CKM matrix is the Wolfenstein parameterization [96], where the CKM matrix is expanded in a small parameter $\lambda \approx 0.225$ [97]

$$V = \begin{pmatrix} V_{ud} & V_{us} & V_{ub} \\ V_{cd} & V_{cs} & V_{cb} \\ V_{td} & V_{ts} & V_{tb} \end{pmatrix} = \begin{pmatrix} 1-\frac{\lambda^2}{2} & \lambda & A\lambda^3(\rho - i\eta) \\ -\lambda & 1-\frac{\lambda^2}{2} & A\lambda^2 \\ A\lambda^3(1-\rho-i\eta) & -A\lambda^2 & 1 \end{pmatrix} + \mathcal{O}(\lambda^4)\,. \tag{2.36}$$

Furthermore, $A \approx 0.826$, $\rho \approx 0.152$, and $\eta = 0.357$ [97]. The CKM matrix exhibits a strong hierarchical structure with dominant diagonal elements. Furthermore, the CP

violating phase arises only for terms of order $\mathcal{O}(\lambda^3)$ in elements V_{td} and V_{ub}. In particular, up to order λ^3, there is no impact of the CP-violating phase in the charm sector of the SM. Therefore, the CP violations in decays of charm hadrons are expected to be tiny and provide good null tests of the SM.

Weak decays can be categorized by the power of λ in the leading contribution of the decay amplitude $\mathcal{A}$. Thus, weak decays of charmed hadrons can be classified into one of the following three categories:

Cabibbo favored (CF):	$\mathcal{A} \propto \lambda^0$,
Singly Cabibbo suppressed (SCS):	$\mathcal{A} \propto \lambda^1$,
Doubly Cabibbo suppressed (DCS):	$\mathcal{A} \propto \lambda^2$.

2.4 Motivation for physics beyond the SM

The SM is an elegant and compactly formulated theory, which has shown impressive agreement with experimental results over the past decades. However, despite the lack of directly detected particles, which are not predicted by the SM, it is known that the SM is at least incomplete. Neutrinos are massless in the SM. However, based on the observation of neutrino oscillations by the Sudbury Neutrino Observatory [11] and the Super-Kamiokande experiment [12], it is known that at least two neutrinos have a small non-vanishing mass. Analogous to the CKM matrix, the mixing mechanism can be explained by a mismatch flavor and mass basis, which is described by the Pontecorvo-Maki-Nakagawa-Sakata (PMNS) matrix [98–100].

Furthermore, the baryon asymmetry in the universe cannot be explained by the SM. According to the Sakharov conditions [101], additional lepton or baryon number violating mechanisms as well as additional CP-violating phases are necessary to explain the amount of visible matter in the universe. Furthermore, visible matter accounts for only $\sim 5\%$ of the energy content of the universe. The SM does not include candidates for dark matter, which is needed to explain e.g. the galaxy rotation curves or the extent of gravitational lensing.

Another theoretical deficiency are the poles in the fundamental coupling constants, which causes the breakdown of perturbation theory for certain energy scales. QCD has a pole for small energy scales. This can be interpreted as a hint that quarks are not the appropriate degrees of freedom for small energies. Instead, QCD's low energy degrees of freedom are hadrons. Moreover, both QED and $U(1)_Y$ have a Landau pole at high energies.

In addition, most of the parameters of the SM are in the quark sector. Both the masses and the entries of the CKM matrix show distinct hierarchies which are not motivated by the SM. There are numerous BSM models which can explain the observed hierarchies by introducing further flavor symmetries. An example are Frogatt-Nielson extensions [102].

Currently there is no evidence for a direct detection of physics beyond the SM. However, there are several hints from indirect searches in B-decay observables and anomalous magnetic moments of charged leptons:

- Deviations of anomalous magnetic moments of up to $4.1\,\sigma$ [15–17] and $2.4\,\sigma$ [18, 19]

for muons and electrons, respectively.

- Deviations in branching ratios of $b \to s\mu^+\mu^-$ decays [20–24].
- Deviations in angular observables of $B \to K^*\mu^+\mu^-$ [25–29].
- Deviations from the lepton flavor universality in $R_{K^{(\star)}}$ [30–35].
- Deviations from the lepton flavor universality in $R_{D^{(\star)}}$ [36–54]. However, the last measurement of $R_{D^{(*)}}$ by Belle is compatible with the SM within 1.2 standard deviations [52].

Due to the large number of deviations in $|\Delta b| = |\Delta s| = 1$ transitions, it is necessary to study $c \to u$ FCNCs, which are the counterparts in the up-type sector, to investigate the flavor structure of the SM and possible new physics.

2.5 Flavor changing neutral currents and the GIM mechanism

Within the Standard Model, the neutral currents via Z boson, photons, and gluons preserve flavor. Changes of the quark flavor are only possible via the charged W bosons. Thus, there are no FCNC transitions at tree level in the SM. However, they are induced at loop level. An example for a Feynman diagram with a $c \to u$ transition is shown in Figure 2.1. The two vertices of the quark line with the virtual W boson change the quark flavor twice, allowing a c quark to be converted into an u quark. Within the loop, all down-type quarks can occur. The generic structure of the decay amplitude for a $c \to u$ transition is given by

$$\mathcal{A}(c \to u) = V_{cd}^* V_{ud} f(\tilde{m}_d^2) + V_{cs}^* V_{us} f(\tilde{m}_s^2) + V_{cb}^* V_{ub} f(\tilde{m}_b^2) \ , \tag{2.37}$$

where $\tilde{m}_i = m_i/m_W$ is the ratio of the down-type quark and W boson masses. Furthermore, f denotes an process dependent, continuous loop function which is suppressed by a factor of $g^2/16\pi^2$. Therefore, all processes that arise only at one-loop level are called loop suppressed. Furthermore, we can make use of the unitarity of the CKM matrix and the relation

$$V_{cd}^* V_{ud} = -V_{cs}^* V_{us} - V_{cb}^* V_{ub} \tag{2.38}$$

to eliminate the factor $V_{cd}^* V_{ud}$. Thus, the amplitude is given by

$$\mathcal{A}(c \to u) = V_{cs}^* V_{us} \left[f(\tilde{m}_s^2) - f(\tilde{m}_d^2) \right] + V_{cb}^* V_{ub} \left[f(\tilde{m}_b^2) - f(\tilde{m}_d^2) \right] \ . \tag{2.39}$$

The first term in (2.39) is suppressed by the small difference in s and d masses compared to the W boson mass, while the second is subject to strong CKM suppression $V_{cb}^* V_{ub} \propto \lambda^5 \approx 5.8 \cdot 10^{-4}$. The suppression of FCNCs in the SM is known as the Glashow-Iliopolus-Maiani (GIM) mechanism [92].

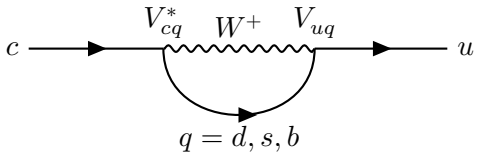

Figure 2.1: Feynman diagramm of the FCNC $c \to u$ in the SM.

2.6 Approximate symmetries of the QCD Lagrangian

The most challenging part of calculating amplitudes of hadron decays is the evaluation of the hadronic matrix elements. Exploiting the approximate symmetries of QCD is a key ingredient in the discussion of charm decays. On the one hand, they allow to determine relations between decay constants, form factors or even whole decay amplitudes, as in the case of $SU(3)_F$. On the other hand they provide a method for a systematic determination of the amplitude in a perturbative series as in the case of chiral perturbation theory (χPT) or the heavy quark effective theory (HQET). As it can be seen from the Lagrangian of QCD (2.11), the couplings to gluons are identical for all quarks. Thus, in QCD, the quarks only differ in their masses (see Table 2.2). Therefore, all mentioned approximate

$m_u(2\,\mathrm{GeV})$	$m_d(2\,\mathrm{GeV})$	$m_s(2\,\mathrm{GeV})$	$m_c(m_c)$	$m_b(m_b)$	$m_t(m_t)$
0.0022 GeV	0.0047 GeV	0.095 GeV	1.275 GeV	4.18 GeV	173.0 GeV

Table 2.2: Quark masses $m_q(\mu)$ at the energy scale μ in the $\overline{\mathrm{MS}}$ scheme [103].

symmetries are based on assumptions concerning the quark masses or their differences, respectively. In general, quarks can be classified into two categories by the typical energy scale of QCD $\lambda_{\mathrm{QCD}} \sim 0.3\,\mathrm{GeV}$. For the light quarks ($u$, d, s) the mass is smaller than λ_{QCD}, while for the heavy quarks (c, b, t) $m_Q > \lambda_{\mathrm{QCD}}$ applies.

2.6.1 $SU(3)_F$

At first, we will focus on the light quarks. Since the mass differences between the light quarks are small compared to λ_{QCD}, we can neglect the mass differences as a first order approximation. Thus, the Lagrangian

$$\mathcal{L}_{\mathrm{QCD}} \supset \bar{q}(i\not{D} + \bar{m})q - \frac{1}{4}G_a^{\mu\nu}G_{a\mu\nu} \tag{2.40}$$

is obtained, where $q = (u, d, s)$ and $\bar{m}$ denotes the mass matrix, which is proportional to the unit matrix. This Lagrangian is invariant under a global $SU(3)_F$ transformation $q \to U_F q$, where q transforms as a triplet. Bound states consisting of two or more light quarks are in irreducible representations which arise from the decomposition of the triplet products [104]. Thus, for the light mesons, an octet and a singlet are obtained. The triplet products of three quark triplets decompose into the light baryon decuplet, octet and a

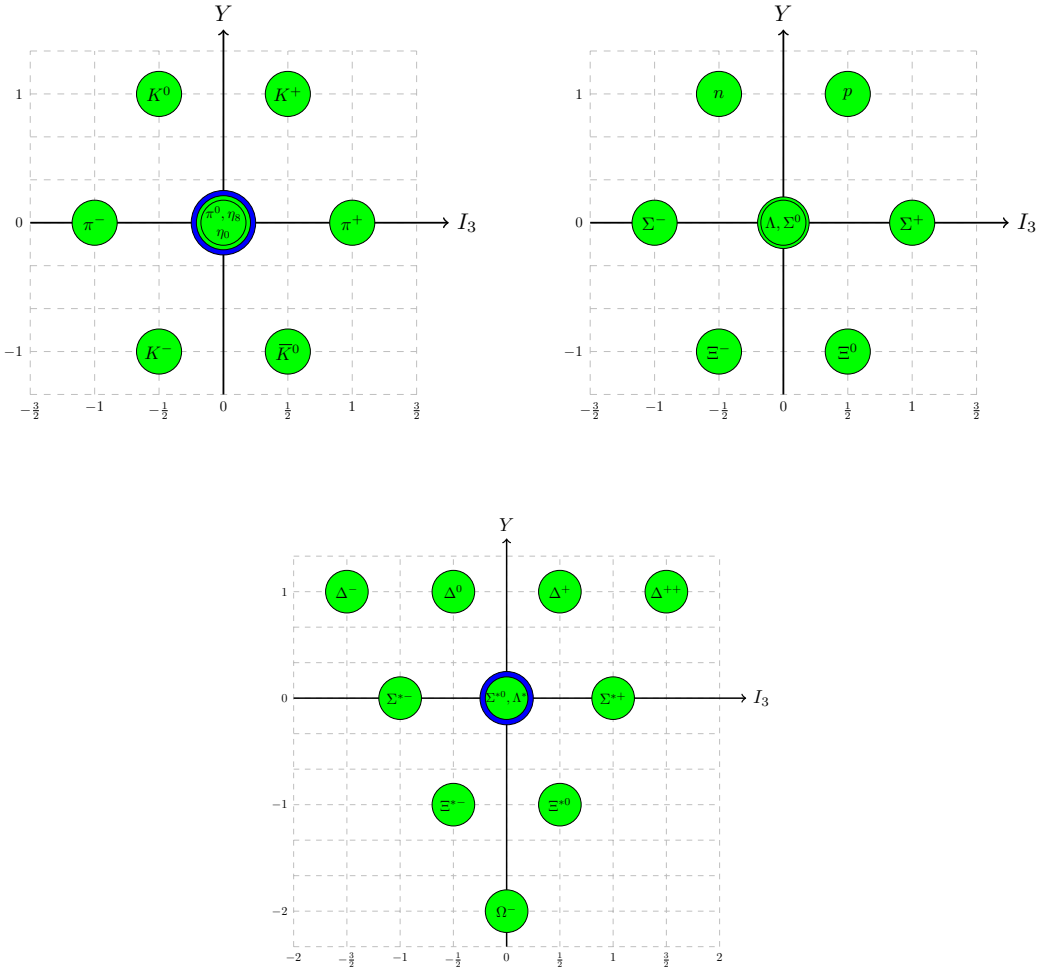

Figure 2.2: Weight diagrams for the octet and singlet of light pseudoscalar mesons as well as the decuplet, octet and singlet of light baryons. The singlet states are denoted by blue circles. I_3 and Y denote the third component of isospin and the hypercharge, respectively. Note that they are not identical to the previously introduced weak isospin and weak hypercharge.

singlet as

$$\begin{aligned} \mathbf{3} \otimes \overline{\mathbf{3}} &= \mathbf{8} \oplus \mathbf{1}\,, \\ \mathbf{3} \otimes \mathbf{3} \otimes \mathbf{3} &= \mathbf{10} \oplus \mathbf{8} \oplus \mathbf{8} \oplus \mathbf{1}\,. \end{aligned} \tag{2.41}$$

Weight diagrams for light meson and baryon multiplets are shown in Fig. 2.2.

Moreover, the heavy hadrons can be arranged in $SU(3)_F$ multipletts according to their light (anti)quarks. The three pseudoscalar charm mesons D^0, D^+ and D_s form a $\overline{\mathbf{3}}$ representation. The same applies for the corresponding vector states. The charm baryons

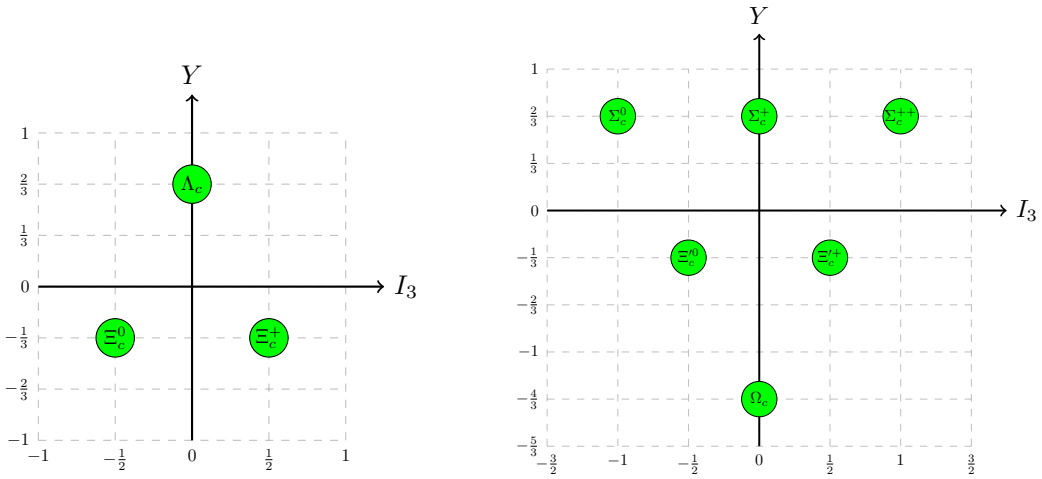

Figure 2.3: Weight diagrams for the anti-triplet and sextet of charm baryons.

form an anti-triplet and a sextet representation according to

$$\mathbf{3} \otimes \mathbf{3} = \overline{\mathbf{3}} \oplus \mathbf{6}\,. \tag{2.42}$$

The $\overline{\mathbf{3}}$ includes the Λ_c, Ξ_c^0 and Ξ_c^+ baryons. The light diquark system has a total spin of $s_l = 0$. Thus, there are no other degenerate baryons with different total spin. The $\mathbf{6}$ representation includes the Σ_c^0, Σ_c^+, Σ_c^{++}, $\Xi_c'^0$, $\Xi_c'^+$ and the Ω_c^0 baryon. Due to the total spin of the diquark system of $s_l = 1$ there is an analogous sextet with spin 3/2. Weight diagrams for the heavy baryon multiplets are shown in Fig. 2.3.

The $SU(3)_F$ has a total of three $SU(2)$ subgroups, each of which acting only on a subset of two quarks. The isospin ($SU(2)_I$), U-Spin ($SU(2)_U$) and V-Spin ($SU(2)_V$) symmetry act on doublets containing (u, d), (d, s) and (u, s), respectively. The representations of quarks as well as all mesons and baryons relevant to this work are given in Table E.1 and E.2. However, the $SU(3)_F$ is just an approximate symmetry. Therefore, the states from the multipletts are not exactly equivalent to the physical states. Thus, the relations between decay constants, form factors and amplitudes are not exact. While the isospin breaking effects $\mathcal{O}\left(\frac{m_u - m_d}{\lambda_{\text{QCD}}}\right)$ are negligible for our purpose, the U- and V-spin breaking effects $\mathcal{O}\left(\frac{m_s - m_{d/u}}{\lambda_{\text{QCD}}}\right)$ are sizable. In our numerical evaluation, we assume corrections of 30%. Note that data on semileptonic charm baryon decays indicate a substantial breaking of $SU(3)_F$ [105]. However, improved data is needed to draw firm conclusions.

2.6.2 Chiral perturbation theory

In the low energy region, the strong coupling constant increases into the non perturbative region, causing quarks and gluons to form bound states. Thus, the normal QCD Lagrangian and the associated perturbation theory are not suitable for calculating hadronic effects.

Therefore, an effective field theories (EFT) framework, which is not described by quark and gluon fields, but in terms of hadronic fields, is required. The EFT is required to satisfy the same symmetries as the usual QCD Lagrangian. Furthermore, a suitable expansion parameter is required, which allows a systematic calculation of hadronic effects using perturbation theory. The concept introduced in this section is known as chiral perturbation theory (χPT) [106–108]. χPT is suitable for the description of hadrons, which consist of u, d and s quarks, and their interactions. This concept is based on an approximate symmetry, which arises when the light quark masses are neglected. In this case, the QCD Lagrangian can be written in terms of left- and right-handed fields as

$$\mathcal{L}_{\mathrm{QCD}} = i\bar{q}_L \not{D} q_L + i\bar{q}_R \not{D} q_R - \frac{1}{4} G_a^{\mu\nu} G_{a\mu\nu} \,. \tag{2.43}$$

Apparently, the Lagrangian is invariant under a global $SU(3)_L \times SU(3)_R$ symmetry, which is commonly known as chiral symmetry. The quark triplets transform as

$$q_L \to U_L q_L \,, \qquad q_R \to U_R q_R \,, \tag{2.44}$$

where $U_L \in SU(3)_L$ and $U_R \in SU(3)_R$. As a consequence of chiral symmetry, degenerate meson multipletts with opposite parity would be expected. However, such a degeneracy could not be confirmed experimentally. The pseudoscalar meson octet is lighter than the scalar states. Thus, the ground state of QCD cannot obey the chiral symmetry. Instead, it breaks the chiral symmetry $SU(3)_L \times SU(3)_R \to SU(3)_{L+R}$. According to the Goldstone theorem [109, 110], eight massless pseudoscalar bosons appear in the theory due to the eight broken axial generators. Moreover, the chiral symmetry is explicitly broken by the non-zero quark masses, giving rise to mass terms for the Goldstone bosons proportional to the quark masses. The Goldstone bosons can be identified as a light pseudoscalar meson octet and combined in the unitary matrix

$$u = \exp\left(\frac{\mathrm{i}\Pi}{f}\right) \,, \qquad \Pi = \begin{pmatrix} \frac{\pi^0}{\sqrt{2}} + \frac{\eta_8}{\sqrt{6}} & \pi^+ & K^+ \\ \pi^- & -\frac{\pi^0}{\sqrt{2}} + \frac{\eta_8}{\sqrt{6}} & K^0 \\ K^- & \overline{K}^0 & -\frac{2\eta_8}{\sqrt{6}} \end{pmatrix} \,, \tag{2.45}$$

which transforms as $u \to U_R u U_L^\dagger$. Here, f denotes the pion decay constant. At this point we are able to define an effective low-energy theory of QCD which is described in terms of mesonic degrees of freedom. To do so, we have to define the most general Lagrangian satisfying P-, C-, T-, Lorentz-invariance as well as the chiral symmetry. In general, the Lagrangian can be written as a series of terms with increasing number of derivatives or momenta, respectively. The small expansion parameter in the p expansion of χPT is $p/\Lambda_{\chi\mathrm{PT}}$, where $\Lambda_{\chi\mathrm{PT}}$ is the energy scale of chiral symmetry breaking of $\mathcal{O}(1\,\mathrm{GeV})$. Due to the parity conservation of QCD, however, only even numbers of derivatives are allowed. To lowest order in derivatives, the effective chiral Lagrangian can be written as

$$\mathcal{L}_2 = \frac{f^2}{4} \mathrm{Tr}\left(\partial_\mu u^\dagger \partial^\mu u\right) \,. \tag{2.46}$$

To this extend, chiral perturbation theory is an effective theory which only describes strong interactions of light octet mesons. To integrate further interactions such as the

electromagnetic or weak interaction into this framework, the Lagrangian in (2.43) has to be generalized to include external hermitian currents called spurions

$$\mathcal{L} = \mathcal{L}_{\mathrm{QCD}} + \bar{q}\gamma^{\mu}(v_{\mu}(x) + \gamma_5 a_{\mu})q - \bar{q}(s(x) - i\gamma_5 p(x))q\,. \tag{2.47}$$

To preserve the chiral symmetry the spurions have to transform according to

$$\begin{aligned} r_{\mu} = v_{\mu} + a_{\mu} &\to U_R r_{\mu} U_R^{\dagger} + i U_R \partial_{\mu} U_R^{\dagger}\,, \\ l_{\mu} = v_{\mu} - a_{\mu} &\to U_L r_{\mu} U_L^{\dagger} + i U_L \partial_{\mu} U_L^{\dagger}\,, \\ s + ip &\to U_R (s + ip) U_L^{\dagger}\,. \end{aligned} \tag{2.48}$$

Since the spurions are supposed to include the electromagnetic and weak interactions, the chiral symmetry becomes a local symmetry. As a consequence, the spurions l_{μ} and r_{μ} can only be incorporated to the Lagrangian by a covariant derivative

$$D_{\mu} u = \partial_{\mu} u - i r_{\mu} u + i u l_{\mu} \tag{2.49}$$

and by non abelian field strength tensors

$$F_l^{\mu\nu} = \partial^{\mu} l^{\mu} - \partial^{\nu} l^{\mu} - i\,[l^{\mu}, l^{\nu}]\,, \qquad F_r^{\mu\nu} = \partial^{\mu} r^{\mu} - \partial^{\nu} r^{\mu} - i\,[r^{\mu}, r^{\nu}]\,. \tag{2.50}$$

Based on the symmetries of QCD and the transformation properties under chiral symmetry, the leading order Lagrangian is given as

$$\mathcal{L}_{\chi\mathrm{PT}} = \frac{f^2}{4}\mathrm{Tr}\left((D_{\mu}u)^{\dagger} D^{\mu} u\right) + \frac{f^2 B_0}{2}\mathrm{Tr}\left((s + ip)u^{\dagger} + u(s - ip)\right)\,, \tag{2.51}$$

where $B_0 = m_{\pi}^2/(m_u + m_d)$.

2.6.3 Heavy quark effective theory

Since the masses of the heavy quarks are larger than λ_{QCD}, neglecting their masses is not a reasonable approximation. Accordingly, they cannot be included in the framework of chiral perturbation theory. Thus, a different approach is required. For quarks with a mass which is large compared to λ_{QCD}, a complementary approximation $m_Q \to \infty$ would be reasonable. The corrections to this approximation arise as an expansion in the small parameter $\lambda_{\mathrm{QCD}}/m_Q$. The effective theory which follows this approach is known as heavy quark effective theory (HQET).

The momentum transfer between the quarks of a meson H, which consists of a heavy quark Q and a light antiquark $\bar{q}$, is of order λ_{QCD}. Thus, the velocity of the heavy quark changes only slightly due to $\Delta v = \Delta p/m_Q$. In the heavy quark limit it is in fact constant. Thus, the heavy quark in the meson acts as a static color source. Therefore, the dynamics of the meson emerge from the $\bar{q}$. Hence, a heavy meson H can be seen as the QCD analogue to the hydrogen atom.

Let us first consider a heavy quark with momentum $p = m_Q v + k$, where $k \ll m_Q$ denotes the residual momentum, which describes how much the quark is off-shell. The Dirac propagator of Q becomes

$$i\frac{\not{p}_Q + m_Q}{p^2 - m_Q^2 + i\epsilon} \to i\frac{1 + \not{v}}{2v \cdot k + i\epsilon} \tag{2.52}$$

in the heavy quark limit. At leading order, the propagator includes a velocity-dependent projector $(1+\not{v})/2$, which would act on the spinor of a heavy quark. Accordingly, for the formulation of an effective Lagrangian, it is convenient to use velocity dependent quark fields

$$\begin{aligned} Q(x) &= \exp(-im_Q v\cdot x)(Q_v(x)+\mathcal{Q}_v(x))\,,\\ Q_v(x) &= \exp(im_Q v\cdot x)\frac{1+\not{v}}{2}Q(x)\,,\\ \mathcal{Q}_v(x) &= \exp(im_Q v\cdot x)\frac{1-\not{v}}{2}Q(x)\,. \end{aligned} \tag{2.53}$$

The field Q_v also contains the projector $(1+\not{v})/2$ and is thus responsible for the leading effects in the $1/m_Q$ evolution. The $\mathcal{Q}_v$ field, on the other hand, is only relevant for corrections in the $1/m_Q$ evolution. By the prefactor $\exp(-im_Q v\cdot x)$ the momentum of the fields Q_v and $\mathcal{Q}_v$ is reduced by $m_Q v$ and thus is equal to the residual momentum. At leading order, the effective Lagrangian

$$\mathcal{L}_Q = \sum_{i=c,b}\bar{Q}_v^i(iv\cdot D)Q_v^i\,. \tag{2.54}$$

depends neither on the masses nor on the spins of the heavy quarks. Therefore, $\mathcal{L}_Q$ has a $U(4)$ spin-flavor symmetry. Consequently, an exchange of the heavy flavors or a change of the spin does not affect the dynamics of a process. The $1/m_Q$ corrections introduce both explicit dependencies on the quark masses and terms that depend on the spin of the quarks, which breaks the spin-flavor symmetry.

In the heavy quark limit, hadrons containing a heavy quark as well as light (anti)quarks and gluons form doublets with total spin $s = s_l \pm 1/2$, where s_l is the spin of the light degrees of freedom, due to the heavy quark spin symmetry. An exception are hadrons with $s_l = 0$. This degeneracy is broken by corrections of order $1/m_Q$ which introduce a dependence on the spin of the heavy quark. For an effective theory of heavy hadrons, it is useful to combine the degenerate states from one spin doublets into one object that transforms linearly under heavy quark symmetry. In the case of heavy $Q\bar{q}$ mesons, such as D and D^* mesons, the doublet is represented by 4×4 matrices

$$\begin{aligned} H_a &= \frac{1+\not{v}}{2}\left(P^\star_{a\mu}\gamma^\mu - P_a\gamma_5\right)\,,\\ \bar{H}_a &= \gamma^0 H_a^\dagger\gamma^0 = \left(P^{\star\dagger}_{a\mu}\gamma^\mu + P_a^\dagger\gamma_5\right)\frac{1+\not{v}}{2}\,, \end{aligned} \tag{2.55}$$

where $P^{\star(\dagger)}_{a\mu}$, $P^{(\dagger)}_a$ annihilate (create) a heavy vector and pseudoscalar meson h_a with quark flavor content $c\bar{q}_a$ and velocity v, respectively. The annihilation operators are normalized as

$$\begin{aligned} \langle 0|P_a|h_a(v)\rangle &= 1\,,\\ \langle 0|P_a^{\star\mu}|h_a^\star(v,\eta)\rangle &= \eta^\mu\,. \end{aligned} \tag{2.56}$$

In section 4.2.2 we use the framework of heavy hadron chiral perturbation theory (HHχPT), which combines chiral and heavy quark symmetry to provide a description of weak radiative D meson decays. For detailed introductions to the concept of heavy quark effective theory we refer to [111–114]

3 The weak effective theory for $c \to u\gamma$ transitions

So far, direct searches for new particles beyond the SM have not been successful. Instead, experimental results agree to an impressive precision with the predictions of the SM, except for the flavor anomalies and the anomalous magnetic moments mentioned in section 2.4. The subsequent tight constraints on BSM physics permit two possibilities. On the one hand, light particles with tiny couplings to the SM content can be introduced, making their production in collider experiments very unlikely. On the other hand, it is possible to introduce new particles with masses which are beyond reach of current collider setups. Thus, the energy scale of new physics will be clearly separated from the electroweak scale. Besides that, we have little knowledge about the nature and structure of BSM physics. A common framework for indirect searches for new physics of the second category are EFTs, which take advantage of the separations between the different energy scales and allow model independent analyses. Model independent in this context means that, with the exception of the separation of scales, there are no explicit requirements on the BSM model. EFTs parameterize interactions by effective operators that include only the relevant, i.e. light, degrees of freedom. The heavy states no longer appear explicitly in the operators, but are absorbed in effective couplings called Wilson coefficients. These, in turn, are independent of the light degrees of freedom. Due to the decoupling of light and heavy degrees of freedom, it is possible to test the SM without explicitly calculating the contributions of a BSM model to an observable. The results of model-independent analyses can subsequently be used as orientation for model-building. The validity of the EFT approach is ensured by the decoupling theorem [115].

3.1 The concept of weak effective theory

A historical example of such an EFT is Fermi's theory of the weak interaction [116]. It describes low energy processes of the weak interaction such as β- or μ-decays without the massive $W^{\pm}$ and Z bosons. Since the typical energy scale of these processes is low compared to the W boson mass, the propagators can be evolved in powers of p^2/m_W^2, where p is the characteristic four momentum of the process. Thus, an effective Lagrangian can be defined as an expansion in local operators

$$\mathcal{L}_{\text{Fermi}} = \frac{4G_F}{\sqrt{2}} J_\mu^\dagger J^\mu + \mathcal{O}\left(\frac{p^2}{m_W^2}\right) , \tag{3.1}$$

where the information on the heavy degrees of freedom are absorbed by the Fermi coupling $G_F = \sqrt{2}g^2/(8m_W^2)$. The charged current of the weak interaction

$$J_\mu = \bar{u}_L'^i \gamma_\mu V_{ij} d_L'^i + \bar{\nu}_L'^i \gamma_\mu e_L'^i \, . \tag{3.2}$$

includes only the relevant light degrees of freedom. However, beyond tree level we have to consider radiative corrections from QED and QCD. The small coupling of QED ensures the applicability of perturbation theory. Moreover, QED loop corrections are small and usually only of interest for leptonic processes in which QCD is not involved. For weak decays containing quarks, QCD corrections are dominant. Due to the large coupling of QCD at low energy scales as well as arising large logarithms, however, problems arise when applying normal perturbation theory. In the following, the method of renormalization group improved perturbation theory, which is used to avoid the problem of large logarithms, is introduced using the example of $b \to cd\bar{u}$ transitions.

The effective Lagrangian for $b \to cd\bar{u}$ transitions is given by

$$\mathcal{L}_{\text{eff}}^{\text{weak}} = \frac{4G_F}{\sqrt{2}} V_{cb} V_{ud}^* \sum_{i=1}^{2} C_i(\mu) O_i(\mu) \,. \tag{3.3}$$

Here, the C_i denote the Wilson Coefficients which parametrize the radiative corrections from QCD (and QED) and incorporate the information from high energy scales. The effective operators describe the low-energy dynamics and are given in terms of light degrees of freedom. All particles with a mass $m > m_b$ are considered to be heavy degrees of freedom and have therefore been integrated out. A common basis for the operators reads

$$O_1 = \left(\bar{d}_L \gamma_\mu T^a u_L\right) \left(c_L \gamma^\mu T^a b_L\right) \,, \qquad O_2 = \left(\bar{d}_L \gamma_\mu u_L\right) \left(c_L \gamma^\mu b_L\right) \,, \tag{3.4}$$

where the operator O_1 arises at one-loop level of QCD due to the non abelian structure of the QCD gauge group. The Wilson coefficients are determined by comparing the amplitudes in the full theory and the effective theory. This procedure is commonly known as matching. When performing the matching up to a fixed and finite order in perturbation theory, it turns out that both the Wilson coefficients and the matrix elements of the local operators can be written as expansions in

$$L_{i,j}^W = \alpha_s^i \ln^j \left(\frac{\mu^2}{m_W^2}\right) \qquad \text{and} \qquad L_{i,j}^b = \alpha_s^i \ln^j \left(\frac{\mu^2}{m_b^2}\right) \tag{3.5}$$

with $0 \leq j \leq i$, respectively. Here, μ denotes the common renormalization scale, whose choice causes a problem. For $\mu \approx m_W$, the expansion of the Wilson coefficients in $L_{i,j}^W$ converges, but not the expansion of the matrix elements of the local operators in $L_{i,j}^b$. For $\mu \approx m_b$ it is the other way around. It is not possible that both expansions converge for a common choice of the renormalization scale. However, the full amplitude cannot depend on the exact choice of the value for μ, since it is an unphysical parameter. Thus, we obtain

$$\frac{\mathrm{d}(C_i(\mu) O_i(\mu))}{\mathrm{d}\ln(\mu)} = \frac{\mathrm{d}C_i(\mu)}{\mathrm{d}\ln(\mu)} O_i(\mu) + C_i(\mu) \frac{\mathrm{d}O_i(\mu)}{\mathrm{d}\ln(\mu)} = 0 \,. \tag{3.6}$$

If the basis of the operators is complete, the logarithmic derivative of the operators can again be expressed in terms of the operators

$$\frac{\mathrm{d}O_i(\mu)}{\mathrm{d}\ln(\mu)} = -\gamma_{ij} O_j \,, \tag{3.7}$$

where the matrix γ is called anomalous dimension matrix (ADM). The ADM can be written as an expansion in the strong coupling constant

$$\gamma_{ij}(\alpha_s) = \sum_k \gamma_{ij}^{(k)} \left(\frac{\alpha_s}{4\pi}\right)^{k+1} . \tag{3.8}$$

Inserting (3.7) in (3.6) yields the renormalization group equation (RGE) for the Wilson Coefficients

$$\frac{\mathrm{d}C_i(\mu)}{\mathrm{d}\ln(\mu)} = (\gamma^T)_{ij} C_j \,. \tag{3.9}$$

The RGE is solved by

$$\begin{aligned} C_i(\mu') &= U_{ij}(\mu', \mu) C_j(\mu) \,, \\ U_{ij}(\mu', \mu) &= \exp\left(\int_{g_s(\mu)}^{g_s(\mu')} \mathrm{d}g_s' \frac{\gamma_{ji}(g_s')}{\beta(g_s')} \right) , \end{aligned} \tag{3.10}$$

where $\beta = \mathrm{d}g_s/\mathrm{d}\ln(\mu)$ is the QCD β-function. Thus, we are able to evaluate the Wilson coefficients at the electroweak scale, where the logarithms vanish and the evolution converges. Subsequently, the RGE can be solved which resumes the large logarithms and provides the Wilson coefficients at the low energy scale. If we only take the leading term in the expansion of the ADMs into account, then only the logarithms of the terms $L_{i,i}^W$ are resumed where the logarithms and couplings appear in the same order. This is known as leading logarithm order (LLO) approximation. In order to resum further logarithms, higher order terms in the expansion of the ADMs have to be taken into account. At next to leading logarithm order (NLLO) the second order terms in the ADM expansion are considered and thus the terms $L_{i,i-1}^W$ are additionally resumed. For a more detailed introduction to the concept of EFTs we refer to [117–123]

3.2 Effective Lagrangian for weak radiative charm decays

For our purpose of describing weak radiative decays of charmed hadrons, we require an EFT analogous to (3.3) which only contains fermions with $m_f \leq m_c$ as well as the photon and gluon as explicit degrees of freedom. However, when performing the matching at the scale μ_W, the b quark has to be considered as a light degree of freedom, and thus emerges in the operators. Since the light quark masses have to be set to zero to be consistent with the factorization of scales in the effective Lagrangian [76], the GIM mechanism yields a perfect cancellation of the loops induced $c \to u$ contributions. Therefore, the effective Lagrangian for $\mu_b \leq \mu \leq \mu_W$ contains exclusively the four quark operators O_1 and O_2. The b quark is integrated out after the RG evolution to μ_b. The corresponding matching of the EFTs with five and four active quark flavors induces contributions to additional operators. After the concluding RG evolution to the charm scale μ_c, the effective $c \to u\gamma$

Lagrangians for CF, SCS and DCS decays are given by [124]

$$\mathcal{L}_{\text{eff}}^{\text{SCS}} = \frac{4G_F}{\sqrt{2}} \left(\sum_{q=d,s} V_{cq}^* V_{uq} \sum_{i=1}^{2} C_i O_i^{(q,q)} + \sum_{i=3}^{6} C_i O_i + \sum_{i=7}^{8} \left(C_i O_i + C_i' O_i' \right) \right) , \tag{3.11}$$

$$\mathcal{L}_{\text{eff}}^{\text{CF}} = \frac{4G_F}{\sqrt{2}} V_{cs}^* V_{ud} \sum_{i=1}^{2} C_i O_i^{(s,d)} , \quad \mathcal{L}_{\text{eff}}^{\text{DCS}} = \frac{4G_F}{\sqrt{2}} V_{cd}^* V_{us} \sum_{i=1}^{2} C_i O_i^{(d,s)} , \tag{3.12}$$

neglecting operators with a mass dimension larger than six. The operators are defined a,s

$$\begin{aligned}
O_1^{(q,q')} &= \left(\bar{u}_L \gamma_\mu T^a q_L'\right) \left(\bar{q}_L \gamma^\mu T^a c_L\right) , & O_2^{(q,q')} &= \left(\bar{u}_L \gamma_\mu q_L'\right) \left(\bar{q}_L \gamma^\mu c_L\right) , \\
O_3 &= \left(\bar{u}_L \gamma_\mu c_L\right) \sum_q \left(\bar{q} \gamma^\mu q\right) , & O_4 &= \left(\bar{u}_L \gamma_\mu T^a c_L'\right) \sum_q \left(\bar{q} \gamma^\mu T^a q\right) , \\
O_5 &= \left(\bar{u}_L \gamma_\mu \gamma_\nu \gamma_\rho c_L\right) \sum_q \left(\bar{q} \gamma^\mu \gamma^\nu \gamma^\rho q\right) , & O_6 &= \left(\bar{u}_L \gamma_\mu \gamma_\nu \gamma_\rho T^a c_L\right) \sum_q \left(\bar{q} \gamma^\mu \gamma^\nu \gamma^\rho T^a q\right) , \\
O_7 &= \frac{e m_c}{16\pi^2} \left(\bar{u}_L \sigma^{\mu\nu} c_R\right) F_{\mu\nu} , & O_7' &= \frac{e m_c}{16\pi^2} \left(\bar{u}_R \sigma^{\mu\nu} c_L\right) F_{\mu\nu} , \\
O_8 &= \frac{g_s m_c}{16\pi^2} \left(\bar{u}_L \sigma^{\mu\nu} T^a c_R\right) G_{a\mu\nu} , & O_8' &= \frac{g_s m_c}{16\pi^2} \left(\bar{u}_R \sigma^{\mu\nu} T^a c_L\right) G_{a\mu\nu} ,
\end{aligned} \tag{3.13}$$

where $\sigma^{\mu\nu} = \frac{i}{2}\left[\gamma^\mu, \gamma^\nu\right]$. The sums in the QCD penguin operators O_{3-6} include all quark fields with $m_q < \mu_c$. The SM Wilson coefficients

$$C_i(\mu) = C_i^{(0)}(\mu) + \frac{\alpha_s(\mu)}{4\pi} C_i^{(1)}(\mu) + \left(\frac{\alpha_s(\mu)}{4\pi}\right)^2 C_i^{(2)}(\mu) + \mathcal{O}(\alpha_s^3(\mu)) \tag{3.14}$$

were calculated up to (partly) next-to-next-to leading logarithmic order (NNLLO) in QCD [76, 125, 126]. The matching of the Wilson coefficients C_1 and C_2 at the electroweak scale was calculated at next-to-next-to leading order (NNLO). Subsequently, the RG-evolution to μ_b was performed at NNLLO. Afterwards, the b-quark was integrated out. The five-to-four flavor matching was carried out at NLO, leading to non-zero coefficients C_{3-8}. Finally, the RG evolution down to the charm scale μ_c was performed at NNLLO. Moreover, the leading QED corrections were calculated, which are negligible for phenomenological purpose. Numerical results are listed in Table 3.1. We confirm the typo noted in [65]. The four-quark operators $O_{1,2}^{(q,q')}$ receive coefficients of order one. The effects of the remaining coefficients can be absorbed into an effective coefficient for O_7, which is strongly suppressed in the SM, $|C_7^{\text{eff}}| \simeq \mathcal{O}(0.001)$ at next-to-next-to leading order [124], due to the efficient GIM-cancellation. The coefficients $C_{7,8}'$ receive an additional suppression of m_u/m_c, and are therefore not included in Table 3.1. Thus, only the four-quark operators are relevant for SM analyses. To quantify the uncertainties regarding the scale μ_c, we vary μ_c within $\left[m_c/\sqrt{2}, \sqrt{2} m_c\right]$. At leading order in α_s, we obtain [124]

$$\begin{aligned}
C_1 &\in [-1.28, -0.83] , & C_2 &\in [1.14, 1.06] , \\
C_+ &= C_2 + \frac{1}{3} C_1 \in [0.76, 0.78] , & C_- &= C_2 - \frac{2}{3} C_1 \in [1.99, 1.61] , \\
\tilde{C} &= \frac{4}{9} C_1 + \frac{1}{3} C_2 \in [-0.189, -0.018] .
\end{aligned} \tag{3.15}$$

$\times(\alpha_s/(4\pi))^i$	$C_1^{(i)}$	$C_2^{(i)}$	$C_3^{(i)}/\lambda_{ds}$	$C_4^{(i)}/\lambda_{ds}$	$C_5^{(i)}/\lambda_{ds}$	$C_6^{(i)}/\lambda_{ds}$	$C_7^{(i)}/\lambda_{ds}$	$C_8^{(i)}/\lambda_{ds}$
$i=0$	-1.0421	1.0949	-0.0038	-0.0625	0.0004	0.0008	0	0
$i=1$	0.3239	-0.0561	-0.0026	-0.0320	0.0000	-0.0002	0.0036	-0.0021
$i=2$	0.0779	-0.0039	-0.0020	-0.0009	0.0001	0.0003	0.0002	-0.0003
$\sum_{i=0}^{2}$	-0.6402	1.0349	-0.0084	-0.0953	0.0005	0.0009	0.0038	-0.0024

Table 3.1: Wilson coefficients of the $c \to u(q\bar{q}')\gamma$ Lagrangian at partly NNLLO in QCD. The given values refer to $\mu_c = m_c$. Note that the Wilson coefficients were determined in a different basis with $O_7 = \frac{em_c}{g_s^2}\,(\bar{u}_L\sigma^{\mu\nu}c_R)\,F_{\mu\nu}$ and $O_8 = \frac{m_c}{g_s}\,(\bar{u}_L\sigma^{\mu\nu}T^a c_R)\,G_{a\mu\nu}$. Furthermore, $\lambda_{ds} = V_{cd}^* V_{ud} + V_{cs}^* V_{us}$. Note that there is a typo in Table 2.2 of [125] regarding the sign of $C_6^{(1)}$.

3.3 Constraints on $C_7^{(\prime)}$

Although the electromagnetic dipole operators are irrelevant for SM predictions due to the negligible effective coefficients, they are of great importance for the search for new physics with radiative decays. BSM physics can significantly increase the Wilson coefficients $C_7^{(\prime)}$. Examples of BSM models that have an impact on $c \to u\gamma$ transitions would be e.g. supersymmetric models with flavor mixing and chirally enhanced gluino loops [124], leptoquarks [124] or dark matter models [127]. The maximum impact of SM extensions on the electromagnetic dipole coefficients is given by the model-independent constraints from experimental data on $D \to \rho^0\gamma$ and $D \to \pi\ell\ell$ decays [68, 75, 128]

$$|C_7^{(\prime)}| \lesssim 0.3\,. \tag{3.16}$$

Moreover, in addition to the modulus, the CP violating phase of $C_7^{(\prime)}$ can be constrained as well. Therefore, we consider the connection between the coefficients of the electromagnetic and chromomagnetic dipole operators at different scales. These are linked by the renormalization-group evolution. At leading order in α_s [124]

$$C_7^{(\prime)}(m_c) \simeq 0.4(C_7^{(\prime)}(\Lambda) - C_8^{(\prime)}(\Lambda))\,, \qquad C_8^{(\prime)}(m_c) \simeq 0.4C_8^{(\prime)}(\Lambda) \tag{3.17}$$

is valid to roughly 20% if Λ, the scale of new physics, is within $1 - 10\,\text{TeV}$. For BSM models predicting dominant chromomagnetic Wilson coefficients $C_8(\Lambda) > C_7(\Lambda)$ at the scale of new physics, the CP asymmetries of radiative and hadronic decays are thus strongly related. In particular, we can constrain the CP violating phase of $C_7^{(\prime)}$ by [129, 130]

$$\Delta A_{\text{CP}} = A_{\text{CP}}(D \to K^+K^-) - A_{\text{CP}}(D \to \pi^+\pi^-)\,, \tag{3.18}$$

which was determined by LHCb as $\Delta A_{\text{CP}} = -(15.4 \pm 2.9)\cdot 10^{-4}$ [131]. The contribution of new physics by the chromomagnetic dipole operators thus obtains the upper limit $\Delta A_{\text{CP}}^{\text{NP}} \sim \text{Im}(C_8(m_c) - C_8'(m_c))\sin(\delta) \lesssim 2\cdot 10^{-3}$, where δ denotes the strong phase difference. Therefore, for $\sin(\delta) \sim 1$ and only one of the coefficients $C_8^{(\prime)}$, we obtain the strong constraint on the $c \to u\gamma$ coupling

$$|\text{Im}\,(C_7^{(\prime)})| \simeq |\text{Im}\,(C_8^{(\prime)})| \lesssim 2\cdot 10^{-3}\,. \tag{3.19}$$

We note that we can ease the ΔA_{CP} constraint by suppressing the strong phase δ. Furthermore, we can bypass the constraint, if $C_7^{(\prime)}(\Lambda) \gg C_8^{(\prime)}(\Lambda)$ or due to different sources of BSM CP violation in the hadronic amplitudes.

4 Three-body decays $D \to PP\gamma$

The most simple hadronic decays based on $c \to u\gamma$ transitions are the resonant two-body decays $D \to V\gamma$ and $D \to A\gamma$, where V and A denote vector mesons and axialvector mesons, respectively. So far, theoretical studies have mainly focused on the $D \to V\gamma$ decays, as in [124, 132–137]. Similarly, the only experimental data obtained up to now fall into this category of decays. The branching ratios and CP asymmetries in Table 4.1 were determined by the Belle, CLEO and BaBar collaborations.

	B (Belle [128])	$A_{\rm CP}$ (Belle [128])	B (CLEO [138])	B (BaBar [139])
$D^0 \to \rho^0\gamma$	$(1.77 \pm 0.31) \cdot 10^{-5}$	0.056 ± 0.156	$< 2.4 \cdot 10^{-4}$	-
$D^0 \to \omega\gamma$	-	-	$< 2.4 \cdot 10^{-4}$	-
$D^0 \to \phi\gamma$	$(2.76 \pm 0.21) \cdot 10^{-5}$	-0.094 ± 0.066	$< 7.6 \cdot 10^{-4}$	$(2.73 \pm 0.40) \cdot 10^{-5}$
$D^0 \to \overline{K}^{*0}\gamma$	$(4.66 \pm 0.30) \cdot 10^{-4}$	-0.003 ± 0.020	$< 1.9 \cdot 10^{-4}$	$(3.22 \pm 0.34) \cdot 10^{-4}$

Table 4.1: Currently available experimental data on weak radiative charm decays.

Following the analysis of resonant decays, the study of non-resonant decays $D \to PP\gamma$ is the next logical step. They provide background to the resonant decays as the vector mesons decay dominantly into two pseudoscalars. However, the additional hadron in the final state makes the description of the decays more complicated. In return, the non-resonant decays provide more information due to their decay distributions and angular observables. Neglecting final states with $\eta^{(\prime)}$, there are a total of 18 different $D \to PP\gamma$ decays, which can be induced by the dimension six operators in (3.12). They are composed of five CF, eight SCS and five DCS modes

$$\begin{aligned}
\text{CF:}\quad & D^0 \to \pi^0\overline{K}^0\gamma,\ D^0 \to \pi^+K^-\gamma,\ D^+ \to \pi^+\overline{K}^0\gamma,\ D_s \to \pi^+\pi^0\gamma,\ D_s \to K^+\overline{K}^0\gamma,\\
\text{SCS:}\quad & D^0 \to \pi^+\pi^-\gamma,\ D^0 \to \pi^0\pi^0\gamma,\ D^0 \to K^+K^-\gamma,\ D^0 \to K^0\overline{K}^0\gamma,\\
& D^+ \to \pi^+\pi^0\gamma,\ D^+ \to K^+\overline{K}^0\gamma,\ D_s \to \pi^+K^0\gamma,\ D_s \to K^+\pi^0\gamma\\
\text{DCS:}\quad & D^0 \to \pi^0K^0\gamma,\ D^0 \to K^+\pi^-\gamma,\ D^+ \to \pi^+K^0\gamma, D^+ \to K^+\pi^0\gamma,\ D_s \to K^+K^0\gamma.
\end{aligned} \tag{4.1}$$

We have covered 14 of them in our previous publications [2, 3] and the remaining four are included in this thesis. $D^+ \to K^+K^0\gamma$ and $D_s \to \pi^+\overline{K}^0\gamma$ are $|\Delta s| = 2$ processes and are thus not induced by dimension six operators. Accordingly, they are not addressed in this thesis.

This chapter is organized as follows: In section 4.1 we describe the kinematics and distributions of the decays. We then provide a description of our QCD frameworks in section 4.2. We use Low's theorem to describe the bremsstrahlung in subsection 4.2.1. We work out decay amplitudes using heavy hadron chiral perturbation theory (HHχPT) in subsection 4.2.2. Finally, we use QCD factorization (QCDF) methods to describe the

leading weak annihilation (WA) contribution in subsection 4.2.3. We provide both SM and BSM predictions for (differential) branching ratios, forward-backward asymmetries and CP asymmetries throughout sections 4.3 to 4.5. Finally, we summarize the results in section 4.6 and outline the best options for NP searches with $D \to PP\gamma$ decays.

4.1 Kinematics and decay distribution

The most general Lorentz and gauge invariant decomposition of the decay amplitude for $D(P) \to P_1(p_1)P_2(p_2)\gamma(k,\epsilon^*)$ reads

$$\begin{aligned}\mathcal{A}(D \to P_1P_2\gamma) = A_-(s,t)\,[(p_1\cdot k)(p_2\cdot\epsilon^*) - (p_2\cdot k)(p_1\cdot\epsilon^*)] \\ + A_+(s,t)\epsilon^{\mu\alpha\beta\gamma}\epsilon^*_\mu p_{1\alpha}p_{2\beta}k_\gamma\,,\end{aligned} \tag{4.2}$$

where A_+ and A_- denote the parity-even and parity-odd contributions, respectively. P, p_1, p_2 and k refer to the four-momenta of the D, P_1, P_2 and photon. The polarization vector of the photon is labeled as ϵ^*. Since the D meson is a pseudoscalar, the amplitude depends on two kinematic quantities. We choose $s = (p_1+p_2)^2$ and $t = (p_2+k)^2$ which are the squared invariant masses of the $P_1 - P_2$ and $P_2 - \gamma$ systems, respectively. P_1 and P_2 are assigned according to the listing in (4.1). Thus, for charged final states, we always denote the positively charged meson as P_1. For the neutral final states, we denote the π^0 or in case of $D^0 \to K^0\overline{K}^0\gamma$ the K^0 as P_1. For the totally antisymmetric Levi-Civita tensor $\epsilon^{\mu\alpha\beta\gamma}$, we use the convention $\epsilon^{0123} = +1$.

As we use squared invariant masses as kinematical variables, the double differential decay distribution is given in the standard Dalitz form and can be written in terms of the parity-even and parity-odd contributions as

$$\frac{\mathrm{d}^2\Gamma}{\mathrm{d}s\mathrm{d}t} = \frac{|A_-|^2 + |A_+|^2}{128(2\pi)^3 m_D^3} f(s,t)\,, \tag{4.3}$$

where

$$\begin{aligned}f(s,t) = m_1^2(t-m_2^2)(s-m_D^2) - m_2^4 m_D^2 \\ - st(s+t-m_D^2) + m_2^2(st + (s+t)m_D^2 - m_D^4)\end{aligned} \tag{4.4}$$

is a kinematical function, depending on s, t and the masses of the pseudoscalars. Furthermore, the singly differential decay distribution reads

$$\begin{aligned}\frac{\mathrm{d}\Gamma}{\mathrm{d}s} &= \int_{t_{\min}}^{t_{\max}} \mathrm{d}t \frac{\mathrm{d}^2\Gamma}{\mathrm{d}s\mathrm{d}t}\,, \\ t_{\min} &= \frac{(m_D^2 - m_1^2 + m_2^2)^2}{4s} - \left(\sqrt{\frac{(s-m_1^2+m_2^2)^2}{4s} - m_2^2} + \frac{m_D^2 - s}{2\sqrt{s}}\right)^2\,, \\ t_{\max} &= \frac{(m_D^2 - m_1^2 + m_2^2)^2}{4s} - \left(\sqrt{\frac{(s-m_1^2+m_2^2)^2}{4s} - m_2^2} - \frac{m_D^2 - s}{2\sqrt{s}}\right)^2\,,\end{aligned} \tag{4.5}$$

where the kinematically allowed range of the di-meson invariant mass is given by $(m_1 + m_2)^2 \le s \le m_D^2$.

4.2 QCD frameworks

Information about the different QCD frameworks are provided in this section. We start with Low's theorem which is used to describe the bremsstrahlung in subsection 4.2.1. Subsequently, HHχPT is introduced and form factors are worked out in 4.2.2. Finally, the leading WA diagram is evaluated using QCDF in 4.2.3. The parity even and parity odd contributions to the decay amplitude are derived for all models. Furthermore, we provide information on parametric input and the regions of applicability.

4.2.1 Low's Theorem

For low photon energies, the distributions of $D \to PP\gamma$ are dominated by bremsstrahlung, which can be described using Low's theorem [140]. This approach relates the decay amplitude of the radiative three-body decays with those of the hadronic two-body decays. Schematic illustrations of the contributions are shown in Figure 4.1. The soft photons

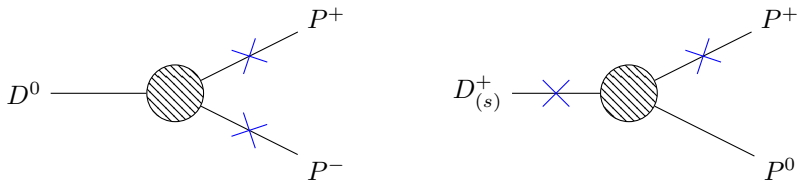

Figure 4.1: Schematic representation of the contributions to the bremsstrahlung according to Low's theorem. The blue crosses indicate the possible radiations of a photon.

are emitted by the charged mesons in the initial and final state. Thus, there is no bremsstrahlung for decays without charged mesons. The parity-odd contributions are given as

$$\begin{aligned} A_-^{\text{Low}}(D^0 \to P_1^+ P_2^- \gamma) &= -\frac{e\mathcal{A}(D^0 \to P_1^+ P_2^-)}{(p_1 \cdot k)(p_2 \cdot k)}\,, \\ A_-^{\text{Low}}(D^+_{(s)} \to P_1^+ P_2^0 \gamma) &= -\frac{e\mathcal{A}(D^+_{(s)} \to P_1^+ P_2^0)}{(p_1 \cdot k)(P \cdot k)}\,, \end{aligned} \tag{4.6}$$

while $A_+^{\text{Low}} = 0$. This approach is valid for photon energies below m_P^2/E_P [141], where P refers to the lighter charged meson. The radiation of the photon and the weak two-body decay factorize. Thus, the only input needed is $\mathcal{A}(D \to P_1 P_2)$, which we do not predict with theoretical models. Instead, we extract the modulus from data on branching ratios using

$$\mathcal{B}(D \to P_1 P_2) = \frac{|\mathcal{A}(D \to P_1 P_2)|^2}{16\pi m_D \Gamma_D} \sqrt{\left(1 - \frac{(m_1+m_2)^2}{m_D^2}\right)\left(1 - \frac{(m_1-m_2)^2}{m_D^2}\right)}\,, \tag{4.7}$$

where Γ_D denotes the total decay witdh of the D mesons. We obtain

$$\begin{aligned}
&\left|\mathcal{A}(D^0 \to \pi^+K^-)\right| = 2.52 \cdot 10^{-6}\,\text{GeV}\,, && \left|\mathcal{A}(D^0 \to K^+\pi^-)\right| = 1.56 \cdot 10^{-7}\,\text{GeV}\,,\\
&\left|\mathcal{A}(D^0 \to \pi^+\pi^-)\right| = 4.62 \cdot 10^{-7}\,\text{GeV}\,, && \left|\mathcal{A}(D^0 \to K^+K^-)\right| = 8.38 \cdot 10^{-7}\,\text{GeV}\\
&\left|\mathcal{A}(D^+ \to \pi^+\pi^0)\right| = 2.74 \cdot 10^{-7}\,\text{GeV}\,, && \left|\mathcal{A}(D_s \to \pi^+\pi^0)\right| < 2.11 \cdot 10^{-7}\,\text{GeV}\,,\\
&\left|\mathcal{A}(D^+ \to \pi^+K^0)\right| < 4.70 \cdot 10^{-8}\,\text{GeV}\,, && \left|\mathcal{A}(D_s \to \pi^+K^0)\right| = 5.75 \cdot 10^{-7}\,\text{GeV}\,,\\
&\left|\mathcal{A}(D^+ \to K^+\pi^0)\right| = 1.16 \cdot 10^{-7}\,\text{GeV}\,, && \left|\mathcal{A}(D_s \to K^+\pi^0)\right| = (2.9 \pm 0.5) \cdot 10^{-7}\,\text{GeV}\,,\\
&\left|\mathcal{A}(D^+ \to K^+\overline{K}^0)\right| = 6.62 \cdot 10^{-7}\,\text{GeV}\,, && \left|\mathcal{A}(D_s \to K^+\overline{K}^0)\right| = 2.10 \cdot 10^{-6}\,\text{GeV}\,,\\
&\left|\mathcal{A}(D^+ \to \pi^+\overline{K}^0)\right| = 1.40 \cdot 10^{-6}\,\text{GeV}\,, && \left|\mathcal{A}(D_s \to K^+K^0)\right| < 5.36 \cdot 10^{-8}\,\text{GeV}\,.
\end{aligned} \tag{4.8}$$

For three decays only upper limits, referring to a 90% confidence level, can be determined. For $D_s \to \pi^+\pi^0$ this is due to the fact that there is only an upper limit on the branching ratio. HHχPT implies that the amplitude is smaller by about two orders of magnitude and, moreover, vanishes in the isospin limit. Excluding $D_s \to K^+\overline{K}^0$, the branching ratios for decays with neutral kaons in the final state are not measured. Instead, there are measurements for the equivalent decays with K^0_S and K^0_L in the final states. The listed values are extracted from those data. However, this method causes large uncertainties for the DCS decays. Consequently, only upper limits are given for $D^+ \to \pi^+K^0$ and $D_s \to K^+K^0$ as well. We consider the sizeable uncertainty of the $D_s \to K^+\pi^0$ amplitude in our analysis, but neglect them for the other decay channels.

Low's theorem predicts a singularity for vanishing photon energies in the D meson's rest frame as the differential decay rate behaves as [142]

$$\frac{\mathrm{d}\Gamma}{\mathrm{d}s} \sim \frac{1}{m_D^2 - s}\,. \tag{4.9}$$

To increase the sensitivity to NP for integrated rates, we perform cuts in s. In this way, we remove the contributions of the singularity's tail, which dominate the distributions for soft photons.

4.2.2 Heavy Hadron chiral Perturbation Theory

Furthermore, we use the framework of heavy hadron chiral perturbation theory (HHχPT) which combines the concepts of chiral perturbation theory (section 2.6.2) and heavy quark effective theory (section 2.6.3) to derive the parity odd and parity even contributions to the decay amplitude. The model was introduced in [143–145] and is formulated in terms of the χPT matrices u (2.45) and the heavy meson fields H (2.55). Subsequently, HHχPT was extended by the light vector resonances, which are described by 3×3 matrices analogous to the χPT matrices [146, 147]

$$\hat{\rho}_\mu = \mathrm{i}\frac{g_v}{\sqrt{2}}\rho_\mu\,, \qquad \rho_\mu = \begin{pmatrix} \frac{\rho^0_\mu+\omega_\mu}{\sqrt{2}} & \rho^+_\mu & K^{\star+}_\mu \\ \rho^-_\mu & \frac{-\rho^0_\mu+\omega_\mu}{\sqrt{2}} & K^{\star0}_\mu \\ K^{\star-}_\mu & \bar{K}^{\star0}_\mu & \Phi_\mu \end{pmatrix}, \tag{4.10}$$

where $g_v = 5.9$ [148–150]. This model has been used previously to determine hadronic form factors in the context of semileptonic decays. In addition, predictions for radiative

two-body decays $D \to V\gamma$ [134, 135] and three-body decays $D^0 \to \pi^+ K^-\gamma$, $D^+ \to \pi^+ \overline{K}^0\gamma$ and $D^0 \to \pi^0(\eta,\eta')\overline{K}^0\gamma$ [151, 152] were made with this approach. To define the Lagrangian and the photon interaction in a simple and compact way, we introduce two currents

$$\begin{aligned} \mathcal{V}_\mu &= \frac{1}{2}\left(u^\dagger D_\mu u + u D_\mu u^\dagger\right) , \\ \mathcal{A}_\mu &= \frac{1}{2}\left(u^\dagger D_\mu u - u D_\mu u^\dagger\right) , \end{aligned} \tag{4.11}$$

where the covariant derivative is given by $D_\mu u^{(\dagger)} = \partial_\mu u^{(\dagger)} + ieB_\mu Q u^{(\dagger)}$. To avoid confusions between the χPT current and the photon field, we label the photon field with B_μ in this section. $Q = \mathrm{diag}(2/3, -1/3, -1/3)$ is the diagonal charge matrix of the light quarks. The parity-even Lagrangian for the light mesons reads [148–150]

$$\mathcal{L}_{\text{light}} = -\frac{f^2}{2}\left[\mathrm{Tr}_F\left(\mathcal{A}_\mu \mathcal{A}^\mu\right) + a\mathrm{Tr}_F\left(\left(\mathcal{V}_\mu - \hat{\rho}_\mu\right)^2\right)\right] + \frac{1}{2g_v^2}\mathrm{Tr}_F\left(F_{\mu\nu}(\hat{\rho})F^{\mu\nu}(\hat{\rho})\right) , \tag{4.12}$$

where the field strength tensor of the vector resonances is given by $F_{\mu\nu}(\hat{\rho}) = \partial_\mu\hat{\rho}_\nu - \partial_\nu\hat{\rho}_\mu + \left[\hat{\rho}_\mu, \hat{\rho}_\nu\right]$. In general, a is a free parameter. For $a = 0$, the vector mesons interact only among themselves. For $a = 2$, vector meson dominance (VMD) is obtained. In this case, there is no direct coupling of a photon to a pseudoscalar. Instead, the photon couples to the pseudoscalar exclusively via a ρ^0, ω or ϕ meson. However, in total, the coupling of photons to pseudoscalars is independent of a. Similarly, the non resonant contribution to the matrix element $\langle P_1 P_2|\bar{q}\gamma^\mu(1-\gamma_5)q'|0\rangle$ vanishes in VMD. However, we neither employ VMD nor exact flavor symmetry. Instead, we set $a = 1$ and take $SU(3)_F$ breaking effects into account by replacing the models coupling $g_v \to \sqrt{2}m_V^2/g_V$, the decay constant f and vector meson masses $m_V = \sqrt{a/2}g_v f$ by the respective measured parameters. Here, g_V denotes the vector meson decay constant with mass dimension two defined by

$$\langle V(q,\eta)|j_V^\mu|0\rangle = \eta^{*\mu}(q)g_V(q^2) , \tag{4.13}$$

where $j^\mu_{K^{*0},\overline{K}^{*0},K^{*\pm},\phi} = \bar{q}\gamma^\mu q'$ and $j^\mu_{\omega,\rho} = \frac{1}{\sqrt{2}}(\bar{u}\gamma^\mu u \pm \bar{d}\gamma^\mu d)$. The four momentum and polarization vector of the vector meson are labeled as q and η, respectively. Due to the replacement of the parameters, the $V\gamma$ interaction from (4.12) modifies to

$$\mathcal{L}_{V\gamma} = -\frac{e}{\sqrt{2}}B_\mu\left(g_\rho\rho^{0\mu} + \frac{1}{3}g_\omega\omega^\mu - \frac{\sqrt{2}}{3}g_\phi\phi^\mu\right) , \tag{4.14}$$

where we assume $g_V(0) \simeq g_V(m_V^2) = m_V f_V$ for our numerical evaluation. Here, f_V is the vector meson decay constant with mass dimension one, which is given in appendix A for the various vector mesons. Furthermore, a parity-odd interaction for the light sector can be defined by [153]

$$\mathcal{L}_{VVP} = -4\frac{C_{VVP}}{f}\epsilon^{\mu\nu\alpha\beta}\mathrm{Tr}(\partial_\mu\rho_\nu\partial_\alpha\rho_\beta\Pi) , \tag{4.15}$$

where $C_{VVP} = 3g_v^2/(32\pi^2)$ in case of exact $SU(3)_F$ symmetry. For our purpose, (4.15) is only relevant for a $VP\gamma$ interaction via $V\gamma$ conversion. Therefore, we neglect (4.15) and use an effective $VP\gamma$ Lagrangian instead

$$\mathcal{L}_{VP\gamma} = -eg_{VP\gamma}\epsilon_{\mu\nu\rho\sigma}\partial^\mu B^\nu \partial^\rho V^\sigma P^\dagger + \text{h.c.} . \tag{4.16}$$

The effective coefficients $g_{VP\gamma}$ can be determined in HHχPT as [137]

$$\begin{aligned} g_{\omega\pi\gamma} &= 4\frac{g_\rho}{m_\rho^2}\frac{C_{VVP}}{f_\pi} > 0\,, \\ g_{\rho\pi\gamma} &= 4\frac{g_\omega}{3m_\omega^2}\frac{C_{VVP}}{f_\pi} > 0\,, \\ g_{K^{*\pm}K^\pm\gamma} &= 2\left(\frac{g_\omega}{3m_\omega^2} + \frac{g_\rho}{m_\rho^2} - \frac{2}{3}\frac{g_\phi}{m_\phi^2}\right)\frac{C_{VVP}}{f_K} > 0\,, \\ g_{K^*K\gamma} &= 2\left(\frac{g_\omega}{3m_\omega^2} - \frac{g_\rho}{m_\rho^2} - \frac{2}{3}\frac{g_\phi}{m_\phi^2}\right)\frac{C_{VVP}}{f_K} < 0\,. \end{aligned} \tag{4.17}$$

However, we replace the modulus of the effective coefficients with values extracted from experimental data

$$\Gamma(V \to P\gamma) = \frac{\alpha_{\rm em} m_V^3}{24} g_{VP\gamma}^2 \left(1 - \frac{m_P^2}{m_V^2}\right)^3 . \tag{4.18}$$

The parity-even heavy-meson Lagrangian reads [137, 151]

$$\begin{aligned} \mathcal{L}_{\rm heavy} = {} & i{\rm Tr}_D\left(H_a v_\mu \left(D^\mu\right)_{ab} \bar{H}_b\right) + ig{\rm Tr}_D\left(H_a\gamma_\mu\gamma_5(\mathcal{A}^\mu)_{ab}\bar{H}_b\right) \\ & + i\tilde{\beta}{\rm Tr}_D\left(H_a v_\mu \left(\mathcal{V}^\mu - \hat{\rho}^\mu\right)_{ab} \bar{H}_b\right) . \end{aligned} \tag{4.19}$$

The covariant derivative acting on the heavy meson fields is defined as $\left(D^\mu\right)_{ab}\overline{H}_b = \partial^\mu \overline{H}_a + \left(\mathcal{V}^\mu\right)_{ab}\overline{H}_b - ieQ_c B^\mu \overline{H}_a$, where $Q_c = 2/3$ is the electric charge of the charm quark. Experimental data on $D^* \to D\pi$ decays determine the parameter $g = 0.59$ [154, 155]. The interaction in the last line is not taken into account as the coupling seems to be negligible small [156]. The parity-odd heavy meson Lagrangian is defined as

$$\mathcal{L} = i\lambda{\rm Tr}\left(H_a\sigma_{\mu\nu}F^{\mu\nu}(\hat{\rho})_{ab}\bar{H}_b\right) - \lambda' e{\rm Tr}\left(H_a\sigma_{\mu\nu}F^{\mu\nu}(B)\bar{H}_a\right) . \tag{4.20}$$

The couplings $\lambda = -0.49\ {\rm GeV}^{-1}$ and $\lambda' = -0.102\ {\rm GeV}^{-1}$ were extracted from ratios $R_\gamma^{0/+} = \Gamma(D^{\star 0/+} \to D^{0/+}\gamma)/\Gamma(D^{\star 0/+} \to D^{0/+}\pi)$. Note that we follow the approach of Fajfer *et al.* and omit the replacement of the parameter g_v in (4.20). The hadronized weak currents are given by [157, 158]

$$\begin{aligned} (\bar{q}_a Q)^\mu_{\text{V-A}} \simeq J^\mu_{Q\bar{q}_a} = {} & \frac{1}{2} i\alpha{\rm Tr}\left(\gamma^\mu(1-\gamma_5)H_b u^\dagger_{ba}\right) + \alpha_1{\rm Tr}\left(\gamma_5 H_b\left(\hat{\rho}^\mu - \mathcal{V}^\mu\right)_{bc} u^\dagger_{ca}\right) \\ & + \alpha_2{\rm Tr}\left(\gamma^\mu\gamma_5 H_b v_\alpha(\hat{\rho}^\alpha - \mathcal{V}^\alpha)_{bc}u^\dagger_{ca}\right) , \\ (\bar{q}_j q_i)^\mu_{\text{V-A}} \simeq J^\mu_{ij} = {} & if^2\left\{u\left[\mathcal{A}^\mu + a\left(\mathcal{V}^\mu - \hat{\rho}^\mu\right)\right]u^\dagger\right\}_{ij} , \end{aligned} \tag{4.21}$$

where the parameter $\alpha = f_h\sqrt{m_h}$ is fixed by the definition of the heavy meson decay constants. The parameters α_1 and α_2 can be determined using the $D \to V$ transition form factors [151]

$$A_1(q^2_{\rm max}) = 2\frac{\sqrt{m_D}}{m_D + m_V}\frac{m_V^2}{g_V}\alpha_1\,, \qquad A_2(q^2_{\rm max}) = 2\frac{m_D + m_V}{m_D^{\frac{3}{2}}}\frac{m_V^2}{g_V}\alpha_2\,. \tag{4.22}$$

Note that unlike [151], we have again replaced g_v. Furthermore, the sign differs due to our conventions of the transition form factors, see appendix B.2. We obtain $\alpha_1 = 0.188\,\mathrm{GeV}^{\frac{1}{2}}$ and $\alpha_2 = 0.086\,\mathrm{GeV}^{\frac{1}{2}}$ using the $D \to K^*$ form factors [159]. The parity-even and parity-odd SM amplitudes are given in terms of four form factors

$$\begin{aligned} A_-^{\mathrm{HH}\chi\mathrm{PT}} &= \frac{G_F e}{\sqrt{2}} \sum_{q,q' \in \{d,s\}} V_{cq}^* V_{uq'} \left[(C_2 - \frac{1}{6} C_1) \sum_i A_i^{(q,q')} + \frac{1}{2} C_1 \sum_i E_i^{(q,q')} \right] , \\ A_+^{\mathrm{HH}\chi\mathrm{PT}} &= \frac{G_F e}{\sqrt{2}} \sum_{q,q' \in \{d,s\}} V_{cq}^* V_{uq'} \left[(C_2 - \frac{1}{6} C_1) \sum_i B_i^{(q,q')} + \frac{1}{2} C_1 \sum_i D_i^{(q,q')} \right] , \end{aligned} \tag{4.23}$$

where A and B belong to the charged current operator $(\bar{u}q')_{\mu V-A}(\bar{q}c)^{\mu}_{V-A} \equiv 4O_2^{(q,q')}$. D and E belong to the neutral current operator $(\bar{q}q')_{\mu V-A}(\bar{u}c)^{\mu}_{V-A} \equiv 8O_1^{(q,q')} + 4O_2^{(q,q')}/3$. All Feynman diagrams as well as the non-zero contributions to the form factors are given in appendix C.1. The form factors are calculated with the naive factorization approximation for the weak matrix elements. We consider the masses of the pseudoscalars only in their propagators and in the phase space, but neglect them otherwise. If the intermediate vector mesons can be on-shell, we use the Breit-Wigner formula for the propagators. A naive calculation of the diagram $A_{6,1}$ using Feynman rules yields an expression which violates gauge invariance. In order to obtain a gauge invariant amplitude one has to remove the contributions of longitudinal polarization of the $D^+_{(s)} \to V^+V_0$ subdiagram. Furthermore, we replace the bremsstrahlung contributions $A_{1,2}$ for D^0 decays and $A_{1,2,3}$ and $E_{1,2}$ for $D^+_{(s)}$ decays by (4.6) to enforce Low's theorem. However, we use the strong and weak phase of the hadronic two body decays predicted by HHχPT, see appendix C.2. The form factors of the hadronic two-body decays are independent of the choice of a. Dependencies of the $D \to PP\gamma$ form factors on a arise from the WA diagramms D_1, D_3 and B_1, B_4 for D^0 and $D^+_{(s)}$ decays, respectively. The form factors in appendix C.1 are obtained for $a = 1$. To recover the general a-dependent expressions, the non-resonant and resonant contributions have to be multiplied with a factor of $(2-a)$ and a, respectively.

To calculate possible BSM contributions of the electromagnetic dipole operators, we further need an expression of the tensor current in terms of HHχPT quantities. Due to the equation of motion for heavy quarks $1/2(1+\not{v})Q = Q$, the heavy V-A and tensor currents are related as

$$\bar{q}\sigma^{0i}(1+\gamma_5)Q = -i\bar{q}_a\gamma^i(1-\gamma_5)Q\,. \tag{4.24}$$

As a consequence, the weak tensor current can be constructed as [160]

$$\begin{aligned} &\bar{q}\sigma^{\mu\nu}(1+\gamma_5)Q \simeq J^{\mu\nu}_{Q\bar{q}_a} \\ &= \frac{1}{2} i\alpha \mathrm{Tr}\left(\sigma^{\mu\nu}(1+\gamma_5)H_b u^\dagger_{ba}\right) \\ &\quad + i\alpha_1 \left(g^{\mu\alpha}g^{\nu\beta} - \frac{1}{2} i\epsilon^{\mu\nu\alpha\beta}\right) \mathrm{Tr}\left(\gamma_5 H_b \left[\gamma_\alpha \left(\hat{\rho}_\beta - \mathcal{V}_\beta\right)_{bc} - \gamma_\beta \left(\hat{\rho}_\alpha - \mathcal{V}_\alpha\right)_{bc}\right] u^\dagger_{ca}\right) \\ &\quad - \alpha_2 \mathrm{Tr}\left(\sigma^{\mu\nu}\gamma_5 H_b v_\alpha \left(\hat{\rho}^\alpha - \mathcal{V}^\alpha\right)_{bc} u^\dagger_{ca}\right) , \end{aligned} \tag{4.25}$$

where the parameters α, α_1 and α_2 are the same as in (4.21). We have added the term $\propto \alpha_2$, however, it is not relevant for the discussed decays. The $D \to P_1P_2$ matrix elements of the tensor currents can be parameterized as

$$\left\langle P_1P_2|\bar{u}\sigma^{\mu\nu}k_\mu(1\pm\gamma_5)c|D\right\rangle = m_D\left[a'p_1^\nu + b'p_2^\nu + c'P^\mu \mp 2ih'\epsilon^{\nu\alpha\beta\gamma}p_{1\alpha}p_{2\beta}k_\gamma\right]. \quad (4.26)$$

The form factors depend on s and t and satisfy

$$a'p_1\cdot k + b'p_2\cdot k + c'P\cdot k = 0 \quad (4.27)$$

due to gauge invariance. The tensor form factors were also determined for $a = 1$. To obtain a general expression, the resonant contributions have to be multiplied by a factor a. Using the parametrization (4.26), the NP amplitudes are obtained as

$$\begin{aligned}\mathcal{A}_-^{\text{NP}} &= i\frac{G_F e}{\sqrt{2}}\frac{m_c}{4\pi^2}(C_7+C_7')\frac{(b'-a')}{v\cdot k}\,,\\ \mathcal{A}_+^{\text{NP}} &= \frac{G_F e}{\sqrt{2}}\frac{m_c m_D}{2\pi^2}(C_7-C_7')h'\,.\end{aligned} \quad (4.28)$$

4.2.3 QCD Factorization

Finally, we use QCDF methods [161–163] to calculate the leading WA contributions $\mathcal{O}(\alpha_s^0(\lambda_{\text{QCD}}/m_c)^1)$ shown in Fig. 4.2. The term factorization refers to the separation of

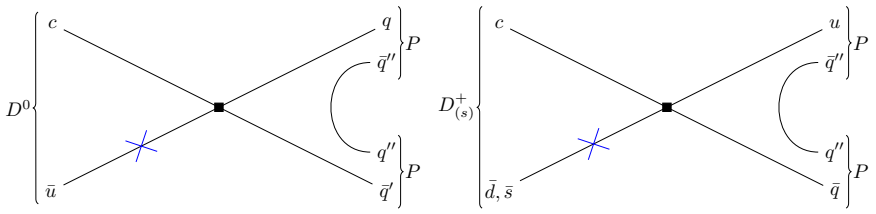

Figure 4.2: The WA diagram for $D^0 \to P_1P_2\gamma$ on the left and $D^+_{(s)} \to P_1^+P_2^0\gamma$ on the right. The blue cross indicates the dominant photon emission from the light quark of the D meson. Photon emission from the other quark lines is suppressed by powers of λ_{QCD}/m_c or α_s.

perturbative short distance and non-perturbative long distance contributions. In contrast, the previously mentioned naive factorization is an approximation in which the matrix element of the four-quark operator is simplified by a product of two matrix elements with single quark currents. However, at order α_s^0, QCDF reproduces the naive factorization [161]. Therefore, the $D \to PP\gamma$ WA amplitude can be written as a product of the PP form factors, see appendix (B.1), and the $D \to \gamma$ matrix element [163]

$$\left\langle\gamma(k,\epsilon^*)|\bar{u}\gamma^\mu(1-\gamma_5)c|D^0(P)\right\rangle = \int\frac{\mathrm{d}\tilde{k}_+}{2\pi}\Phi^{D^0}_{\alpha\beta}(\tilde{k}_+)T^\mu_{\beta\alpha}(\tilde{k}_+)\,. \quad (4.29)$$

The light-cone wave function $\Phi^{D^0}_{\alpha\beta}$ is a universal non-perturbative quantity [161]. $T^\mu_{\beta\alpha}$ denotes the hard-scattering kernel which is a perturbatively calculable kinematical function

given in [163]. QCDF is an established method for the calculation of the transition matrix element (4.29) and has already been used in the context of $B^- \to \ell\bar{\nu}_l\gamma$ [163], $B^- \to \ell\bar{\nu}_l\ell'\bar{\ell}'$ [164] decays as well as radiative two body decays $B \to V\gamma$ [162] and $D \to V\gamma$ [124]. The parity-even and parity-odd amplitudes

$$\begin{aligned}
\mathcal{A}_-^{\mathrm{WA}}(D^0 \to P_1P_2\gamma) &= i\frac{G_F e}{\sqrt{2}}\tilde{C}\frac{f_D Q_u}{\lambda_D(v\cdot k)}\sum_{q,q'\in\{d,s\}} V_{cq}^* V_{uq'} f_{(q,q')}^{P_1P_2}(s)\,,\\
\mathcal{A}_+^{\mathrm{WA}}(D^0 \to P_1P_2\gamma) &= \frac{G_F e}{\sqrt{2}}\tilde{C}\frac{f_D Q_u}{\lambda_D(v\cdot k)}\sum_{q,q'\in\{d,s\}} V_{cq}^* V_{uq'} f_{(q,q')}^{P_1P_2}(s)\,,\\
\mathcal{A}_-^{\mathrm{WA}}(D_{(s)}^+ \to P_1^+P_2^0\gamma) &= i\frac{G_F e}{\sqrt{2}}C_2\frac{f_{D_{(s)}} Q_d}{\lambda_{D_{(s)}}(v\cdot k)}\sum_{q\in\{d,s\}} V_{cd(s)}^* V_{uq} f_{(q)}^{P_1^+P_2^0}(s)\,,\\
\mathcal{A}_+^{\mathrm{WA}}(D_{(s)}^+ \to P_1^+P_2^0\gamma) &= \frac{G_F e}{\sqrt{2}}C_2\frac{f_{D_{(s)}} Q_d}{\lambda_{D_{(s)}}(v\cdot k)}\sum_{q\in\{d,s\}} V_{cd(s)}^* V_{uq} f_{(q)}^{P_1^+P_2^0}(s)\,.
\end{aligned} \tag{4.30}$$

are given in terms of three non-perturbative quantities. The decay constants of the D mesons $f_{D_{(s)}}$ as well as the PP form factors are well known. In contrast, $\lambda_{D_{(s)}} \sim \lambda_{\mathrm{QCD}}$ is poorly known and thus source of large theoretical uncertainties. In the following, we use $\lambda_{D_{(s)}} = 0.1\,\mathrm{GeV}$ [124], which can be seen as a lower bound. The amplitudes for the neutral D meson depend on the color suppressed combination of the Wilson coefficients $\tilde{C}$ (3.15). Therefore, the WA amplitudes are suppressed and subject to large scale uncertainties. However, the $D_{(s)}^+$ decays are neither suppressed nor do they have a large scale uncertainty. Furthermore, the WA contributions are independent of t.

Using the isospin relations

$$\begin{aligned}
f_{(d,d)}^{\pi^+\pi^-}(s) &= -F^{\mathrm{em}}(s)\,, & f_{(d)}^{\pi^+\pi^0}(s) &= -\sqrt{2}F^{\mathrm{em}}(s)\,,\\
f_{(d,d)}^{K^+K^-}(s) &= 3F_{K^+}^{(I=0)}(s) - F_{K^+}^{(I=1)}(s)\,, & f_{(d,d)}^{K^0\bar{K}^0}(s) &= 3F_{K^+}^{(I=0)}(s) + F_{K^+}^{(I=1)}(s)\\
f_{(s,s)}^{K^+K^-}(s) &= -3F_{K^+}^{s}(s)\,, & f_{(s,s)}^{K^0\bar{K}^0}(s) &= -3F_{K^+}^{s}(s)\,,\\
f_{(s,d)}^{\pi^+K^-}(s) &= -f_+^{\bar{K}\pi^-}(s)\,, & f_{(d,s)}^{K^+\pi^-}(s) &= -f_+^{\bar{K}\pi^-}(s)\,,\\
f_{(s,d)}^{\pi^0\bar{K}^0}(s) &= \frac{1}{\sqrt{2}}f_+^{\bar{K}\pi^-}(s)\,, & f_{(d,s)}^{\pi^0K^0}(s) &= -\frac{1}{\sqrt{2}}f_+^{\bar{K}\pi^-}(s)\,,\\
f_{(s)}^{\pi^+K^0}(s) &= f_+^{\bar{K}\pi^-}(s) & f_{(s)}^{K^+\pi^0}(s) &= -\frac{1}{\sqrt{2}}f_+^{\bar{K}\pi^-}(s)\,,\\
f_{(d)}^{K^+\bar{K}^0}(s) &= 2F_{K^+}^{(I=1)}(s)\,,
\end{aligned} \tag{4.31}$$

all required form factors can be obtained by the electromagnetic pion and kaon form factors, as well as the form factors extracted from $\tau^- \to \nu_\tau K_S^0\pi^-$ decays. Details on the form factors as well as the isospin relations can be found in appendix B.1 and E.1, respectively. The decays $D^+ \to \pi^+\bar{K}^0\gamma$, $D_s \to K^+K^0\gamma$, and $D^0 \to \pi^0\pi^0\gamma$ do not receive WA contributions due to their involved quark flavors and isospin symmetry, respectively. The validity of the QCDF predictions is limited to energetic photons as it is a simultaneous expansion in $\lambda_{\mathrm{QCD}}/m_c$ and $\lambda_{\mathrm{QCD}}/E_\gamma$. Therefore, we restrict our QCDF predictions to

$$E_\gamma \gtrsim 0.5\,\mathrm{GeV} \quad \to \quad s \lesssim 1.5\,\mathrm{GeV}^2\,. \tag{4.32}$$

Leading order QCDF does not include contributions from t and u channel resonances. These could be added in a phenomenological approach by combining $D \to PV$ amplitudes [165–167] with the effective $VP\gamma$ interaction in (4.16). Furthermore, QCDF does not include non-resonant or bremsstrahlung contributions. However, the latter is of minor importance in the considered region of phase space.

4.3 Branching ratios

We start the discussion of observables with the most simple ones, the branching ratios. In Figure 4.3 and 4.4, the double differential branching ratios based on HHχPT are shown in form of Dalitz plots. For decays with charged mesons, the bremsstrahlung is dominant for high s. For charged D mesons, the largest contributions are located at the diagonal edge of the phase space. This is not the case for neutral D mesons due to the interchange of momenta in the denominator of (4.6). Large branching ratios also arise at the horizontally extending edge of the phase space. The exact shape of the bremsstrahlung is determined by the mass difference of the pseudoscalars in the final state. If the masses are identical, the bremsstrahlung is symmetrically distributed along both edges of the phase space. For decays without charged mesons, there is no bremsstrahlung.

Furthermore, the bands generated by resonances in s, t and the third Mandelstam variable $u = (p_1 + k)^2$ are particularly apparent. For $D^+_{(s)} \to K^+\overline{K}^0\gamma$, $D^+ \to \pi^+\overline{K}^0\gamma$, and $D_s \to K^+K^0\gamma$, a preference of the u channel resonance can be observed, since the u channel contributions of the B and D form factors interfere constructively, while the t channel contributions interfere destructively. For $D^+ \to \pi^+\overline{K}^0\gamma$, $D^0 \to \pi^0\pi^0\gamma$ and $D_s \to K^+K^0\gamma$ there are no s channel resonances due to the involved quark flavors. Moreover, the ρ^+ resonance is not included in phase space for $D_s \to K^+\overline{K}^0\gamma$ and $D^+ \to K^+\overline{K}^0\gamma$. Thus, no bands in s are seen for these five decays. Furthermore, the large $\omega\pi\gamma$ coupling results in distinctive bands for ω resonances. The non-resonant effects are rather small and only of importance beyond the bremsstrahlung and the resonances.

In Figure 4.5 and 4.6, we show SM predictions for the SM-like and BSM sensitive decays, respectively. The results of QCDF, HHχPT and Low's theorem are shown in blue, green and red, respectively. The width of the bands represent the theoretical uncertainties concerning the μ_c dependence of the Wilson coefficients as well as the uncertainty of the $D_s \to K^+\pi^0$ amplitude. The uncertainties of the QCDF predictions for neutral D mesons are particularly conspicuous. These are an outcome of the color suppressed combination of the Wilson coefficients $\tilde{C}$ (3.15). The bands have a width of about two orders of magnitude due to the quadratic dependence of the branching ratios on $\tilde{C}$. The shape of the QCDF results is essentially given by the $P_1 - P_2$ form factors. For the final states $K^+\overline{K}^0\gamma$ no resonance peak can be identified, since the lowest ρ resonance is not included in the phase space.

For low photon energies, the HHχPT distributions exhibit the soft photon pole. Due to the replacement of the model's own bremsstrahlung contributions by Low's theorem, the results asymptotically converge towards the large s endpoint. Without the replacement, the differential branching ratios in this region would be about an order of magnitude larger. For small and intermediate s, the distributions are dominated by the resonances.

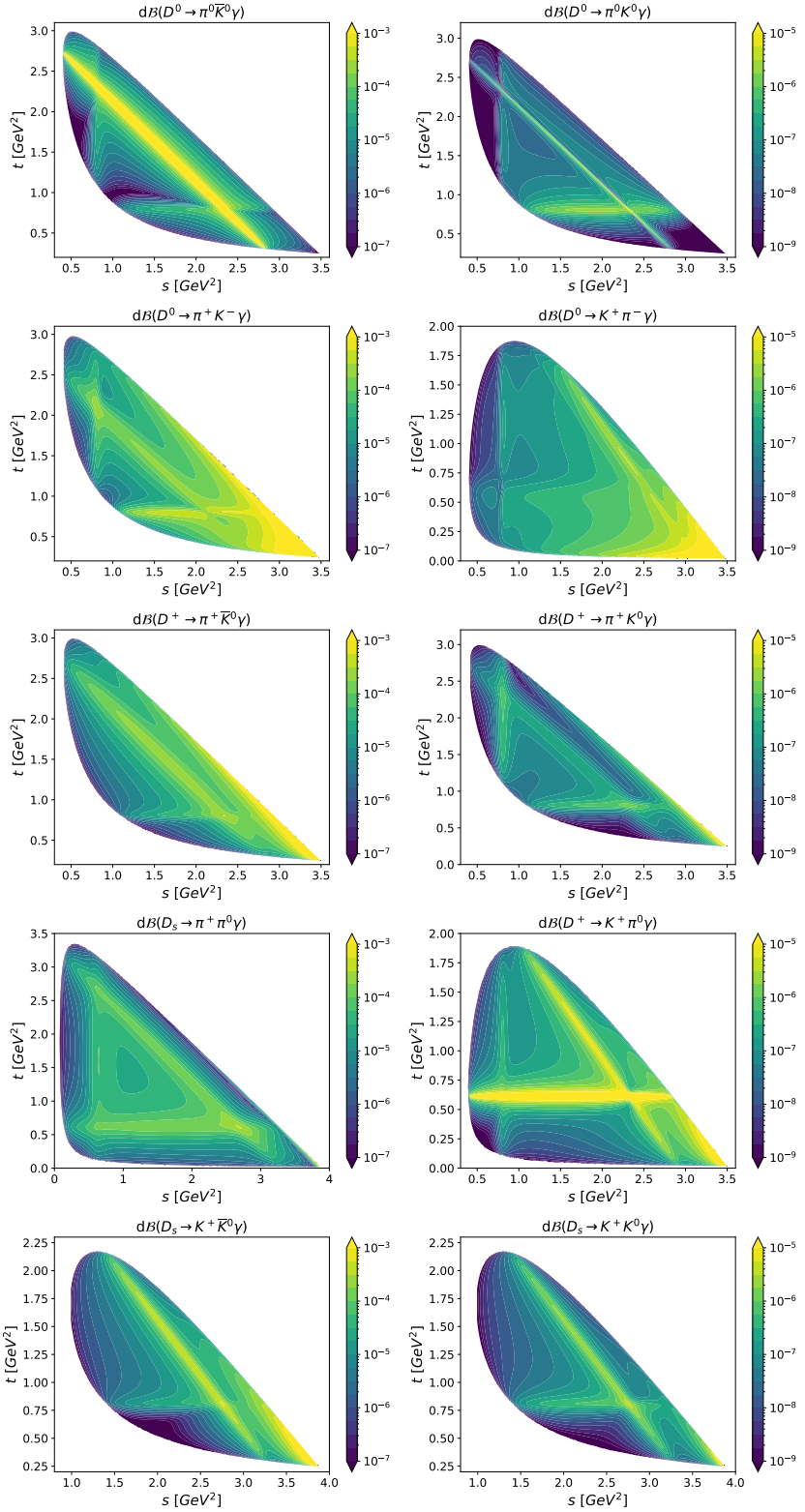

Figure 4.3: Dalitz plots for the CF and DCS decay modes based on HHχPT for $\mu_c = m_c$ and the mean value of the $D \to P_1 P_2$ amplitude.

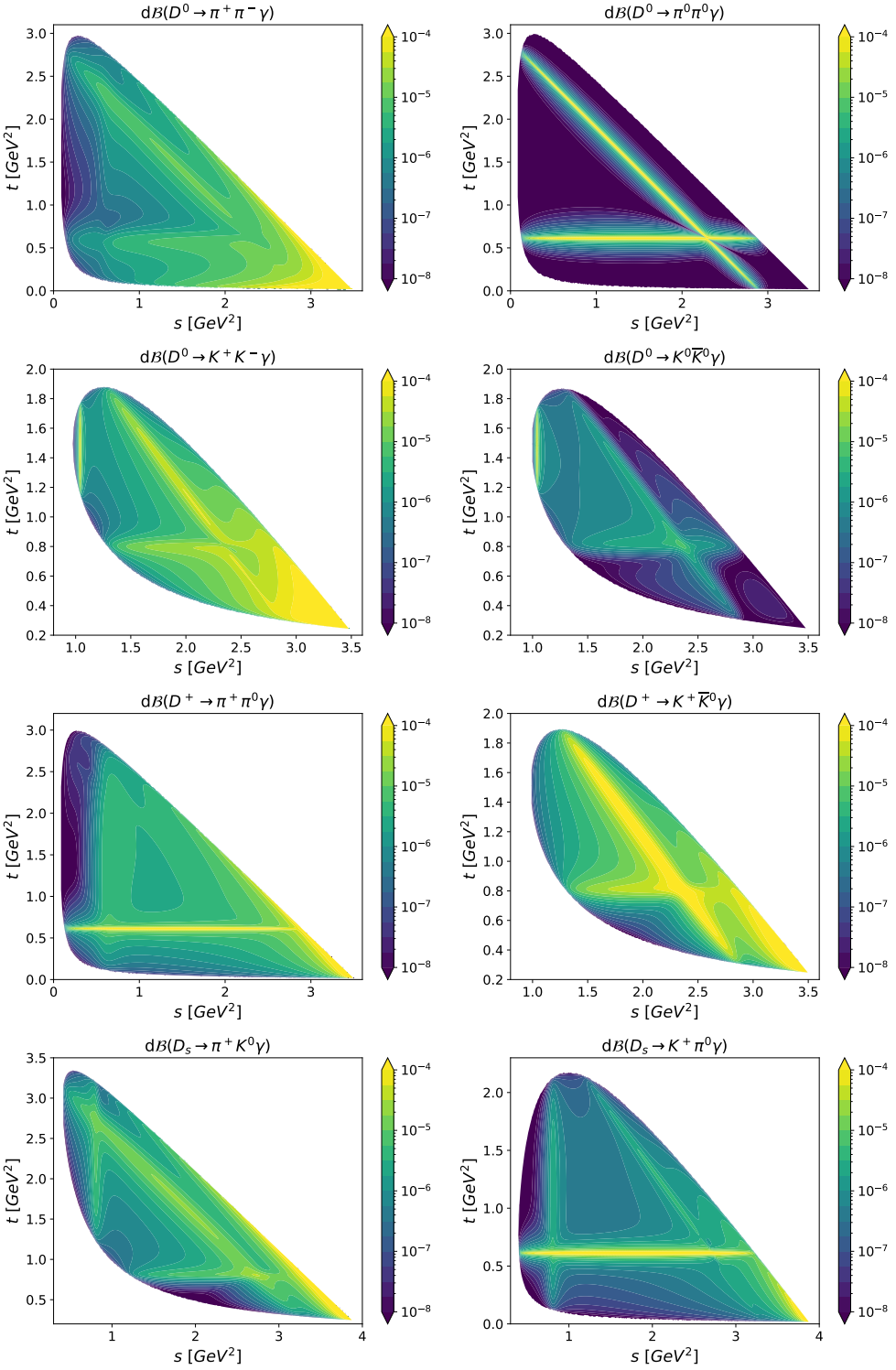

Figure 4.4: Dalitz plots for the SCS decay modes based on HHχPT for $\mu_c = m_c$ and the mean value of the $D \to P_1P_2$ amplitude.

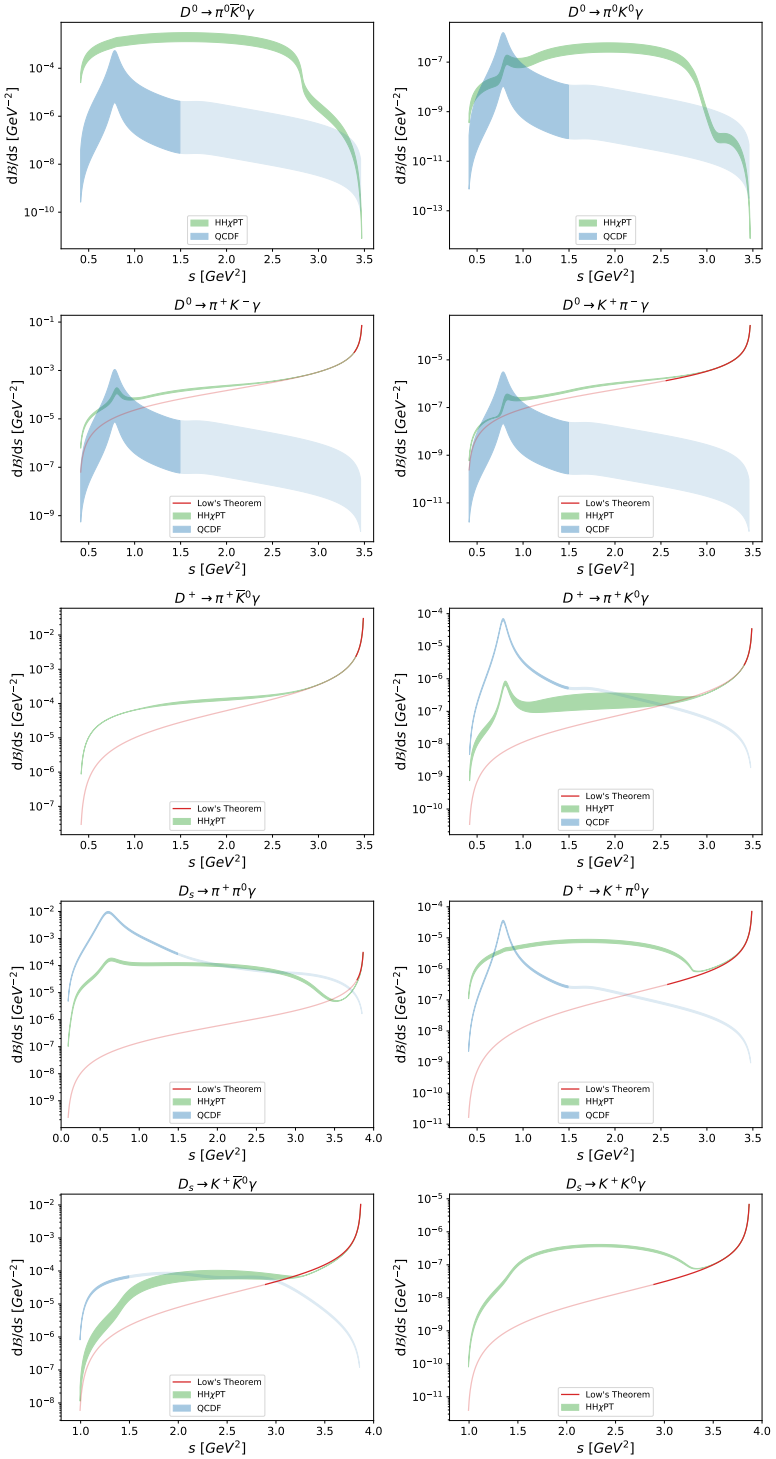

Figure 4.5: Differential branching ratios based on Low's Theorem (red), HHχPT (green) and QCDF(blue) for CF and DCS decays. The darker areas and lines correspond to the region of applicability for the different models. The QCDF predictions are given for $\lambda_{D_{(s)}} = 0.1\,\text{GeV}$ and scale with $(0.1\,\text{GeV}/\lambda_{D_{(s)}})^2$.

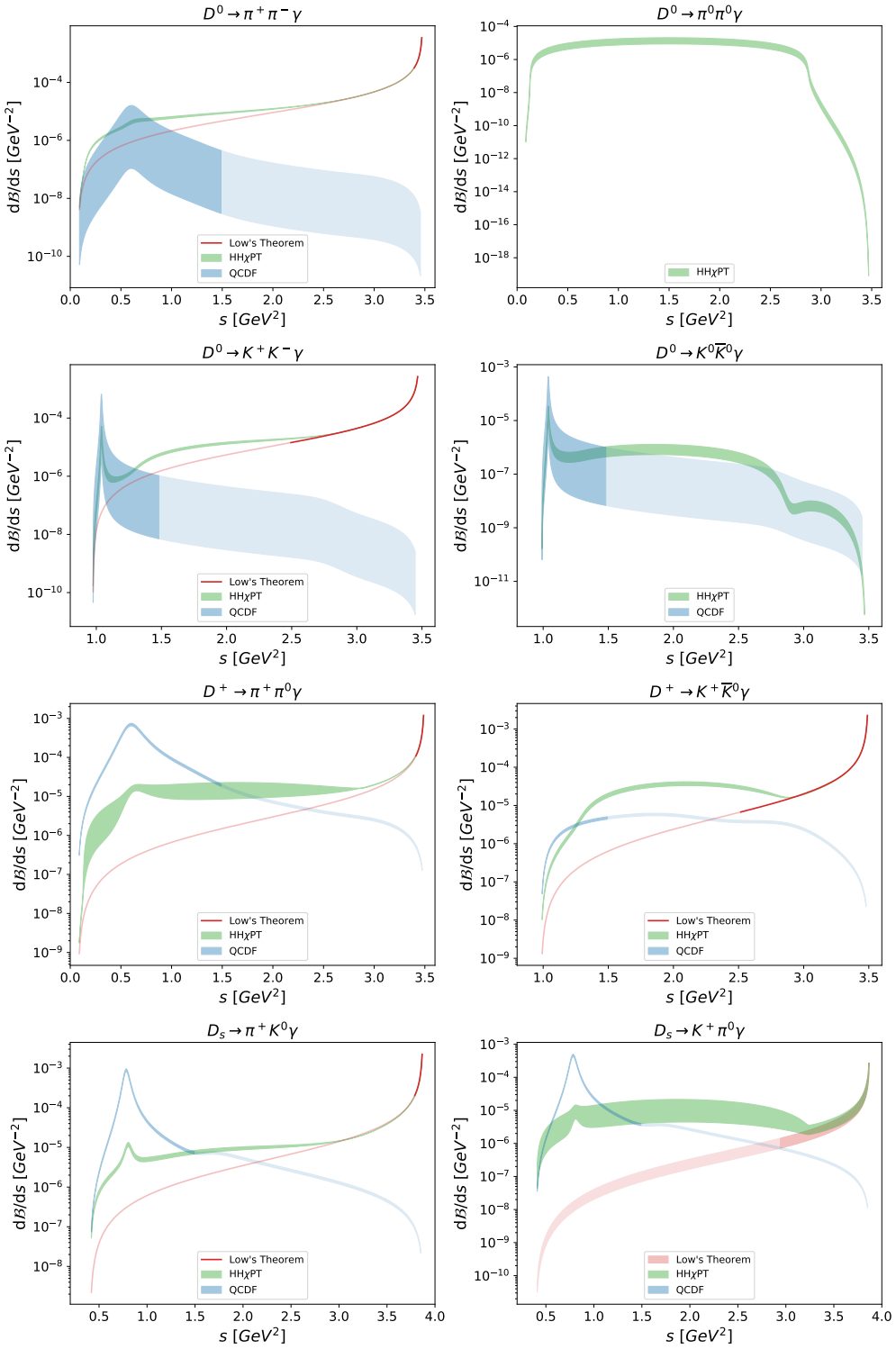

Figure 4.6: Differential branching ratios based on Low's Theorem (red), HHχPT (green) and QCDF(blue) for SCS decays. The darker areas and lines correspond to the region of applicability for the different models. The QCDF predictions are given for $\lambda_{D_{(s)}} = 0.1\,\text{GeV}$ and scale with $(0.1\,\text{GeV}/\lambda_{D_{(s)}})^2$.

Comparing the QCDF and HHχPT distributions, we notice that the s-channel contributions of the QCDF results are about two orders of magnitude larger for charged D mesons. On the one hand, this can be explained by the small value for $\lambda_{D_{(s)}}$ that we use for our numerical evaluation. On the other hand, however, HHχPT takes the radiation of the photon from the c quark into account. By replacing the remaining parameter g_v in the WA contributions of the HHχPT form factors, we obtain a simplified expressions $\sim \lambda' + Q_q\lambda$, where Q_q is the charge of the light quark of the D meson. Thus, for charged D mesons, there is a strong destructive interference between the leading WA term $\sim \lambda$ and the emission of the photon from the c quark. For the neutral D meson, the terms interfere constructively.

In Figure 4.7 and 4.8, we compare the SM predictions for decays of neutral and charged D mesons with different BSM scenarios. The SM amplitudes are based on HHχPT. We set one of the BSM coefficients $C_7^{(\prime)}$ to zero and exploit the limit (3.16) for the other. Moreover, we vary the CP violating phase in steps of $\pi/2$. For $D^0 \to \pi^0\pi^0\gamma$, the NP effects are negligible as they are purely non-resonant. The contributions from dipole operators are also negligible for decays with two kaons, since the phase space does not include the ρ and ω. For the other decay channels, the differential branching ratios can be increased by up to one order of magnitude in the region of the s-channel resonance.

The same comparison between SM predictions and BSM scenarios is shown in Figure 4.9 and 4.10 for QCDF. At the s-channel peak, SM and BSM predictions differ marginally, especially for $C_7^{(\prime)} = 0$. The largest discrepancies can be seen above the s-channel resonances. For $\lambda_{D_{(s)}} = 0.1\,\text{GeV}$ these are less than an order of magnitude. As mentioned before, leading order QCDF does not include contributions from the t- and u-channel resonances. These would dominate the distributions above the s-channel peak and significantly reduce the sensitivity to new physics.

Table 4.2 provides the integrated branching ratios for all decay modes for QCDF and HHχPT. The branching ratios are given in the region of applicability of the QCD factorization for both QCDF and HHχPT to enable a comparison. In addition, the HHχPT branching ratios are given for $E_\gamma \geq 0.1\,\text{GeV}$ to avoid the soft photon pole. Here, $E_\gamma = (m_D^2 - s)/(2m_D)$ is the photon energy in the rest frame of the D meson. Applying the same cuts to both models yields values of comparable magnitude for the neutral decay modes. A large difference only exists for $D^0 \to \pi^0\overline{K}^0\gamma$, due to the ω which is included in the HHχPT prediction. As with the differential branching ratios, QCDF results in larger values for the decays $D_s \to \pi^+\pi^0\gamma$, $D_s \to K^+\overline{K}^0\gamma$ and $D^+ \to \pi^+K^0\gamma$. We note that the branching ratio of $D_s \to K^+\overline{K}^0\gamma$ is two orders of magnitude smaller than that of $D_s \to \pi^+\pi^0\gamma$, even though both are CF.

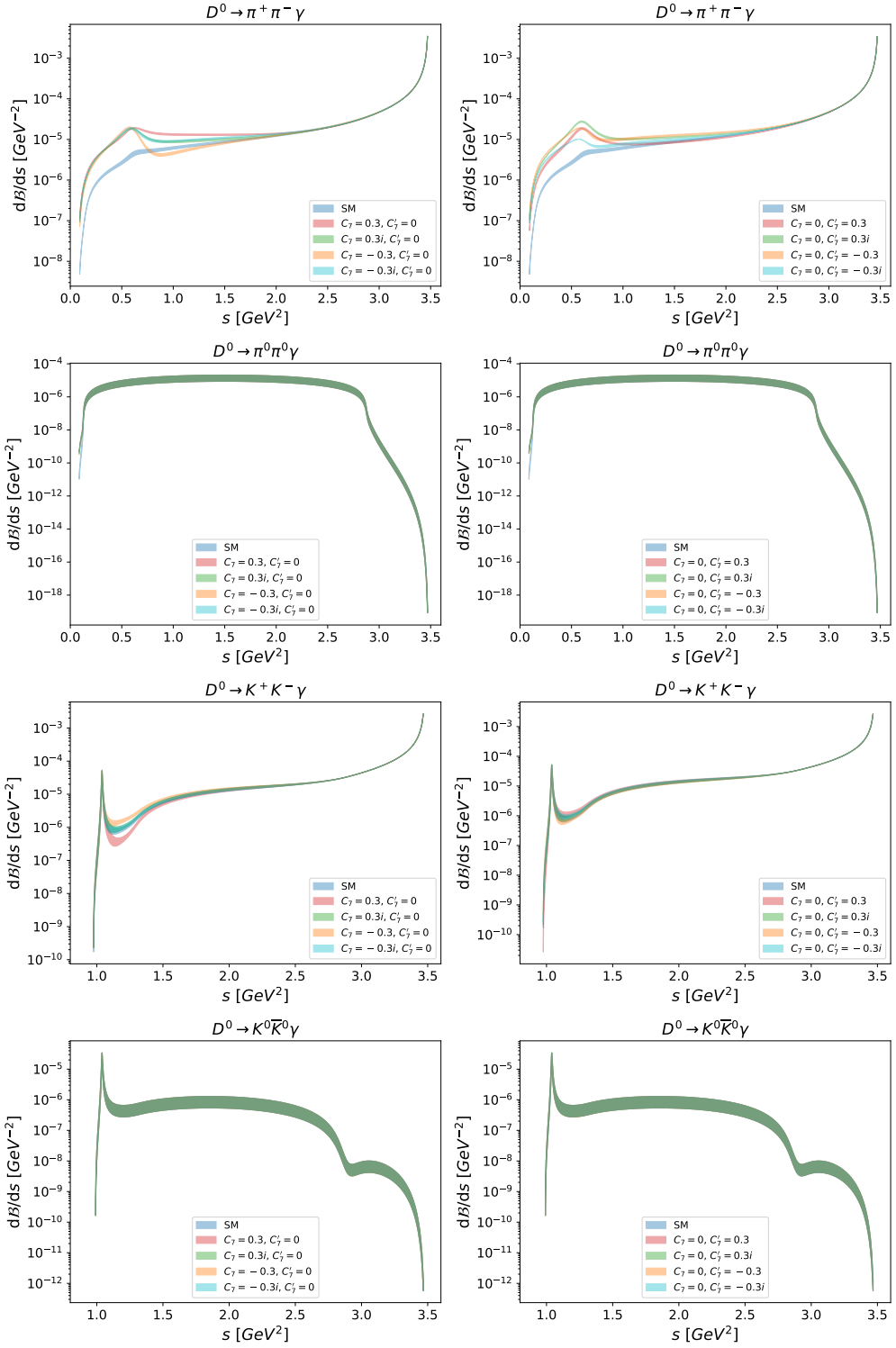

Figure 4.7: Differential branching ratios for several BSM scenarios of D^0 decays based on HHχPT.

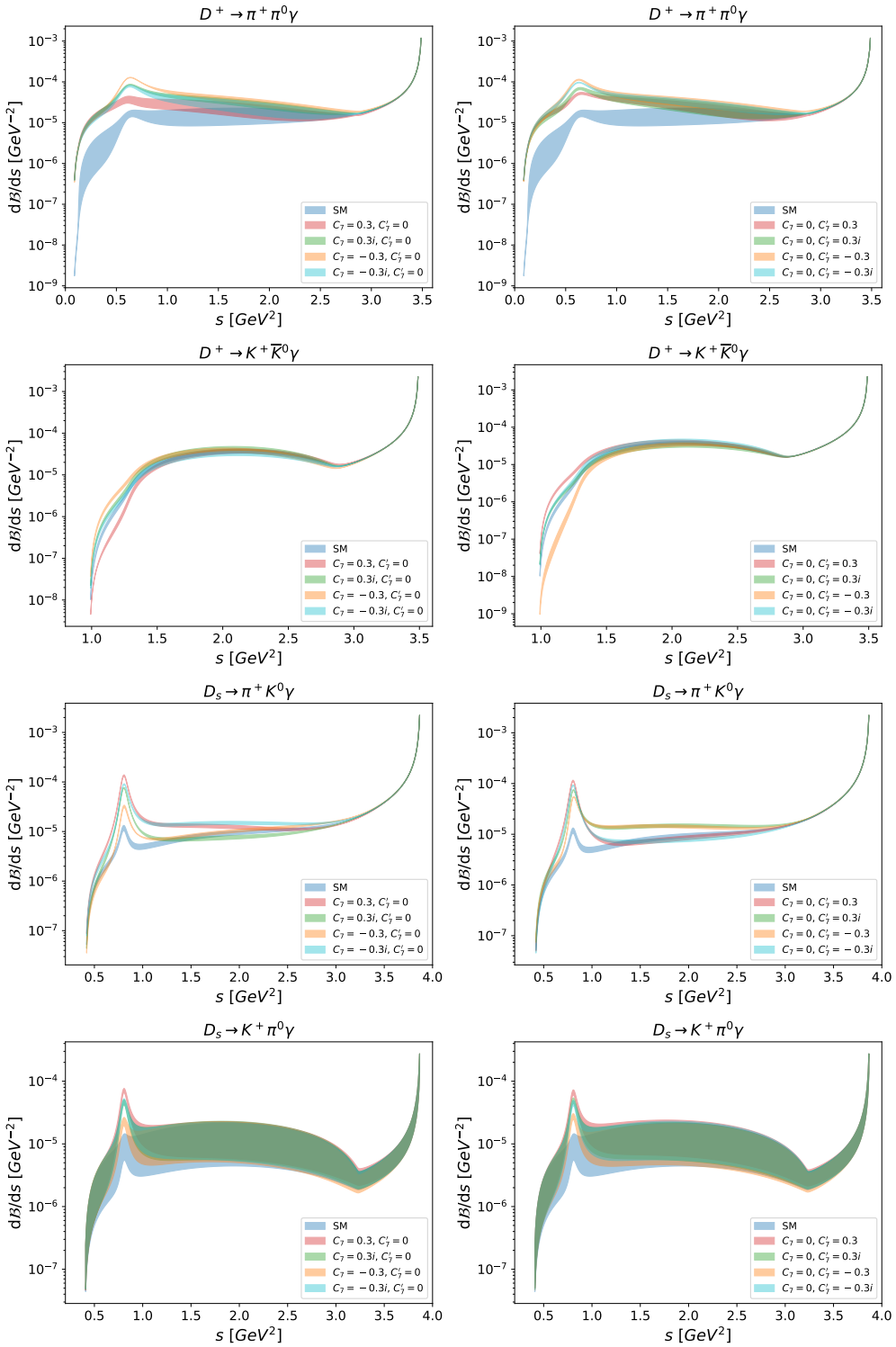

Figure 4.8: Differential branching ratios for several BSM scenarios of $D^+_{(s)}$ decays based on HHχPT.

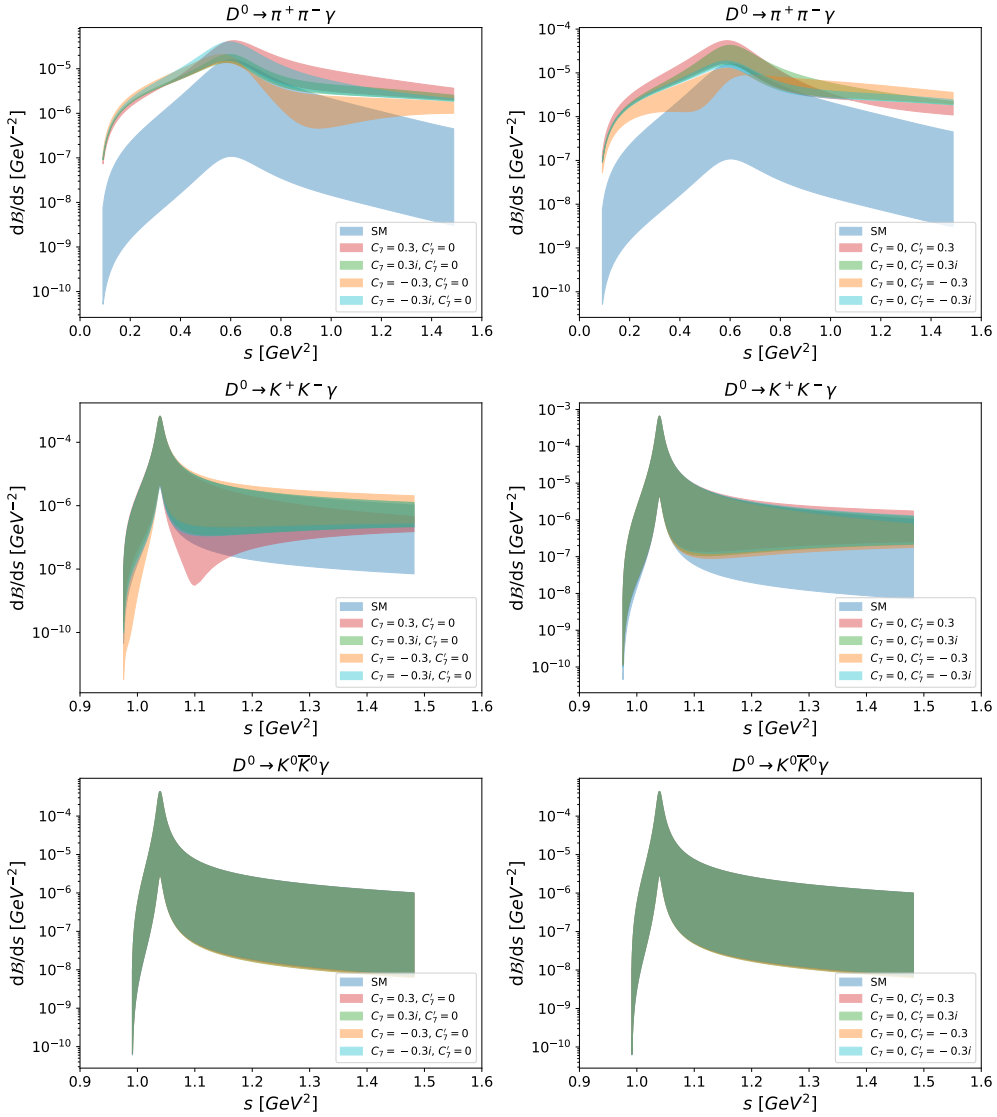

Figure 4.9: Differential branching ratios for several BSM scenarios of D^0 decays based on QCDF SM predictions.

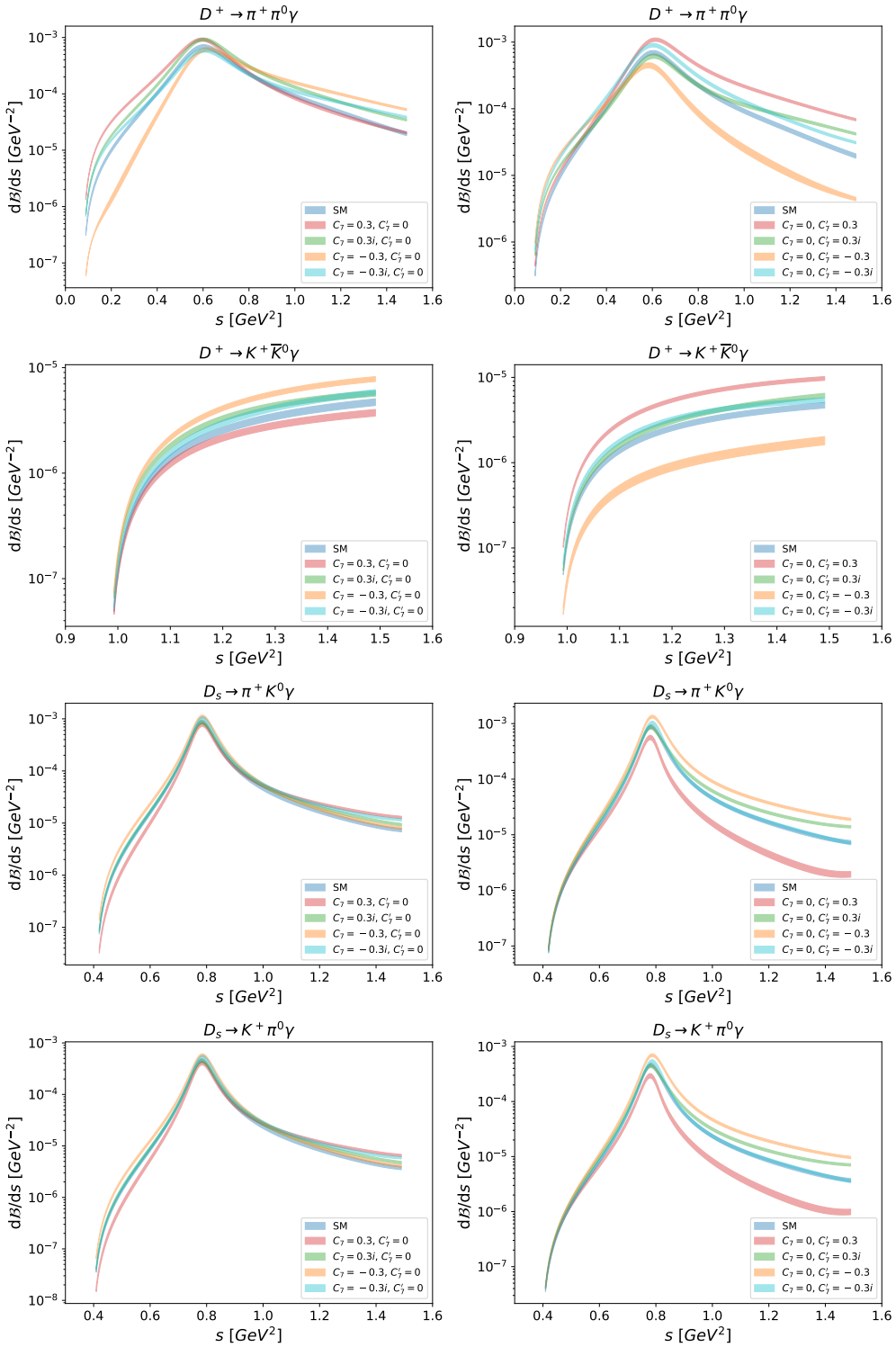

Figure 4.10: Differential branching ratios for several BSM scenarios of $D^+_{(s)}$ decays based on QCDF SM predictions.

decay	$\text{QCDF}\big\vert^{\text{SM}}_{s\leq 1.5\,\text{GeV}^2}$	$\text{HH}\chi\text{PT}\big\vert^{\text{SM}}_{s\leq 1.5\,\text{GeV}^2}$	$\text{HH}\chi\text{PT}\big\vert^{\text{SM}}_{E_\gamma\geq 0.1\,\text{GeV}}$	$\text{QCDF}\big\vert^{\text{BSM}}_{s\leq 1.5\,\text{GeV}^2}$	$\text{HH}\chi\text{PT}\big\vert^{\text{BSM}}_{s\leq 1.5\,\text{GeV}^2}$	$\text{HH}\chi\text{PT}\big\vert^{\text{BSM}}_{E_\gamma\geq 0.1\,\text{GeV}}$
$D^0 \to \pi^0\bar{K}^0\gamma$	$(0.04-6.36)\cdot 10^{-5}$	$(0.9-2.2)\cdot 10^{-3}$	$(2.1-4.9)\cdot 10^{-3}$	-	-	-
$D^0 \to \pi^+K^-\gamma$	$(0.09-12.9)\cdot 10^{-5}$	$(7.2-9.2)\cdot 10^{-5}$	$(6.7-7.2)\cdot 10^{-4}$	-	-	-
$D^+ \to \pi^+\bar{K}^0\gamma$	-	$(6.1-6.5)\cdot 10^{-5}$	$(3.6-3.8)\cdot 10^{-4}$	-	-	-
$D_s \to \pi^+\pi^0\gamma$	$(2.8-3.2)\cdot 10^{-3}$	$(1.1-1.5)\cdot 10^{-4}$	$(2.4-3.0)\cdot 10^{-4}$	-	-	-
$D_s \to K^+\bar{K}^0\gamma$	$(1.8-2.1)\cdot 10^{-5}$	$(1.5-3.4)\cdot 10^{-6}$	$(1.1-1.7)\cdot 10^{-4}$	-	-	-
$D^0 \to \pi^+\pi^-\gamma$	$(0.04-5.16)\cdot 10^{-6}$	$(6.2-7.1)\cdot 10^{-6}$	$(3.9-4.1)\cdot 10^{-5}$	$(0.6-1.7)\cdot 10^{-5}$	$(0.9-1.7)\cdot 10^{-5}$	$(4.3-5.2)\cdot 10^{-5}$
$D^0 \to \pi^0\pi^0\gamma$	-	$(0.8-1.9)\cdot 10^{-5}$	$(1.6-3.8)\cdot 10^{-5}$	-	$(0.8-1.9)\cdot 10^{-5}$	$(1.6-3.8)\cdot 10^{-5}$
$D^0 \to K^+K^-\gamma$	$(0.05-9.88)\cdot 10^{-6}$	$(1.2-1.8)\cdot 10^{-6}$	$(3.3-3.5)\cdot 10^{-5}$	$(0.07-10.43)\cdot 10^{-6}$	$(0.9-2.2)\cdot 10^{-6}$	$(3.2-3.7)\cdot 10^{-5}$
$D^0 \to K^0\bar{K}^0\gamma$	$(0.04-6.80)\cdot 10^{-6}$	$(3.4-8.0)\cdot 10^{-7}$	$(0.8-2.0)\cdot 10^{-6}$	$(0.04-6.81)\cdot 10^{-6}$	$(3.4-8.0)\cdot 10^{-7}$	$(0.9-2.0)\cdot 10^{-6}$
$D^+ \to \pi^+\pi^0\gamma$	$(2.1-2.4)\cdot 10^{-4}$	$(1.0-2.2)\cdot 10^{-5}$	$(3.0-5.4)\cdot 10^{-5}$	$(1.2-4.2)\cdot 10^{-4}$	$(2.7-7.7)\cdot 10^{-5}$	$(0.5-1.2)\cdot 10^{-4}$
$D^+ \to K^+\bar{K}^0\gamma$	$(1.3-1.5)\cdot 10^{-6}$	$(2.5-3.2)\cdot 10^{-6}$	$(4.4-5.4)\cdot 10^{-5}$	$(0.5-3.1)\cdot 10^{-6}$	$(1.7-4.8)\cdot 10^{-6}$	$(4.0-6.1)\cdot 10^{-5}$
$D_s \to \pi^+K^0\gamma$	$(9.7-11.2)\cdot 10^{-5}$	$(4.9-6.1)\cdot 10^{-6}$	$(3.0-3.3)\cdot 10^{-5}$	$(0.5-1.8)\cdot 10^{-4}$	$(0.8-2.5)\cdot 10^{-5}$	$(3.6-5.5)\cdot 10^{-5}$
$D_s \to K^+\pi^0\gamma$	$(5.0-5.8)\cdot 10^{-5}$	$(0.3-1.3)\cdot 10^{-5}$	$(1.0-4.3)\cdot 10^{-5}$	$(2.7-9.5)\cdot 10^{-5}$	$(0.5-2.2)\cdot 10^{-5}$	$(1.3-5.5)\cdot 10^{-5}$
$D^0 \to \pi^0K^0\gamma$	$(0.01-1.81)\cdot 10^{-7}$	$(0.7-1.8)\cdot 10^{-7}$	$(3.3-8.0)\cdot 10^{-7}$	-	-	-
$D^0 \to K^+\pi^-\gamma$	$(0.02-3.66)\cdot 10^{-7}$	$(2.0-2.5)\cdot 10^{-7}$	$(2.7-2.9)\cdot 10^{-6}$	-	-	-
$D^+ \to \pi^+K^0\gamma$	$(7.2-8.3)\cdot 10^{-6}$	$(1.3-2.4)\cdot 10^{-7}$	$(4.3-7.9)\cdot 10^{-7}$	-	-	-
$D^+ \to K^+\pi^0\gamma$	$(3.7-4.3)\cdot 10^{-6}$	$(4.5-5.8)\cdot 10^{-6}$	$(1.2-1.5)\cdot 10^{-5}$	-	-	-
$D_s \to K^+K^0\gamma$	-	$(1.1-1.4)\cdot 10^{-8}$	$(4.8-5.7)\cdot 10^{-7}$	-	-	-

Table 4.2: Branching ratios for all decay modes. The top, middle and bottom part correspond to CF, SCS and DCS decays, respectively. The predictions are given in the region of applicability of QCDF $s \leq 1.5\,\text{GeV}^2$ and for $E_\gamma \geq 0.1\,\text{GeV}$.

4.4 Forward-Backward asymmetries

For a decay of a D meson into at least three final state particles, it is possible to define angular observables. In the following we consider a forward-backward (FB) asymmetry, which is defined by

$$A_{\mathrm{FB}}(s) = \frac{\int_{t_{\min}}^{t_0} dt \frac{\mathrm{d}^2\Gamma}{\mathrm{d}s\mathrm{d}t} - \int_{t_0}^{t_{\max}} dt \frac{\mathrm{d}^2\Gamma}{\mathrm{d}s\mathrm{d}t}}{\int_{t_{\min}}^{t_0} dt \frac{\mathrm{d}^2\Gamma}{\mathrm{d}s\mathrm{d}t} + \int_{t_0}^{t_{\max}} dt \frac{\mathrm{d}^2\Gamma}{\mathrm{d}s\mathrm{d}t}} \,, \qquad t_0 = \frac{1}{2s}\left(-s^2 + s(m_D^2 + m_1^2 + m_2^2) + m_D^2(m_2^2 - m_1^2)\right) \,, \tag{4.33}$$

where the first (second) term in the numerator corresponds to $0 \leq \cos(\theta_{2\gamma}) \leq 1$ ($-1 \leq \cos(\theta_{2\gamma}) \leq 0$). Here, $\theta_{2\gamma}$ is the angle between P_2 and the photon in the $P_1 - P_2$ center-of-mass frame. Thus, for a FB asymmetry greater than zero, the photon is preferentially emitted in the direction of the P_2. For a non-vanishing FB asymmetry, the form factors must exhibit a dependence on t. Since this is not the case for the leading order WA contribution in QCDF, $A_{\mathrm{FB}}(s) = 0$ is predicted for all decay modes.

Figure 4.11 and 4.12 show SM FB asymmetries based on the predictions of HHχPT for SM-like and BSM sensitive decays, respectively. A_{FB} is dominated by the virtual vector resonances and bremsstrahlung. To illustrate this, the FB asymmetries are also shown without and only with single resonance contributions. The s-channel resonance can only contribute to A_{FB} through interference terms, since they have no dependence on t. The decays $D^+ \to \pi^+\bar{K}^0\gamma$, $D^0 \to \pi^0\pi^0\gamma$, $D_s \to K^+K^0\gamma$ have no s-channel resonances. Thus, the associated distributions would be identical to the non-resonant case. The bremsstrahlung does not lead to an asymmetry for decays of neutral D mesons, provided that the masses of the pseudoscalars are identical. If there is a mass difference, the bremsstrahlung leads to an asymmetry which dominates the large s region. For decays of charged D mesons, bremsstrahlung always leads to an asymmetry, since only one of the final state pseudoscalars is charged and thus can emit a photon.

The decay $D^0 \to \pi^0\pi^0\gamma$ is symmetric in the two pseudoscalars. Therefore, the form factors are antisymmetric under the permutation of $p_1 \leftrightarrow p_2$. Consequently, the contributions in the forward and backward regions cancel each other. Thus, $A_{\mathrm{FB}} = 0$ holds for all s. In case of $D^0 \to K^0\bar{K}^0\gamma$, the flavor structure leads to the fact that only WA-like diagrams are possible. Since K^0 and $\bar{K}^0$ are antiparticles of each other, this also yields form factors which are antisymmetric under the permutation $p_1 \leftrightarrow p_2$. Thus, $A_{\mathrm{FB}}(s) = 0$ holds here as well. Similarly, the BSM contributions of $D^0 \to \pi^0\pi^0\gamma$ and $D^0 \to K^0\bar{K}^0\gamma$ also exhibit the antisymmetry under permutation of $p_1 \leftrightarrow p_2$. Therefore, these decay channels will not be considered later in the discussion of NP-induced effects.

For $D^0 \to \pi^+\pi^-\gamma$ and $D^0 \to K^+K^-\gamma$ the t- and u-channel resonances of the neutral current operator provide the same contributions to the forward and backward region of phase space. This symmetry does not exist for the D^0 decays with $P_1 \neq \bar{P}_2$. In the case of the charged current operator, the resonances contribute differently to the forward and backward region due to the asymmetric factorization of the B_3 diagrams. This effect is mainly responsible for the shape of the forward-backward asymmetries of $D^0 \to \pi^+\pi^-\gamma$ and $D^0 \to K^+K^-\gamma$.

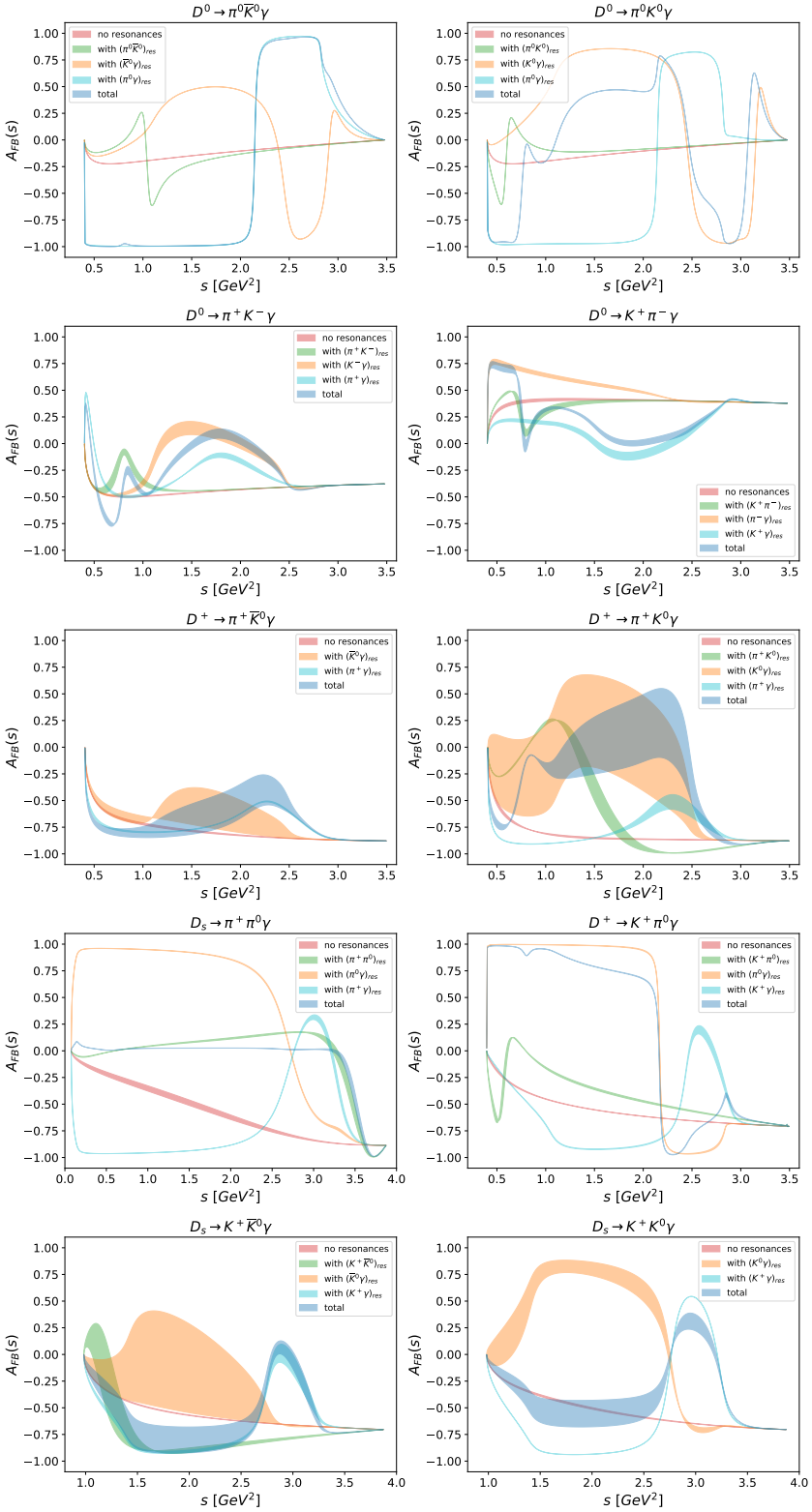

Figure 4.11: Forward backward asymmetry based on SM HHχPT predictions for CF and DCS decays.

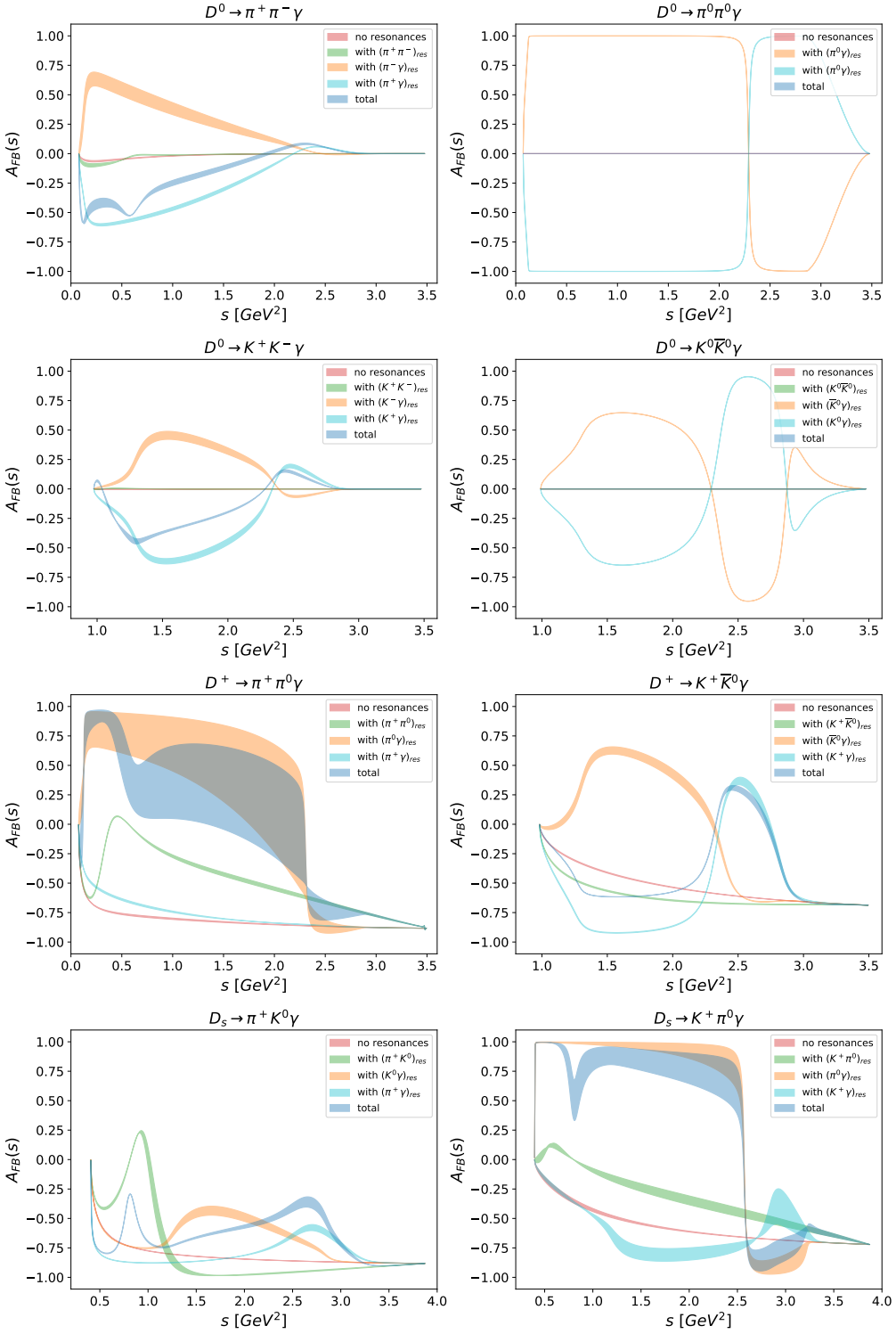

Figure 4.12: Forward backward asymmetry based on SM HHχPT predictions for SCS decays.

$D^0 \to \pi^0 \overline{K}^0 \gamma$ is dominated by the ω resonance just like $D^+ \to \pi^+\pi^0\gamma$ and $D^+_{(s)} \to K^+\pi^0\gamma$. For $D^0 \to \pi^0 K^0\gamma$, the effects of the ω are much smaller than for $D^0 \to \pi^0\overline{K}^0\gamma$ due to different relative signs and the ensuing destructive interference. The ω does not contribute to $D_s \to \pi^+\pi^0\gamma$ despite the π^0 in the final state. The t and u channel contributions do not cancel exactly due to the small difference of the $\rho^0\pi^0\gamma$ un $\rho^\pm\pi^\pm\gamma$ couplings.

Large scale uncertainties in the t-channel contributions occur for the decays $D^+ \to \pi^+\overline{K}^0\gamma$, $D_s \to K^+\overline{K}^0\gamma$, $D^+ \to \pi^+\pi^0\gamma$ and $D^+ \to \pi^+K^0\gamma$ due to interference of the form factors B and D. Since the t-channel resonances dominate the forward region for small and intermediate s, the uncertainties are clearly visible in the plots.

We consider the same BSM scenarios for A_{FB} as for the branching ratios in section 4.3. Since the only t- dependencies of the dipole operators $O_7^{(\prime)}$ arise from non-resonant contributions, the most significant BSM effects show up in the form of suppressions of the partially large SM forward-backward asymmetries predicted by HHχPT. The most obvious example of this is the decay $D^+ \to \pi^+\pi^0\gamma$. Apart from this, the largest effects can be seen for $D^0 \to \pi^+\pi^-\gamma$ and $D_s \to \pi^+K^0\gamma$. All non-trivial predictions of HHχPT are shown in Figure 4.13 and 4.14.

The SM QCDF amplitudes with $\lambda_{D_{(s)}} = 0.1\,\mathrm{GeV}$ yield values for $A_{\mathrm{FB}}^{\mathrm{BSM}}(s)$ in the range of $\mathcal{O}(10^{-3}) - \mathcal{O}(10^{-2})$ for charged D mesons. For $\lambda_{D_{(s)}} = 0.3\,\mathrm{GeV}$, the SM contributions are significantly suppressed, leading to larger asymmetries. These are usually in the range of $\mathcal{O}(10^{-2})$, but occasionally reach values of $|A_{\mathrm{FB}}(s)| \lesssim 0.15$. The SM amplitudes are color-suppressed for neutral D mesons, leading to asymmetries of $|A_{\mathrm{FB}}(s)| \lesssim 0.25$ even for small values of of the non-perturbative parameter $\lambda_{D_{(s)}} = 0.1\,\mathrm{GeV}$. It should be noted, however, that leading order QCDF is not a good model for predicting A_{FB} as it does not describe any of the mechanisms inducing an FB asymmetry within the SM.

Overall, it can be stated that new physics can have a significant impact on A_{FB}. However, due to the complicated interplay of s, t and u channel resonances and the intrinsic uncertainty of the Breit-Wigner approach, it is difficult to draw firm conclusions for BSM physics. A_{FB} is therefore more suitable for testing QCD models.

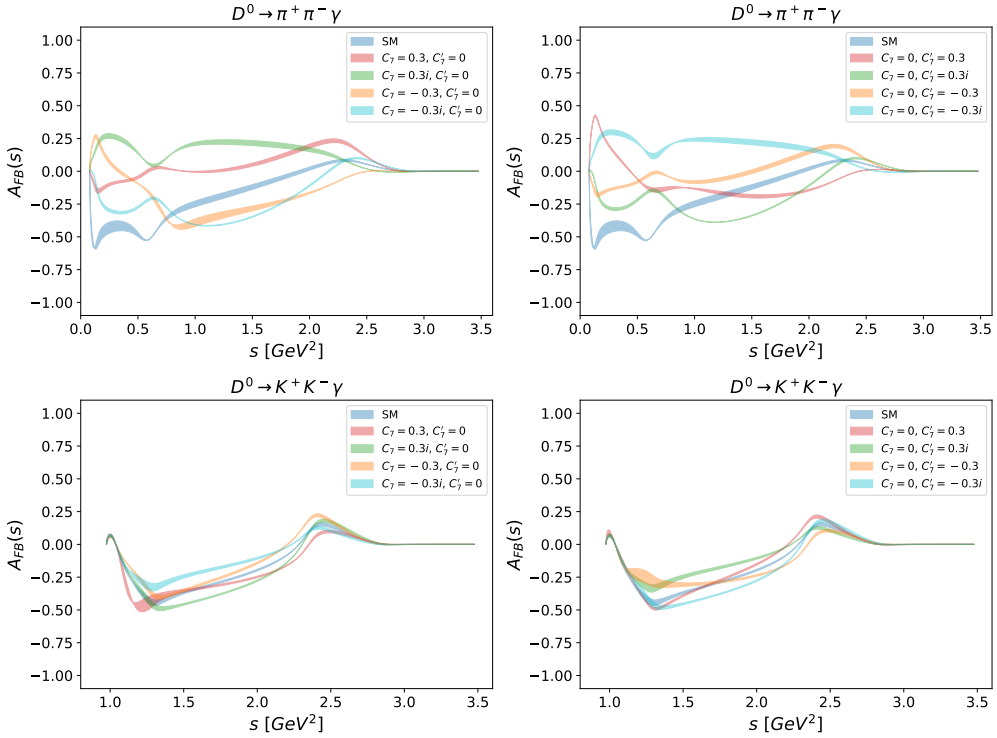

Figure 4.13: Forward backward asymmetries beyond the SM for decays of neutral D mesons.

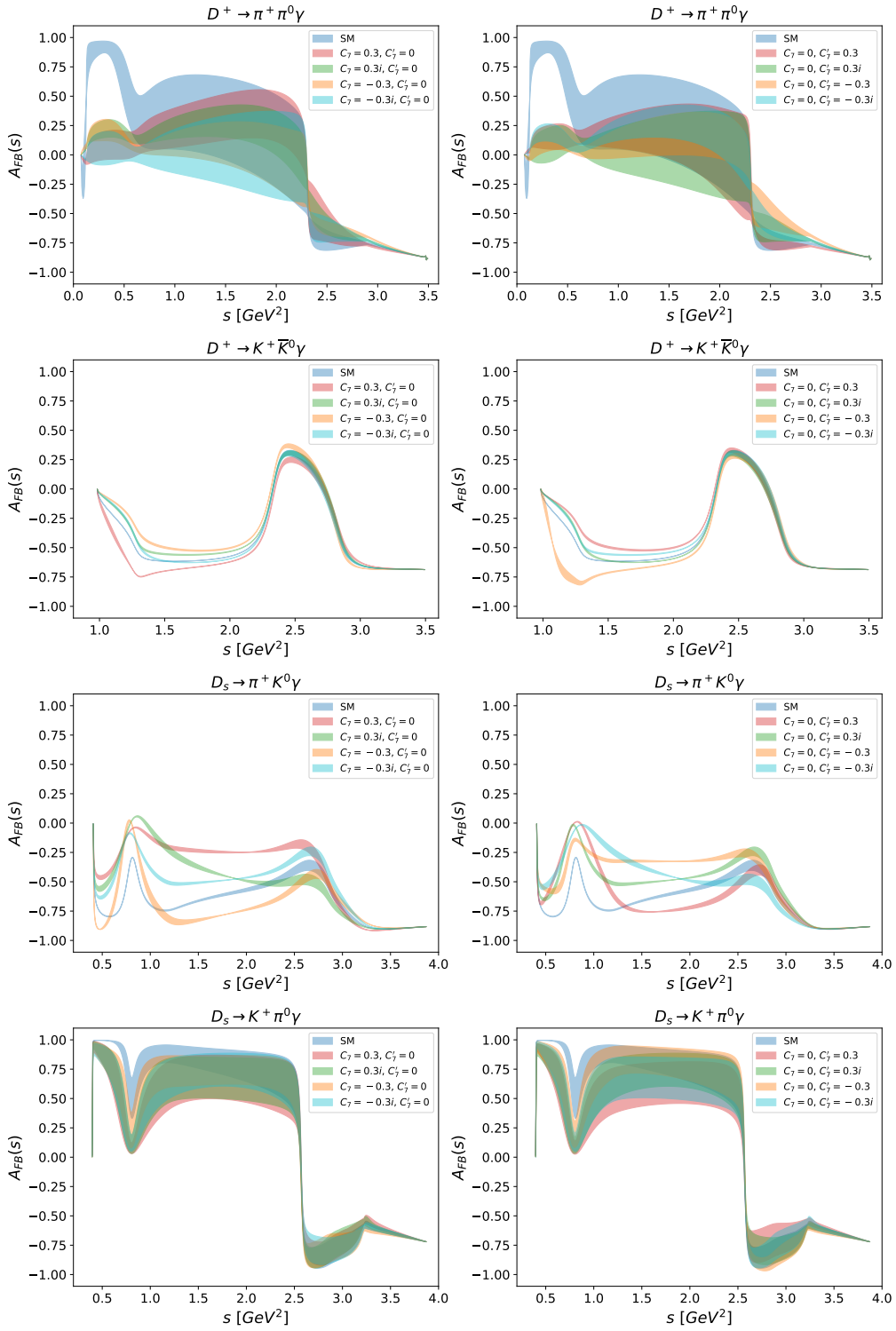

Figure 4.14: Forward backward asymmetries beyond the SM for decays of charged D mesons.

4.5 CP asymmetries

Following branching ratios and FB asymmetries, we finally discuss the single- and double-differential CP asymmetries

$$A_{\mathrm{CP}}(s) = \int \mathrm{d}t A_{\mathrm{CP}}(s,t)\,, \quad A_{\mathrm{CP}}(s,t) = \frac{1}{\Gamma + \overline{\Gamma}} \left(\frac{\mathrm{d}^2\Gamma}{\mathrm{d}s\mathrm{d}t} - \frac{\mathrm{d}^2\overline{\Gamma}}{\mathrm{d}s\mathrm{d}t} \right)\,, \tag{4.34}$$

which are the most promising observables for the search of BSM signatures. Here, $\overline{\Gamma}$ denotes the decay rate of the CP-conjugated decay. For both normalization and differential distributions, we only take the valid phase space into account for QCDF. For HHχPT, we restrict the phase space to $s \leq 2\,\mathrm{GeV}^2$ to avoid large bremsstrahlung contributions in the normalization and the associated suppression of A_{CP}. CP asymmetries are only possible for SCS decays, since all contributions have the same weak phase for CF and DCS decays.

In the SM, $D^0 \to K^+K^-\gamma$ and $D^0 \to K^0\overline{K}^0\gamma$ are the only decays that have a non-vanishing CP asymmetry of $|A_{\mathrm{CP}}(s)| \lesssim 10^{-4}$ and $|A_{\mathrm{CP}}(s)| \lesssim 6 \cdot 10^{-4}$ in leading order QCDF, respectively. In both cases, the maxima are located at the ϕ peak. Since the ϕ is a narrow resonance, the CP asymmetries decrease rapidly with increasing distance from the resonance. For each of the remaining decay modes, there is only one WA contribution with a single weak phase and therefore no CP-violation. However, taking into account further decay topologies and $SU(3)_F$ breaking effects, they also do obtain non-zero CP asymmetries.

Since HHχPT includes further decay topologies, non-vanishing SM CP asymmetries are obtained for a total of five decay modes. Figure 4.15 shows Dalitz plots for these decays. For $D^0 \to K^+K^-\gamma$, $D^+ \to K^+\overline{K}^0\gamma$, $D_s \to \pi^+K^0\gamma$, and $D_s \to K^+\pi^0\gamma$, significant cancellations occur when integrating over t. CP asymmetries of $|A_{\mathrm{CP}}(s)| \lesssim 6 \cdot 10^{-5}$, $|A_{\mathrm{CP}}(s)| \lesssim 1.2 \cdot 10^{-5}$, $|A_{\mathrm{CP}}(s)| \lesssim 1.2 \cdot 10^{-4}$ and $|A_{\mathrm{CP}}(s)| \lesssim 4.5 \cdot 10^{-5}$ are obtained, respectively, where the maxima always occur at the s-channel resonance except for $D^+ \to K^+\overline{K}^0\gamma$. For $D^0 \to K^0\overline{K}^0\gamma$, there is no cancellation regarding the t integration. Thus, the maximum of $|A_{\mathrm{CP}}(s)| \lesssim 2.5 \cdot 10^{-4}$ does not arise at the ϕ peak, but from the constructive increase of the t and u channel resonances. The remaining decay modes have no SM CP violation. However, taking into account $SU(3)_F$ breaking effects and rescattering of the light mesons, which is possible at one-loop levels and above, CP asymmetries are induced for the remaining SCS decays as well.

Due to NP, the dipole coefficients $C_7^{(\prime)}$ can obtain considerable contributions with large CP-violating phases. Thus, all FCNC decay modes can obtain significant CP asymmetries. We begin the discussion of BSM CP asymmetries with the QCDF SM contributions. Since the QCDF amplitudes do not incorporate t- or u-channel resonances, the only sources of strong phases are the s-channel resonances. Therefore, we omit a representation of the BSM effects in terms of Dalitz plots. In Figure 4.16 and 4.17, we compare the SM predictions with different BSM scenarios for neutral and charged D mesons, respectively. We set one of the BSM coefficients to zero and a magnitude of 0.05 or 0.2 to the other one. To maximize the CP asymmetries, we set the weak phase to $\phi_w = \pm\pi/2$. $A_{\mathrm{CP}}(s)$ can take $\mathcal{O}(0.01)$ values for $D^+ \to K^+\overline{K}^0\gamma$ and $\mathcal{O}(1)$ values for $D^0 \to \pi^+\pi^-\gamma$ and $D^0 \to K^+K^-\gamma$. For the remaining decays, the values are of order $\mathcal{O}(0.1)$. The distributions of $D_s \to \pi^+K^0\gamma$ and $D_s \to K^+\pi^0\gamma$ are almost identical. Essentially, their amplitudes differ by an isospin

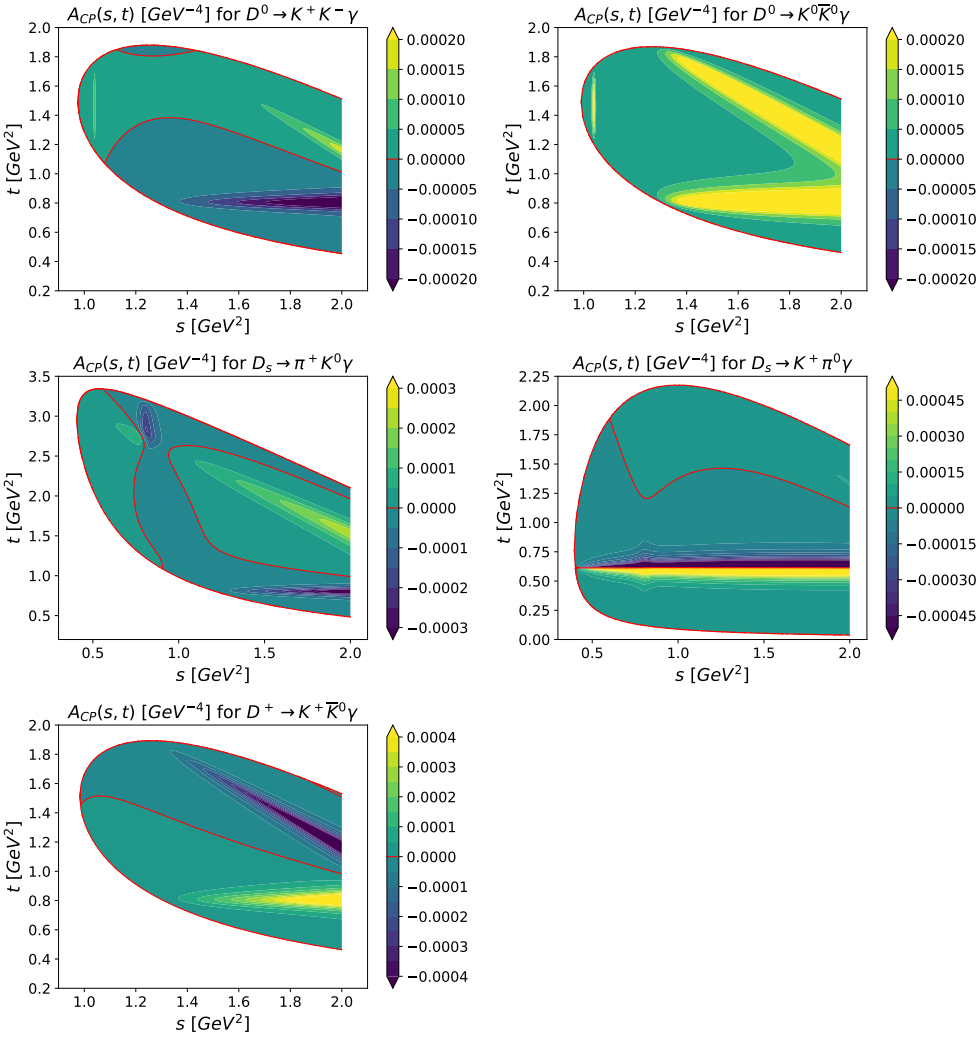

Figure 4.15: Dalitz plots of SM CP asymmetry.

factor of $-1/\sqrt{2}$. The small differences are a consequence of different momenta in the heavy meson propagators of the tensor form factors and differently shaped phase spaces. Analogously, similarities can be seen between the distributions of $D^0 \to K^+K^-\gamma$ and $D^0 \to K^0\bar{K}^0\gamma$, as the SM amplitudes differ only by the relative sign in (4.31).

In Figure 4.18 and 4.19 we show Dalitz plots of the double differential CP asymmetries based on HHχPT. Again, one of the coefficients has been set to zero. The second one has a value of $0.1i$. It can be seen that the CP asymmetries are increased by a factor of $\sim 10^3$ compared to the SM for all decay channels except $D^0 \to K^0\bar{K}^0\gamma$. In Figure 4.20 and 4.21, we show the same BSM scenarios as in 4.16 and 4.17 for HHχPT. For $D^0 \to \pi^+\pi^-\gamma$, $D^+ \to \pi^+\pi^0\gamma$, and $D_s \to K^+\pi^0\gamma$, the contributions of parity even and parity odd amplitude are of the same order of magnitude. Thus, the relative sign between C_7 and C_7' in (4.28) leads to a constructive increase for C_7' and to a cancellation of CP

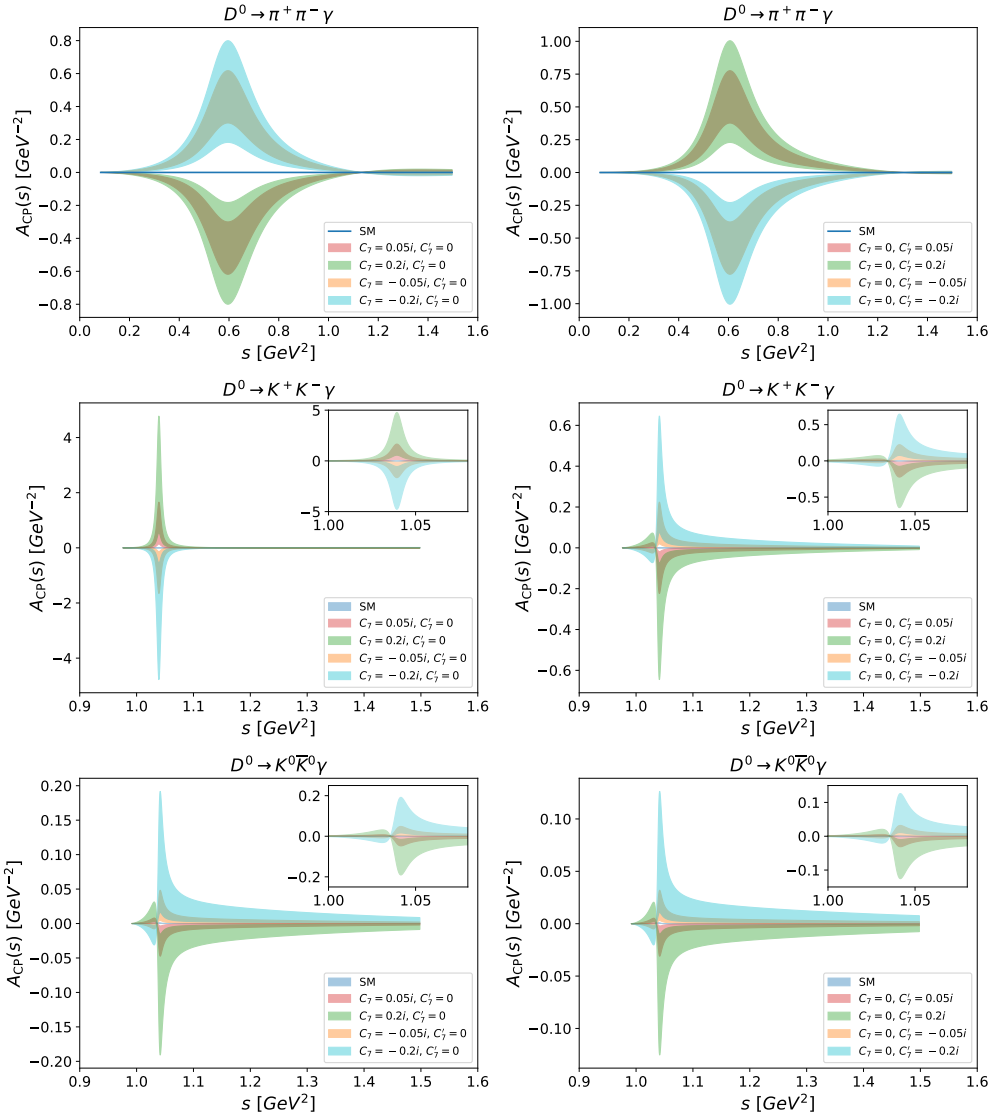

Figure 4.16: CP asymmetries for D^0 decays as a function of s based on QCDF SM predictions.

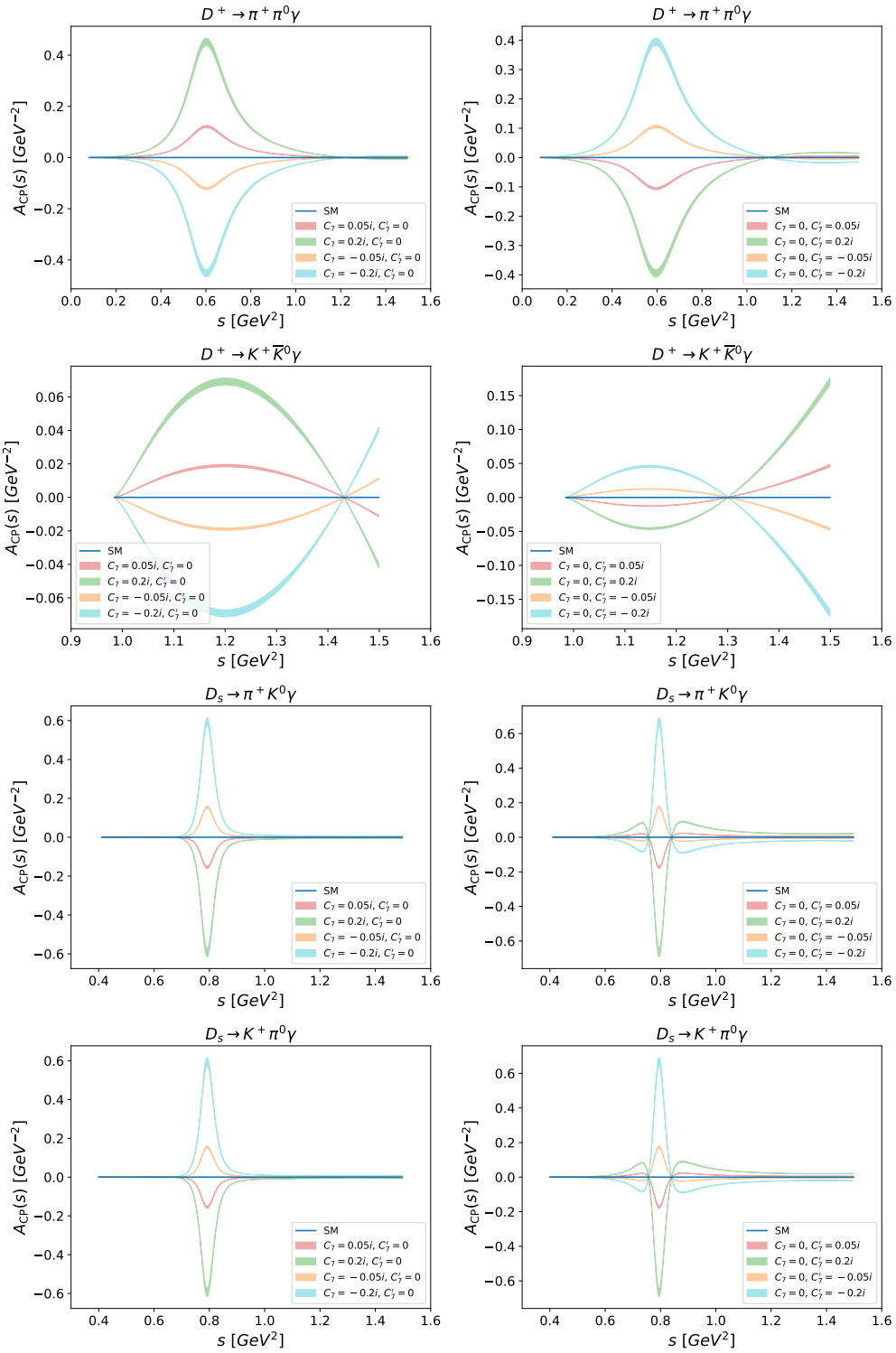

Figure 4.17: CP asymmetries for $D^+_{(s)}$ as a function of s based on QCDF SM predictions.

asymmetries for C_7. In case of $D^0 \to K^+K^-\gamma$ and $D^0 \to K^0\overline{K}^0\gamma$, the ϕ contributes only to A_+. Accordingly, the distribution is dominated by the parity even amplitude. For $D_s \to \pi^+K^0\gamma$, on the other hand, the s-channel peak is dominated by A_-. The tails of the distributions arising from the t- and u-channel resonances have a different sign in the two scenarios. Thus, the tails of the CP asymmetries originate from A_+.

For many decays, integration over t leads to cancellations of t- and u-channel contributions. This effect is particularly severe if the resonances are antiparticles of each other. To avoid this cancellation, it is useful to consider the double differential distributions in the form of Dalitz plots.

As stated in section 3.3, the imaginary parts of $C_7^{(\prime)}$ can be constrained to $|\mathrm{Im}(C_7^{(\prime)})| \lesssim 2 \cdot 10^{-3}$ by data from ΔA_{CP} in some BSM model. This corresponds to a suppression by a factor of 50 compared to the Dalitz plots in 4.18 and 4.19. Since the CP asymmetries scale approximately linearly with $\mathrm{Im}(C_7^{(\prime)})$ for $|C_7^{(\prime)}| \lesssim 0.1$, this also causes A_{CP} to be suppressed by a factor of 50. However, the resulting CP asymmetries are still in the per mile range and over an order of magnitude larger than the SM CP asymmetries. For values of $|C_7^{(\prime)}| \gtrsim 0.1$, the BSM contributions can lead to enhanced decay rates and thus affect the normalization of A_{CP}. Consequently, the CP asymmetries of some decay modes do not scale linearly with $\mathrm{Im}(C_7^{(\prime)})$ for large BSM coefficients.

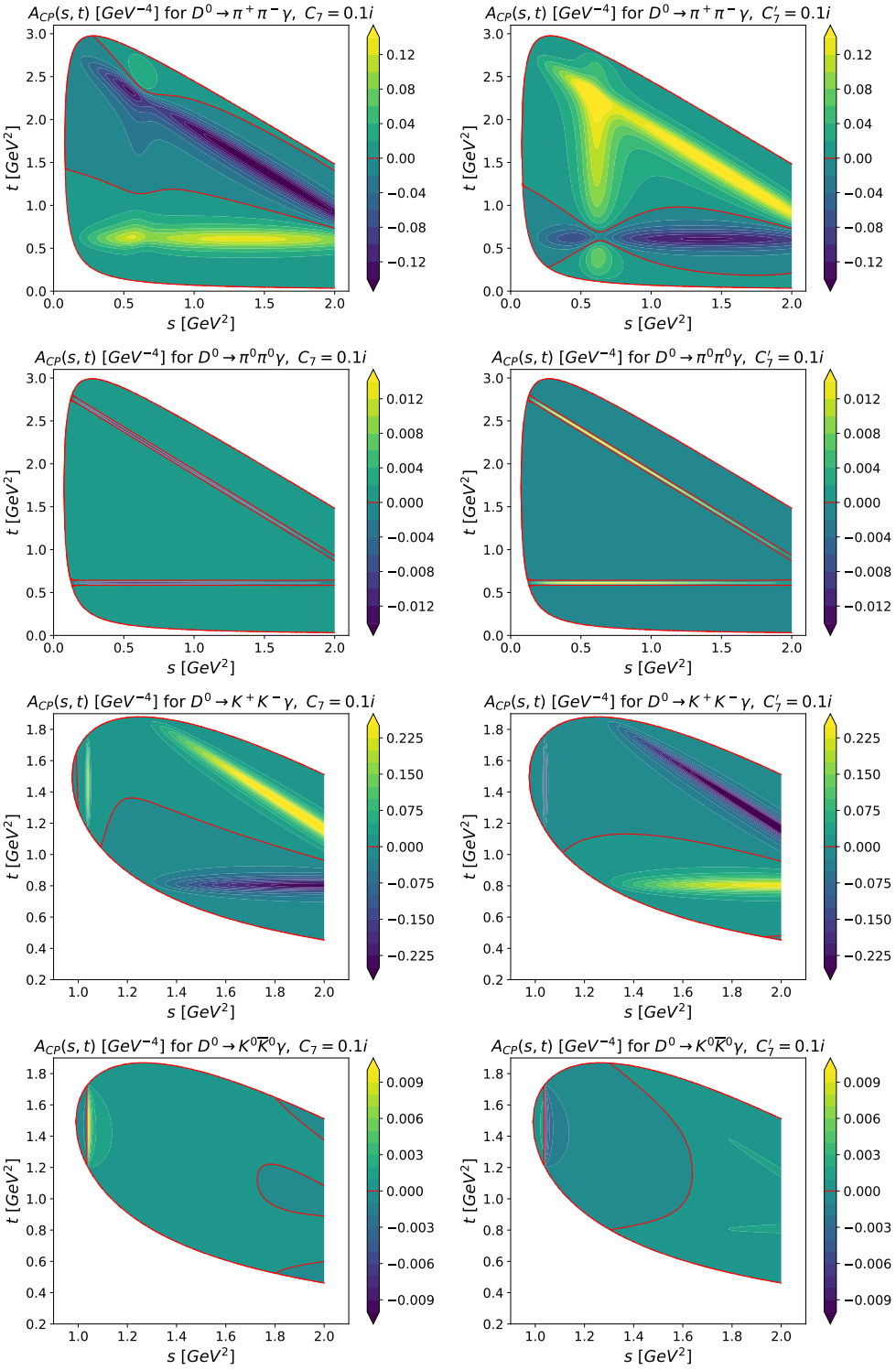

Figure 4.18: Dalitz plots of BSM CP asymmetries for decays of neutral D mesons.

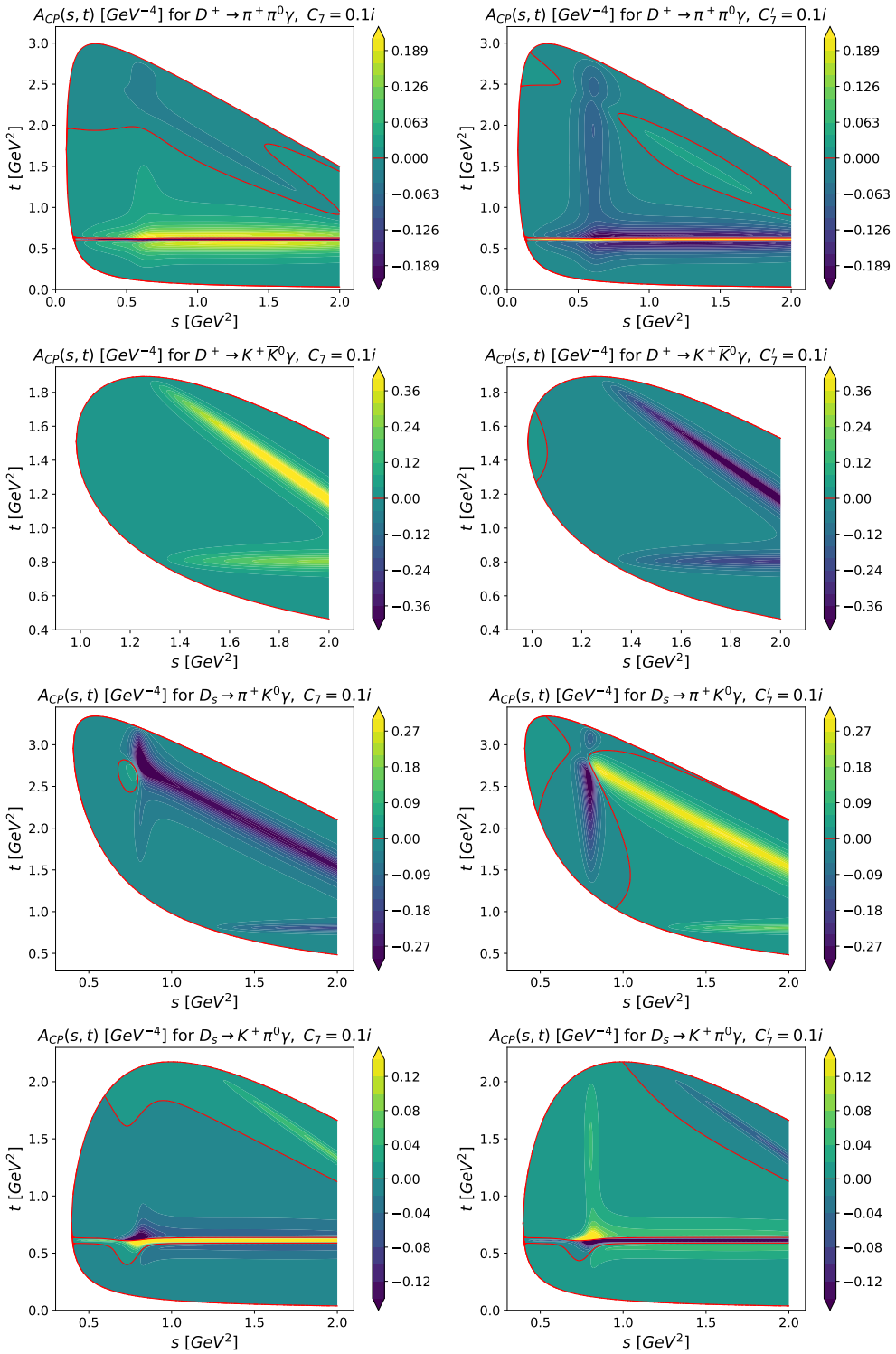

Figure 4.19: Dalitz plots of BSM CP asymmetries for decays of charged D mesons.

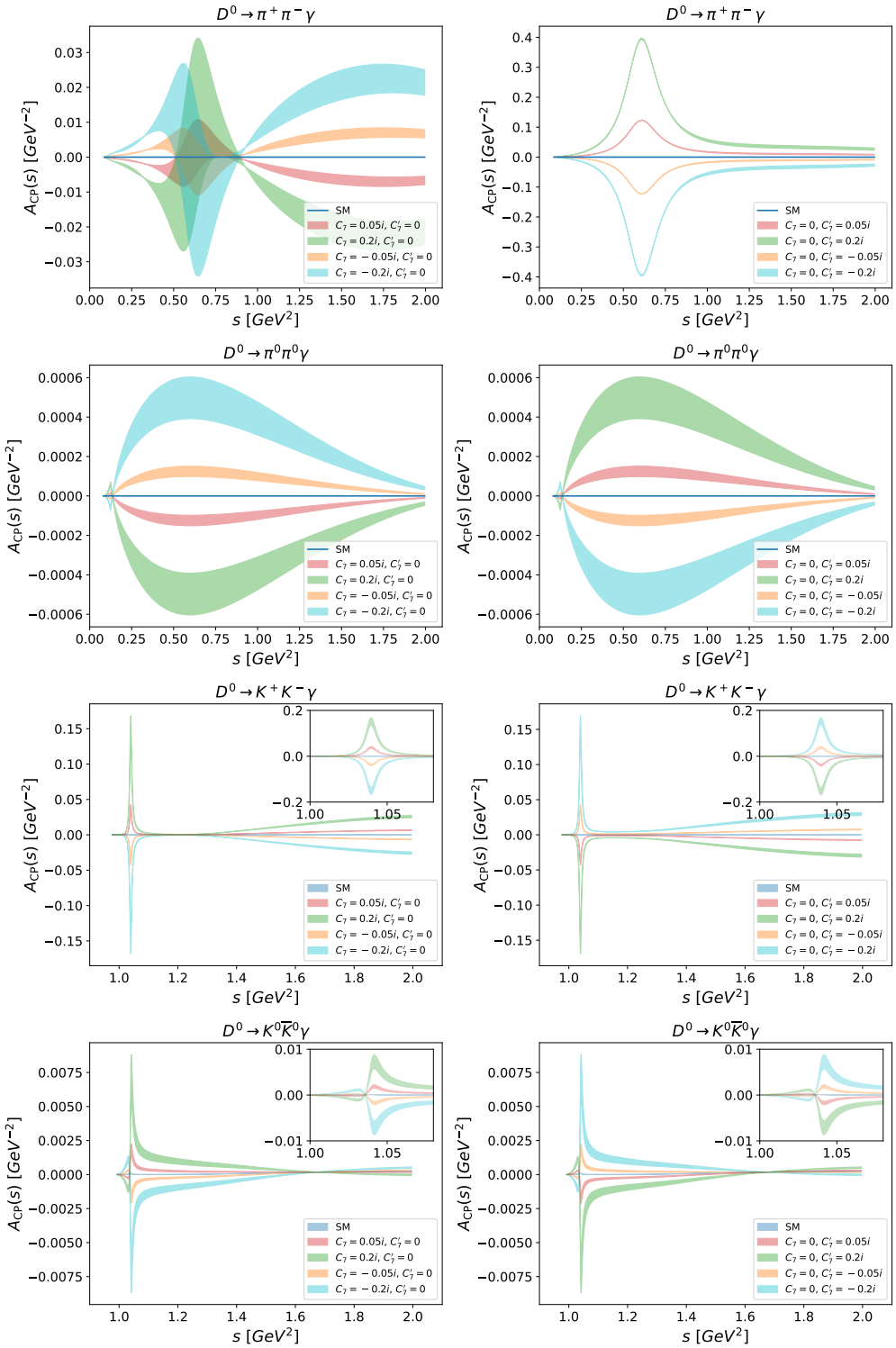

Figure 4.20: CP asymmetries for D^0 decays as a function of s based on HHχPT predictions.

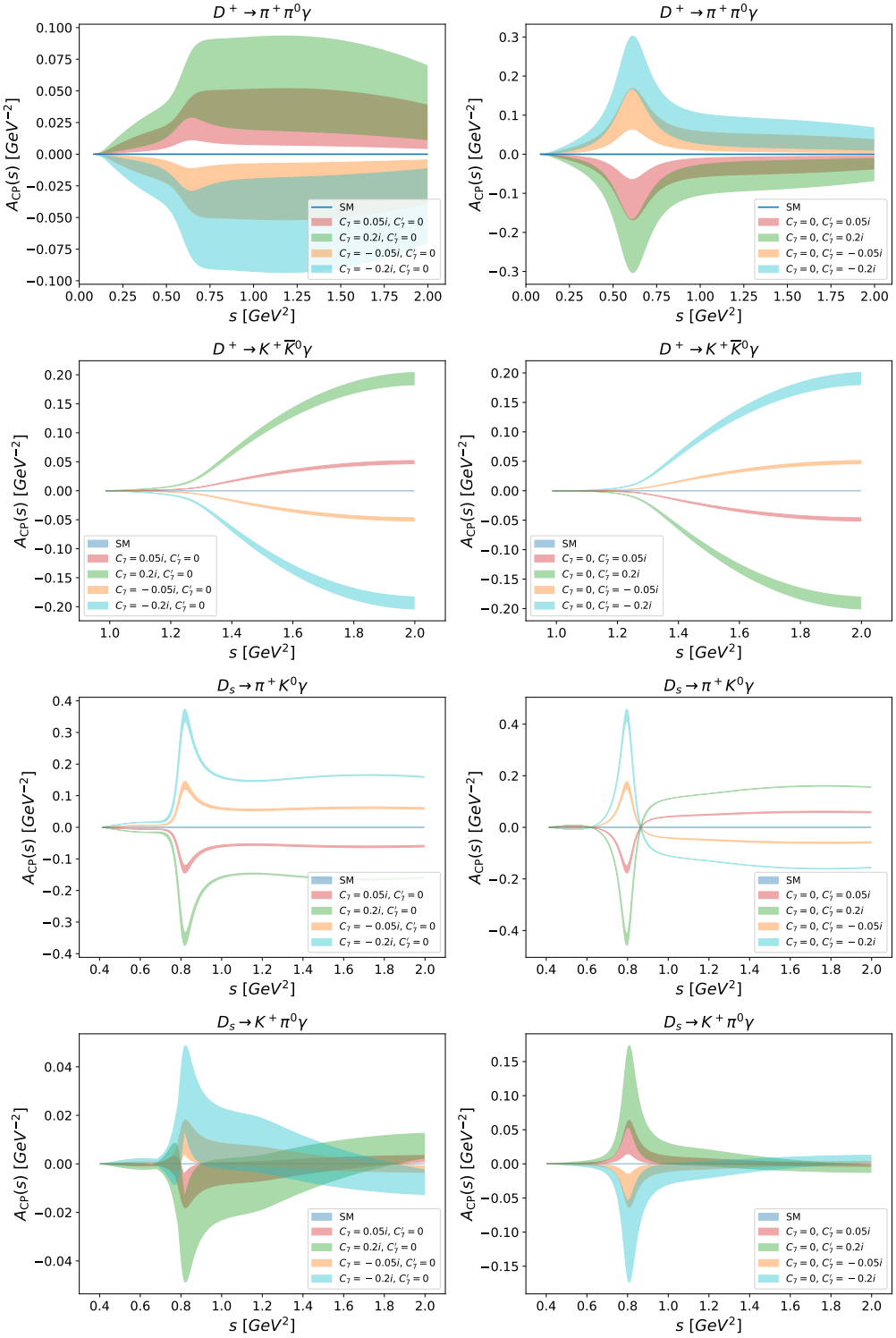

Figure 4.21: CP asymmetry for $D^+_{(s)}$ decays as a function of s based on HHχPT predictions.

4.6 Summary

In this chapter, we have discussed radiative three-body decays $D \to PP\gamma$. We have used Low's theorem, HHχPT, and QCDF to determine SM predictions for branching ratios, FB asymmetries, and CP asymmetries for all 18 decay modes involving pions and kaons. The CF and DCS modes are SM-like and thus well suited for testing the QCD frameworks. Of particular interest is the FB asymmetry, which vanishes when the amplitudes have no t dependence. This is the case for leading order QCDF. HHχPT, on the other hand, acquires diverse distributions due to the non-resonant contributions and especially due to the t and u channel resonances.

The eight SCS decays are FCNC processes and thus sensitive to new physics. We have shown the maximum impact of new physics in the electromagnetic dipole operators on branching ratios and FB asymmetries. Branching ratios of the SCS modes are mainly in the range of $10^{-5} - 10^{-4}$. They can be affected by new physics, however, this observable is not sufficiently clean and subject to too many uncertainties to unambiguously identify new physics. The FB asymmetry, on the other hand, reveals significant qualitative differences between SM predictions and BSM scenarios for some decays. Therefore, this observable is more appropriate to signal influences of BSM physics. Nevertheless, due to the intrinsic uncertainty of the Breit Wigner approach and the uncertainties associated with a leading order calculation, it is also difficult to claim sensitivity to new physics for A_{FB}.

Due to the small CP-violating phase in the charm sector of the SM, the CP asymmetries have the greatest sensitivity to BSM physics. If the CP-violating phase of the new physics is maximized, the CP asymmetries can be increased by up to three orders of magnitude compared to the SM. Taking into account the constraints of ΔA_{CP}, which will be relevant for some NP models, the CP asymmetries can still be increased by more than one order of magnitude by new physics. We note that double differential CP- asymmetries in the form of Dalitz plots are advantageous since they avoid cancellations. Moreover, cuts in s are helpful to avoid the large contributions of bremsstrahlung in the normalization and the accompanying suppression. We provide a review of the most interesting decay modes and point out opportunities. The best decay channels for

- testing QCD frameworks with branching ratios, see Fig. 4.5 and 4.6: In general, all CF and DCS modes are suitable for this purpose. Particularly interesting are the modes $D^+ \to \pi^+ \overline{K}^0 \gamma$ (CF) and $D_s \to K^+ K^0 \gamma$ (DCS), which do not have an s-channel resonance due to the involved flavor and, therefore, do not have a leading order QCDF contribution.

- testing QCD frameworks with A_{FB}, see Fig. 4.11 and 4.12: $D^0 \to \pi^0 \overline{K}^0 \gamma$ (CF), $D_s \to \pi^+ \pi^0 \gamma$ (CF) and $D^+ \to K^+ \pi^0 \gamma$ (DCS) have small uncertainties. In addition, the distributions have very distinctive shapes, which are reasonably well understood.

- testing the SM with A_{FB}, see Fig. 4.13 and 4.14: $D^0 \to \pi^+ \pi^- \gamma$, $D^+ \to \pi^+ \pi^0 \gamma$ and $D_s \to \pi^+ K^0 \gamma$, since the other decay modes have small differences between SM and BSM asymmetries or large uncertainties.

- testing the SM with A_{CP}: Dalitz plots are suitable for all decay modes. For the singly differential CP asymmetries, the decays $D^+ \to \pi^+ \pi^0 \gamma$ and $D_s \to \pi^+ K^0 \gamma$ can

M_c	$f(c \to h_c)$	$N(h_C)$ FCC-ee	$N(h_C)$ Belle II
D^0	0.59	$\sim 3 \cdot 10^{11}$	$\sim 4 \cdot 10^{10}$
D^+	0.24	$\sim 1 \cdot 10^{11}$	$\sim 2 \cdot 10^{10}$
D_s	0.10	$\sim 6 \cdot 10^{10}$	$\sim 7 \cdot 10^{9}$

Table 4.3: Charm fragmentation fractions $f(c \to M_c)$ [168] and number of charmed mesons for $c\bar{c}$ production rates of $550 \cdot 10^9$ (FCC-ee) and $65 \cdot 10^9$ (Belle II with $50\,\mathrm{ab}^{-1}$) [81]. Table is adopted from [66]

be pointed out. They are sensitive in both BSM coefficients and do not suffer from strong cancellation between the t- and u-channel contributions. $D^0 \to K^+K^-\gamma$ is also a valid option in the region of the ϕ peak. The remaining modes are only sensitive in one BSM coefficient or substantially smaller asymmetries have to be expected. We also note that the cut in s is in fact not required for the decays $D^0 \to \pi^0\pi^0\gamma$ and $D^0 \to K^0\overline{K}^0\gamma$, since all mesons are neutrally charged and thus no bremsstrahlung is emitted. Therefore, it is possible to study the whole phase space without suppression. However, it turns out that the expected CP asymmetries are small compared to the other modes.

$D \to PP\gamma$ decays are well-suited for investigations at current e^+e^- facilities as Belle II and BES III as well as future e^+e^- colliders such as the FCC-ee. The branching ratios (see Table 4.2) are roughly in the range of 10^{-7} to 10^{-3}. With the fragmentation fractions and the number of charm mesons given in Table 4.3, the lowest number of unreconstructed events of $3 \cdot 10^4$ (FCC-ee) and $3.5 \cdot 10^3$ (Belle II) is obtained for $D_s \to K^+K^0\gamma$. The largest number of events are expected for $D^0 \to \pi^0\overline{K}^0\gamma$. We obtain $3 \cdot 10^8$ and $4 \cdot 10^7$ for the FCC-ee and Belle II, respectively.

5 Photon polarization in $D \to K\pi\pi\gamma$ decays

Besides branching ratios, angular observables and CP asymmetries of radiative charm decays, the photon polarization is an interesting observable to test the SM. Since the detectors do not measure the polarization of photons directly, it has to be reconstructed from the momenta of the final states and the angular distributions. As the photon helicity is odd under parity, the angular distributions of a radiative D meson decay only exhibit a dependence on the photon polarization if a pseudoscalar quantity can be constructed using the final state momenta. In case of a four-body decay $D \to P_1P_2P_3\gamma$, a triple product $\vec{p}_1 \cdot (\vec{p}_2 \times \vec{p}_3)$ can be formed, which is also parity odd [169]. For three-body decays, which were discussed in the previous chapter, the three momenta of the final states are linearly dependent and thus the triple product vanishes. Therefore, we do not have access to the photon polarization in $D \to PP\gamma$ decays via the angular distribution.

In this chapter, we use an up-down asymmetry A_{UD} in the angular distribution to extract the photon polarization of $D^+_{(s)} \to K_1^+(\to K\pi\pi)\gamma$ decays, where K_1 is an axial-vector meson. The adaptation of this method, which is known from B physics [169, 170], to charm physics offers the advantage of partner decays. Both the D^+ and the D_s decay are color-allowed and induced by weak annihilation. In the SM, the photon polarizations of the D^+ and D_s decays are identical up to U-spin breaking effects. However, the DCS $D^+ \to K_1^+\gamma$ decay is SM-like, while the SCS $D_s \to K_1^+\gamma$ decay is an FCNC process and therefore sensitive to new physics in the dipole operators, which can alter the polarization of the photon. Thus, the photon polarization can be extracted from the SM-like D^+ decay and subsequently compared to the BSM sensitive D_s decay. Since the spectra of the $K_1^+ \to K\pi\pi$ decay are universal for both decays, the hadronic prefactors between A_{UD} and the photon polarization are identical for D^+ and D_s decays. Consequently, precise knowledge of the $K\pi\pi$ spectrum and a theoretical prediction of the photon polarization is not necessary. Instead, the ratio of the up-down asymmetries, which is identical to the ratio of the polarisations, can be used as a null test of the SM.

This chapter is organized as follows: In section 5.1, the kinematics and angular distributions for $D^+_{(s)} \to K_1^+(\to K\pi\pi)\gamma$ are described. Furthermore, we define an up-down asymmetry which allows to extract the polarization of the photon in the $D^+_{(s)} \to K_1^+\gamma$ decay. Subsequently, the unmeasured branching ratios of $D^+ \to K_1^+\gamma$ and $D_s \to K_1^+\gamma$ are estimated using QCDF methods in section 5.2. In addition, the impact of new physics in the electromagnetic dipole operator on the photon polarization is estimated. In section 5.3, the helicity amplitudes of the decay $K_1 \to K\pi\pi$ are discussed. We analyze the hadronic factor in the up-down asymmetry and provide its distribution in section 5.4. Finally, we summarize the results in section 5.5.

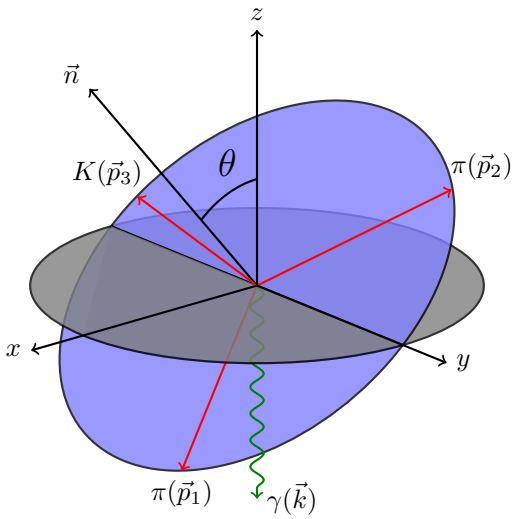

Figure 5.1: Kinematics of the $K_1 \to K\pi\pi$ decay in the $K\pi\pi$ center-of-mass frame. The z-axis is defined as the direction opposite to the photon. θ is the angle between the z-axis and the normal $\vec{n} = (\vec{p}_1 \times \vec{p}_2)/|\vec{p}_1 \times \vec{p}_2|$.

5.1 Angular distribution and kinematics

The angular distribution for $D^+_{(s)} \to K_1^+(\to K\pi\pi)\gamma$ decays can be written as

$$\frac{\mathrm{d}^4\Gamma}{\mathrm{d}s\mathrm{d}s_{13}\mathrm{d}s_{23}\mathrm{d}\cos(\theta)} \propto \left[|\vec{\mathcal{J}}|^2(1+\cos^2(\theta)) + 2\lambda_\gamma Im\left[\vec{n}\cdot(\vec{\mathcal{J}}\times\vec{\mathcal{J}}^*)\right]\cos(\theta)\right] PS\,, \tag{5.1}$$

where $s = (p_1+p_2+p_3)^2$ and $s_{ij} = (p_i+p_j)^2$ denote the $K\pi\pi$ and the P_iP_j invariant mass squared, respectively. The momenta p_2, p_3 and p_1 refer to the positively charged pion, the kaon and the remaining pion as specified in (5.12). The angle θ is defined by the direction opposite to the photon and the normal $\vec{n} = \vec{p_1}\times\vec{p_2}/|\vec{p_1}\times\vec{p_2}|$, see Fig. 5.1. The spatial components of the $K_1 \to K\pi\pi$ helicity amplitude, which we discuss in section 5.3, are denoted by $\vec{\mathcal{J}}$. The photon polarization parameter is defined as

$$\lambda_\gamma^{D^+_{(s)}} = -\frac{1-r^2_{D^+_{(s)}}}{1+r^2_{D^+_{(s)}}}\,, \qquad r_{D^+_{(s)}} = \left|\frac{A_R^{D^+_{(s)}}}{A_L^{D^+_{(s)}}}\right|, \tag{5.2}$$

where $A^{D^+_{(s)}}_{L/R}$ denote the $D^+_{(s)} \to K_1^+\gamma$ decay amplitudes for left-handed and right-handed polarized photons, see Sec. (5.2) for details. The factor

$$PS = \frac{1-s/m^2_{D_{(s)}}}{256(2\pi)^5 m_{D_{(s)}} s} \tag{5.3}$$

is obtained from the phase space which has the non-trivial boundaries

$$\begin{aligned}
&(m_1+m_2+m_3)^2 \le s \le m^2_{D^+_{(s)}}\,,\\
&(m_1+m_3)^2 \le s_{13} \le (\sqrt{s}-m_2)^2\,,\\
&s_{23\text{min}} \le s_{23} \le s_{23\text{max}}\,,\\
&s_{23\text{min/max}} = (E^*_2+E^*_3)^2 - \left(\sqrt{E^{*2}_2-m^2_2} \pm \sqrt{E^{*2}_3-m^2_3}\right)^2\,,
\end{aligned} \tag{5.4}$$

where $E^*_2 = (s-s_{13}-m^2_2)/(2\sqrt{s_{13}})$ and $E^*_3 = (s_{13}-m^2_1+m^2_3)/(2\sqrt{s_{13}})$ denote the energies in the P_2P_3 center-of-mass frame. From the definition of the angular distribution (5.1), it is evident that the polarization of the photon has no effect on integrated branching ratios or CP asymmetries as λ_γ only appears in combination with $\cos(\theta)$. However, the photon polarization can be extracted from an up-down asymmetry A_{UD}, which is linear in the photon polarization parameter and defined by

$$\begin{aligned}
A_{\text{UD}} &= \left(\int_0^1 \frac{\mathrm{d}^2\Gamma}{\mathrm{d}s\mathrm{d}\cos(\theta)}\mathrm{d}\cos(\theta) - \int_{-1}^0 \frac{\mathrm{d}^2\Gamma}{\mathrm{d}s\mathrm{d}\cos(\theta)}\mathrm{d}\cos(\theta)\right) \Big/ \int_{-1}^1 \frac{\mathrm{d}^2\Gamma}{\mathrm{d}s\mathrm{d}\cos(\theta)}\mathrm{d}\cos(\theta)\\
&= \frac{3}{4}\frac{\left\langle \text{Im}[\vec{n}\cdot(\vec{\mathcal{J}}\times\vec{\mathcal{J}}^*)]\,\kappa\right\rangle}{\left\langle|\vec{\mathcal{J}}|^2\right\rangle}\lambda_\gamma\,,
\end{aligned} \tag{5.5}$$

The $\langle ...\rangle$-brackets denote the integration over the invariant mass squares s_{13} and s_{23}. The parameter $\kappa = \text{sgn}(s_{13}-s_{23})$ for $K^+_1 \to \pi^0\pi^+K^0$ and $\kappa = 1$ for $K^+_1 \to \pi^-\pi^+K^+$ does not directly arise from the definition of the angular distribution and A_{UD}. The reason for the introduction of κ is given in section 5.3. Since the helicity amplitudes are the same for D^+ and D_s decays, the proportionality factors between A_{UD} and λ_γ are identical. Thus, they drop out from the ratio of the up-down asymmetries

$$\frac{A^{D_s}_{\text{UD}}}{A^{D^+}_{\text{UD}}} = \frac{\lambda^{D_s}_\gamma}{\lambda^{D^+}_\gamma} = \frac{1-r^2_{D_s}}{1+r^2_{D_s}}\frac{1+r^2_{D^+}}{1-r^2_{D^+}}\,. \tag{5.6}$$

In the SM, r_{D^+} and r_{D_s} are identical and thus the ratio is equal to one up to U-spin breaking corrections. In section 5.2, we consider the impact of U-spin breaking as well as the contributions from new physics in the electromagnetic dipole operators on the photon polarization and the ratio (5.6).

Note that the relation between A_{UD} and λ_γ gets more complicated when considering more than one K_1 resonance, since $r_{D_{(s)^+}}$ and λ_γ varies with s. Therefore, λ_γ is not identical for the different K_1 resonances. This effect can be controlled by cuts [1]. A generally valid formula can be found in appendix C of [1]. However, the SM prediction that (5.6) is equal to one up to U-spin breaking effects is not effected.

5.2 The $D^+_{(s)} \to K^+_1\gamma$ decay

The decay rate of the two-body decay $D^+_{(s)} \to K^+_1\gamma$ can be written as [124]

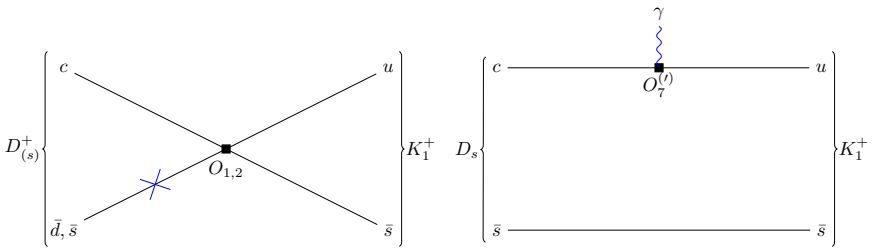

Figure 5.2: The Feynman diagram for the leading weak annihilation contribution is shown on the left. The blue cross indicates where the photon is emitted. Further contributions are suppressed by λ_{QCD}/m_c. BSM diagram of the photonic dipole operator for $D_s \to K_1^+\gamma$ is shown on the right.

$$\Gamma = \frac{\alpha_e G_F^2 m_{D^+_{(s)}}^3}{32\pi^4}\left(1 - \frac{m_{K_1}^2}{m_{D^+_{(s)}}^2}\right)^3 \left(|A_L^{D^+_{(s)}}|^2 + |A_R^{D^+_{(s)}}|^2\right), \tag{5.7}$$

where α_e denotes the fine structure constant. $A_{L,R}$ refer to the decay amplitudes for left-handed and right-handed polarized photons as in (5.2). As no experimental data on $D^+_{(s)} \to K_1^+\gamma$ decays is available, we use QCDF methods to estimate the SM branching ratios as well as the BSM potential of the photon polarization. Figure 5.2 shows the leading weak annihilation diagram on the left, where the blue cross indicates that the photon is dominantly emitted by the light quark inside the $D^+_{(s)}$ meson. Photon emissions from the other quark lines are suppressed by λ_{QCD}/m_c and will be neglected. The BSM contribution of the electromagnetic dipole operator to $D_s \to K_1^+\gamma$ is shown on the right. For the left-handed amplitudes we obtain analogously to $D \to V\gamma$ [124]

$$\begin{aligned} A_{L\,\text{SM}}^{D} &= -\frac{2\pi^2 Q_d f_D f_{K_1} m_{K_1}}{m_D \lambda_D} V_{cd}^* V_{us} C_2 \frac{m_D^2}{m_D^2 - m_{K_1}^2}, \\ A_{L\,\text{SM}}^{D_s} &= -\frac{2\pi^2 Q_d f_{D_s} f_{K_1} m_{K_1}}{m_{D_s} \lambda_{D_s}} V_{cs}^* V_{us} C_2 \frac{m_{D_s}^2}{m_{D_s}^2 - m_{K_1}^2}, \end{aligned} \tag{5.8}$$

where $A_{R\,\text{SM}}^{D^+_{(s)}} = 0$. The extra minus sign is a result of the $V - A$ structure of the four quark operators. However, substantial corrections have to be expected due to the poor convergence of the heavy quark and α_s expansion. Leading order QCDF leads to purely left-handed photons, but contributions to right-handed photons are also expected. For instance, a mechanism for generating right-handed photons is given by a quark loop with an $O_{1,2}$ insertion, where the photon and a gluon are coupled to the loop [171]. However, this mechanism is at least perturbatively subject to GIM suppression [124].

For the SM branching ratios we obtain

$$\begin{aligned}
B(D^+ \to K_1^+(1270)\gamma) &= [(1.3 \pm 0.3), (1.5 \pm 0.4)] \times 10^{-5} \left(\frac{0.1\ \text{GeV}}{\lambda_D}\right)^2 , \\
B(D^+ \to K_1^+(1400)\gamma) &= [(1.4 \pm 0.6), (1.6 \pm 0.7)] \times 10^{-5} \left(\frac{0.1\ \text{GeV}}{\lambda_D}\right)^2 , \\
B(D_s \to K_1^+(1270)\gamma) &= [(1.9 \pm 0.4), (2.2 \pm 0.5)] \times 10^{-4} \left(\frac{0.1\ \text{GeV}}{\lambda_{D_s}}\right)^2 , \\
B(D_s \to K_1^+(1400)\gamma) &= [(2.0 \pm 0.9), (2.4 \pm 1.0)] \times 10^{-4} \left(\frac{0.1\ \text{GeV}}{\lambda_{D_s}}\right)^2 ,
\end{aligned} \tag{5.9}$$

where the first and second entry correspond to the lower and upper end of the range of the Wilson coefficient C_2 (3.15), respectively. We added the parametric uncertainties from decay constants, masses, lifetimes, and CKM matrix elements in quadrature. However, the largest uncertainty arises from the non-perturbative parameter $\lambda_{D^+_{(s)}}$, which we scale with 0.1 GeV as in section 4.2.3. The difference of one order of magnitude between D^+ and D_s decays essentially follows from the CKM matrix elements and the different lifetimes $|V_{cd}/V_{cs}|^2(\tau_{D^+}/\tau_{D_s}) \approx 0.1$.

The dipole operators $O_7^{(\prime)}$ contribute only to the left- or right-handed amplitude

$$A^{D_s}_{L\,\text{NP}} = m_c C_7 T^{K_1}, \quad A^{D_s}_{R\,\text{NP}} = m_c C_7' T^{K_1}\,, \tag{5.10}$$

respectively. $T^{K_1} = T_1^{D_s\to K_1^+}(0)$ denotes the form factor of a $D_s \to K_1^+$ transition via a tensor current, which is defined in appendix B.3. This form factor is unknown to date. Therefore, we will assume in the following that the ratios of the tensor form factors are the same as in B physics. From the data on radiative B decays, see appendix A for details, the ratios $T_1^{B\to K_1(1400)}/T_1^{B\to K_1(1270)} \simeq 0.5$ and $T_1^{B\to K_1(1270)}/T_1^{B\to K^*(892)} \simeq 1.1$ can be determined. By using $T_1^{D_s\to K^*(892)} \simeq 0.7$ [124], we obtain $T^{K_1(1270)} \simeq 0.8$ and $T^{K_1(1400)} \simeq 0.4$. The ratios of left-handed and right-handed amplitudes for D^+ and D_s decays read as follows

$$r_{D^+} = \left|\frac{A^{D^+}_{R\,\text{SM}}}{A^{D^+}_{L\,\text{SM}}}\right|, \qquad r_{D_s} = \left|\frac{m_c T^{K_1} C_7'^{\,\text{eff}} + A^{D_s}_{R\,\text{SM}}}{m_c T^{K_1} C_7^{\text{eff}} + A^{D_s}_{L\,\text{SM}}}\right|. \tag{5.11}$$

In order to estimate whether one can search for new physics by comparing the photon polarizations or A_{UD}, it is essential to examine how large the effects of U-spin breaking can be. There are numerous sources for the U-spin breaking. The phase space, the CKM matrix elements as well as parameters like masses, decay constants and $\lambda_{D_{(s)}}$ can be taken into account in a simple way. Sources which require an exact calculation of the amplitudes are problematic. For example, the contributions to right-handed photons mentioned before are only possible for FCNC decays. U-spin breaking effects are usually of the order $\mathcal{O}(0.2-0.3)$ [172–174]. It is advantageous that we consider the ratios of left- and right-handed amplitudes and thus only the residual breaking is of importance. In

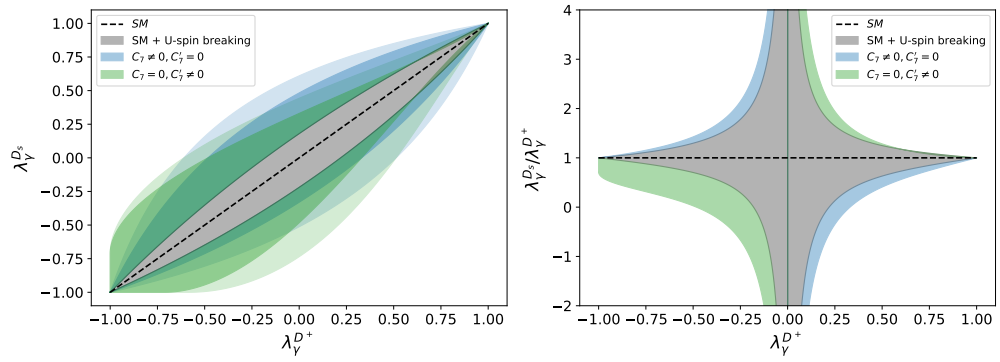

Figure 5.3: Estimation of the BSM reach in $D^+_{(s)} \to K_1(1270)\gamma$ decays. $\lambda_\gamma^{D_s}$ (left) and $\lambda_\gamma^{D_s}/\lambda_\gamma^{D^+}$ (right) are shown as a function of $\lambda_\gamma^{D^+}$. The black dashed line refers to the SM in the exact U-spin limit. $\pm 20\%$ U-spin breaking between $r_{\text{SM}}^{D^+}$ and $r_{\text{SM}}^{D_s}$ are illustrated by the gray shaded area. The blue (green) region illustrates the BSM reach in C_7 (C_7'). We set $C_7' = 0$ ($C_7 = 0$) and varied the other coefficient within $-0.3 \leq C_7^{(\prime)} \leq 0.3$. For the darker shaded area we used the exakt U-spin limit of the SM amplitudes. The lighter shaded area in the left plot includes the $\pm 20\%$ U-spin breaking. We used the leading order QCDF result (5.8) for the left-handed SM amplitude.

the following, we assume $\pm 20\%$ U-spin breaking between r_{D^+} and r_{D_s}. In Figure 5.3 we estimate the BSM reach and U-spin breaking effects on $\lambda_\gamma^{D_s}$ for a given value of $\lambda_\gamma^{D^+}$. The dashed line shows the case of the exact U-spin limit and the gray area includes $\pm 20\%$ U-spin breaking between r_{D_s} and r_{D^+}. The BSM reach in C_7 and C_7' is shown in blue and green, respectively. One of the dipole coefficients is set to zero, while the other one is varied in the allowed range according to (3.16). For the darker shaded regions, we used the exact U-spin for the SM amplitudes. The lighter shaded region include both the U-spin breaking effects and variations in one dipole coefficient. The small value of $\lambda_{D_{(s)}} = 0.1\,\text{GeV}$ suppresses the effects of new physics. Nevertheless, NP effects caused by enlarged dipole coefficients can be significant. However, for the SM test using (5.6), small values of $\lambda_\gamma^{D^+}$ are problematic. In this case, U-spin breaking can lead to huge discrepancies of $\lambda_\gamma^{D_s}/\lambda_\gamma^{D^+} \approx 1$. However, if we assume that the photon in $D^+ \to K_1^+\gamma$ is dominantly left-handed polarized $\lambda_\gamma^{\text{SM}} \lesssim -0.5$, as implied by QCDF, values exceeding $0.8 \lesssim A_{\text{UD}}^{D_s}/A_{\text{UD}}^{D^+} = \lambda_\gamma^{D_s}/\lambda_\gamma^{D^+} \lesssim 1.2$ hint new physics.

5.3 The $K_1 \to K\pi\pi$ decay

Even though an exact knowledge of the helicity amplitudes is not necessary for the null test of the SM using (5.6), they determine the sensitivity for the photon polarization in the up-down asymmetry. If the factor $\left\langle \text{Im}[\vec{n} \cdot (\vec{\mathcal{J}} \times \vec{\mathcal{J}}^*)]\,\kappa \right\rangle / \left\langle |\vec{\mathcal{J}}|^2 \right\rangle$ is small or even zero, we do not have access to λ_γ. Therefore, we use a phenomenological model to describe the helicity amplitudes and estimate the proportionality factor between A_{UD} and λ_γ. In general, there

is a variety of resonances contributing to the final state $K\pi\pi$ including the K_1 axial vector mesons with spin parity $J^P = 1^+$. Due to the stronger phase space suppression in charm physics compared to B physics, we restrict ourselves to a two-resonance approach, which takes the $K_1(1270)$ and $K_1(1400)$ into account and we neglect the remaining members of the $K_J(1400)$ family as well as the $K_1(1650)$ resonance. We consider two different combinations of charges in the final state

$$\begin{aligned} \text{I}: \quad & K_1^+(1270/1400) \to \pi \underbrace{{}^0(p_1)\overbrace{\pi^+(p_2)K}^{K^{*+}}{}^0(p_3)}_{K^{*0}}\,, \\ \text{II}: \quad & K_1^+(1270/1400) \to \pi \underbrace{{}^-(p_1)\pi^+(p_2)K^+(p_3)}_{K^{*0}}\,, \end{aligned} \tag{5.12}$$

where the brackets indicate the possible intermediate vector resonances. The helicity amplitude is defined by the $K_1 \to K\pi\pi$ decay amplitude as

$$\mathcal{A}(K_1 \to K\pi\pi) = \epsilon^\mu \mathcal{J}_\mu\,, \tag{5.13}$$

where ϵ^μ is the polarization vector of the K_1. For $\mathcal{J}_\mu$, we use a Breit-Wigner approach. A general Lorentz decomposition of the helicity amplitude requires two functions $C_{1,2}$ for parametrization. Thus, $\mathcal{J}_\mu$ can be written as

$$\mathcal{J}_\mu^{I,II} = \sum_{K_{\text{res}}} \xi_{K_{\text{res}}} \left[C_{1K_{\text{res}}}^{I,II}(s, s_{13}, s_{23}) p_{1\mu} - C_{2K_{\text{res}}}^{I,II}(s, s_{13}, s_{23}) p_{2\mu} \right] BW_{K_{\text{res}}}(s)\,. \tag{5.14}$$

The definition of the Breit Wigner function is given in (C.1). The parameter $\xi_{K_{\text{res}}}$ accounts for the differences in the productions of the various resonances in weak decays. The discrepancies follow from different hadronic parameters such as masses m_{K_1}, decay constants f_{K_1} and also form factors $T_1^{K_1}$. This approach is an approximation of the general formula from Appendix C in [1] and allows the use of (5.5). In addition, $\xi_{K_{\text{res}}}$ allows individual resonances to be added or removed from the calculation individually. The functions $C_{1,2}$ are determined by quasi-two-body decays $K_1 \to V(\to PP)P$. For the two different final states, we obtain [175]

$$\begin{aligned} C_1^I &= \frac{\sqrt{2}}{3}(a_{13}^{K^*} - b_{13}^{K^*}) + \frac{\sqrt{2}}{3} b_{23}^{K^*} + \frac{1}{\sqrt{3}} a_{12}^{\rho}\,, & C_2^I &= \frac{\sqrt{2}}{3} b_{13}^{K^*} + \frac{\sqrt{2}}{3}(a_{23}^{K^*} - b_{23}^{K^*}) - \frac{1}{\sqrt{3}} b_{12}^{\rho}\,, \\ C_1^{II} &= -\frac{2}{3}(a_{13}^{K^*} - b_{13}^{K^*}) - \frac{1}{\sqrt{6}} a_{12}^{\rho}\,, & C_2^{II} &= -\frac{2}{3} b_{13}^{K^*} + \frac{1}{\sqrt{6}} b_{12}^{\rho}\,. \end{aligned} \tag{5.15}$$

On the one hand, the two modes obtain different isospin factors. However, the essential difference is that there is no vector resonance decaying into π^+K^+ for channel II. For the functions

$$\begin{aligned} a_{ij}^V &= g_{VP_iP_j} BW_V(s_{ij})[f^V + h^V\sqrt{s}(E_i - E_j) - \Delta_{ij}]\,, \\ b_{ij}^V &= g_{VP_iP_j} BW_V(s_{ij})[-f^V + h^V\sqrt{s}(E_i - E_j) - \Delta_{ij}]\,, \\ \Delta_{ij} &= \frac{(m_i^2 - m_j^2)}{m_V^2}[f^V + h^V\sqrt{s}(E_i + E_j)]\,, \end{aligned} \tag{5.16}$$

a Breit-Wigner approach is used for the vector resonances as well. The energies of the final state pseudoscalars in the K_1 rest frame are given by

$$\begin{aligned} E_1 &= \frac{s - s_{23} + m_1^2}{2\sqrt{s}}\,, \qquad E_2 = \frac{s - s_{13} + m_2^2}{2\sqrt{s}}\,, \\ E_3 &= \frac{s - s_{12} + m_3^2}{2\sqrt{s}} = \frac{s_{23} + s_{13} - m_1^2 - m_2^2}{2\sqrt{s}}\,. \end{aligned} \tag{5.17}$$

The coupling g_{VPP} can be extracted from data on decay widths [176]

$$B(V \to P_1 P_2) = \frac{g_{VP_1P_2}^2 |\vec{p}|^3}{6\pi m_V^2 \Gamma_V}\,, \tag{5.18}$$

with a positive sign for $K^* \to K\pi$ and and a negative sign for $\rho \to \pi\pi$. The hadronic form factors f^V and h^V are defined by the $K_1 \to VP$ decay amplitude

$$\mathcal{A}(K_1 \to VP) = \varepsilon_{K_1}^{\mu}(f^V g_{\mu\nu} + h^V p_{V\mu} p_{K_1\nu})\varepsilon_V^{\nu *}\,. \tag{5.19}$$

They have been calculated in [175] using the $^3P_0$ quark pair creation model (QPCM) [177] and are given in appendix D

5.4 Up-down asymmetry

The sensitivity of A_{UD} to the polarization of the photon is determined by the hadronic prefactor in (5.5) For two resonances $a = K_1(1270)$ and $b = K_1(1400)$, the numerator of A_{UD} (5.5) is given by

$$\begin{aligned} \mathrm{Im}[\vec{n} \cdot (\vec{\mathcal{J}} \times \vec{\mathcal{J}}^*)] = -2\mathrm{Im}[&\xi_a^2 C_{1a} C_{2a}^* |BW_a|^2 + \xi_b^2 C_{1b} C_{2b}^* |BW_b|^2 \\ &+ \xi_a \xi_b (C_{1a} C_{2b}^* - C_{2a} C_{1b}^*) BW_a BW_b^*] \, |\vec{p}_1 \times \vec{p}_2|\,, \end{aligned} \tag{5.20}$$

where superscripts and kinematical variables were dropped to simplify the notation. Analogously, the denominator can be written as

$$\begin{aligned} |\vec{\mathcal{J}}|^2 = {} & \xi_a^2 |BW_a|^2 \left(|C_{1a}|^2 |\vec{p}_1|^2 + |C_{2a}|^2 |\vec{p}_2|^2 - 2\mathrm{Re}(C_{1a} C_{2a}^*) \vec{p}_1 \cdot \vec{p}_2\right) \\ & + \xi_b^2 |BW_b|^2 \left(|C_{1b}|^2 |\vec{p}_1|^2 + |C_{2b}|^2 |\vec{p}_2|^2 - 2\mathrm{Re}(C_{1b} C_{2b}^*) \vec{p}_1 \cdot \vec{p}_2\right) \\ & + 2\xi_a \xi_b \mathrm{Re}\left[BW_a BW_b^* \left(C_{1a} C_{1b}^* |\vec{p}_1|^2 + C_{2a} C_{2b}^* |\vec{p}_2|^2 - (C_{1a} C_{2b}^* + C_{2a} C_{1b}^*) \vec{p}_1 \cdot \vec{p}_2\right)\right] \end{aligned} \tag{5.21}$$

Due to isospin symmetry, a permutation of $s_{13} \leftrightarrow s_{23}$ leads to an interchange of the functions $C_1 \leftrightarrow C_2$ for $K_1 \to K^0\pi^+\pi^0$. Since $\mathrm{Im}[\vec{n} \cdot (\vec{\mathcal{J}} \times \vec{\mathcal{J}}^*)] \propto \mathrm{Im}(C_1 C_2^*)$, (5.20) is thus antisymmetric in the $s_{13} - s_{23}$ Dalitz plane as shown in Figure 5.4. The upper plots include only the $K_1(1270)$ resonance and show a Dalitz plot for an invariant mass square of $s = m_{K_1(1270)}^2$. Similarly, the lower plots are made using only the contributions of the $K_1(1400)$ resonance at an invariant mass square of $s = m_{K_1(1400)}^2$. A_{UD} would always vanish due to the integration over the whole $s_{13} - s_{23}$ Dalitz plane. To prevent the cancellation and to obtain a non-zero up-down asymmetry it is necessary to introduce

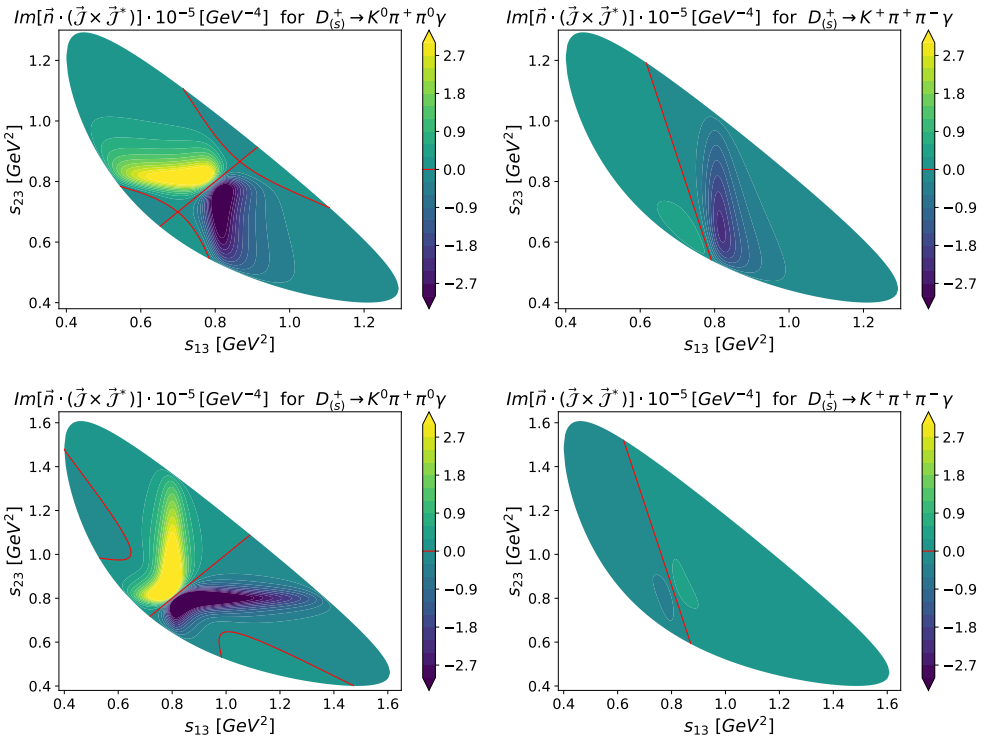

Figure 5.4: Dalitz plots of $\mathrm{Im}[\vec{n}\cdot(\vec{\mathcal{J}}\times\vec{\mathcal{J}}^*)]$ for $K^0\pi^+\pi^0$ (plot to the left) and $K^+\pi^+\pi^-$ (plot to the right) at $s = m^2_{K_1(1270)}$ (upper plots) and $s = m^2_{K_1(1400)}$ (lower plots). The upper and lower plots were made for individual resonances $K_1(1270)$ and $K_1(1400)$, respectively.

the parameter κ in (5.5). The plots on the right-hand side of Figure 5.4 show analogous plots for $K_1 \to K^+\pi^+\pi^-$. Particularly striking is the straight zero line arising from $\mathrm{Im}\left[BW_{K^*}(s_{13})BW^*_\rho(s_{12})\right] = 0$. The exact shape depends on s due to the relation $s_{12}+s_{13}+s_{23} = s + 2m^2_\pi + m^2_K$. This property occurs only in the case of a single K_1 resonance.

On the one hand, the necessary relative strong phases originate from the interferences of the different K_1 resonances. On the other hand, the $C_{1,2}$ functions involve interferences between the $K^*\pi$ and $K\rho$ contributions. The origin of the phases in the QPCM are exclusively the Breit-Wigner functions. The largest imaginary parts are expected for $K_1 \to K^0\pi^+\pi^0$ since there are more interfering amplitudes involved. The smallest imaginary parts are expected if $K_1(1400) \to K^+\pi^+\pi^-$ is considered exclusively, since the $K_1(1400)$ decays mainly into $K^*\pi$. These features are well illustrated in the Dalitz plots in Figure 5.4.

In Figure 5.5, the distributions of $\left\langle|\vec{\mathcal{J}}|^2\right\rangle\cdot PS$ are shown on the left as a function of s. The distributions for the individual resonances $K_1(1270)$ and $K_1(1400)$ are given in black and blue, respectively. For the red, green and orange curves, $\xi_{K_1(1270)} = 1$ is fixed and different values of $\xi_{K_1(1400)} = 0.5, 1, -1$ are used. A comparison of the plots with the measured spectra of $B^+ \to K^+\pi^+\pi^-\gamma$ decays [178–180] suggests a ratio of $\xi_{K_1(1400)}/\xi_{K_1(1270)} \approx +1$.

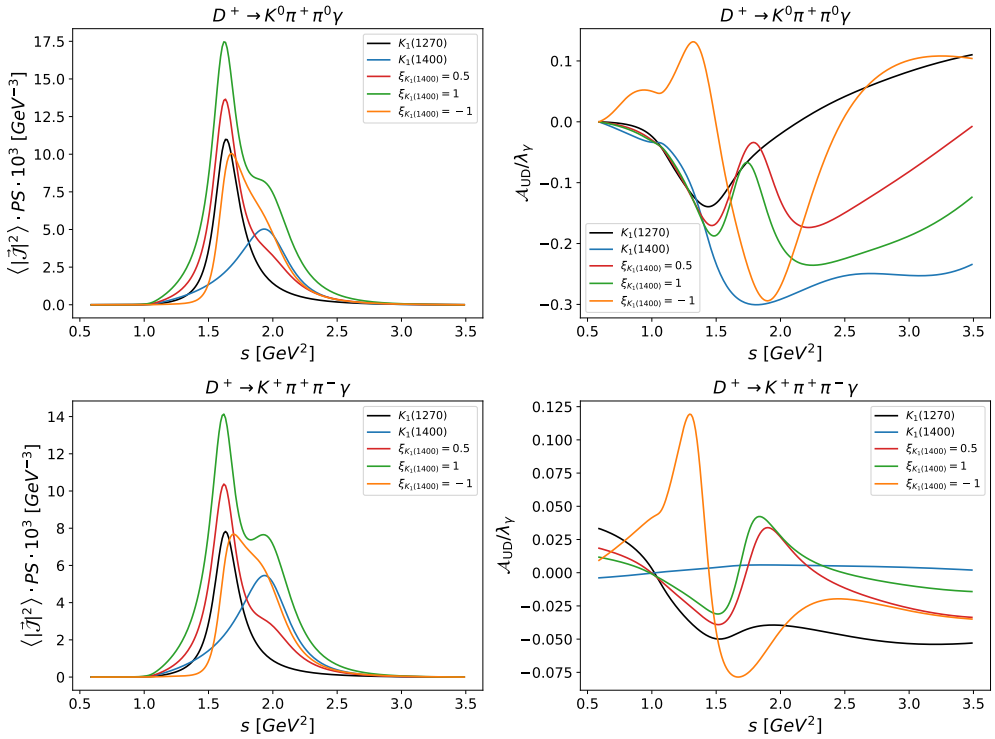

Figure 5.5: $\left\langle|\vec{\mathcal{J}}|^2\right\rangle \cdot PS$ (plots to the left) and $A_{\mathrm{UD}}/\lambda_\gamma$ (plots to the right) as a function of the invariant $K^0\pi^+\pi^0$ (upper plots) and $K^+\pi^+\pi^-$ (lower plots) mass for individual resonances $K_1(1270, 1400)$ and with different relative fraction $\xi_{K_1(1400)}$.

Both distributions exhibit a dominant peak regarding the $K_1(1270)$ resonance as well as a subdominant signal at $\sqrt{s} \approx 1.4\,\mathrm{GeV}$.

On the right-hand side of Figure 5.5, we show A_{UD} in units of λ_γ as a function of s. We consider the same scenarios as for the distributions of $\left\langle|\vec{\mathcal{J}}|^2\right\rangle \cdot PS$. As the Dalitz plots, the distributions confirm the conjecture that larger up-down asymmetries are expected for the final state $K^0\pi^+\pi^0$. A_{UD} can locally obtain values of order $\mathcal{O}(0.2 - 0.3)$. Moreover, A_{UD} is negligibly small for $K^+\pi^+\pi^-$ when only the $K_1(1400)$ resonance is taken into account. In general, up-down asymmetries are of order $\mathcal{O}(0.1)$ for this final state.

The QPCM predicts no further relative phases. However, analyses from the Belle collaboration on $B^+ \to J/\psi K^+\pi^+\pi^-$ and $B^+ \to \psi' K^+\pi^+\pi^-$ decays indicate a non-zero phase

$$\delta_\rho = \arg\left[\frac{\mathcal{A}(K_1(1270) \to (K\rho)_S) \times \mathcal{A}(\rho \to \pi\pi)}{\mathcal{A}(K_1(1270) \to (K^*\pi)_S) \times \mathcal{A}(K^* \to K\pi)}\right] \tag{5.22}$$

of $\delta_\rho = -(43.8 \pm 4.0 \pm 7.3)^\circ$ [178]. A similar conclusion was drawn by the Babar collaboration when they re-analyzed ACCMOR data [181]. They obtain a value of $\delta_\rho = -(31 \pm 1)^\circ$ [182]. Even though such a phase has no appreciable effect on $\left\langle|\vec{\mathcal{J}}|^2\right\rangle$, $\mathrm{Im}[\vec{n} \cdot (\vec{\mathcal{J}} \times \vec{\mathcal{J}}^*)]$ is sensitive to such phases. Therefore, we examine the influence of $\delta_\rho = -40^\circ$ on the up-down asymmetry in Figure 5.6. The solid lines correspond to the predictions from

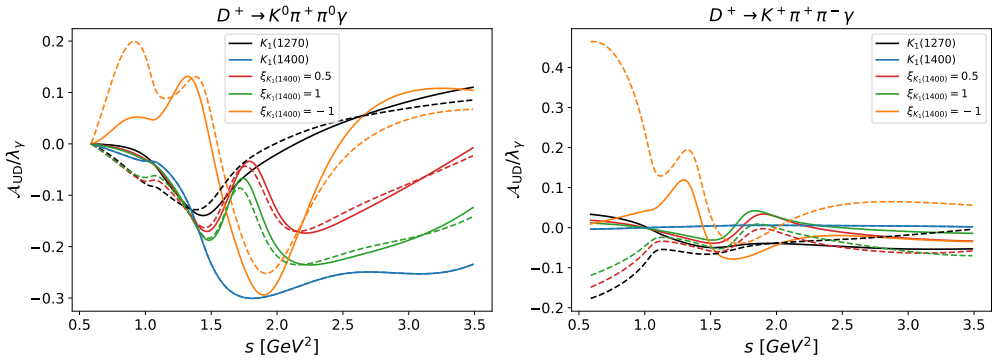

Figure 5.6: $A_{\rm UD}/\lambda_\gamma$ as a function of the invariant $K^0\pi^+\pi^0$ (left plot) and $K^+\pi^+\pi^-$ (right plot) mass for individual resonances $K_1(1270, 1400)$ and with different relative fraction $\xi_{K_1(1400)}$. Solid lines correspond to the pure quark model prediction. Dashed lines illustrate the effect of the additional phase $\delta_\rho = -40^\circ$.

Figure 5.5, while the dashed lines include the additional phase δ_ρ. Analogously, we analyze the influence of an additional phase

$$\delta_D = \arg\left[\frac{\mathcal{A}(K_1(1270) \to (K^*\pi)_D)}{\mathcal{A}(K_1(1270) \to (K^*\pi)_S)}\right] = 90^\circ\,. \tag{5.23}$$

In Figure 5.7, we compare the results of the QPCM with the effects of the additional phase δ_D, which are again indicated by dashed lines. Adding the $\delta_\rho = -40^\circ$ phase has slight effects on the $A_{\rm UD}/\lambda_\gamma$ spectra for $K^0\pi^+\pi^0$. Qualitatively, the shapes of the curves agree well. The largest differences are in the region of small s. The additional peak for $\xi_{K_1(1400)} = -1$ is particularly prominent. However, $A_{\rm UD}/\lambda_\gamma$ remain of order $\mathcal{O}(0.2 - 0.3)$. For $K^+\pi^+\pi^-$, more pronounced changes in the spectra occur, again primarily found in the region of smaller s. Thus, much larger values of the order $\mathcal{O}(0.4)$ can occur locally. The phase δ_D, on the other hand, also has a significant influence on the shape of the distributions for large values of s.

Assuming $K_1(1270)$ dominance, the s-integrated up-down asymmetry yields values in the range of $[-30\%, +2\%]$ and $[-13\%, -2\%]$ for $K^0\pi^+\pi^0$ and $K^+\pi^+\pi^-$, respectively. We note that binning is beneficial to prevent cancellations associated with the sign changes of $A_{\rm UD}$. We emphasize that the estimates have sizable uncertainties. In addition, the used model does not take into account resonances beyond $K_1(1400)$, which yield visible signals in the data of $B^+ \to K^+\pi^+\pi^-\gamma$ [179]. Moreover, the region of high s is expected to be dominated by bremsstrahlung, as it is the case for the three-body decays. Overall, the model oversimplifies the situation for $s \gtrsim 2\,\text{GeV}^2$ and has to be considered as a zeroth order study. However, the estimates indicate that $A_{\rm UD}/\lambda_\gamma$ can at least locally acquire sizable values. Thus, the sensitivity for the null test is given.

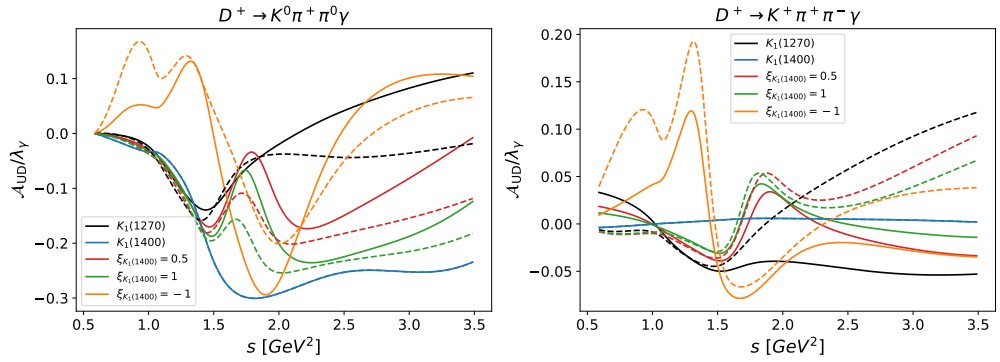

Figure 5.7: $A_{\rm UD}/\lambda_\gamma$ as a function of the invariant $K^0\pi^+\pi^0$ (left plot) and $K^+\pi^+\pi^-$ (right plot) mass for individual resonances $K_1(1270, 1400)$ and with different relative fraction $\xi_{K_1(1400)}$. Solid lines correspond to the pure quark model prediction. Dashed lines illustrate the effect of the additional phase $\delta_D = 90°$.

5.5 Summary

In addition to branching ratios, CP asymmetries, and angular observables, the photon polarization in radiative charm decays is an interesting observable for testing the SM. An extraction of the photon polarization from the angular distribution of D meson decays requires a final state with at least three hadrons. In this chapter we have discussed the up-down asymmetry of $D^+_{(s)} \to K_1^+(\to K\pi\pi)\gamma$, which is proportional to the photon polarization parameter. A direct determination of λ_γ by means of $A_{\rm UD}$ poses the same challenge as in B physics. An exact knowledge of the helicity amplitudes and in particular of all relative phases is required. However, charm physics offers an advantage over B physics. With $D^+ \to K_1^+(\to K\pi\pi)\gamma$ and $D_s \to K_1^+(\to K\pi\pi)\gamma$ there are partner decays, the first of which is SM-like, while the second is an FCNC and thus sensitive to new physics in the electromagnetic dipole operators. Since the helicity amplitudes for both decays are universal, the hadronic prefactor drops out of the ratio of up-down asymmetries. In the SM, the ratio is one in the U-spin limit. Assuming that the photons in the D^+ decay are mainly left-handed polarized ($\lambda_\gamma < -0.5$), as implied by leading order QCDF, all ratios beyond $0.8 \lesssim A_{\rm UD}^{D_s}/A_{\rm UD}^{D^+} = \lambda_\gamma^{D_s}/\lambda_\gamma^{D^+} \lesssim 1.2$ are a hint of new physics in $O_7^{(\prime)}$. The estimate of the BSM potential in Figure 5.3 shows that much larger effects can be obtained with the current limits on $C_7^{(\prime)}$ (3.16).

We used an phenomenological model based on quasi two-body decays to estimate the proportionality factor between the up-down asymmetry and the photon polarization parameter. $A_{\rm UD}/\lambda_\gamma$ is of order $\mathcal{O}(10\%)$ for $K_1^+ \to K^+\pi^+\pi^-$, and in extreme cases even $\mathcal{O}(40\%)$. For $K_1^+ \to K^0\pi^+\pi^0$, the proportionality factor can reach values of $\mathcal{O}(30\%)$, as shown in Figures 5.5-5.7. The uncertainties of these estimates are sizeable, as in B physics, but this does not affect the null test. However, it can be reasonably expected that the sensitivity of $A_{\rm UD}$ to λ_γ is at least given for some bins of the invariant mass squared s.

6 Rare radiative decays of charm baryons

In chapter 5 we have seen that the polarization of photons in rare radiative charm decays is a good observable to test the SM. On the one hand, current limits on the dipole coefficients still allow for huge NP effects. On the other hand, an accurate SM prediction is not necessarily needed to search for NP effects. Instead, it is sufficient to compare the photon polarizations of partner decays, i.e., a SM-like and a BSM sensitive decay mode, which are connected by the $SU(3)_F$ symmetry. Despite the uncertainties of flavor relations of order 30%, this method works as the effects of new physics can be much larger.

However, for D mesons we need at least a four-body decay to access the photon polarization via the angular distribution. Four body decays are both experimentally and theoretically challenging. Although the hadronic prefactor drops out in the ratio of up-down asymmetries (5.6), it determines the sensitivity of the up-down asymmetry to the photon polarization. Moreover, without the exact knowledge of the $K_1 \to K\pi\pi$ helicity amplitude, only a determination of the ratio of the polarizations is possible. If the polarization parameter of the SM-like decay mode is close to zero, U-spin breaking effects can have a huge impact on the ratio $\lambda_\gamma^{D_s}/\lambda_\gamma^{D^+}$.

In comparison, radiative decays of charmed baryons B_c have a great advantage. Due to their spin, the angular distribution of the two-body decay $B_c \to B\gamma$ already depends on the polarization parameter, if the B_c is polarized. For unpolarized charm baryons, the photon polarization can be extracted from the angular distribution of the decay chain $B_c \to B(\to B'P)\gamma$, provided that the B is a weakly decaying hyperon.

Thus, in this chapter weak radiative decays of charmed anti-triplet baryons $B_{c\bar{3}}$ (Λ_c, Ξ_c^+, Ξ_c^0) and sextet baryons B_{c6} (Σ_c^{++}, Σ_c^+, Σ_c^0, $\Xi_c'^+$, $\Xi_c'^0$, Ω_c) are discussed. The analysis is restricted to the spin 1/2 multiplet of the sextet baryons. Furthermore, the emphasis is on decays in the light octet baryons B_8, as the decuplet baryons B_{10} are spin 3/2 baryons which decay strongly and electromagnetically. In section 6.1 we define the decay amplitude and present the long-distance and short distance $c \to u\gamma$ contributions. In section 6.2 we provide flavor relations between the decay amplitudes based on U-spin and $SU(3)_F$, which we use to bypass the difficulty in the calculation of the dominant weak annihilation contributions. We present the observables for the two-body decays $B_c \to B\gamma$ and the decay chains $B_c \to B(\to B'P)\gamma$ in section 6.3 and 6.4, respectively. Beside the photon polarization, branching ratios and CP asymmetries are studied. In 6.5 the BSM reach of branching ratios and the photon polarization is estimated. To conclude, the results are summarized in section 6.6.

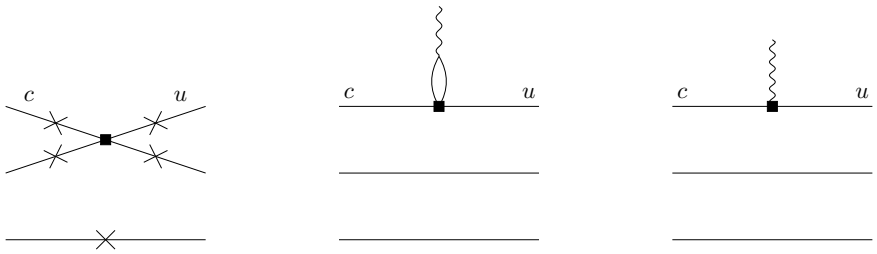

Figure 6.1: Contributions to $B_c \to B\gamma$ decays. The left diagram shows weak annihilation inside the baryons. Possible emissions of photons are marked by crosses. Long distance $c \to u\gamma$ contributions with a photon coupling to the weak current via the light vector mesons ρ^0, ω and ϕ are illustrated in the middle. On the right, short distance $c \to u\gamma$ contributions from the electromagnetic dipole operators $O_7^{(\prime)}$ are shown.

6.1 Decay amplitude

The general Lorentz decomposition of the $B_{c\bar{3}/c6} \to B_8\gamma$ decay amplitude

$$\mathcal{A}(B_c \to B\gamma) = \frac{G_F e}{\sqrt{2}} \bar{u}(q, s_B) \left[F_L P_R + F_R P_L\right] \not{k} \not{\epsilon}^* u(P, s_{B_c}) \tag{6.1}$$

is given in terms of contributions for left-handed photons F_L and right-handed photons F_R. P_L and P_R denote the chiral projectors defined in (2.13). s_{B_c} and s_B refer to the spin of the $B_{c\bar{3}/c6}$ and B_8, respectively. Furthermore, P and q denote the four momenta of the $B_{c\bar{3}/c6}$ and B_8. The four momentum and polarization vector of the photon are labeled as k and ϵ, respectively. Note that in the literature the general Lorentz decomposition is usually given in terms of a parity-even and parity-odd component F_1 and F_2, respectively. The left- and right-handed contributions can be expressed by F_1 and F_2 with the simple relation $F_{L/R} = F_1 \pm F_2$. However, as the emphasis of this chapter is on the photon polarization, the given representation of the decay amplitude is beneficial.

In Fig. 6.1, we show Feynman diagrams for different decay mechanisms contributing to $B_c \to B\gamma$. From the shown decay mechanisms, only weak annihilation contributes to the SM-like CF and DCS decays. Within the SM, the SCS decays are also dominated by WA. At leading order, the WA amplitude scales with the color-allowed coefficient C_-. However, we do not rely on the theory prediction of the weak annihilation amplitude, as theory methods are subject to large uncertainties. Theory predictions [183–185] for the branching ratios and polarizations are summarized in Table 25 of [186]. The branching ratios of the CF decays $\Lambda_c \to \Sigma^+\gamma$ and $\Xi_c^0 \to \Xi^0\gamma$ vary between $0.3 \cdot 10^{-4}$ and $3 \cdot 10^{-4}$. Photon polarizations vary between -0.49 and 0.86. Note that some works did not take into account the Wilson coefficients which enhance the amplitude by C_-. Instead we suggest to extract the contributions from weak annihilation to $F_{L/R}$ from the SM-like decay modes. Subsequently, the flavor relations determined in the next section can be used to estimate the SM contribution of the BSM sensitive SCS decay modes.

The middle diagram in Fig. 6.1 shows the long distance $c \to u\gamma$ contributions where the photon is connected to the weak current via intermediate vector mesons ρ^0, ω and

ϕ. The long distance $c \to u\gamma$ contributions are induced by the four quark operators $O_{1,2}$. A naive combination of the factorization approach $\langle V|(\bar{q}q)_{V-A}|0\rangle \langle B|(\bar{u}c)_{V-A}|B_c\rangle$ and the Lagrangian for $V\gamma$ conversion (4.14) would lead to an amplitude violating $U(1)_{\text{EM}}$ gauge invariance. To prevent the violation of gauge invariance, only the transversal polarized states of the vector mesons may be taken into account. Following [187–189], the longitudinal and transversal parts can be separated using the Gordan identity

$$m_c \bar{u}\gamma^\mu(1-\gamma_5)c = (2P^\mu - q^\mu)\bar{u}(1+\gamma_5)c - i\bar{u}\sigma^{\mu\nu}q_\nu(1+\gamma_5)c\,, \tag{6.2}$$

where terms $\sim m_u$ are neglected. Here, P and q denote the momentum of the c quark and the momentum transfer, respectively. The first and second term vanish for transversal and longitudinal polarization vectors, respectively. Thus, the long distance $c \to u\gamma$ amplitude is described by an operator with tensor structure. The long distance amplitude reads

$$F_L^{\text{LD}} = -2\frac{\tilde{C}C_{\text{VMD}}}{m_c} h_\perp^{B_c\to B}(k^2=0)\,, \qquad F_R^{\text{LD}} = 0\,, \tag{6.3}$$

where $\tilde{C}$ is the color-suppressed combination of Wilson coefficients (3.15) and

$$C_{\text{VMD}} = V_{cs}^* V_{us}\left(-\frac{1}{3}f_\phi^2\right) + V_{cd}^* V_{ud}\left(-\frac{1}{2}f_{\rho^0}^{(d)\,2} + \frac{1}{6}f_\omega^{(d)\,2}\right). \tag{6.4}$$

As in section 4.2.2, we assume that the vector meson decay constants vary only slightly between the mass shell of the mesons and the photon $f_V(k^2=0) \approx f_V(k^2=m_V^2)$. Due to GIM cancellations and similar values for the decay constants, one obtains $C_{\text{VMD}} \approx -6.3\cdot 10^{-4}$ GeV^2 which is about two orders of magnitude smaller than the individual contributions $\lambda f_V^2 \sim 10^{-2}$ GeV^2. Furthermore, $h_\perp^{B_c\to B}$ is the tensor form factor, which is defined in appendix B.4. In writing down (6.5) we used the endpoint relation $h_\perp^{B_c\to B}(k^2=0) = \tilde{h}_\perp^{B_c\to B}(k^2=0)$ of the tensor form factors [190]. For $\Lambda_c \to p$ they are known from lattice QCD [191] and relativistic quark models [192]. Moreover, results from light cone sum rules are available for $\Xi_c \to \Sigma$ [193]. For the estimation of the BSM reach in section 6.5, results from lattice QCD $h_\perp^{\Lambda_c\to p}(k^2=0) = 0.511 \pm 0.027$ and the flavor relations in section 6.2 are used.

Due to the GIM suppression, the long distance contributions are negligible for branching ratios and the photon polarization. The same holds for the SM contributions of the electromagnetic dipole operators, which are shown on the right of Fig. 6.1. However, BSM physics can induce sizable dipole coefficients. The left- and right-handed NP amplitudes are given by

$$\begin{aligned} F_L^{\text{NP}} &= -\frac{m_c}{2\pi^2} C_7 h_\perp^{B_c\to B}(k^2=0)\,, \\ F_R^{\text{NP}} &= -\frac{m_c}{2\pi^2} C_7' h_\perp^{B_c\to B}(k^2=0)\,. \end{aligned} \tag{6.5}$$

6.2 Flavor symmetry relations

In this section the flavor relations between the different decay modes are derived. As stated before, we will focus on the decays of charmed anti-triplet and sextet baryons

into light octet baryons as the decuplet baryons have spin 3/2 and decay strongly and electromagnetically. We will also comment on $B_{c\bar{3}/c6} \to B_{10}\gamma$ in this section. However, group theoretical decompositions of the decay amplitudes and the resulting relations are only given in appendix E.2.3. Once branching ratios and photon polarizations of the SM-like decays are determined experimentally, the left-and right-handed SM amplitudes of the BSM sensitive decay can be estimated using those relations. We use both the approximate $SU(2)_U$ and $SU(3)_F$ symmetries to derive flavor relations between the amplitudes. $SU(2)_{I,U,V}$ and $SU(3)_F$ wave functions are given in Table E.2. We start with the simpler U-spin symmetry. Following [172], we express the SM Lagrangian in terms of U-spin operators

$$\begin{aligned} \mathcal{L}_{\text{eff}}^{\text{CF}} &\propto -V_{cs}^* V_{ud}(1,-1)_U\,, \\ \mathcal{L}_{\text{eff}}^{\text{SCS}} &\propto \sqrt{2}\,(\Sigma(1,0)_U + \Delta(0,0)_U)\,, \\ \mathcal{L}_{\text{eff}}^{\text{DCS}} &\propto V_{cd}^* V_{us}(1,1)_U\,, \end{aligned} \tag{6.6}$$

where $(i,j)_U = \mathcal{O}^{U=i}_{U_3=j}$. i and j denote the total U-spin and the third component of the operator, respectively.

$$\Sigma = \frac{V_{cs}^* V_{us} - V_{cd}^* V_{ud}}{2} \sim \lambda \qquad \text{and} \qquad \Delta = \frac{V_{cs}^* V_{us} + V_{cd}^* V_{ud}}{2} = -\frac{V_{cb}^* V_{ub}}{2} \sim \lambda^5 \tag{6.7}$$

are the CKM leading and subleading combinations of the CKM matrix elements. Due to the CKM suppression, the singlet operator is negligible for branching ratios and the photon polarization. However, it is crutial for SM CP asymmetries as it provides the necessary second CP violating phase. The long distance and short distance $c \to u\gamma$ contributions are also described by an U-spin preserving singlet operator. However, in the following we distinguish between the contributions of the two singlet operators as we consider $O_7^{(\prime)}$ as a source of NP. Furthermore, this allows us to use additional simple isospin relations between amplitudes of dipole operators. Thus, the corresponding Lagrangian for the long distance and short distance $c \to u\gamma$ contributions can be written as

$$\begin{aligned} \mathcal{L}_{\text{eff}}^{c\to u\gamma} &\propto (0,0)_U \\ &\propto (1/2,1/2)_I\,. \end{aligned} \tag{6.8}$$

The general U-spin decompositions of the SM decay amplitudes are given in Table E.3, E.5 and E.11 for $B_{c\bar{3}} \to B_8\gamma$, $B_{c6} \to B_8\gamma$ and $B_{c6} \to B_{10}\gamma$, respectively. For $B_{c\bar{3}} \to B_8\gamma$, two amplitudes are required for both the triplet and singlet operator to parametrize all decay modes. Since the Σ_c^{++} does not decay into $B_8\gamma$, there is no decay of a B_{c6} U-spin singlet, however, the B_{c6} includes the U-spin triplet states (Σ_c^0, $\Xi_c^{\prime 0}$, Ω_c), see Fig. 2.3. With an U-spin triplet in the initial state, both the singlet and triplet component of the Λ and Σ^0 can contribute to the decay amplitude. Thus, a total number of three amplitudes is needed to parametrize the contributions of $(1,j)_U$ operators for $B_{c6} \to B_8\gamma$. For $B_{c6} \to B_{10}\gamma$, the number of independent contributions of the U-spin triplet operators is reduced to two as the Σ^{*0} is a pure triplet state and no spin 3/2 analogue of the Λ is part of the decuplet. However, three amplitudes are needed for the parametrization of $(0,0)_U$ as singlets, doublets and triplets are part of the B_{c6} and B_{10} multiplets. In Table E.4, E.6 and

E.10 the iso- and U-spin decompositions of the $c \to u\gamma$ long distance and short distance contributions are shown. Using U-spin, the same number of independent amplitudes is required to describe the $c \to u\gamma$ contribution as for the SM singlet component. However, the simple isospin structure of (6.8) allows to reduce the number of $c \to u\gamma$ amplitudes to one for each of the categories $B_{c\bar{3}} \to B_8\gamma$, $B_{c6} \to B_8\gamma$ and $B_{c6} \to B_{10}\gamma$.

Similarly, the SM Lagrangians can be written in terms of $SU(3)_F$ operators. In general, four quark operators $(\bar{q}^l \Gamma q_j)(\bar{q}^k \Gamma c)$ with $q_i = (u, d, s)$ decompose as $\mathbf{3} \otimes \overline{\mathbf{3}} \otimes \mathbf{3} = \mathbf{3} \oplus \mathbf{3} \oplus \overline{\mathbf{6}} \oplus \mathbf{15}$. Thus, the Lagrangian consists of $SU(3)_F$ operators with three different representations, where the triplet operator exclusivly appears in SCS transitions. In detail, the Lagrangians for CF, SCS and DCS decays are given by

$$\begin{aligned}
\mathcal{L}_{\text{eff}}^{\text{CF}} &= V_{cs}^* V_{ud} \left(\overline{\mathbf{6}}_{-\frac{2}{3},1,1} + \mathbf{15}_{-\frac{2}{3},1,1} \right) , \\
\mathcal{L}_{\text{eff}}^{\text{SCS}} &= \Sigma \left(\sqrt{2}\, \overline{\mathbf{6}}_{\frac{1}{3},\frac{1}{2},\frac{1}{2}} + \frac{2}{\sqrt{3}} \mathbf{15}_{\frac{1}{3},\frac{1}{2},\frac{1}{2}} - \sqrt{\frac{2}{3}} \mathbf{15}_{\frac{1}{3},\frac{3}{2},\frac{1}{2}} \right) \\
&\quad + \Delta \left(\mathbf{3}_{\frac{1}{3},\frac{1}{2},\frac{1}{2}} + \frac{1}{\sqrt{3}} \mathbf{15}_{\frac{1}{3},\frac{1}{2},\frac{1}{2}} + \sqrt{\frac{2}{3}} \mathbf{15}_{\frac{1}{3},\frac{3}{2},\frac{1}{2}} \right) , \\
\mathcal{L}_{\text{eff}}^{\text{DCS}} &= V_{cd}^* V_{us} \left(-\overline{\mathbf{6}}_{\frac{4}{3},0,0} + \mathbf{15}_{\frac{4}{3},1,0} \right) ,
\end{aligned} \tag{6.9}$$

where $\mathbf{R}_{Y,I,I_3}$ denotes a $SU(3)_F$ operator with irreducible representation $\mathbf{R}$, hypercharge Y and isospin I, I_3. Furthermore, the SM $c \to u\gamma$ contributions refers to the triplet operator $\mathbf{3}_{\frac{1}{3},\frac{1}{2},\frac{1}{2}}$. NP effects by $O_7^{(\prime)}$ are described by an triplett operator with the same quantum numbers. The products of the operators with the $SU(3)_F$ states of the charm baryons decompose into irreducible representations as follows

$$\begin{aligned}
&\mathbf{3} \otimes \overline{\mathbf{3}} = \mathbf{8} \oplus \mathbf{1} , && \mathbf{3} \otimes \mathbf{6} = \mathbf{10} \oplus \mathbf{8} , \\
&\overline{\mathbf{6}} \otimes \overline{\mathbf{3}} = \overline{\mathbf{10}} \oplus \mathbf{8} , && \overline{\mathbf{6}} \otimes \mathbf{6} = \mathbf{27} \oplus \mathbf{8} \oplus \mathbf{1} , \\
&\mathbf{15} \otimes \overline{\mathbf{3}} = \mathbf{27} \oplus \mathbf{10} \oplus \mathbf{8} , && \mathbf{15} \otimes \mathbf{6} = \mathbf{35} \oplus \mathbf{27} \oplus \mathbf{10} \oplus \overline{\mathbf{10}} \oplus \mathbf{8} .
\end{aligned} \tag{6.10}$$

Two important facts can be inferred from the decomposition. On the one hand, the only non-zero contribution to $B_{c\bar{3}} \to B_{10}\gamma$ arises from the **15** operator. Thus, such decays are not suitable for the search for NP in $O_7^{(\prime)}$. On the other hand, the sextet operator does not contribute to $B_{c6} \to B_{10}\gamma$. Therefore, in contrast to U-spin symmetry, only three, three and two independent amplitudes are needed to parametrize the $B_{c\bar{3}} \to B_8\gamma$, $B_{c6} \to B_8\gamma$ and $B_{c6} \to B_{10}\gamma$ decay amplitudes, respectively. In appendix E.2.2 the explicit decompositions for all individual operators and charm baryons are given. $SU(3)$ Clebsch Gordan coefficients are determined using the isoscalar factors from [194]. The $SU(3)_F$ decompositions of the decay amplitudes are shown in Table E.7 and E.8.

Finally, we use the $SU(3)_F$ irreducible representation approach (IRA) to derive the flavor relations. In the $SU(3)_F$ IRA, the effective Lagrangian for $c \to u\gamma$ transitions can be written analogously to [195] as

$$\mathcal{L}_{\text{eff}} = \frac{G_F}{\sqrt{2}} \left(C_- H(\overline{\mathbf{6}})_j^{lk} + C_+ H(\mathbf{15})_j^{lk} + H(\mathbf{3})^l \right) . \tag{6.11}$$

The tensor representation $H(\mathbf{3})^l$ denotes the contributions of triplet operators such as $O_7^{(\prime)}$. For $c \to u$ transitions, the only non zero entry is $H(\mathbf{3})^1 = 1$. The tensor representations $H(\overline{\mathbf{6}})^{lk}_j$ and $H(\mathbf{15})^{lk}_j$ correspond to the operators

$$\mathcal{O}_{\overline{\mathbf{6}}} \propto \left(\bar{q}^l q_j \bar{q}^k - \bar{q}^k q_j \bar{q}^l\right) c\,, \qquad \mathcal{O}_{\mathbf{15}} \propto \left(\bar{q}^l q_j \bar{q}^k + \bar{q}^k q_j \bar{q}^l\right) c\,, \tag{6.12}$$

where we neglected the Lorentz structure to ease the notation. The tensors $H(\overline{\mathbf{6}})^{lk}_j$ and $H(\mathbf{15})^{lk}_j$ are antisymmetric and symmetric in the upper indices, respectively. A set of traceless tensors ($\sum_j H^{ij}_j = \sum_j H^{ji}_j = 0$) which satisfy the conditions are given in [196, 197]. For Cabibbo favored $c \to su\bar{d}$ transitions the non-zero elements are

$$H(\overline{\mathbf{6}})^{31}_2 = -H(\overline{\mathbf{6}})^{13}_2 = 1\,, \qquad H(\mathbf{15})^{31}_2 = H(\mathbf{15})^{13}_2 = 1\,, \tag{6.13}$$

with an overall factor of $V^*_{cs}V_{ud}$. For doubly Cabibbo suppressed $c \to du\bar{s}$ transitions the non-zero elements are

$$-H(\overline{\mathbf{6}})^{21}_3 = H(\overline{\mathbf{6}})^{12}_3 = 1\,, \qquad H(\mathbf{15})^{21}_3 = H(\mathbf{15})^{12}_3 = -1\,, \tag{6.14}$$

with an overall factor of $V^*_{cd}V_{us}$. It turns out that the tensors for SCS decays have more non-zero elements, since the down type quarks have the same flavour and the tensors are traceless. As a consequence also elements whose indices do not match the flavours of the operators in (6.12) obtain non-vanishing entries. The structural differences compared to the CF and DCS transitions can be understood as effects of further decay topologies such as penguin-like diagrams, which are only possible for SCS modes. For $c \to ud\bar{d}$ transitions the non-zero elements are given by

$$\begin{aligned} &H(\overline{\mathbf{6}})^{21}_2 = -H(\overline{\mathbf{6}})^{12}_2 = H(\overline{\mathbf{6}})^{13}_3 = -H(\overline{\mathbf{6}})^{31}_3 = \frac{1}{2}\,, \\ &\frac{1}{3}H(\mathbf{15})^{21}_2 = \frac{1}{3}H(\mathbf{15})^{12}_2 = -\frac{1}{2}H(\mathbf{15})^{11}_1 = -H(\mathbf{15})^{13}_3 = -H(\mathbf{15})^{31}_3 = \frac{1}{4}\,, \end{aligned} \tag{6.15}$$

with an overall factor of $V^*_{cd}V_{ud}$. Analogously, the non.zero elements of the tensors for $c \to us\bar{s}$ transitions read

$$\begin{aligned} &-H(\overline{\mathbf{6}})^{21}_2 = H(\overline{\mathbf{6}})^{12}_2 = -H(\overline{\mathbf{6}})^{13}_3 = H(\overline{\mathbf{6}})^{31}_3 = \frac{1}{2}\,, \\ &-H(\mathbf{15})^{21}_2 = -H(\mathbf{15})^{12}_2 = -\frac{1}{2}H(\mathbf{15})^{11}_1 = \frac{1}{3}H(\mathbf{15})^{13}_3 = \frac{1}{3}H(\mathbf{15})^{31}_3 = \frac{1}{4}\,, \end{aligned} \tag{6.16}$$

with an overall factor of $V^*_{cs}V_{us}$.

The $SU(3)_F$ multiplets of the baryons are also represented as tensors in flavor space. For the charm baryons we obtain

$$B_{c\bar{3}} = (\Xi_c^0, -\Xi_c^+, \Lambda_c)\,, \quad B_{c6} = \begin{pmatrix} \Sigma_c^{++} & \frac{1}{\sqrt{2}}\Sigma_c^+ & \frac{1}{\sqrt{2}}\Xi_c^{\prime +} \\ \frac{1}{\sqrt{2}}\Sigma_c^+ & \Sigma_c^0 & \frac{1}{\sqrt{2}}\Xi_c^{\prime 0} \\ \frac{1}{\sqrt{2}}\Xi_c^{\prime +} & \frac{1}{\sqrt{2}}\Xi_c^{\prime 0} & \Omega_c \end{pmatrix}. \tag{6.17}$$

The light baryon octet B_8 and decuplet B_{10} can be written as

$$B_8 = \begin{pmatrix} \frac{\Lambda}{\sqrt{6}} + \frac{\Sigma^0}{\sqrt{2}} & \Sigma^+ & p \\ \Sigma^- & \frac{\Lambda}{\sqrt{6}} - \frac{\Sigma^0}{\sqrt{2}} & n \\ \Xi^- & \Xi^0 & -\frac{2\Lambda}{\sqrt{6}} \end{pmatrix}, \tag{6.18}$$

$$B_{10} = \frac{1}{\sqrt{3}} \left(\begin{pmatrix} \sqrt{3}\Delta^{++} & \Delta^+ & \Sigma^{*+} \\ \Delta^+ & \Delta^0 & \frac{\Sigma^{*0}}{\sqrt{2}} \\ \Sigma^{*+} & \frac{\Sigma^{*0}}{\sqrt{2}} & \Xi^{*0} \end{pmatrix}, \begin{pmatrix} \Delta^+ & \Delta^0 & \frac{\Sigma^{*0}}{\sqrt{2}} \\ \Delta^0 & \sqrt{3}\Delta^- & \Sigma^{*-} \\ \frac{\Sigma^{*0}}{\sqrt{2}} & \Sigma^{*-} & \Xi^{*-} \end{pmatrix}, \begin{pmatrix} \Sigma^{*+} & \frac{\Sigma^{*0}}{\sqrt{2}} & \Xi^{*0} \\ \frac{\Sigma^{*0}}{\sqrt{2}} & \Sigma^{*-} & \Xi^{*-} \\ \Xi^{*0} & \Xi^{*-} & \sqrt{3}\Omega^- \end{pmatrix} \right).$$

The decay amplitudes are obtained from the sum of all possible contractions of the flavour indices of the tensors H and the baryon tensors. The addends are weighted with generic coefficients that parameterize the decay amplitudes. Thus, the amplitudes can be written as [198]

$$\begin{aligned} \mathcal{A}(B_{c\bar{3}} \to B_8\gamma) = {} & b_1 H(\mathbf{3})^k (B_{c\bar{3}})^{[ij]} (B_8)_{[ij]k} + b_2 H(\mathbf{3})^k (B_{c\bar{3}})^{[ij]} (B_8)_{j[ik]} \\ & + \left(\tilde{b}_1 H(\overline{\mathbf{6}})^{lk}_j + \tilde{b}_4 H(\mathbf{15})^{lk}_j\right) (B_{c\bar{3}})^{[ij]} (B_8)_{k[il]} \\ & + \left(\tilde{b}_2 H(\overline{\mathbf{6}})^{lk}_j + \tilde{b}_5 H(\mathbf{15})^{lk}_j\right) (B_{c\bar{3}})^{[ij]} (B_8)_{l[ik]} \\ & + \left(\tilde{b}_3 H(\overline{\mathbf{6}})^{lk}_j + \tilde{b}_6 H(\mathbf{15})^{lk}_j\right) (B_{c\bar{3}})^{[ij]} (B_8)_{i[lk]}\,, \end{aligned} \tag{6.19}$$

$$\begin{aligned} \mathcal{A}(B_{c6} \to B_8\gamma) = {} & b'_1 H(\mathbf{3})^k (B_{c6})^{ij} (B_8)_{j[ik]} \\ & + \left(\tilde{b}'_1 H(\overline{\mathbf{6}})^{lk}_j + \tilde{b}'_4 H(\mathbf{15})^{lk}_j\right) (B_{c6})^{ij} (B_8)_{k[il]} \\ & + \left(\tilde{b}'_2 H(\overline{\mathbf{6}})^{lk}_j + \tilde{b}'_5 H(\mathbf{15})^{lk}_j\right) (B_{c6})^{ij} (B_8)_{l[ik]} \\ & + \left(\tilde{b}'_3 H(\overline{\mathbf{6}})^{lk}_j + \tilde{b}'_6 H(\mathbf{15})^{lk}_j\right) (B_{c6})^{ij} (B_8)_{i[lk]}\,, \end{aligned} \tag{6.20}$$

$$\mathcal{A}(B_{c6} \to B_{10}\gamma) = b''_1 H(\mathbf{3})^k (B_{c6})^{ij} (B_{10})_{ijk} + \tilde{b}''_1 H(\mathbf{15})^{lk}_j (B_{c6})^{ij} (B_{10})_{ilk}\,, \tag{6.21}$$

where $(B_{c\bar{3}})^{[ij]} = \epsilon^{ijk}(B_{c\bar{3}})_k$ and $(B_8)_{i[jk]} = \epsilon_{jkx}(B_8)_i{}^x$. Due to the symmetry properties of the tensors H, the number of necessary coefficients can be reduced as follows

$$\tilde{b}^{(\prime)}_2 = -\tilde{b}^{(\prime)}_1\,, \quad \tilde{b}^{(\prime)}_4 = \tilde{b}^{(\prime)}_5\,, \quad \tilde{b}^{(\prime)}_6 = 0\,. \tag{6.22}$$

In the following, the explicit determination of an amplitude is shown using the example of $\Lambda_c \to p\gamma$. The relevant elements of the baryon tensors for this decay are $(B_{c\bar{3}})^{[12]} = -(B_{c\bar{3}})^{[21]} = \Lambda_c$ and $(B_8)_{1[12]} = -(B_8)_{1[21]} = p$. Thus, all contractions contributing to $\Lambda_c \to p\gamma$ are given by

$$\begin{aligned} \mathcal{A}(\Lambda_c \to p\gamma) = {} & b_1 H(\mathbf{3})^1 \left((B_{c\bar{3}})^{[12]} (B_8)_{1[12]} + (B_{c\bar{3}})^{[21]} (B_8)_{1[21]}\right) \\ & + b_2 H(\mathbf{3})^1 (B_{c\bar{3}})^{[21]} (B_8)_{1[21]} \\ & + \left(\tilde{b}_1 H(\overline{\mathbf{6}})^{21}_2 + \tilde{b}_4 H(\mathbf{15})^{21}_2\right) (B_{c\bar{3}})^{[12]} (B_8)_{1[12]} \\ & + \left(-\tilde{b}_1 H(\overline{\mathbf{6}})^{12}_2 + \tilde{b}_4 H(\mathbf{15})^{12}_2\right) (B_{c\bar{3}})^{[12]} (B_8)_{1[12]} \\ & + 2\tilde{b}_4 H(\mathbf{15})^{11}_1 (B_{c\bar{3}})^{[21]} (B_8)_{1[21]} \\ & + \tilde{b}_3 \left(H(\overline{\mathbf{6}})^{12}_2 (B_{c\bar{3}})^{[12]} (B_8)_{1[12]} + H(\overline{\mathbf{6}})^{21}_2 (B_{c\bar{3}})^{[12]} (B_8)_{1[21]}\right). \end{aligned} \tag{6.23}$$

Decay	U-Spin	$SU(3)_F$	$SU(3)_F$ IRA
$\Lambda_c \to \Sigma^+\gamma$	$V_{cs}^* V_{ud} A_\Sigma$	$V_{cs}^* V_{ud} B_\Sigma$	$V_{cs}^* V_{ud} D$
$\Xi_c^0 \to \Xi^0\gamma$	$V_{cs}^* V_{ud} A'_\Sigma$	$V_{cs}^* V_{ud} B'_\Sigma$	$V_{cs}^* V_{ud} D'$
$\Lambda_c \to p\gamma$	$-\Sigma A_\Sigma + \Delta A_\Delta + A_7$	$\Sigma B_\Sigma - \Delta B_\Delta + B_7$	$\Sigma D - \Delta \tilde{b}_4 + D_7$
$\Xi_c^+ \to \Sigma^+\gamma$	$\Sigma A_\Sigma + \Delta A_\Delta + A_7$	$-\Sigma B_\Sigma - \Delta B_\Delta + B_7$	$\Sigma D + \Delta \tilde{b}_4 - D_7$
$\Xi_c^0 \to \Lambda\gamma$	$-\sqrt{\frac{3}{2}}\Sigma A'_\Sigma - \frac{1}{2}(\Delta A'_\Delta + A'_7)$	$\sqrt{\frac{3}{2}}\Sigma B'_\Sigma + \sqrt{\frac{3}{2}}\Delta B_\Delta + \frac{1}{\sqrt{6}} B_7$	$-\sqrt{\frac{3}{2}}\Sigma D' + \sqrt{\frac{3}{2}}\Delta \tilde{b}_4 + \frac{1}{\sqrt{6}} D_7$
$\Xi_c^0 \to \Sigma^0\gamma$	$-\frac{1}{\sqrt{2}}\Sigma A'_\Sigma + \frac{\sqrt{3}}{2}(\Delta A'_\Delta + A'_7)$	$-\frac{1}{\sqrt{2}}\Sigma B'_\Sigma + \frac{3}{\sqrt{2}}\Delta B_\Delta + \sqrt{\frac{1}{2}} B_7$	$\frac{1}{\sqrt{2}}\Sigma D' + \frac{3}{\sqrt{2}}\Delta \tilde{b}_4 + \frac{1}{\sqrt{2}} D_7$
$\Xi_c^+ \to p\gamma$	$V_{cd}^* V_{us} A_\Sigma$	$V_{cd}^* V_{us} B_\Sigma$	$V_{cd}^* V_{us} D$
$\Xi_c^0 \to n\gamma$	$-V_{cd}^* V_{us} A'_\Sigma$	$V_{cd}^* V_{us} B'_\Sigma$	$-V_{cd}^* V_{us} D'$

Table 6.1: Comparison of the U-spin, $SU(3)_F$ and $SU(3)_F$ IRA relations for the $B_{c\bar{3}} \to B_8\gamma$ decays. $A_\Sigma^{(\prime)}$ and $A_\Delta^{(\prime)}$ denote to the U-spin triplet and singlet SM contributions of the W-exchange diagrams. $A_7^{(\prime)} = A_{\rm NP}^{(\prime)} + A_{\rm LD}^{(\prime)}$ refers to the $c \to u\gamma$ short distance and long distance contributions with intermediate vector resonances. Note that $A_7^{(\prime)}$ originates from U-spin singlet operators and $A_{\rm LD}^{(\prime)}$ also scales with Δ in the limit $f_\phi = f_\rho^{(d)} = f_\omega^{(d)}$. Furthermore, $A_7 = \sqrt{\frac{2}{3}} A'_7$ in the isospin limit. Analogously, we used the notation $B_\Sigma = \sqrt{\frac{2}{3}} A_{\bar{6}} - \frac{2}{\sqrt{15}} A_{15}$, $B'_\Sigma = \sqrt{\frac{2}{3}} A_{\bar{6}} + \frac{2}{\sqrt{15}} A_{15}$, $B_\Delta = \frac{1}{\sqrt{15}} A_{15}$ and $B_7 = B_{\rm NP} + \Delta A_3$ for the $SU(3)_F$ relations. Similarly, $D = -2(\tilde{b}_1 - \tilde{b}_3 + \tilde{b}_4)$, $D' = 2(\tilde{b}_1 - \tilde{b}_3 - \tilde{b}'_4)$ and $D_7 = 2b_1 + b_2$ denote the W exchange and $c \to u\gamma$ contributions, respectively.

By inserting the tensor elements and replacing the CKM matrix elements by $V_{cd}^* V_{ud} = \Delta - \Sigma$ and $V_{cs}^* V_{us} = \Delta + \Sigma$, we obtain

$$\mathcal{A}(\Lambda_c \to p\gamma) = 2b_1 + b_2 - 2\Sigma(\tilde{b}_1 + \tilde{b}_4 - \tilde{b}_3) - \Delta \tilde{b}_4 \,. \tag{6.24}$$

Note that in some literature, see for instance [195], a simpler construction of $H(\overline{\mathbf{6}}/\mathbf{15})$ is used for the SCS transitions, where the tensors have an analogous structure to the CF and DCS transitions. The additional topologies which are possible for SCS transitions are thus neglected. As expected, however, this only affects the contributions $\propto \Delta$ and is thus just relevant for SM CP violation.

In Table 6.1, 6.2 and E.9, the results for $SU(2)_U$ and $SU(3)_F$ relations are shown. Furthermore, the results are compared with the $SU(3)_F$ IRA. Several differences with regard to the results from [198] become apparent, which are caused by missing contractions in [198].

Based on the relation in Table 6.1 and 6.2, sum rules for the decay amplitudes can be derived. Using the U-spin, relations for CF and SCS decays

$$\begin{aligned} &\mathcal{A}(\Lambda_c \to p\gamma) - \mathcal{A}(\Xi_c^+ \to \Sigma^+\gamma) + 2\frac{\Sigma}{V_{cs}^* V_{ud}} \mathcal{A}(\Lambda_c \to \Sigma^+\gamma) = 0 \,, \\ &\sqrt{3}\mathcal{A}(\Xi_c^0 \to \Lambda\gamma) + \mathcal{A}(\Xi_c^0 \to \Sigma^0\gamma) + 2\sqrt{2}\frac{\Sigma}{V_{cs}^* V_{ud}} \mathcal{A}(\Xi_c^0 \to \Xi^0\gamma) = 0 \,, \end{aligned} \tag{6.25}$$

Decay	U-Spin	$SU(3)_F$	$SU(3)_F$ IRA
$\Sigma_c^+ \to \Sigma^+\gamma$	$V_{cs}^* V_{ud} E_\Sigma$	$V_{cs}^* V_{ud} F_\Sigma$	$V_{cs}^* V_{ud} G$
$\Sigma_c^0 \to \Lambda\gamma$	$V_{cs}^* V_{ud} \left(\frac{\sqrt{3}}{2\sqrt{2}} E'_\Sigma + \frac{1}{2\sqrt{3}} E''_\Sigma\right)$	$-\frac{1}{\sqrt{3}} V_{cs}^* V_{ud} (2F'_\Sigma - F_\Sigma)$	$\frac{1}{\sqrt{3}} V_{cs}^* V_{ud} (2G' - G)$
$\Sigma_c^0 \to \Sigma^0\gamma$	$V_{cs}^* V_{ud} \left(\frac{1}{2\sqrt{2}} E'_\Sigma - \frac{1}{2} E''_\Sigma\right)$	$V_{cs}^* V_{ud} F_\Sigma$	$-V_{cs}^* V_{ud} G$
$\Xi_c'^0 \to \Xi^0\gamma$	$V_{cs}^* V_{ud} \frac{1}{\sqrt{2}} E'_\Sigma$	$V_{cs}^* V_{ud} F'_\Sigma$	$V_{cs}^* V_{ud} G'$
$\Sigma_c^+ \to p\gamma$	$-\Sigma E_\Sigma + \Delta E_\Delta + E_7$	$\Sigma F_\Sigma + \frac{3}{\sqrt{2}} \Delta F_\Delta - F_7$	$\Sigma G + \frac{3}{\sqrt{2}} \Delta \tilde{b}'_4 - G_7$
$\Sigma_c^0 \to n\gamma$	$-\Sigma E'_\Sigma + \Delta E'_\Delta + E'_7$	$\sqrt{2}\Sigma F'_\Sigma - \Delta F_\Delta - \sqrt{2} F_7$	$\sqrt{2}\Sigma G' - \Delta \tilde{b}'_4 - \sqrt{2} G_7$
$\Xi_c'^+ \to \Sigma^+\gamma$	$\Sigma E_\Sigma + \Delta E_\Delta + E_7$	$\Sigma F_\Sigma - \frac{3}{\sqrt{2}} \Delta F_\Delta + F_7$	$\Sigma G - \frac{3}{\sqrt{2}} \Delta \tilde{b}'_4 + G_7$
$\Xi_c'^0 \to \Lambda\gamma$	$\frac{1}{\sqrt{6}} \Sigma E''_\Sigma + \frac{\sqrt{3}}{2} (\Delta E'_\Delta + E'_7)$	$\frac{1}{\sqrt{6}} (2F_\Sigma - F'_\Sigma) - \frac{\sqrt{3}}{2} \Delta F_\Delta - \sqrt{\frac{3}{2}} F_7$	$-\frac{1}{\sqrt{6}} (2G - G') + \frac{\sqrt{3}}{2} \Delta \tilde{b}'_4 + \sqrt{\frac{3}{2}} G_7$
$\Xi_c'^0 \to \Sigma^0\gamma$	$-\frac{1}{\sqrt{2}} \Sigma E''_\Sigma + \frac{1}{2} (\Delta E'_\Delta + E'_7)$	$\frac{1}{\sqrt{2}} \Sigma (2F_\Sigma - F'_\Sigma) + \frac{1}{2} \Delta F_\Delta + \frac{1}{\sqrt{2}} F_7$	$-\frac{1}{\sqrt{2}} \Sigma (2G - G') - \frac{1}{2} \Delta \tilde{b}'_4 - \frac{1}{\sqrt{2}} G_7$
$\Omega_c \to \Xi^0\gamma$	$\Sigma E'_\Sigma + \Delta E'_\Delta + E'_7$	$\sqrt{2}\Sigma F'_\Sigma + \Delta F_\Delta + \sqrt{2} F_7$	$\sqrt{2}\Sigma G' + \Delta \tilde{b}'_4 + \sqrt{2} G_7$
$\Xi_c'^+ \to p\gamma$	$V_{cd}^* V_{us} E_\Sigma$	$-V_{cd}^* V_{us} F_\Sigma$	$V_{cd}^* V_{us} G$
$\Xi_c'^0 \to n\gamma$	$V_{cd}^* V_{us} \frac{1}{\sqrt{2}} E'_\Sigma$	$-V_{cd}^* V_{us} F'_\Sigma$	$V_{cd}^* V_{us} G'$
$\Omega_c \to \Lambda\gamma$	$V_{cd}^* V_{us} \left(\frac{\sqrt{3}}{2\sqrt{2}} E'_\Sigma - \frac{1}{2\sqrt{3}} E''_\Sigma\right)$	$-\sqrt{\frac{1}{3}} V_{cd}^* V_{us} (F_\Sigma + F'_\Sigma)$	$-\sqrt{\frac{1}{3}} V_{cd}^* V_{us} (G + G')$
$\Omega_c \to \Sigma^0\gamma$	$V_{cd}^* V_{us} \left(\frac{1}{2\sqrt{2}} E'_\Sigma + \frac{1}{2} E''_\Sigma\right)$	$-V_{cd}^* V_{us} (F_\Sigma - F'_\Sigma)$	$-V_{cd}^* V_{us} (G - G')$

Table 6.2: Comparison of the U-spin, $SU(3)_F$ and $SU(3)_F$ IRA relations for the $B_{c6} \to B_8\gamma$ decays. Analogously to Table 6.1, $E_\Sigma^{(\prime,\prime\prime)}$, $E_\Delta^{(\prime)}$ and $E_7^{(\prime)}$ refer to the U-spin triplet, U-spin singlet and the $c \to u\gamma$ contributions, respectively. Note that $\sqrt{2}E_7 = E'_7$ in the isospin limit. Analogously, we used the notation $F_\Sigma = \sqrt{\frac{2}{5}} A'_{\overline{6}} - \frac{2}{3\sqrt{5}} A'_{15}$, $F'_\Sigma = \sqrt{\frac{2}{5}} A'_{\overline{6}} + \frac{2}{3\sqrt{5}} A'_{15}$, $F_\Delta = \frac{\sqrt{2}}{3\sqrt{5}} A'_{15}$ and $F_7 = \sqrt{\frac{1}{3}} (F_{\rm NP} + \Delta A'_3)$ for the $SU(3)_F$ relations. Similarly, $G = -\sqrt{2}(\tilde{b}'_1 - \tilde{b}'_3 + \tilde{b}'_4)$, $G' = -\sqrt{2}(\tilde{b}'_1 - \tilde{b}'_3 - \tilde{b}'_4)$ and $G_7 = \frac{1}{\sqrt{2}} b'_1$ denote the weak annihilation and $c \to u\gamma$ contributions in the $SU(3)_F$ IRA. The $SU(3)_F$ and U-spin decompositions are identical up to global signs for $E''_\Sigma = \frac{1}{\sqrt{2}} E'_\Sigma - 2E_\Sigma$ and $E_\Delta = -\frac{3}{\sqrt{2}} E'_\Delta$.

are obtained for charmed anti-triplet baryons and

$$\begin{aligned}
&\mathcal{A}(\Sigma_c^+ \to p\gamma) - \mathcal{A}(\Xi_c'^+ \to \Sigma^+\gamma) + 2\frac{\Sigma}{V_{cs}^* V_{ud}} \mathcal{A}(\Sigma_c^+ \to \Sigma^+\gamma) = 0\,, \\
&\frac{\sqrt{3}}{2} \mathcal{A}(\Sigma_c^0 \to n\gamma) - \mathcal{A}(\Xi_c'^0 \to \Lambda\gamma) + \sqrt{2}\frac{\Sigma}{V_{cs}^* V_{ud}} \mathcal{A}(\Sigma_c^0 \to \Lambda\gamma) = 0\,, \\
&2\mathcal{A}(\Sigma_c^0 \to n\gamma) - \mathcal{A}(\Xi_c'^0 \to \Sigma^0\gamma) - 2\sqrt{2}\frac{\Sigma}{V_{cs}^* V_{ud}} \mathcal{A}(\Sigma_c^0 \to \Sigma^0\gamma) = 0\,, \\
&\mathcal{A}(\Sigma_c^0 \to n\gamma) - \mathcal{A}(\Omega_c \to \Xi^0\gamma) + 2\sqrt{2}\frac{\Sigma}{V_{cs}^* V_{ud}} \mathcal{A}(\Xi_c'^0 \to \Xi^0\gamma) = 0\,.
\end{aligned} \tag{6.26}$$

for the charmed sextet baryons. Note that by neglecting the CKM suppressed contributions $\sim \Delta$, simpler sum rules can be established. Those sum rules only relate two SCS decay modes. However, such sum rules only apply within the SM.

Furthermore, the flavor symmetries connect the $c \to u\gamma$ components of the amplitudes, leading to relations between the hadronic transition form factors. This allows to employ the $\Lambda_c \to p$ form factors from lattice QCD for all $B_{c\bar{3}} \to B_8\gamma$ decay modes. Based on U-spin/isospin, we obtain from Table 6.1

$$-\sqrt{6} h_\perp^{\Xi_c^0 \to \Lambda} = \sqrt{2} h_\perp^{\Xi_c^0 \to \Sigma^0} = h_\perp^{\Xi_c^+ \to \Sigma^+} = h_\perp^{\Lambda_c \to p}\,. \tag{6.27}$$

Currently, none of the $B_{c6} \to B_8\gamma$ form factors are known. Moreover, they cannot be related to the $B_{c\bar{3}} \to B_8\gamma$ form factors as the charm baryons belong to different multiplets. However, at least relations for the sextet decays can be inferred from Table 6.2

$$h_\perp^{\Sigma_c^+\to p} = h_\perp^{\Xi_c'^+\to\Sigma^+} = \frac{1}{\sqrt{2}} h_\perp^{\Sigma_c^0\to n} = \sqrt{\frac{2}{3}} h_\perp^{\Xi_c'^0\to\Lambda} = \sqrt{2} h_\perp^{\Xi_c'^0\to\Sigma^0} = \frac{1}{\sqrt{2}} h_\perp^{\Omega_c\to\Xi^0} \,. \tag{6.28}$$

Note that form factors based on operators with the same U-spin preserving and isospin changing $\bar{u}c$ flavor structure, such as the form factors for semileptonic $c \to u\ell\ell$ transitions, see i.e. [65, 199], obey the same relations. We do not specify the sum rules and form factor relations for $B_{c6} \to B_{10}\gamma$ at this point. However, they can be determined analogously from Table E.9.

The amplitudes of all SCS decay modes exhibit the same structure $x_\Sigma \Sigma X_\Sigma + x_\Delta \Delta X_\Delta + x_7 X_7$. Due to the strong CKM suppression, the terms $\sim \Delta$ are negligible. Thus, the ratio $|x_7/x_\Sigma|$ is a measure for the NP sensitivity. Looking at the $SU(3)_F$ relations in Table 6.1 and 6.2, it becomes evident that this ratio is unity. The only two exceptions are the decays with final state $\Lambda\gamma$. For $\Xi_c^0 \to \Lambda\gamma$ and $\Xi_c'^0 \to \Lambda\gamma$ we obtain 1/3 and 3, respectively. Thus, the sensitivity hierarchie is inverted between the charmed anti-triplet and charm sextet, exhibiting a relative suppression and enhancement for $\Xi_c^0 \to \Lambda\gamma$ and $\Xi_c'^0 \to \Lambda\gamma$, respectively. To conclude, the relative NP sensitivity hierarchy is given by

$$\begin{aligned} &\left|\frac{\mathcal{A}^{\rm NP}(\Lambda_c \to p\gamma)}{\mathcal{A}^{\rm SM}(\Lambda_c \to p\gamma)}\right| \approx \left|\frac{\mathcal{A}^{\rm NP}(\Xi_c^+ \to \Sigma^+\gamma)}{\mathcal{A}^{\rm SM}(\Xi_c^+ \to \Sigma^+\gamma)}\right| \approx \left|\frac{\mathcal{A}^{\rm NP}(\Xi_c^0 \to \Sigma^0\gamma)}{\mathcal{A}^{\rm SM}(\Xi_c^0 \to \Sigma^0\gamma)}\right| > \left|\frac{\mathcal{A}^{\rm NP}(\Xi_c^0 \to \Lambda\gamma)}{\mathcal{A}^{\rm SM}(\Xi_c^0 \to \Lambda\gamma)}\right| , \\ &\left|\frac{\mathcal{A}^{\rm NP}(\Xi_c'^0 \to \Lambda\gamma)}{\mathcal{A}^{\rm SM}(\Xi_c'^0 \to \Lambda\gamma)}\right| > \left|\frac{\mathcal{A}^{\rm NP}(\Sigma_c^+ \to p\gamma)}{\mathcal{A}^{\rm SM}(\Sigma_c^+ \to p\gamma)}\right| \approx \text{remaining sextet decay modes} \,. \end{aligned} \tag{6.29}$$

6.3 Observables of the two-body decay

Rare radiative decays of charm baryons provide a variety of observables. In this section, we review the various observables of the two body decay $B_c \to B\gamma$. In section 6.3.1, we determine the angular distribution, define the polarization parameter and show how it can be measured in two-body decays of polarized charm baryons. In section 6.3.2, we use the flavor relations from 6.2 to determine SM relations between branching ratios of SM-like CF decays and BSM sensitive SCS decays. Finally, we address CP asymmetries in section 6.3.3.

6.3.1 Decay distribution and photon polarization

Since the decay of polarized charm baryons is considered in this section, it is not possible to use the spin-averaged absolute square of the matrix element (6.1) for the calculation of the angular distribution. Instead, each configuration of baryon spins and photon helicity has to be considered explicitly. Therefore, we write the decay amplitude (6.1) in terms of helicity amplitudes

$$\mathcal{A}(B_c \to B\gamma) = \frac{G_F e}{\sqrt{2}} H_1^{h_\gamma}(s_{B_c}, s_B) \,, \tag{6.30}$$

where h_γ denotes the helicity of the photon. Using the explicit spinor representations from [200, 201], four non-zero helicity amplitudes are obtained

$$\begin{aligned} H_1^{-1}\left(+1/2,-1/2\right) &= -\sqrt{2}F_L(m_{B_c}^2 - m_B^2)\sin\left(\theta_\gamma/2\right) , \\ H_1^{-1}\left(-1/2,-1/2\right) &= +\sqrt{2}F_L(m_{B_c}^2 - m_B^2)\cos\left(\theta_\gamma/2\right) , \\ H_1^{+1}\left(+1/2,+1/2\right) &= +\sqrt{2}F_R(m_{B_c}^2 - m_B^2)\cos\left(\theta_\gamma/2\right) , \\ H_1^{+1}\left(-1/2,+1/2\right) &= +\sqrt{2}F_R(m_{B_c}^2 - m_B^2)\sin\left(\theta_\gamma/2\right) . \end{aligned} \tag{6.31}$$

Here, F_L and F_R refer to the contributions for left-handed and right-handed photons, respectively. m_{B_c} and m_B denote the masses of the charm baryon and the octet baryon, respectively. All values are listed in appendix A. The angle θ_γ is between the polarization axis of the spins in the B_c rest frame and the momentum of the photon. The decay probability is given by the sum of the absolute squares of the helicity amplitudes which have to be weighted with a corresponding element of the polarization density matrix ρ [202]

$$w = \frac{G_F^2 e^2}{2} \sum_{h_\gamma, s_{B_c}, s_B} \rho_{s_{B_c}, s_{B_c}} \left| H_1^{h_\gamma}(s_{B_c}, s_B) \right|^2 . \tag{6.32}$$

The polarization density matrix ρ accounts for the imbalance of the spin states for a source of polarized B_c baryons. The diagonal elements of ρ are normalized as $\rho_{+1/2,+1/2} + \rho_{-1/2,-1/2} = 1$ and define the B_c polarization $P_{B_c} = \rho_{+1/2,+1/2} - \rho_{-1/2,-1/2}$. Using the decay probability in (6.32), the differential branching ratio is given by

$$\frac{\mathrm{d}B}{\mathrm{d}\cos(\theta_\gamma)} = \frac{G_F^2 e^2}{64\pi\Gamma_{B_c}} m_{B_c}^3 \left(1 - \frac{m_B^2}{m_{B_c}^2}\right)^3 \left(|F_L|^2 + |F_R|^2\right) \left[1 + P_{B_c}\lambda_\gamma \cos(\theta_\gamma)\right] , \tag{6.33}$$

where Γ_{B_c} is the total decay width of the charm baryon, see appendix A. λ_γ is the photon polarization parameter which is defined analogously to (5.2)

$$\lambda_\gamma = \frac{|F_R|^2 - |F_L|^2}{|F_R|^2 + |F_L|^2} = -\frac{1 - r^2}{1 + r^2} , \qquad r = \left|\frac{F_R}{F_L}\right| . \tag{6.34}$$

Note that we used a different sign convention for the photon polarization parameter than [183–185]. We chose the convention in (6.34) to be consistent with chapter 5. Furthermore, a polarization parameter of $\lambda_\gamma = -1$ corresponds to a purely left-handed photon with helicity $h_\gamma = -1$ in this convention. The angular distribution (6.33) proves that the photon polarization is only accessible if the B_c is polarized. For $P_{B_c} = 0$ the dependence on λ_γ drops out. The total branching ratio is obtained by integrating over the angle θ_γ, whereby the dependence on λ_γ drops out

$$B(B_c \to B\gamma) = \int_{-1}^{+1} \frac{\mathrm{d}B}{\mathrm{d}\cos(\theta_\gamma)} \mathrm{d}\cos(\theta_\gamma) = \frac{G_F^2 e^2}{32\pi\Gamma_{B_c}} m_{B_c}^3 \left(1 - \frac{m_B^2}{m_{B_c}^2}\right)^3 \left(|F_L|^2 + |F_R|^2\right) . \tag{6.35}$$

Thus, branching ratios are not sensitive to the photon polarization. However, the angular dependence of (6.33) allows to define a forward-backward asymmetry in θ_γ

$$A_{\mathrm{FB}}^{\gamma} = \frac{1}{B}\left(\int_0^1 \mathrm{d}\cos(\theta_\gamma)\frac{\mathrm{d}B}{\mathrm{d}\cos(\theta_\gamma)} - \int_{-1}^0 \mathrm{d}\cos(\theta_\gamma)\frac{\mathrm{d}B}{\mathrm{d}\cos(\theta_\gamma)}\right) = \frac{P_{B_c}\lambda_\gamma}{2}\,, \tag{6.36}$$

which only depends on P_{B_c} and λ_γ. One way to measure A_{FB}^{γ} is via the average longitudinal momentum $\left\langle k_\parallel \right\rangle_\beta$ of the photon in the lab frame with respect to the B_c boost axis [203]

$$\left\langle k_\parallel \right\rangle_\beta = \gamma E_\gamma(\beta + \frac{2}{3}A_{\mathrm{FB}}^{\gamma})\,, \tag{6.37}$$

where $E_\gamma = (m_{B_c}^2 - m_B^2)/(2m_{B_c})$ is the photon energy in the B_c rest frame and $\beta = |\vec{P}|/E_{B_c}$.

6.3.2 Flavor relations for standard model branching ratios

The flavor relations from section 6.2 can be used to determine relations between branching ratios. Neglecting the strongly CKM suppressed contributions $\propto \Delta$, the SM amplitude of SCS decays only depends on the contributions X_Σ, just like the CF and DCS modes. Thus, SM predictions for the branching ratios of SCS decays can be made based on the CF modes. Furthermore, hierarchies can be identified. Based on Table 6.1 and the differences in life times, phase space factors and CKM elements, the branching ratios of the SCS decays of charmed anti-triplet baryons can be written as

$$\begin{aligned}
B(\Lambda_c \to p\gamma) &\approx \lambda^2 \frac{(m_{\Lambda_c}^2 - m_p^2)^3}{(m_{\Lambda_c}^2 - m_{\Sigma^+}^2)^3} B(\Lambda_c \to \Sigma^+\gamma) \approx 0.072 \cdot B(\Lambda_c \to \Sigma^+\gamma)\,,\\
B(\Xi_c^+ \to \Sigma^+\gamma) &\approx \lambda^2 \frac{m_{\Lambda_c}^3 \Gamma_{\Lambda_c}}{m_{\Xi_c^+}^3 \Gamma_{\Xi_c^+}} \frac{(m_{\Xi_c^+}^2 - m_{\Sigma^+}^2)^3}{(m_{\Lambda_c}^2 - m_{\Sigma^+}^2)^3} B(\Lambda_c \to \Sigma^+\gamma) \approx 0.160 \cdot B(\Lambda_c \to \Sigma^+\gamma)\,,\\
B(\Xi_c^0 \to \Lambda\gamma) &\approx \frac{3\lambda^2}{2} \frac{(m_{\Xi_c^0}^2 - m_\Lambda^2)^3}{(m_{\Xi_c^0}^2 - m_{\Xi^0}^2)^3} B(\Xi_c^0 \to \Xi^0\gamma) \approx 0.104 \cdot B(\Xi_c^0 \to \Xi^0\gamma)\,,\\
B(\Xi_c^0 \to \Sigma^0\gamma) &\approx \frac{\lambda^2}{2} \frac{(m_{\Xi_c^0}^2 - m_{\Sigma^0}^2)^3}{(m_{\Xi_c^0}^2 - m_{\Xi^0}^2)^3} B(\Xi_c^0 \to \Xi^0\gamma) \approx 0.030 \cdot B(\Xi_c^0 \to \Xi^0\gamma)\,.
\end{aligned} \tag{6.38}$$

Flavor relations cannot be used to relate $\Lambda_c \to \Sigma^+\gamma$ and $\Xi_c^0 \to \Xi^0\gamma$. However, in the $SU(3)_F$ limit, the amplitudes of the CF decays only differ by the sign of A_{15}. As A_{15} is suppressed by a smaller Wilson coefficient compared to $A_{\overline{6}}$, we assume $B_\Sigma \approx B'_\Sigma$. Thus, we expect only small differences in the branching ratios as

$$\frac{B(\Lambda_c \to \Sigma^+\gamma)}{B(\Xi_c^0 \to \Xi^0\gamma)} \approx \frac{m_{\Xi_c^0}^3 \Gamma_{\Xi_c^0}}{m_{\Lambda_c}^3 \Gamma_{\Lambda_c}} \frac{(m_{\Lambda_c}^2 - m_{\Sigma^+}^2)^3}{(m_{\Xi_c^0}^2 - m_{\Xi^0}^2)^3} \approx 1.1\,. \tag{6.39}$$

Based on the prefactors in (6.38) and the ratio (6.39), the largest branching ratios are expected for $\Xi_c^+ \to \Sigma^+\gamma$. Subsequently, $\Xi_c^0 \to \Lambda\gamma$ and $\Lambda_c \to p\gamma$ have the second and third

largest branching ratios, respectively. The suppression compared to the CF decays is about one order of magnitude. The smallest branching ratio is obtained for $\Xi_c^0 \to \Sigma^0\gamma$ with a suppression factor of $\sim 3\%$.

Analogously, relations for the decays $B_{c6} \to B_8\gamma$ are obtained using Table 6.2

$$\begin{aligned}
B(\Sigma_c^+ \to p\gamma) &\approx \lambda^2 \frac{(m_{\Sigma_c^+}^2 - m_p^2)^3}{(m_{\Sigma_c^+}^2 - m_{\Sigma^+}^2)^3} B(\Sigma_c^+ \to \Sigma^+\gamma) \approx 0.070 \cdot B(\Sigma_c^+ \to \Sigma^+\gamma)\,, \\
B(\Xi_c'^+ \to \Sigma^+\gamma) &\approx \lambda^2 \frac{m_{\Sigma_c^+}^3 \Gamma_{\Sigma_c^+}}{m_{\Xi_c'^+}^3 \Gamma_{\Xi_c'^+}} \frac{(m_{\Xi_c'^+}^2 - m_{\Sigma^+}^2)^3}{(m_{\Sigma_c^+}^2 - m_{\Sigma^+}^2)^3} B(\Sigma_c^+ \to \Sigma^+\gamma)\,, \\
B(\Sigma_c^0 \to n\gamma) &\approx 2\lambda^2 \frac{m_{\Xi_c'^0}^3 \Gamma_{\Xi_c'^0}}{m_{\Sigma_c^0}^3 \Gamma_{\Sigma_c^0}} \frac{(m_{\Sigma_c^0}^2 - m_n^2)^3}{(m_{\Xi_c'^0}^2 - m_{\Xi^0}^2)^3} B(\Xi_c'^0 \to \Xi^0\gamma)\,, \\
B(\Omega_c \to \Xi^0\gamma) &\approx 2\lambda^2 \frac{m_{\Xi_c'^0}^3 \Gamma_{\Xi_c'^0}}{m_{\Omega_c}^3 \Gamma_{\Omega_c}} \frac{(m_{\Omega_c}^2 - m_{\Xi^0}^2)^3}{(m_{\Xi_c'^0}^2 - m_{\Xi^0}^2)^3} B(\Xi_c'^0 \to \Xi^0\gamma)\,.
\end{aligned} \tag{6.40}$$

Note that no relations for $\Xi_c'^0 \to \Lambda\gamma$ and $\Xi_c'^0 \to \Sigma^0\gamma$ are given, since two SM-like decays are necessary to construct their amplitudes. Furthermore, the decay widths of the Ξ_c' are unknown up to now. Thus, we cannot evaluate the prefactors for the last three relations. However, the branching ratios $\Xi_c', \Sigma_c \to B\gamma$ are strongly suppressed by large total widths as Ξ_c' and Σ_c decay strongly and electromagnetically, respectively. Thus, decays of charmed anti-triplet baryons have significantly larger branching ratios. For example, $\Sigma_c^+ \to \Sigma^+\gamma$ has a relative suppression of $\Gamma_{\Lambda_c}/\Gamma_{\Sigma_c^+} > 7 \cdot 10^{-10}$ compared to $\Lambda_c \to \Sigma^+\gamma$ due to a significant difference in the decay widths. The only exception among the charmed sextet baryons is the Ω_c which exclusively decays weakly. Thus, the $\Omega_c \to B\gamma$ decay should have significantly larger branching ratios $\sim B(B_{c\bar{3}} \to B_8\gamma)$. For the decays of charmed sextet baryons into decuplet baryons, we obtain by using Table E.9

$$\begin{aligned}
B(\Sigma_c^{++} \to \Delta^{++}\gamma) &\approx \frac{3}{2}\lambda^{10} \frac{m_{\Sigma_c^+}^3 \Gamma_{\Sigma_c^+}}{m_{\Sigma_c^{++}}^3 \Gamma_{\Sigma_c^{++}}} \frac{(m_{\Sigma_c^{++}}^2 - m_{\Delta^{++}}^2)^3}{(m_{\Sigma_c^+}^2 - m_{\Sigma^{*+}}^2)^3} B(\Sigma_c^+ \to \Sigma^{*+}\gamma) \\
&\lesssim 1.7 \cdot 10^{-6} \cdot B(\Sigma_c^+ \to \Sigma^{*+}\gamma)\,, \\
B(\Sigma_c^+ \to \Delta^+\gamma) &\approx \lambda^2 \frac{(m_{\Sigma_c^+}^2 - m_{\Delta^+}^2)^3}{(m_{\Sigma_c^+}^2 - m_{\Sigma^{*+}}^2)^3} B(\Sigma_c^+ \to \Sigma^{*+}\gamma) \approx 0.067 \cdot B(\Sigma_c^+ \to \Sigma^{*+}\gamma)\,, \\
B(\Sigma_c^0 \to \Delta^0\gamma) &\approx 2\lambda^2 \frac{(m_{\Sigma_c^0}^2 - m_{\Delta^0}^2)^3}{(m_{\Sigma_c^0}^2 - m_{\Sigma^{*0}}^2)^3} B(\Sigma_c^0 \to \Sigma^{*0}\gamma) \approx 0.133 \cdot B(\Sigma_c^0 \to \Sigma^{*0}\gamma)\,, \\
B(\Xi_c'^+ \to \Sigma^{*+}\gamma) &\approx \lambda^2 \frac{m_{\Sigma_c^+}^3 \Gamma_{\Sigma_c^+}}{m_{\Xi_c'^+}^3 \Gamma_{\Xi_c'^+}} \frac{(m_{\Xi_c'^+}^2 - m_{\Sigma^{*+}}^2)^3}{(m_{\Sigma_c^+}^2 - m_{\Sigma^{*+}}^2)^3} B(\Sigma_c^+ \to \Sigma^{*+}\gamma)\,, \\
B(\Xi_c'^0 \to \Sigma^{*0}\gamma) &\approx \frac{1}{2}\lambda^{10} \frac{(m_{\Xi_c'^0}^2 - m_{\Sigma^{*0}}^2)^3}{(m_{\Xi_c'^0}^2 - m_{\Xi^{*0}}^2)^3} B(\Xi_c'^0 \to \Xi^{*0}\gamma) \approx 2.2 \cdot 10^{-7} B(\Xi_c'^0 \to \Xi^{*0}\gamma)\,, \\
B(\Omega_c \to \Xi^{*0}\gamma) &\approx 2\lambda^2 \frac{m_{\Sigma_c^0}^3 \Gamma_{\Sigma_c^0}}{m_{\Omega_c}^3 \Gamma_{\Omega_c}} \frac{(m_{\Omega_c}^2 - m_{\Xi^{*0}}^2)^3}{(m_{\Sigma_c^0}^2 - m_{\Sigma^{*0}}^2)^3} B(\Sigma_c^0 \to \Sigma^{*0}\gamma) \approx 9.7 \cdot 10^7 B(\Sigma_c^0 \to \Sigma^{*0}\gamma)\,,
\end{aligned} \tag{6.41}$$

where the first relation is only valid in $SU(3)_F$. Note that the SM branching ratios of $\Sigma_c^{++} \to \Delta^{++}\gamma$ and $\Xi_c'^0 \to \Sigma^{*0}\gamma$ are strongly CKM suppressed as they do not receive a X_Σ contribution. Thus, they are sensitive to NP in the dipole operators. However, the Ξ_c' and Σ_c decay modes are probably unusable due to the large total decay widths.

6.3.3 CP asymmetries

For a two-body decay, the CP asymmetry is defined by

$$A_{\rm CP} = \frac{|A|^2 - |\bar{A}|^2}{|A|^2 + |\bar{A}|^2}\,, \tag{6.42}$$

where $\bar{A}$ is the amplitude of the CP-conjugated decay. In the SM, the only origin of a CP violating phase is the CKM matrix. Due to its structure, the CP violation is negligible in charm decays. By neglecting terms $\mathcal{O}(\Delta^2/\Sigma^2)$, the SM CP asymmetry can be written as

$$A_{\rm CP}^{\rm SM} \approx {\rm Im}\left(\frac{-2\Delta}{\Sigma}\right) {\rm Im}\left(\frac{A_\Delta}{A_\Sigma}\right) \approx -6\times 10^{-4}\ {\rm Im}\left(\frac{A_\Delta}{A_\Sigma}\right)\,. \tag{6.43}$$

Thus, CP asymmetries of order $\mathcal{O}(10^{-4} - 10^{-3})$ are expected at most in the SM. However, beyond the SM, CP asymmetries can be significantly larger due to new sources of CP violating phases. Taking into account the constraints from $\Delta A_{\rm CP}$ (3.19) and neglecting the contributions X_Δ, the factor including the weak phases becomes

$$\left|{\rm Im}\left(\frac{-2C_7^{(\prime)}}{\Sigma}\right)\right| \lesssim 2\cdot 10^{-2}\,. \tag{6.44}$$

This is equivalent to an increase of the CP-violation by a factor of ~ 30. Note that the CP violation can be enhanced even more by bypassing the constraints from $\Delta A_{\rm CP}$. Thus, percent level CP asymmetries are possible beyond the SM.

Furthermore, the flavor relations can be used to derive sum rules for the CP asymmetries. Based on Table 6.1, 6.2 and E.9, we obtain the following sum rules for the $B_{c\bar{3}} \to B_8\gamma$ decays

$$\begin{aligned} &A_{\rm CP}(\Lambda_c \to p\gamma) + A_{\rm CP}(\Xi_c^+ \to \Sigma^+\gamma) = 0\,,\\ &A_{\rm CP}(\Xi_c^0 \to \Sigma^0\gamma) + 3A_{\rm CP}(\Xi_c^0 \to \Lambda\gamma) = 0\,, \end{aligned} \tag{6.45}$$

the $B_{c6} \to B_8\gamma$ decays

$$\begin{aligned} &A_{\rm CP}(\Sigma_c^+ \to p\gamma) + A_{\rm CP}(\Xi_c'^+ \to \Sigma^{*+}\gamma) = 0\,,\\ &A_{\rm CP}(\Sigma_c^0 \to n\gamma) + A_{\rm CP}(\Omega_c \to \Xi^0\gamma) = 0\,,\\ &A_{\rm CP}(\Xi_c'^0 \to \Lambda\gamma) + 3A_{\rm CP}(\Xi_c'^0 \to \Sigma^0\gamma) = 0\,, \end{aligned} \tag{6.46}$$

and the $B_{c6} \to B_{10}\gamma$ decays

$$\begin{aligned} &A_{\rm CP}(\Sigma_c^+ \to \Delta^+\gamma) + A_{\rm CP}(\Xi_c'^+ \to \Sigma^+\gamma) = 0\,,\\ &A_{\rm CP}(\Sigma_c^0 \to \Delta^0\gamma) + A_{\rm CP}(\Omega_c \to \Xi^{*0}\gamma) = 0\,. \end{aligned} \tag{6.47}$$

The sum rules are valid in both $SU(2)_U$ and $SU(3)_F$. Furthermore, the sum rules are valid within the SM and beyond, since the electromagnetic dipole operators are $(0,0)_U$ operators. Thus, the X_7 obey the same flavor relations as the X_Δ. Therefore, the sum rules cannot be used to test the SM, but to test the precision of the flavor symmetries. Note that the sum rules reflect the inverted NP sensitivity hierarchy between $B_{c\bar{3}} \to B_8\gamma$ and $B_{c6} \to B_8\gamma$ decays, see (6.29).

6.4 Photon polarization in the decay chain $B_c \to B(\to B'P)\gamma$

Section 6.3.1 has pointed out that the polarization of the photon can be extracted from the two-body decay $B_c \to B\gamma$ only if the initial state baryon is polarized. For unpolarized B_c, there is another method for extracting λ_γ, which uses the decay chain $B_c \to B(\to B'P)\gamma$. Here, B has to be a weakly decaying hyperon and P denotes a pseudoscalar meson. The $B \to B'P$ decay amplitude is given by [200]

$$\mathcal{A}(B \to B'P) = N\bar{u}(q, s_B)\,(\xi\gamma_5 + \omega)\,u(q_1, s_{B'}) = N H_2(s_B, s_{B'})\,, \tag{6.48}$$

where q and q_1 denote the momenta of B and B', respectively. Analogously, s_B and $s_{B'}$ refer to the spin of the initial and final state baryon. ξ and ω denote contributions of opposite parity. For weak hyperon decays the normalization is given by $\frac{4G_F}{\sqrt{2}}V_{ud}^*V_{us}$. Analogously to (6.30), the decay amplitude can be written in terms of helicity amplitudes [200]

$$\begin{aligned}
H_2(+1/2,+1/2) &= (\sqrt{r_+}\omega - \sqrt{r_-}\xi)\cos(\theta_B/2)\,,\\
H_2(+1/2,-1/2) &= (\sqrt{r_+}\omega + \sqrt{r_-}\xi)\sin(\theta_B/2)e^{i\phi_B}\,,\\
H_2(-1/2,+1/2) &= (-\sqrt{r_+}\omega + \sqrt{r_-}\xi)\sin(\theta_B/2)e^{-i\phi_B}\,,\\
H_2(-1/2,-1/2) &= (\sqrt{r_+}\omega + \sqrt{r_-}\xi)\cos(\theta_B/2)\,,
\end{aligned} \tag{6.49}$$

where θ_B denotes the angle between the B and B' momenta in the $B'P$ rest frame. ϕ_B is the corresponding azimuth angle. The differential branching ratio is calculated using a decay probability similarly to (6.32)

$$\frac{\mathrm{d}B}{\mathrm{d}\cos(\theta_B)} = \frac{|N|^2\sqrt{r_+r_-}}{32\pi m_B^3\Gamma_B}\left(r_+|\omega|^2 + r_-|\xi|^2\right)\left(1 + P_B\alpha_B\cos(\theta_B)\right)\,. \tag{6.50}$$

Here, $r_\pm$ are kinematical functions depending on the masses $r_\pm = (m_B \pm m_{B'})^2 - m_P^2$. P_B is the polarization of the initial state baryon B. Furthermore, the parity violating parameter is given by

$$\alpha_B = \frac{-2Re(\omega^*\xi)}{\sqrt{\frac{r_-}{r_+}}|\xi|^2 + \sqrt{\frac{r_+}{r_-}}|\omega|^2}\,. \tag{6.51}$$

The double differential branching ratio of the decay chain $B_c \to B(\to B'P)\gamma$ is given by

$$\frac{\mathrm{d}^2B}{\mathrm{d}\cos(\theta_\gamma)\mathrm{d}\cos(\theta_B)} \propto \left[1 + P_{B_c}\alpha_B\cos(\theta_\gamma)\cos(\theta_B) + \alpha_B\lambda_\gamma\cos(\theta_B) + P_{B_c}\lambda_\gamma\cos(\theta_\gamma)\right]\,, \tag{6.52}$$

Decay	B	α_B
$\Lambda(1116) \to p\pi^-$	$(63.9 \pm 0.5)\%$	0.732 ± 0.014
$\Sigma^+(1189) \to p\pi^0$	$(51.57 \pm 0.30)\%$	-0.982 ± 0.014
$\Xi^0(1315) \to \Lambda\pi^0$	$(99.52 \pm 0.012)\%$	-0.356 ± 0.011

Table 6.3: Branching ratio B and parity violating parameter α_B of weakly decaying hyperons [103]. The $\Xi^-(1322)$, which is dominantly decaying into $\Lambda\pi^-$ with a sizable parity violating parameter, is not produced in rare charm baryon decays.

where the normalization can be inferred from $B(B_c \to B(\to B'P)\gamma) = B(B_c \to B\gamma)B(B \to B'P)$. The angular distribution (6.52) provides two different ways to determine the photon polarization. On the one hand, by integrating over θ_B we get the same angular distribution as in (6.33). Thus, as in the case of two-body decays, we can determine λ_γ by means of $A_{\rm FB}^\gamma$ if the charm baryon is polarized. On the other hand, the same angular dependence as in (6.50) emerges when integrating over θ_γ. However, since the non-zero helicity amplitudes (6.31) of right- and left-handed photons are always accompanied by a baryon spin of $s_B = +1/2$ and $s_B = -1/2$, respectively, P_B and λ_γ coincide. Therefore, the obtained angular distribution depends on λ_γ, while being independent of the polarization of the charm baryon. Thus, λ_γ can be extracted by a forward-backward asymmetry in θ_B

$$A_{\rm FB}^B = \frac{1}{B}\left(\int_0^1 \mathrm{d}\cos(\theta_B)\frac{\mathrm{d}B}{\mathrm{d}\cos(\theta_B)} - \int_{-1}^0 \mathrm{d}\cos(\theta_B)\frac{\mathrm{d}B}{\mathrm{d}\cos(\theta_B)}\right) = \frac{\alpha_B\lambda_\gamma}{2}\,. \tag{6.53}$$

Note that the secondary baryon B has to decay weakly for $\alpha_B \neq 0$. Thus, the spin 3/2 baryons of the decuplet can only be used to study branching ratios, CP violation and $A_{\rm FB}^\gamma$. In Table 6.3 we provide branching ratios and parity violating parameters for all weakly decaying hyperons which are relevant for rare radiative charm decays.

6.5 Estimates of the BSM reach

After defining the observables and explaining different ways to determine them in section 6.3 and 6.4, this section estimates the scope of new physics. Since none of the $B_{c6} \to B_8$ tensor form factors is known, we omit estimates for the $B_{c6} \to B_8\gamma$ decays and restrict the analysis to $B_{c\bar{3}} \to B_8\gamma$. However, the procedure would be the same. Once the branching ratios $B^{\rm CF}$ and polarization parameters $\lambda_\gamma^{\rm CF}$ of the CF decays are experimentally determined, we can extract the left and right handed amplitudes $F_{L/R}^{\rm CF}$. First, the polarization parameter is used to calculate the ratio of the right- and left-handed amplitude

$$r^{\rm CF} = \sqrt{\frac{1+\lambda_\gamma^{\rm CF}}{1-\lambda_\gamma^{\rm CF}}}\,. \tag{6.54}$$

Subsequently, $F_{L/R}^{\rm CF}$ can be determined using $r^{\rm CF}$ and the branching ratio $B^{\rm CF}$

$$|F_L^{\rm CF}| = \sqrt{\frac{B^{\rm CF}}{C^{\rm CF}(1+(r^{\rm CF})^2)}}\,, \qquad |F_R^{\rm CF}| = r^{\rm CF}\sqrt{\frac{B^{\rm CF}}{C^{\rm CF}(1+(r^{\rm CF})^2)}}\,. \tag{6.55}$$

Here, C^{CF} is the proportionality factor defined by

$$B^{\mathrm{CF}} = C^{\mathrm{CF}}(|F_L^{\mathrm{CF}}|^2 + |F_R^{\mathrm{CF}}|^2)\,, \tag{6.56}$$

which includes couplings, masses and total widths. The factor C^{CF} can be inferred from (6.35). After the determination of $F_{L/R}^{\mathrm{CF}}$, the SM amplitudes of the SCS decays are obtained by applying the flavor symmetry relations from Table 6.1 and 6.2. For example, by dividing the $\Xi_c^0 \to \Xi^0\gamma$ amplitude by $V_{cs}^* V_{ud}$ and then multiplying by $-\sqrt{\frac{3}{2}}\Sigma$, the $\Xi_c^0 \to \Lambda\gamma$ amplitudes $F_{L/R}^{\mathrm{SCS}}$ are obtained. Note that the DCS decay channels can also be used to calculate the SM amplitudes. (6.55) shows that we can only determine the modulus of the left- and right-handed amplitudes. Thus, the phase is uncertain. However, the SM weak phase is negligible and since we vary the dipole coefficients between -0.3 and 0.3 when estimating the BSM reach, the unknown sign does not affect our results.

Since neither branching ratios nor photon polarizations have been measured so far and predictions of different theory methods greatly differ, see Table 25 of [186], we base our benchmark $B^{\mathrm{CF}} = 5 \cdot 10^{-41}$ on the measured branching ratio $B(D^0 \to \overline{K}^{*0}\gamma) = (4.1 \pm 0.7) \cdot 10^{-4}$ [103]. Compared to the resonant decays $D \to V\gamma$, the leading order WA contribution for $B_c \to B\gamma$ is enhanced by a factor of $C_-/\tilde{C}$. However, the hadronic matrix elements may be subject to a suppression as indicated by the theory predictions [183–185]. Furthermore, we use $\lambda_\gamma^{\mathrm{CF}} = -0.5$ as an assumption.

The branching ratios of the SCS decays is affected by NP contributions and can be written as

$$B^{\mathrm{SCS}} = C^{\mathrm{SCS}}(|F_L^{\mathrm{SCS}} + F_L^{\mathrm{NP}}|^2 + |F_R^{\mathrm{SCS}} + F_R^{\mathrm{NP}}|^2)\,. \tag{6.57}$$

The ratio of right- and left-handed amplitudes is altered by NP effects as well

$$r^{\mathrm{SCS}} = \left|\frac{F_R^{\mathrm{SCS}} + F_R^{\mathrm{NP}}}{F_L^{\mathrm{SCS}} + F_L^{\mathrm{NP}}}\right|\,, \tag{6.58}$$

which gives the polarization parameter

$$\lambda_\gamma^{\mathrm{SCS}} = -\frac{1 - (r^{\mathrm{SCS}})^2}{1 + (r^{\mathrm{SCS}})^2}\,. \tag{6.59}$$

The SM is tested by comparing B^{CF} and B^{SCS} or $\lambda_\gamma^{\mathrm{CF}}$ and $\lambda_\gamma^{\mathrm{SCS}}$. In the exact U-spin limit, the polarization parameters are identical. The relations for the SM branching ratios were discussed in section 6.3.2.

In Fig. 6.2 the NP potential in branching ratios of the BSM sensitive SCS decays is shown as a function of the branching ratio of the CF partner decay. The SM prediction in the exact U-spin limit is illustrated by the black dashed line. The impact of $\pm 30\%$ U-spin breaking effects on both F_L^{SCS} and F_R^{SCS} are included in the gray shaded area. The BSM reach in C_7 ($C_7' = 0$) and C_7' ($C_7 = 0$) is shown in blue and green. Besides the variation in the dipole coefficients, these regions also include the 30% U-spin breaking of the SM amplitudes. The plots show a greater impact of C_7 than C_7' as we used a fixed polarization parameter of the CF decay of $\lambda_\gamma^{\mathrm{CF}} = -0.5$.

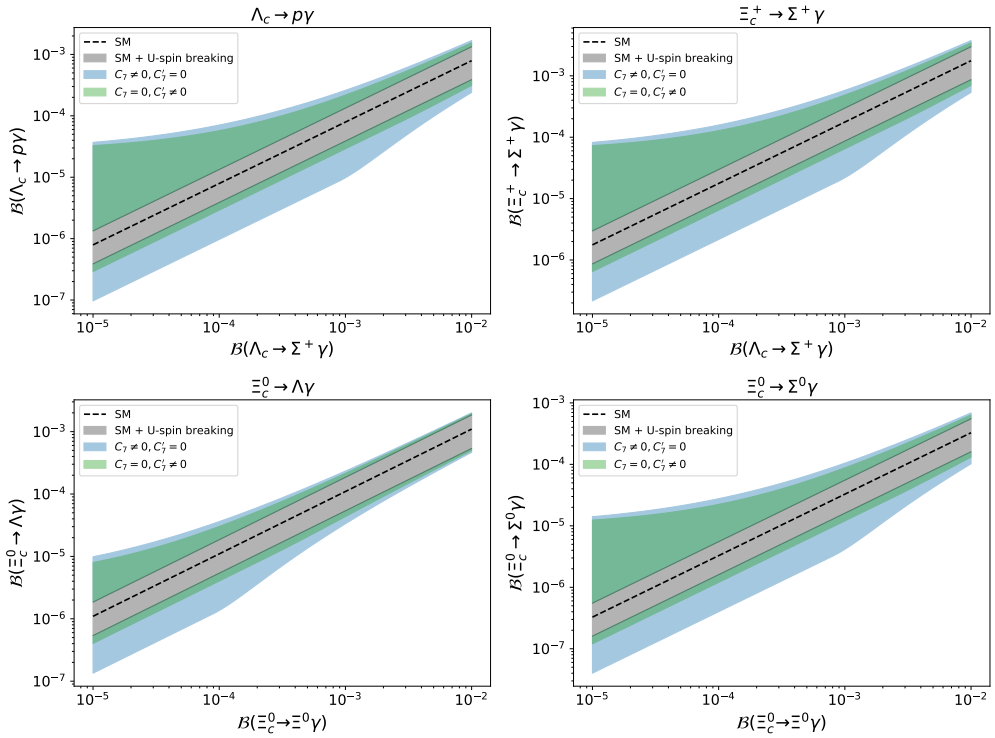

Figure 6.2: NP potential in the branching ratios of the BSM sensitive decay modes as a function of the branching ratios of the CF partner decay. The polarization parameter is fixed to $\lambda_\gamma^{\rm CF} = -0.5$. The black dashed line refers to the SM in the exact U-spin limit. $\pm 30\%$ U-spin breaking effects on $\mathcal{A}_{L/R}^{\rm SM}$ are illustrated by the gray shaded area. The blue (green) region shows the BSM reach in C_7 (C_7'). We set $C_7' = 0$ ($C_7 = 0$) and varied the other coefficient within $-0.3 \leq C_7^{(\prime)} \leq 0.3$. The BSM regions also take the $\pm 30\%$ U-spin breaking of the SM amplitudes into account.

Analogously, the BSM reach of the polarization parameter $\lambda_\gamma^{\rm SCS}$ is shown in Fig. 6.3 as a function of the polarization parameter of the partner decay. Again, the black dashed line shows the SM prediction in the exact U-spin limit. As the U-spin breaking effects should reduce in the ratio of right- and left-handed amplitudes, the impact of $\pm 20\%$ U-spin braking between $r_{\rm SM}^{\rm CF}$ and $r_{\rm SM}^{\rm SCS}$ [1] is shown by the gray shaded area. The NP potential in C_7 ($C_7' = 0$) and C_7' ($C_7 = 0$) is shown in blue and green. For the darker shaded area, we used the exact U-spin limit for the SM amplitudes. The lighter shaded area includes $\pm 30\%$ U-spin breaking in $F_{L/R}^{\rm SM}$, while keeping the U-spin breaking of the ratio $r_{\rm SM}^{\rm SCS}$ limited to $\pm 20\%$.

It turns out that both branching ratios and photon polarization can be altered by physics beyond the SM beyond the level of $SU(3)_F$ breaking effects. In particular, λ_γ shows good sensitivity to NP. With the current limits on the dipole coefficients, most of

[1] After the submission of the thesis, the first upper limts of $B(\Lambda_c \to \Sigma^+\gamma) < 2.6 \cdot 10^{-4}$ and $B(\Xi_c^0 \to \Xi^0\gamma) < 1.7 \cdot 10^{-4}$ were published by Belle II [204].

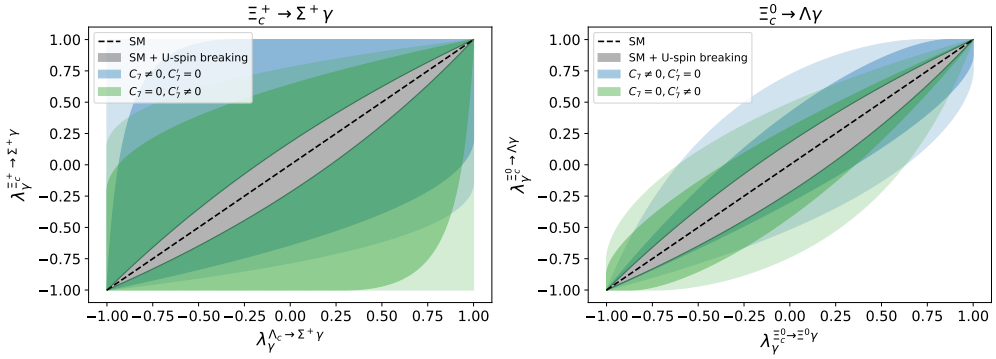

Figure 6.3: NP potential of λ_γ of the BSM sensitive decay modes $\Xi_c^+ \to \Sigma^+\gamma$ (left) and $\Xi_c^0 \to \Lambda\gamma$ (right) as a function of the photon polarization of the CP partner decay $\Lambda_c \to \Sigma^+\gamma$ and $\Xi_c^0 \to \Xi^0\gamma$, respectively. The branching ratios of the partner modes are fixed to $B^{\rm CF} = 5 \cdot 10^{-4}$. The black dashed line refers to the SM in the exact U-spin limit. $\pm 20\%$ U-spin breaking between $r_{\rm SM}^{\rm CF}$ and $r_{\rm SM}^{\rm SCS}$ are illustrated by the gray shaded area. The blue (green) region illustrates the BSM reach in C_7 (C_7'). We set $C_7' = 0$ ($C_7 = 0$) and varied the other coefficient within $-0.3 \leq C_7^{(\prime)} \leq 0.3$. For the darker shaded area we used the exakt U-spin limit of the SM amplitudes. The lighter shaded area includes $\pm 30\%$ U-spin breaking in $F_{L/R}^{\rm SM}$, while keeping the U-spin breaking of the ratio $r_{\rm SM}^{\rm SCS}$ limited to $\pm 20\%$. The BSM reach of $\Lambda_c \to p\gamma$ and $\Xi_c^0 \to \Sigma^0\gamma$ is not shown as it coincides with $\Xi_c^+ \to \Sigma^+\gamma$.

the phase space is still possible with the chosen benchmark. In general, the sensitivity to new physics decreases with increasing branching ratios $B^{\rm CF}$. Furthermore, the sensitivity in the individual dipole coefficients depends on the SM polarization. Both observables reflect the sensitivity hierarchy (6.29).

6.6 Summary

Rare radiative decays of charm baryons offer a variety of observables including branching ratios, CP asymmetries and photon polarizations. A precise theoretical prediction within the SM is currently not possible, since theory methods lack sufficient control. Thus, flavor symmetries are crucial as they allow to extract the SM amplitudes from CF and DCS decays. Although subject to significant systematic uncertainties of $\sim 30\%$, $SU(2)_U$ and $SU(3)_F$ relations are a key ingredient, as current limits on NP allow for much larger effects.

Currently none of the weak radiative charm baryon decay modes have been observed. Thus, an analysis of BSM sensitive decays regarding new physics is not possible yet. Instead, the sensitivity to new physics can be estimated as functions of SM-like decays.

NP effects can alter the branching ratios beyond the level of $SU(3)_F$ breaking effects, see Fig. 6.2. The sensitivity to physics beyond the SM strongly depends on the branching ratio of the partner decays. The BSM reach is suppressed for increasing $B^{\rm CF}$.

BSM sensitive (SCS) decay	CF decay
$\Xi_c^+ \to \Sigma^+\gamma$	$\Lambda_c \to \Sigma^+\gamma$
$\Xi_c^0 \to \Lambda\gamma$	$\Xi_c^0 \to \Xi^0\gamma$
$\Omega_c \to \Xi^0\gamma$	$\Xi_c'^0 \to \Xi^0\gamma$
$\Xi_c'^+ \to \Sigma^+\gamma$	$\Sigma_c^+ \to \Sigma^+\gamma$
$\Xi_c'^0 \to \Lambda\gamma$	$\Sigma_c^0 \to \Lambda\gamma$, $\Xi_c'^0 \to \Xi^0\gamma$

Table 6.4: Partner modes which can be analyzed using the decay chains $B_c \to B(\to B'P)\gamma$ and the U-spin relations in Table 6.1 and 6.2. Only self-analyzing secondary baryons (Λ, Σ^+, Ξ^0) are included.

BSM sensitive (SCS) decay	CF decay	DCS decays
$\Lambda_c \to p\gamma$	$\Lambda_c \to \Sigma^+\gamma$	$\Xi_c^+ \to p\gamma$
$\Xi_c^0 \to \Sigma^0\gamma$	$\Xi_c^0 \to \Xi^0\gamma$	$\Xi_c^0 \to n\gamma$
$\Omega_c \to \Xi^0\gamma$	-	$\Omega_c \to \Lambda\gamma$, $\Omega_c \to \Sigma^0\gamma$

Table 6.5: Additional partner modes including non self-analyzing secondary baryons. Thus, the decay chain $B_c \to B(\to B'P)\gamma$ cannot be used for all decay modes to determine the photon polarization. Decays of Σ_c and Ξ_c' are excluded as they are probably unusable due to their large total decay widths.

CP asymmetries serve as null test as $A_{\rm CP}^{\rm SM}$ is subject to strong parametric suppression. Within the SM, CP asymmetries of order $\mathcal{O}(10^{-4} - 10^{-3})$ are expected at most. The flavor symmetries yield sum rules for $A_{\rm CP}$ which are valid in both, the SM and beyond. Thus, they cannot be used to test the SM. However, they can be used to validate the flavor relations.

We stress the possibility to test the SM by measuring the photon polarization of partner decays using the decay chain $B_c \to B(\to B'P)\gamma$, which is possible for both polarized and unpolarized charm baryons if the secondary baryon B is a weakly decaying hyperon. Fig. 6.3 shows the SM prediction including U-spin breaking effects as well as the BSM reach. A list of partner decays which allow to measure the photon polarizations using the decay chains with self-analyzing secondary baryons is provided in Table 6.4. Two partner decays are needed to extract the SM amplitude E_Σ'' for the SCS decay $\Xi_c'^0 \to \Lambda\gamma$. Note that partner decays including Ξ_c' and Σ_c are probably unusable due to the suppression of the branching ratios based on the large decay widths. Thus, the decays of charmed sextet baryons are unfavorable. Furthermore, the SCS decay $\Xi_c^+ \to \Sigma^+\gamma$ and the corresponding CF partner decay $\Lambda_c \to \Sigma^+\gamma$ are preferable due to the NP sensitivity hierarchy.

In case of polarized charm baryons, the photon polarization can also be determined for decays into non self-analyzing baryons. A list of partner decays excluding the Ξ_c^0 and Σ_c is provided in Table 6.5. The SCS decay $\Omega_c \to \Xi^0\gamma$ is disadvantageous as two DCS partner decays are required to extract the SM amplitude.

Branching ratios of rare radiative charm anti-triplet baryon decays are expected to be comparable with those of D mesons. The fragmentation fractions and the corresponding number of charm baryons for current and future e^+e^- colliders, which are shown in Table

B_c	$f(c \to h_c)$	$N(h_C)$ FCC-ee	$N(h_C)$ Belle II
Λ_c	0.06	$\sim 3 \cdot 10^{10}$	$\sim 4 \cdot 10^9$
Ξ_c^+	0.00024	$\sim 1 \cdot 10^8$	$\sim 1 \cdot 10^7$
Ξ_c^0	0.00024	$\sim 1 \cdot 10^8$	$\sim 1 \cdot 10^7$
Ω_c	0.004	$\sim 2 \cdot 10^9$	$\sim 2 \cdot 10^8$

Table 6.6: Charm fragmentation fractions $f(c \to B_c)$ [168] and number of charmed baryons for $c\bar{c}$ production rates of $550 \cdot 10^9$ (FCC-ee) and $65 \cdot 10^9$ (Belle II with $50\,\text{ab}^{-1}$) [81].

6.6, are significantly smaller compared to charm mesons (see Table 4.3). Thus, the number of unreconstructed events is also decreased. Based on our benchmark $B^{\text{CF}} = 5 \cdot 10^{-4}$, we expect only ~ 10 unreconstructed events for the DCS decays $\Xi_c^+ \to p\gamma$ and $\Xi_c^0 \to n\gamma$ at Belle II. However, those decays are not mandatory for the proposed test of the SM and can be replaced by CF modes with significantly larger production rates. The only DCS decay modes which cannot be replaced by CF ones are $\Omega_c \to \Lambda\gamma$ and $\Omega_c \to \Sigma^0\gamma$. which are mandatory to determine the SM amplitude of the SCS decay $\Omega_c \to \Xi^0\gamma$.

7 Conclusion and Outlook

This thesis presents different opportunities to test the SM with radiative $|\Delta c| = |\Delta u| = 1$ transitions beyond the resonant decays $D \to V\gamma$ and $D \to A\gamma$. Chapter 2 summarizes the SM and introduces the approximate symmetries of QCD which are a key ingredient for studying radiative charm decays. Furthermore, searches for physics beyond the SM are motivated. Subsequently, chapter 3 discusses the concept of weak effective theory. The effective Lagrangian for $c \to u\gamma$ transitions is given together with the SM Wilson coefficients. Current bounds on the electromagnetic dipole coefficients are summarized.

In chapter 4, radiative three body decays $D \to PP\gamma$ are discussed. Low's theorem, HHχPT and leading order QCD factorization have been used to calculate the decay amplitude for all 18 decays with $P = \pi, K$ which are induced by dimension six operators. HHχPT form factors have been worked out including the resonance contributions for all decay channels. (Differential) branching ratios, the forward-backward asymmetry and CP asymmetries are determined within the SM and in different BSM scenarios. The main results can be summarized as follows, see also section 4.6:

- Decay distributions are dominated by resonances and bremsstrahlung.
- Branching ratios can be affected by new physics in the region of the s-channel resonance. However, a separation of new physics effects is challenging in view of hadronic uncertainties. Branching ratios of CF and DCS modes can be used to validate the used theory models.
- Forward-backward asymmetries exhibit significant qualitative differences between SM prediction and BSM scenarios in some cases. The most reasonable $c \to u\gamma$ modes to search for new physics are $D^0 \to \pi^+\pi^-\gamma$, $D^+ \to \pi^+\pi^0\gamma$ and $D_s \to \pi^+K^0\gamma$ as they provide the greatest impact of NP contributions and smallest SM uncertainties. However, it is difficult to claim sensitivity to new physics effects due to the intrinsic uncertainty of the Breit Wigner approach and the complicated interplay of s-, t- and u-channel contributions. Therefore, SM-like modes should be utilized beforehand to estimate the accuracy of the predictions. For this purpose $D^0 \to \pi^0\overline{K}^0\gamma$, $D_s \to \pi^+\pi^0\gamma$ and $D^+ \to K^+\pi^0\gamma$ are suitable as they provide small uncertainties and a disinctive shape which is reasonably well understood.
- CP asymmetries provide a null-test of the SM due to negligible CP violating phases in the charm sector of the SM. Dalitz plots are suitable to search for new physics in all SCS decay modes. For the singly differential CP asymmetries, $D^+ \to \pi^+\pi^0\gamma$ and $D_s \to \pi^+K^0\gamma$ are the most suitable as they are sensitive to both dipole coefficients and not subject to cancellations between t- and u-channel contributions.

In chapter 5, a SM test using the photon polarization in $D^+_{(s)} \to K_1^+(\to K\pi\pi)\gamma$ decays is discussed. The polarization parameter can be extracted from an up-down asymmetry,

analogously to $B \to K_1(\to K\pi\pi)\gamma$ decays. However, precise knowledge of the helicity amplitudes and all relativ phases is needed for the extraction. Charm physics is advantageous as partner decay exist. $D^+ \to K_1^+(\to K\pi\pi)\gamma$ is SM-like and $D_s \to K_1^+(\to K\pi\pi)\gamma$ is a BSM sensitive FCNC transition. Due to the universality of the helicity amplitudes, the ratio of their up-down asymmetries coincides with the ratio of the polarization parameters, which is equal to one within the SM up to U-spin breaking corrections. Thus, a significant deviation of the ratio from one may be an indication of new physics in the dipole operators.

Finally, rare radiative decays of charm baryons are discussed in chapter 6. To bypass the difficulties in the calculation of the weak annihilation contributions, flavor symmetries can be used to extract the SM amplitudes of the BSM sensitive decays from SM-like partner decays. Flavor relations have been worked out for $B_{c\bar{3}} \to B_8\gamma$, $B_{c6} \to B_8\gamma$ and, for completeness, $B_{c6} \to B_{10}\gamma$. Estimates of the NP potential are provided for branching ratios, CP asymmetries and photon polarizations. The main results can be summarized as follows, see also section 6.6:

- Decays of Ξ_c' and Σ_c are unusable as they decay strongly and electromagnetically, respectively.
- NP effects can alter branching ratios beyond the level of $SU(3)_F$ breaking effects.
- CP asymmetries serve as null test within the SM. NP can enhance CP asymmetries up to few percent.
- A comparison of the photon polarizations in SM-like and BSM sensitive partner decays serve as null test of the SM. Within the SM, they are identical up to $SU(3)_F$ breaking effects.
- For unpolarized charm baryons, the photon polarizations can be determined using the decay chains $B_c \to B(\to B'P)\gamma$ with self-analyzing secondary baryons. The BSM sensitive decays $\Xi_c^+ \to \Sigma^+\gamma$ and $\Xi_c^0 \to \Lambda\gamma$ are suitable for this type of analysis. The corresponding partner decays are $\Lambda_c \to \Sigma^+\gamma$ and $\Xi_c^0 \to \Xi^0\gamma$. For $\Xi_c^+ \to \Sigma^+\gamma$, a better sensitivity for new physics is expected.
- In case of polarized charm baryons, the determination of the photon polarization is also possible for the BSM sensitive decays $\Lambda_c \to p\gamma$, $\Xi_c^0 \to \Sigma^0\gamma$, $\Omega_c \to \Xi^0\gamma$ and their partner decays, allowing further null tests of the SM

Charm decays provide the opportunity to test the flavor structure in the up-type sector of the SM. Precise calculations of the SM contributions are challenging with current methods. This is due to systematic problems such as poor convergence of α_s and heavy quark expansion as well as dominant resonance contributions. This makes it difficult to distinguish between SM and BSM physics in simple observables such as branching ratios. However, these problems can be circumvented with specific observables, which serve as a null test of the SM, and (approximate) symmetries of the SM. Radiative decays complement searches for new physics with $D^0 - \overline{D}^0$-mixing, hadronic, semileptonic and dineutrino decays.

So far, no weak radiative charm decays beyond the resonant two-body decays of D mesons have been observed. Experimental searches in all modes and observables are

desirable as they allow to improve our understanding of QCD, valididate theoretical methods and models and search for new physics in the up-type sector of the SM. With branching ratios of order $\mathcal{O}(10^{-7} - 10^{-3})$, radiative charm decays are not only in reach of current and future experiments such as LHCb, Belle II, BES III, Super charm-tau factory and FCC, but also allow analyses with decent statistics.

A Parameters

Masses m, mean life times τ and decay widths $\Gamma = \frac{\hbar}{\tau}$, where $\hbar = 6.582119569 \cdot 10^{-25}\,\mathrm{GeV}\cdot\mathrm{s}$ is the reduced Planck constant, are taken from the PDG [103]. Upper limits refer to a 90% confidence level. Parameters are provided with uncertainties. However, the uncertainties are negligible for the numerical evaluation in this thesis. The parameters for the mesons are given by

$$
\begin{aligned}
&m_{\pi^0} = (0.1349768 \pm 0.0000005)\,\mathrm{GeV}\,, \\
&m_{\pi^\pm} = (0.13957039 \pm 0.0000018)\,\mathrm{GeV}\,, \\
&m_{\eta} = (0.547862 \pm 0.000017)\,\mathrm{GeV}\,, \\
&m_{\eta'} = (0.95778 \pm 0.00006)\,\mathrm{GeV}\,, \\
&m_{K^0} = (0.497611 \pm 0.000013)\,\mathrm{GeV}\,, \\
&m_{K^\pm} = (0.493677 \pm 0.000016)\,\mathrm{GeV}\,, \\
&m_{\rho} = (0.77526 \pm 0.00023)\,\mathrm{GeV}\,, && \Gamma_{\rho} = (0.1474 \pm 0.0008)\,\mathrm{GeV}\,, \\
&m_{\omega} = (0.78266 \pm 0.00013)\,\mathrm{GeV}\,, && \Gamma_{\omega} = (0.00868 \pm 0.00013)\,\mathrm{GeV}\,, \\
&m_{\phi} = (1.019461 \pm 0.000016)\,\mathrm{GeV}\,, && \Gamma_{\phi} = (0.004249 \pm 0.000013)\,\mathrm{GeV}\,, \\
&m_{K^{*0}} = (0.89555 \pm 0.00020)\,\mathrm{GeV}\,, && \Gamma_{K^{*0}} = (0.0473 \pm 0.0005)\,\mathrm{GeV}\,, \\
&m_{K^{*\pm}} = (0.89267 \pm 0.00026)\,\mathrm{GeV}\,, && \Gamma_{K^{*\pm}} = (0.0514 \pm 0.0008)\,\mathrm{GeV}\,, \\
&m_{K_1(1270)} = (1.253 \pm 0.007)\,\mathrm{GeV}\,, && \Gamma_{K_1(1270)} = (0.090 \pm 0.020)\,\mathrm{GeV}\,, \\
&m_{K_1(1400)} = (1.403 \pm 0.007)\,\mathrm{GeV}\,, && \Gamma_{K_1(1400)} = (0.174 \pm 0.013)\,\mathrm{GeV}\,, \\
&m_{D^0} = (1.86484 \pm 0.00005)\,\mathrm{GeV}\,, && \tau_{D^0} = (4.101 \pm 0.015) \cdot 10^{-13}\,\mathrm{s}\,, \\
&m_{D^+} = (1.86966 \pm 0.00005)\,\mathrm{GeV}\,, && \tau_{D^+} = (1.040 \pm 0.007) \cdot 10^{-12}\,\mathrm{s}\,, \\
&m_{D_s} = (1.96835 \pm 0.00007)\,\mathrm{GeV}\,, && \tau_{D_s} = (5.04 \pm 0.04) \cdot 10^{-13}\,\mathrm{s}\,.
\end{aligned}
\tag{A.1}
$$

The mass of the η_8 is obtained from the Gell-Mann-Okubo mass formula [104, 205]

$$
m_{\eta_8} = \sqrt{\frac{4m_K^2 - m_\pi^2}{3}} = (0.56929 \pm 0.00003)\,\mathrm{GeV}\,. \tag{A.2}
$$

Masses, lifetimes and decay widths for the charm baryons are given by

$$
\begin{aligned}
&m_{\Lambda_c} = (2.28646 \pm 0.00014)\,\text{GeV}\,, && \tau_{\Lambda_c} = (2.024 \pm 0.031) \cdot 10^{-13}\,\text{s}\,,\\
&m_{\Xi_c^+} = (2.46794^{+0.00017}_{-0.00020})\,\text{GeV}\,, && \tau_{\Xi_c^+} = (4.56 \pm 0.05) \cdot 10^{-13}\,\text{s}\,,\\
&m_{\Xi_c^0} = (2.47090^{+0.00022}_{-0.00029})\,\text{GeV}\,, && \tau_{\Xi_c^0} = (1.53 \pm 0.06) \cdot 10^{-13}\,\text{s}\,,\\
&m_{\Sigma_c^{++}} = (2.45397 \pm 0.00014)\,\text{GeV}\,, && \Gamma_{\Sigma_c^{++}} = (0.00185 \pm 0.00014)\ \text{GeV}\,,\\
&m_{\Sigma_c^+} = (2.4529 \pm 0.0004)\,\text{GeV}\,, && \Gamma_{\Sigma_c^+} < 0.0046\ \text{GeV}\,,\\
&m_{\Sigma_c^0} = (2.45375 \pm 0.00014)\,\text{GeV}\,, && \Gamma_{\Sigma_c^0} = (0.00179 \pm 0.00015)\ \text{GeV}\,,\\
&m_{\Xi_c'^+} = (2.5782 \pm 0.0005)\,\text{GeV}\,,\\
&m_{\Xi_c'^0} = (2.5787 \pm 0.0005)\,\text{GeV}\,,\\
&m_{\Omega_c} = (2.6952 \pm 0.0017)\,\text{GeV}\,, && \tau_{\Omega_c} = (2.68 \pm 0.026) \cdot 10^{-13}\,\text{s}\,.
\end{aligned}
\tag{A.3}
$$

Finally, the masses for the relevant members of the light baryon octet and decuplet are provided

$$
\begin{aligned}
&m_p = (0.938272081 \pm 0.000000006)\,\text{GeV}\,, && \tau_p > 3.6 \cdot 10^{29}\,\text{years}\,,\\
&m_n = (0.9389565413 \pm 0.000000006)\,\text{GeV}\,, && \tau_n = (879.4 \pm 0.6)\,\text{s}\,,\\
&m_{\Sigma^0} = (1.192642 \pm 0.000024)\,\text{GeV}\,, && \tau_{\Sigma^0} = (74 \pm 7) \cdot 10^{-21}\,\text{s}\,,\\
&m_{\Sigma^+} = (1.18937 \pm 0.000007)\,\text{GeV}\,, && \tau_{\Sigma^+} = (8.018 \pm 0.026) \cdot 10^{-11}\,\text{s}\,,\\
&m_{\Lambda} = (1.115683 \pm 0.000006)\,\text{GeV}\,, && \tau_{\Lambda} = (2.632 \pm 0.020) \cdot 10^{-10}\,\text{s}\,,\\
&m_{\Xi^0} = (1.31486 \pm 0.00020)\,\text{GeV}\,, && \tau_{\Xi^0} = (2.90 \pm 0.09) \cdot 10^{-10}\,\text{s}\,,\\
&m_{\Delta^{++/+/0}} \approx (1.232 \pm 0.002)\,\text{GeV}\,, && \Gamma_{\Delta^{++/+/0}} \approx (0.117 \pm 0.003)\,\text{GeV}\,,\\
&m_{\Sigma^{*0}} = (1.3837 \pm 0.0010)\,\text{GeV}\,, && \Gamma_{\Sigma^{*0}} = (0.036 \pm 0.005)\,\text{GeV}\,,\\
&m_{\Sigma^{*+}} = (1.38280 \pm 0.00035)\,\text{GeV}\,, && \Gamma_{\Sigma^{*+}} = (0.036 \pm 0.007)\,\text{GeV}\,,\\
&m_{\Xi^{*0}} = (1.53180 \pm 0.00032)\,\text{GeV}\,, && \Gamma_{\Xi^{*0}} = (0.0091 \pm 0.0001)\,\text{GeV}\,.
\end{aligned}
\tag{A.4}
$$

Fermi's constant G_F, electromagnetic coupling α_{em} and charm quark $\overline{\text{MS}}$ mass $m_c(\mu)$ are given by [103]

$$
\begin{aligned}
&G_F = 1.166379 \cdot 10^{-5}\,\text{GeV}^2\,,\\
&\alpha_{\text{em}} = 7.29735257 \cdot 10^{-3}\,,\\
&m_c(m_c) = 1.27 \pm 0.02\,.
\end{aligned}
\tag{A.5}
$$

The modulus of the $D \to PP$ amplitudes, which are needed to describe the bremsstrahlung according to Low's theorem (see Sec. 4.2.1), are obtained from the branching ratios [103]

$$\begin{aligned}
&B(D^0 \to \pi^+ K^-) = (3.946 \pm 0.030) \cdot 10^{-2}\,, && B(D^0 \to K^+ \pi^-) = (1.50 \pm 0.07) \cdot 10^{-4}\,,\\
&B(D^0 \to \pi^+ \pi^-) = (1.453 \pm 0.024) \cdot 10^{-3}\,, && B(D^0 \to K^+ K^-) = (4.08 \pm 0.06) \cdot 10^{-3}\\
&B(D^+ \to \pi^+ \pi^0) = (1.247 \pm 0.033) \cdot 10^{-3}\,, && B(D_s \to \pi^+ \pi^0) < 3.4 \cdot 10^{-4}\,,\\
&B(D^+ \to \pi^+ K^0_{\rm S}) = (1.562 \pm 0.031) \cdot 10^{-2}\,, && B(D_s \to \pi^+ K^0_{\rm S}) = (1.19 \pm 0.05) \cdot 10^{-3}\,,\\
&B(D^+ \to \pi^+ K^0_{\rm L}) = (1.46 \pm 0.05) \cdot 10^{-2}\,, &&\\
&B(D^+ \to K^+ \pi^0) = (2.08 \pm 0.21) \cdot 10^{-4}\,, && B(D_s \to K^+ \pi^0) = (6.1 \pm 2.1) \cdot 10^{-4}\,,\\
&B(D^+ \to K^+ K^0_{\rm S}) = (3.04 \pm 0.09) \cdot 10^{-3}\,, && B(D_s \to K^+ \overline{K}^0) = (2.95 \pm 0.14) \cdot 10^{-2}\,,\\
&B(D^+ \to K^+ K^0_{\rm L}) = (3.21 \pm 0.16) \cdot 10^{-3}\,. &&
\end{aligned} \tag{A.6}$$

For the extraction of the couplings $g_{VP\gamma}$ (see eq. (4.16)) and g_{VPP} (see eq. (5.18)) we use [103]

$$\begin{aligned}
&B(\rho^\pm \to \pi^\pm \gamma) = (4.5 \pm 0.5) \cdot 10^{-4}\,,\\
&B(\rho^0 \to \pi^0 \gamma) = (4.7 \pm 0.8) \cdot 10^{-4}\,,\\
&B(\omega \to \pi^0 \gamma) = (8.34 \pm 0.26) \cdot 10^{-2}\,,\\
&B(K^{*\pm} \to K^\pm \gamma) = (9.8 \pm 0.9) \cdot 10^{-4}\,,\\
&B(K^{*0} \to K^0 \gamma) = (2.46 \pm 0.21) \cdot 10^{-3}\,,\\
&B(\rho \to \pi^+ \pi^-) \approx 1\,,\\
&B(K^{*0} \to (K\pi)^0) = 0.99754 \pm 0.00021\,.
\end{aligned} \tag{A.7}$$

Branching ratios and parity violating parameters of hadronic two body decays of baryons are given by [103]

$$\begin{aligned}
&B(\Lambda \to p\pi^-) = (63.9 \pm 0.5)\%\,, && \alpha_B(\Lambda \to p\pi^-) = 0.732 \pm 0.014\,,\\
&B(\Sigma^+ \to p\pi^0) = (53.57 \pm 0.30)\%\,, && \alpha_B(\Sigma^+ \to p\pi^0) = -0.981 \pm 0.016\,,\\
&B(\Sigma^+ \to n\pi^+) = (48.31 \pm 0.30)\%\,, && \alpha_B(\Sigma^+ \to n\pi^+) = 0.068 \pm 0.013\,,\\
&B(\Xi^0 \to \Lambda\pi^0) = (99.52 \pm 0.012)\%\,, && \alpha_B(\Xi^0 \to \Lambda\pi^0) = -0.356 \pm 0.011\,.
\end{aligned} \tag{A.8}$$

Branching ratios for radiative B decays are given by [103]

$$\begin{aligned}
B(B^0 \to K^{0*}(892)\gamma) &= (4.18 \pm 0..25) \times 10^{-5}\,,\\
B(B^+ \to K_1^+(1270)\gamma) &= (4.4^{+0.7}_{-0.6}) \times 10^{-5}\,,\\
B(B^+ \to K_1^+(1400)\gamma) &= (10^{+5}_{-4}) \times 10^{-5}\,.
\end{aligned} \tag{A.9}$$

The CKM matrix elements are taken from the UTfit collaboration [97]

$$\begin{aligned}
&V_{ud} = 0.97431 \pm 0.00012, && V_{us} = 0.22514 \pm 0.00055,\\
&V_{cd} = (-0.22500 \pm 0.00054) \exp\left[i(0.0351 \pm 0.0010)^\circ\right], &&\\
&V_{cs} = (0.97344 \pm 0.00012) \exp\left[i(-0.001880 \pm 0.000055)^\circ\right]. &&
\end{aligned} \tag{A.10}$$

The decay constants are given by [1, 22, 206, 207]

$$\begin{aligned}
&f_D = (0.21215 \pm 0.00127)\,\text{GeV}\,, && f_{D_s} = (0.24883 \pm 0.00127)\,\text{GeV}\,,\\
&f_\pi = (0.1302 \pm 0.0014)\,\text{GeV}\,, && f_K = (0.1556 \pm 0.0004)\,\text{GeV}\\
&f_\rho = (0.216 \pm 0.003)\,\text{GeV}\,, && f_{\rho^{(d)}} = (0.2097 \pm 0.0003)\,\text{GeV}\,,\\
&f_\omega = (0.197 \pm 0.008)\,\text{GeV}\,, && f_{\omega^{(d)}} = (0.2013 \pm 0.0008)\,\text{GeV}\,,\\
&f_\phi = (0.233 \pm 0.004)\,\text{GeV}\,,\\
&f_{K_1(1270)} = (0.17 \pm 0.02)\,\text{GeV}\,, && f_{K_1(1400)} = (0.175 \pm 0.037)\,\text{GeV}\,.
\end{aligned} \tag{A.11}$$

χPT [208] and the $q\bar{q} - s\bar{s}$ mixing scheme [209] provide decay constants for singlet and octet states η_0 and η_8

$$\begin{aligned}
f_{\eta_8} &= \sqrt{\frac{4}{3}f_K^2 - \frac{1}{3}f_\pi^2} = (0.1632 \pm 0.0006)\,\text{GeV}\,,\\
f_{\eta_0} &= \sqrt{\frac{2}{3}f_K^2 + \frac{1}{3}f_\pi^2} = (0.1476 \pm 0.0005)\,\text{GeV}\,,
\end{aligned} \tag{A.12}$$

which are in agreement with values extracted from $\eta^{(\prime)} \to \gamma\gamma$ decays [209]

$$f_{\eta_8} = (0.164 \pm 0.006)\,\text{GeV}\,, f_{\eta_0} = (0.152 \pm 0.004)\,\text{GeV}\,. \tag{A.13}$$

B Transition form factors

In this appendix we provide information about the vacuum $\to PP$ (section B.1), $D \to V$ (section B.2) and $B_c \to B$ (section B.4) transition form factors. The HHχPT form factors are given in appendix C

B.1 vacuum $\to PP$

The vacuum $\to PP$ form factors are the main ingredient for the QCDF predictions (section 4.2.3) of the $D \to PP\gamma$ decay amplitude and primarily responsible for the shape of the distributions. Due to the discrete symmetries of QCD and conservation of angular momentum, the axialvector current does not contribute. The remaining matrix element can generally be parametrized by two form factors

$$\left\langle P_1(p_1)P_2(p_2)|\bar{q}\gamma_\mu q'|0\right\rangle = f_+^{P_1P_2}(s)(p_1-p_2)_\mu + f_-^{P_1P_2}(s)(p_1+p_2)_\mu\,, \tag{B.1}$$

where the labeling has been adopted from [210]. Here, $s = (p_1+p_2)^2$ is the invariant mass squared of the two pseudoscalars. If the masses of the pseudoscalars are identical, $f_-(s) = 0$ has to hold due to current conservation. Furthermore, the remaining form factor f_+ has to vanish if the final state is symmetric in the pseudoscalars. However, the QCDF amplitude depends only on the form factor f_+. Therefore, we neglect f_- in the following. This section is split up into three subsections, one for each of the final states $\pi\pi$, KK and $K\pi$.

B.1.1 Pion form factors

The electromagnetic pion form factor $F_\pi^{\rm em}$ is defined as

$$\left\langle \pi^+(p_1)\pi^-(p_2)|j_\mu^{\rm em}|0\right\rangle = F_\pi^{\rm em}(s)(p_1-p_2)_\mu\,, \tag{B.2}$$

where the electromagnetic current can be decomposed into an isotriplet ($I=1$), an isosinglet ($I=0$) and a strangeness current

$$\begin{aligned} j_\mu^{\rm em} &= \frac{2}{3}\overline{u}\gamma_\mu u - \frac{1}{3}\overline{d}\gamma_\mu d - \frac{1}{3}\overline{s}\gamma_\mu s \\ &= \frac{1}{2}(\overline{u}\gamma_\mu u - \overline{d}\gamma_\mu d) + \frac{1}{6}(\overline{u}\gamma_\mu u + \overline{d}\gamma_\mu d) - \frac{1}{3}\overline{s}\gamma_\mu s \\ &= \frac{1}{\sqrt{2}} j_\mu^{(I=1)} + \frac{1}{3\sqrt{2}} j_\mu^{(I=0)} - \frac{1}{3} j_\mu^s \\ &= J_\mu^{(I=1)} + J_\mu^{(I=0)} + J_\mu^s\,. \end{aligned} \tag{B.3}$$

In the isospin symmetry limit, only the $I = 1$ current contributes to $F_\pi^{\rm em}$, which can be written as [211]

$$F_\pi^{\rm em}(s) = \left[\sum_{n=0}^{3} c_n BW_n^{KS}(s)\right]_{fit} + \left[\sum_{n=4}^{\infty} c_n BW_n^{KS}(s)\right]_{\text{dual-QCD}_{N_C=\infty}} . \tag{B.4}$$

The coefficients c_{0-3} are fitted to data, while the remaining coefficients c_n are given by the dual-QCD model

$$\begin{aligned} c_0 &= 1.171 \pm 0.007\,, & c_1 &= -0.119 \pm 0.011\,, \\ c_2 &= 0.0115 \pm 0.0064\,, & c_3 &= -0.0438 \pm 0.02\,, \\ c_n &= \frac{2(-1)^n \Gamma(1.8) m_\rho^2}{\sqrt{\pi} m_n^2 \Gamma(n+1)\Gamma(1.3-n)} & n &\geq 4\,. \end{aligned} \tag{B.5}$$

The Breit-Wigner function takes into account an s-dependent width

$$\begin{aligned} BW_n^{KS}(s) &= \frac{m_n^2}{m_n^2 - s - i\sqrt{s}\Gamma_n(s)}\,. \\ \Gamma_n(s) &= \frac{0.2 m_n^3}{s}\left(\frac{p(s)}{p(m_n^2)}\right)^3 \Gamma_n\,, \\ p(s) &= \sqrt{s - 4m_\pi^2}/2\,. \end{aligned} \tag{B.6}$$

The masses and widths of the ρ meson and its first excitation are fitted to data

$$\begin{aligned} m_\rho &= (0.7739 \pm 0.0006)\,\text{GeV}\,, & m_{\rho'} &= (1.357 \pm 0.018)\,\text{GeV}\,, \\ \Gamma_\rho &= (0.1149 \pm 0.0010)\,\text{GeV}\,, & \Gamma_{\rho'} &= (0.437 \pm 0.060)\,\text{GeV}\,. \end{aligned} \tag{B.7}$$

The remaining masses and widths are given by

$$m_n^2 = m_\rho^2(1+2n)\,, \qquad \Gamma_n = 0.2\,\text{m}_n\,. \tag{B.8}$$

$F_\pi^{\rm em}$ is shown in Figure B.1.

B.1.2 Kaon form factors

The electromagnetic kaon form factor $F_{K^+}^{\rm em}$, defined as

$$\left\langle K^+(p_1)K^-(p_2)|j_\mu^{\rm em}|0\right\rangle = F_{K^+}^{\rm em}(s)(p_1 - p_2)_\mu\,, \tag{B.9}$$

is taken from [211] and shown in Figure B.2. Here, the isospin-zero components contribute to the form factor via ω and ϕ resonances

$$\begin{aligned} F_{K^+}^{\rm em}(s) &= F_{K^+}^{(I=1)}(s) + F_{K^+}^{(I=0)}(s) + F_{K^+}^{s}(s), \\ F_{K^+}^{(I=1)}(s) &= \frac{1}{2}(c_\rho^K BW_\rho(s) + c_{\rho'}^K BW_{\rho'}(s) + c_{\rho''}^K BW_{\rho''}(s)), \\ F_{K^+}^{(I=0)}(s) &= \frac{1}{6}(c_\omega^K BW_\omega(s) + c_{\omega'}^K BW_{\omega'}(s) + c_{\omega''}^K BW_{\omega''}(s)), \\ F_{K^+}^{s}(s) &= \frac{1}{3}(c_\phi BW_\phi(s) + c_{\phi'} BW_{\phi'}(s)). \end{aligned} \tag{B.10}$$

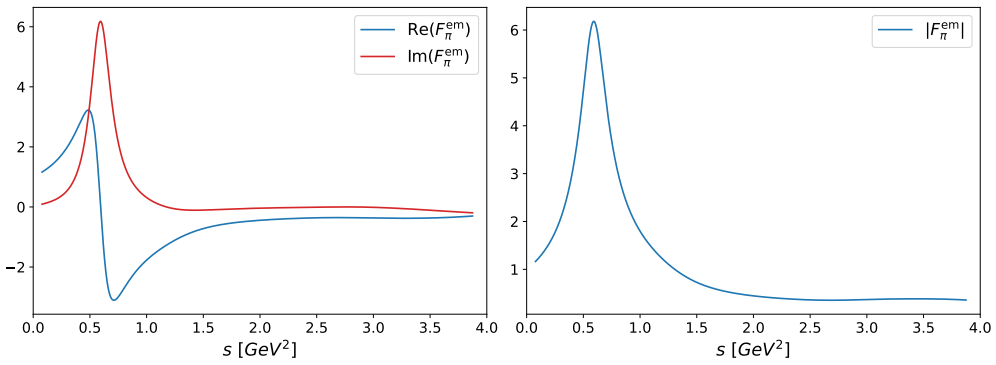

Figure B.1: The real and imaginary part (left) as well as the absolut values (right) of the electromagnetic pion form factor F_π^{em} (B.4) as a function of the invariant mass squared s.

The fit parameters are given by

$$\begin{aligned}
&m_\phi = 1.019372\,\text{GeV}, \quad m_\phi = 1.68\,\text{GeV}, \quad m_{\rho'} = 1.465\,\text{GeV},\\
&m_{\rho''} = 1.720\,\text{GeV}, \quad m_{\omega'} = 1.425\,\text{GeV}, \quad m_{\omega''} = 1.67\,\text{GeV},\\
&\Gamma_\phi = 0.00436\,\text{GeV}, \quad \Gamma_{\phi'} = 0.150\,\text{GeV}, \quad \Gamma_\rho = 0.150\,\text{GeV}, \quad \Gamma_{\rho'} = 0.400\,\text{GeV},\\
&\Gamma_{\rho''} = 0.250\,\text{GeV}, \quad \Gamma_\omega = 0.0084\,\text{GeV}, \quad \Gamma_{\omega'} = 0.215\,\text{GeV}, \quad \Gamma_{\omega''} = 0.315\,\text{GeV},\\
&c_\phi = (1.018 \pm 0.006), \quad c_{\phi'} = (-0.018 \pm 0.006),\\
&c_\rho^K = (1.195 \pm 0.009), \quad c_{\rho'}^K = (-0.112 \pm 0.010), \quad c_{\rho''}^K = (-0.083 \pm 0.019),\\
&c_\omega^K = (1.195 \pm 0.009), \quad c_{\omega'}^K = (-0.112 \pm 0.010), \quad c_{\omega''}^K = (-0.083 \pm 0.019).
\end{aligned} \tag{B.11}$$

B.1.3 $K\pi$ form factors

The $\bar{K}^0\pi^-$ form factors are defined as

$$\left\langle \bar{K}^0(p_1)\pi^-(p_2)|\bar{s}\gamma_\mu u|0\right\rangle = f_+^{\bar{K}^0\pi^-}(s)\,(p_1-p_2)_\mu + f_-^{\bar{K}^0\pi^-}(s)\,(p_1+p_2)_\mu\,. \tag{B.12}$$

The vector form factor $f_+^{\bar{K}^0\pi^-}$, shown in Figure B.3, can be parametrized with a dispersion relation [212]

$$f_+^{\bar{K}^0\pi^-}(s) = f_+^{\bar{K}^0\pi^-}(0)\cdot\exp\left[\lambda_+'\frac{s}{m_\pi^2} + \frac{1}{2}\left(\lambda_+'' - \lambda_+'^2\right)\frac{s^2}{m_\pi^4} + \frac{s^3}{\pi}\int_{s_{K\pi}}^{s_{cut}} \mathrm{d}s'\,\frac{\delta_1^{K\pi}(s')}{(s')^3(s'-s-i\epsilon)}\right], \tag{B.13}$$

with $s_{K\pi} = (m_K + m_\pi)^2$. The phase $\delta_1^{K\pi}(s)$ is extracted from a two resonance model [212]

$$\tilde{f}_+^{\bar{K}^0\pi^-}(s) = \frac{f_+^{\bar{K}^0\pi^-}(s)}{f_+^{\bar{K}^0\pi^-}(0)} = \frac{m_{K^\star}^2 - \kappa_{K^\star}\tilde{H}_{K\pi}(0) + \beta s}{D(K^\star)} - \frac{\beta s}{D(K^{\star\prime})}\,, \tag{B.14}$$

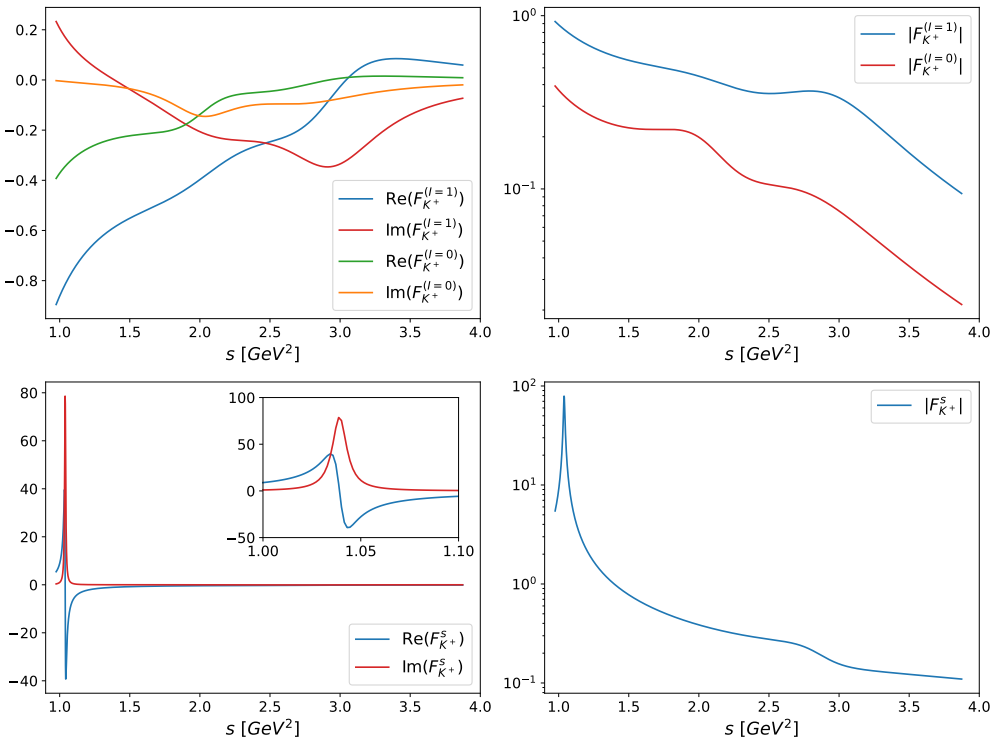

Figure B.2: The real and imaginary parts (left) as well as the absolut values (right) of the electromagnetic kaon form factors (B.10) as a function of s. The upper (lower) plots show $F_{K^+}^{(I=1,0)}$ ($F_{K^+}^{s}$).

where

$$
\begin{aligned}
D(n) &= m_n^2 - s - \kappa_n \mathrm{Re}\left(\tilde{H}_{K\pi}(s)\right) - i m_n \gamma_n(s)\,, \\
\gamma_n(s) &= \gamma_n \frac{s}{m_n^2} \frac{\sigma_{K\pi}^3(s)}{\sigma_{K\pi}^3(m_n^2)}, \qquad \gamma_n = \gamma_n(m_n^2)\,, \\
\sigma_{K\pi}(s) &= \frac{2 q_{K\pi}(s)}{\sqrt{s}} = \frac{1}{s}\sqrt{(s-(m_K+m_\pi)^2)\,(s-(m_K-m_\pi)^2)}\,, \\
\kappa_n &= \frac{192\pi f_K f_\pi}{\sigma_{K\pi}^3(m_n^2)} \frac{\gamma_n}{m_n}\,.
\end{aligned}
\tag{B.15}
$$

The χPT loop integral functions [213]

$$
\tilde{H}_{K\pi}(s) = H_{K\pi}(s) - \frac{2}{3 f_\pi^2} L_{K\pi}^r s = \frac{1}{f_\pi^2}\left[s M_{K\pi}^r(s) - L_{K\pi}(s)\right] \tag{B.16}
$$

can be found in chapter 8 of Ref. [214]:

$$
\begin{aligned}
M^r_{K\pi}(s) &= \frac{1}{12s}(s-2\Sigma)\overline{J}_{K\pi}(s) + \frac{\Delta^2}{3s^2}\overline{\overline{J}}_{K\pi}(s) - \frac{1}{6}k_{K\pi}(\mu) + \frac{1}{288\pi^2}\,,\\
L_{K\pi}(s) &= \frac{\Delta^2}{4s}\overline{J}_{K\pi}(s)\,,\\
k_{K\pi}(\mu) &= \frac{1}{32\pi^2}\frac{1}{\Delta}\left(m_K^2\ln\left(\frac{m_K^2}{\mu^2}\right) - m_\pi^2\ln\left(\frac{m_\pi^2}{\mu^2}\right)\right)\,,\\
\overline{\overline{J}}_{K\pi}(s) &= \overline{J}_{K\pi}(s) - s\overline{J}'_{K\pi}(0)\,,\\
\overline{J}_{K\pi}(s) &= J_{K\pi}(s) - J_{K\pi}(0)\\
&= \frac{1}{32\pi^2}\left(2 + \left[\frac{\Delta}{s} - \frac{\Sigma}{\Delta}\right]\ln\left(\frac{m_\pi^2}{m_K^2}\right) - \frac{v}{s}\ln\left(\frac{(s+v)^2-\Delta^2}{(s-v)^2-\Delta^2}\right)\right)\,,\\
\overline{J}'_{K\pi}(0) &= \frac{1}{32\pi^2}\left(\frac{\Sigma}{\Delta^2} + 2\frac{m_K^2 m_\pi^2}{\Delta^3}\ln\left(\frac{m_\pi^2}{m_K^2}\right)\right)\,,\\
v(s) &= s\sigma_{K\pi}(s)\,,\\
\Sigma &= m_K^2 + m_\pi^2\,,\\
\Delta &= m_K^2 - m_\pi^2\,.
\end{aligned}
\tag{B.17}
$$

The renormalization scale μ is set to the physical resonance mass $\mu = m_{K^\star}$ [212]. The resonance masses and width parameters are unphysical fitting parameters. They are obtained as [212]

$$
\begin{aligned}
&m^{\text{fit}}_{K^\star} = (0.94341 \pm 0.00058)\,\text{GeV}\,, \qquad \gamma^{\text{fit}}_{K^\star} = (0.06672 \pm 0.00086)\,\text{GeV}\,,\\
&m^{\text{fit}}_{K^{\star\prime}} = (1.374 \pm 0.030)\,\text{GeV}\,, \qquad \gamma^{\text{fit}}_{K^{\star\prime}} = (0.24 \pm 0.10)\,\text{GeV}\,,\\
&s_{cut} = 4\,\text{GeV}^2\,, \qquad \mu = m^{\text{phy}}_{K^\star} = 0.892\,\text{GeV}\,, \qquad \beta = (-3.9 \pm 1.5)\cdot 10^{-2}\,,\\
&\lambda'_+ = (24.66 \pm 0.69)\cdot 10^{-3}\,, \qquad \lambda''_+ = (11.99 \pm 0.19)\cdot 10^{-4}\,,\\
&|V_{us}| f_+^{\overline{K}^0\pi^-}(0) = 0.21664 \pm 0.00048\,.
\end{aligned}
\tag{B.18}
$$

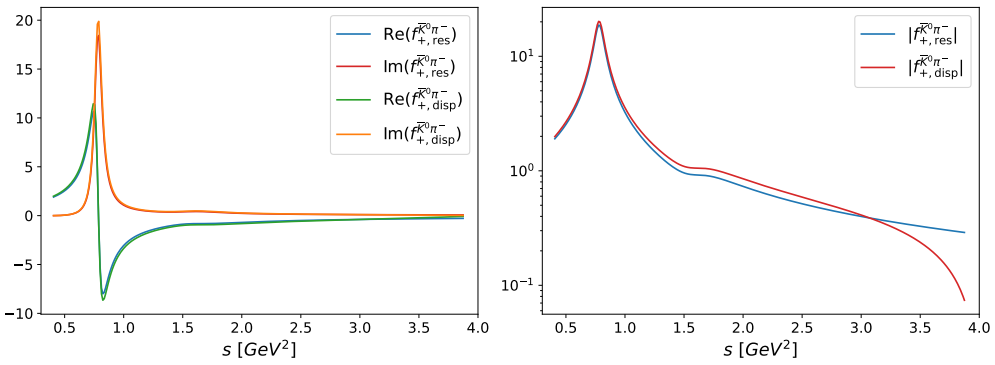

Figure B.3: The real and imaginary part (left) as well as the absolut value of the $f_+^{\bar{K}^0\pi^-}$ form factor (B.12) functions of s. Results from the two resonance model as well as the dispersive description are shown. The form factor is extracted from $\tau^- \to \nu_\tau K_s \pi^-$ decays [212].

B.2 $D \to V$ form factors

We use the $D \to V$ form factors to determine the HHχPT couplings α_1 and α_2 (4.22). The matrix element of the $V-A$ current can be defined in terms of four form factors V and $A_{0,1,2}$ [159]

$$\begin{aligned}\langle V(p_V,\epsilon)|\bar{q}\gamma_\mu(1-\gamma_5)c|D(p_D)\rangle = &-\frac{V(q^2)}{m_D+m_V}\epsilon_{\mu\alpha\beta\gamma}\epsilon^{*\alpha}P^\beta q^\gamma \\ &+ iA_1(q^2)(m_D+m_V)\left(q_\mu\frac{\epsilon^*\cdot P}{q^2}-\epsilon_\mu^*\right) \\ &- iA_2(q^2)\frac{\epsilon^*\cdot P}{m_D+m_V}\left(q_\mu\frac{m_D^2-m_V^2}{q^2}-P_\mu\right) \\ &- iA_0(q^2)2m_V\frac{\epsilon^*\cdot P}{q^2}q_\mu\,,\end{aligned} \tag{B.19}$$

with $P = p_D + p_V$ and $q = p_D - p_V$. The individual form factors can be parametrized in terms of three parameters

$$F(q^2) = \frac{F(0)}{1 - a\frac{q^2}{m_D^2} + b\left(\frac{q^2}{m_D^2}\right)^2}\,. \tag{B.20}$$

For the extraction of α_1 and α_2 we used the $D \to K^*$ form factors obtained from the covariant light-front model. The necessary parameters are given by [159]

$$\begin{aligned} A_1(0) &= 0.72 \pm 0.01\,, & a_{A_1} &= 0.45 \pm 0.02\,, & b_{A_1} &= 0.01 \pm 0.00\,, \\ A_2(0) &= 0.60 \pm 0.00\,, & a_{A_2} &= 0.89 \pm 0.01\,, & b_{A_2} &= 0.21 \pm 0.02\,, \end{aligned} \tag{B.21}$$

where uncertainties are added in quadrature. We note that one could also use other transitions such as $D \to \rho$, $D \to \omega$, $D_s \to K^*$ and $D_s \to \phi$ to determine the parameters.

In addition, calculations with other methods [215–219] as well as first measurements [220, 221] of the form factors are available.

B.3 $D_s \to K_1^+$ tensor form factors

The $D_s \to K_1^+$ matrix element of a tensor current can be parametrized as

$$\begin{aligned}\langle K_1^+(\varepsilon,k)|\bar{u}\sigma_{\mu\nu}(1\pm\gamma_5)q^\nu c|D_s(p)\rangle &= T_2^{K_1}(q^2)\left[\varepsilon_\mu^*(m_{D_s}^2-m_{K_1}^2)-(\varepsilon^* p)(p+k)_\mu\right]\\ &+T_3^{K_1}(q^2)(\varepsilon^* p)\left[q_\mu-\frac{q^2}{m_{D_s}^2-m_{K_1}^2}(p+k)_\mu\right]\\ &\pm 2T_1^{K_1}(q^2)i\epsilon_{\mu\nu\rho\sigma}\varepsilon^{\nu *}p^\rho k^\sigma\,,\end{aligned} \tag{B.22}$$

with $T_1^{K_1}(0)=T_2^{K_1}(0)$.

B.4 $B_c \to B$ form factors

The $B_c \to B$ form factors can be written as

$$\begin{aligned}&\langle B(q,\,s_B)|\overline{u}\mathrm{i}\sigma^{\mu\nu}k_\nu c|B_c(P,\,s_{B_c})\rangle =\\ &\quad -\overline{u}(q,\,s_B)\left[\frac{h_+^{B_c\to B}(k^2)}{s_+}k_\nu\left(k^\nu s^\mu-s^\nu k^\mu\right)\right.\\ &\qquad \left.+h_\perp^{B_c\to B}(k^2)\left(-i\sigma^{\mu\nu}k_\nu+\frac{1}{s_+}k_\nu\left(s^\nu k^\mu-k^\nu s^\mu\right)\right)\right]u(P,\,s_{B_c})\end{aligned} \tag{B.23}$$

$$\begin{aligned}&\langle B(q,\,s_B)|\overline{u}\mathrm{i}\sigma^{\mu\nu}k_\nu\gamma_5 c|B_c(P,\,s_{B_c})\rangle =\\ &\quad -\overline{u}(q,\,s_B)\gamma_5\left[\frac{\tilde{h}_+^{B_c\to B}(k^2)}{s_-}k_\nu\left(k^\nu s^\mu-s^\nu k^\mu\right)\right.\\ &\qquad \left.+\tilde{h}_\perp^{B_c\to B}(k^2)\left(-i\sigma^{\mu\nu}k_\nu+\frac{1}{s_-}k_\nu\left(s^\nu k^\mu-k^\nu s^\mu\right)\right)\right]u(P,\,s_{B_c})\end{aligned} \tag{B.24}$$

with $k=P-q$, $s=P+q$ and $s_\pm=(m_{B_c}\pm m_B)^2-k^2$. The definition of the tensor form factors h and $\tilde{h}$ are identical to those in [191]. We have only rearranged the expressions using the Gordan-identity into a more practical notation for radiative decays. The fit results and correlation matrices are given in [191] for $\Lambda_c \to p$ in terms of the z-expansion

$$f(k^2)=\frac{1}{1-k^2/(m_{pole}^f)^2}\sum_{n=0}^{n_{max}}a_n^f|z(k^2)|^n \tag{B.25}$$

with

$$z(k^2) = \frac{\sqrt{t_+ - k^2} - \sqrt{t_+ - t_0}}{\sqrt{t_+ - k^2} + \sqrt{t_+ - t_0}} \tag{B.26}$$

and

$$t_+ = (m_D + m_\pi)^2\,, \qquad t_0 = (m_{\Lambda_c} - m_p)^2\,. \tag{B.27}$$

C HHχPT form factors

In this appendix we provide the HHχPT form factors derived from the effective Lagrangian and weak currents defined in section 4.2.2. Section C.1 covers the radiative three body decays $D \to PP\gamma$. In App. C.2 we define and list the form factors of the hadronic two body decays $D \to PP$.

C.1 radiative three body decays

To provide a better overview, we divide this section into three parts. The form factors of the CF, SCS and DCS decays are given in sections C.1.1, C.1.2 and C.1.3, respectively. Furthermore, we show all corresponding HHχPT Feynman diagrams in Fig. C.1-C.19. The order of the decays is arranged as in 4.1. The form factors for 14 of the 18 decays are taken from [2, 3]. The missing modes $D \to \pi^0\pi^0\gamma$, $D \to K^0\overline{K}^0\gamma$, $D \to \pi^0 K^0\gamma$ and $D \to K^+\pi^-\gamma$ are included in this thesis. In the following we denote the Breit-Wigner function and the $D^* - D$ mass difference as

$$\begin{aligned} BW_n(x) &= \frac{1}{x - m_n^2 + i m_n \Gamma_n}\,, \\ \Delta &= m_{D^*} - m_D\,. \end{aligned} \tag{C.1}$$

C.1.1 Cabibbo favored modes

$\underline{D^0 \to \pi^0 \overline{K}^0 \gamma}$

$$\begin{aligned} E_1^{(s,d)} &= ig\frac{f_D f_K}{f_\pi}\frac{v\cdot k}{v\cdot k + v\cdot p_1 + \Delta}\left(\frac{1}{v\cdot k + \Delta} - \frac{1}{v\cdot p_1 + \Delta}\right) \\ &\quad \times \left(\sqrt{2}\lambda' + \frac{1}{2}\lambda g_v\left(\frac{g_\omega}{3m_\omega^2} + \frac{g_\rho}{m_\rho^2}\right)\right) \end{aligned} \tag{C.2}$$

$$D_1^{(s,d)} = -\sqrt{2}\frac{f_D f_K}{f_\pi}\lambda'\left(\frac{1}{v\cdot k + \Delta} + g\frac{v\cdot p_2}{v\cdot p_1 + v\cdot k}\left[\frac{1}{v\cdot k + \Delta} + \frac{1}{v\cdot p_1 + \Delta}\right]\right) \tag{C.3}$$

$$\begin{aligned} D_2^{(s,d)} &= -\frac{1}{2}\frac{f_D f_K}{f_\pi}\lambda g_v\left(\frac{g_\omega}{3m_\omega^2} + \frac{g_\rho}{m_\rho^2}\right) \\ &\quad \times \left(\frac{1}{v\cdot k + \Delta} + g\frac{v\cdot p_2}{v\cdot p_1 + v\cdot k}\left[\frac{1}{v\cdot k + \Delta} + \frac{1}{v\cdot p_1 + \Delta}\right]\right) \end{aligned} \tag{C.4}$$

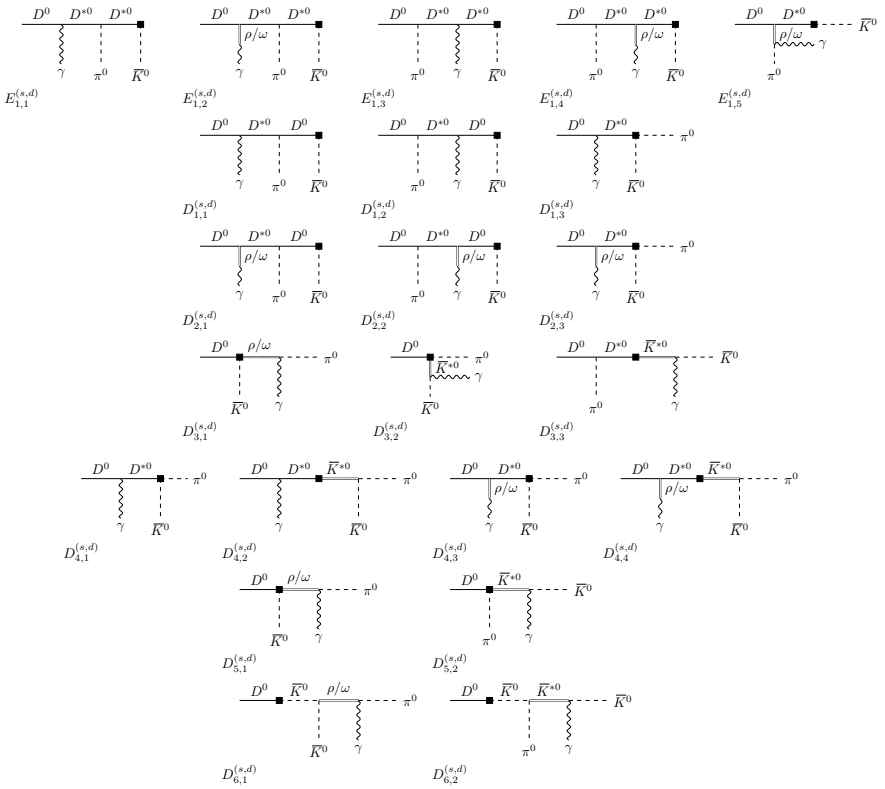

Figure C.1: HHχPTFeynman diagrams for the decay $D^0 \to \pi^0 \overline{K}^0 \gamma$.

$$
\begin{aligned}
D_3^{(s,d)} &= -\sqrt{\frac{2}{m_D}} f_K (\alpha_1 m_D - \alpha_2 v\cdot p_2) \left(\frac{m_\rho^2 g_{\rho\pi\gamma}}{g_\rho} BW_\rho(u) + \frac{m_\omega^2 g_{\omega\pi\gamma}}{g_\omega} BW_\omega(u) \right) \\
&\quad + \frac{1}{\sqrt{2}} g_{K^*} g_{K^*K\gamma} \frac{f_D}{f_\pi} \left(1 + g \frac{m_D - v\cdot p_1}{v\cdot p_1 + \Delta} \right) BW_{\overline{K}^*}(t)
\end{aligned} \tag{C.5}
$$

$$
D_4^{(s,d)} = -f_D \frac{1}{v\cdot k + \Delta} \left(1 - m_{K^*}^2 BW_{\overline{K}^*}(s)\right) \left(\sqrt{2}\lambda' + \frac{1}{2}\lambda g_v \left(\frac{g_\omega}{3m_\omega^2} + \frac{g_\rho}{m_\rho^2} \right) \right) \tag{C.6}
$$

$$
\begin{aligned}
D_5^{(s,d)} &= \frac{1}{\sqrt{2}} \frac{f_D}{f_K} (g_\rho g_{\rho\pi\gamma} BW_\rho(u) - g_\omega g_{\omega\pi\gamma} BW_\omega(u)) \\
&\quad + \frac{1}{\sqrt{2}} \frac{f_D}{f_\pi} g_{K^*} g_{K^*K\gamma} BW_{\overline{K}^*}(t)
\end{aligned} \tag{C.7}
$$

$$
\begin{aligned}
D_6^{(s,d)} &= \frac{1}{\sqrt{2}} f_D f_K \frac{m_D^2}{m_D^2 - m_K^2} \left(\frac{m_\rho^2}{g_\rho} g_{\rho\pi\gamma} BW_\rho(u) - \frac{m_\omega^2}{g_\omega} g_{\omega\pi\gamma} BW_\omega(u) \right. \\
&\quad \left. - \frac{m_{K^*}^2}{g_{K^*}} g_{K^*K\gamma} BW_{\overline{K}^*}(t) \right)
\end{aligned} \tag{C.8}
$$

$\underline{D^0 \to \pi^+ K^- \gamma}$

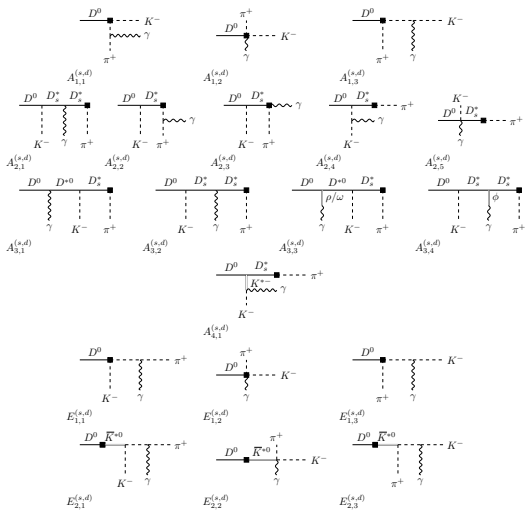

a) Contributions to the parity-even form factors A and E. For each of the diagrams $A_{1,1}$, $A_{1,2}$, $A_{1,3}$, $A_{2,2}$, $A_{2,3}$, $A_{2,4}$, $E_{1,1}$, $E_{1,2}$, $E_{1,3}$, $E_{2,1}$ and $E_{2,3}$ there are additional diagrams where the photon is coupled to the pseudoscalar via a ρ^0-, ω-, ϕ-mesons.

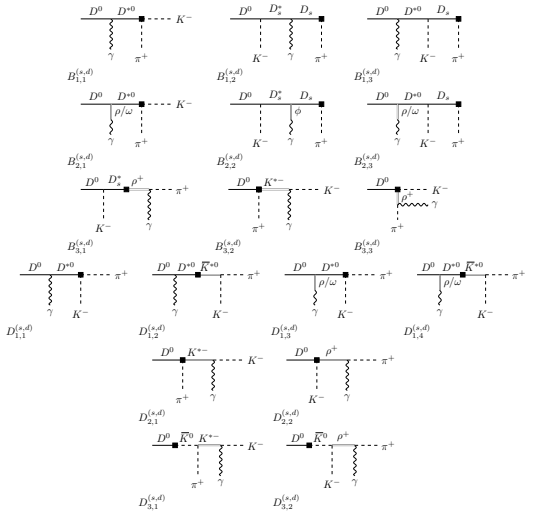

b) Contributions to the parity-odd form factors B and D.

Figure C.2: HHχPTFeynman diagrams for the decay $D^0 \to \pi^+ K^- \gamma$.

$$A_1^{(s,d)} = i\frac{f_D f_\pi}{f_K}\frac{p_1\cdot k - m_D(v\cdot k + v\cdot p_1)}{(p_1\cdot k)(p_2\cdot k)} \tag{C.9}$$

$$\begin{aligned} A_2^{(s,d)} = &-i\sqrt{m_D m_{D_s}}\frac{f_{D_s} f_\pi}{f_K}\frac{g}{(p_1\cdot k)(p_2\cdot k)}\left(\frac{p_2\cdot k(m_D - v\cdot p_2)}{m_D(v\cdot p_2 + \Delta)}\right.\\ &+ \frac{p_2\cdot k\,[p_1\cdot p_2 - (v\cdot p_1)(v\cdot p_2)]}{m_D(v\cdot p_2+\Delta)(v\cdot p_2 + v\cdot k + \Delta)}\\ &\left.+ \frac{(m_D - v\cdot p_1)p_1\cdot k + m_D p_1\cdot p_2 + m_D(v\cdot p_1)(v\cdot p_2)}{m_D(v\cdot p_2 + v\cdot k + \Delta)}\right) \end{aligned} \tag{C.10}$$

$$\begin{aligned} A_3^{(s,d)} = &\, i\sqrt{\frac{m_{D_s}}{m_D}}\frac{f_{D_s} f_\pi}{f_K} g\frac{v\cdot k}{v\cdot k + v\cdot p_2 + \Delta}\\ &\times\left(\frac{2\lambda' - \frac{\sqrt{2}}{3}\lambda g_v\frac{g_\phi}{m_\phi^2}}{v\cdot p_2 + \Delta} - \frac{2\lambda' + \frac{1}{\sqrt{2}}\lambda g_v\left(\frac{g_\omega}{3m_\omega^2} + \frac{g_\rho}{m_\rho^2}\right)}{v\cdot k + \Delta}\right) \end{aligned} \tag{C.11}$$

$$B_1^{(s,d)} = 2\frac{f_D f_\pi}{f_K}\lambda'\left(\frac{1}{v\cdot k + \Delta} + g\frac{f_{D_s}}{f_D}\sqrt{\frac{m_{D_s}}{m_D}}\frac{v\cdot p_1}{(v\cdot p_2 + v\cdot k)}\left[\frac{1}{v\cdot k + \Delta} + \frac{1}{v\cdot p_2 + \Delta}\right]\right) \tag{C.12}$$

$$B_2^{(s,d)} = \frac{1}{\sqrt{2}}\frac{f_\pi}{f_K}\lambda g_v\left(\frac{g_\omega}{3m_\omega^2}+\frac{g_\rho}{m_\rho^2}\right)\frac{1}{v\cdot k+\Delta}\left(f_D+g\sqrt{\frac{m_{D_s}}{m_D}}f_{D_s}\frac{v\cdot p_1}{(v\cdot p_2+v\cdot k)}\right)$$
$$- g\lambda g_v\sqrt{\frac{m_{D_s}}{m_D}}\frac{f_{D_s}f_\pi}{f_K}\frac{\sqrt{2}g_\phi}{3m_\phi^2}\frac{v\cdot p_1}{(v\cdot p_2+v\cdot k)(v\cdot p_2+\Delta)} \tag{C.13}$$

$$B_3^{(s,d)} = \frac{2}{\sqrt{m_D}}f_\pi\frac{m_{K^*}^2 g_{K^{*\pm}K^\pm\gamma}}{g_{K^*}}(\alpha_1 m_D-\alpha_2 v\cdot p_1)BW_{K^{*-}}(t)$$
$$- g_\rho g_{\rho^\pm\pi^\pm\gamma}\frac{f_D}{f_K}\left(1+g\sqrt{\frac{m_{D_s}}{m_D}}\frac{f_{D_s}}{f_D}\frac{m_D-v\cdot p_2}{v\cdot p_2+\Delta}\right)BW_{\rho^+}(u) \tag{C.14}$$

$$D_1^{(s,d)} = \frac{f_D}{v\cdot k+\Delta}\left(1-m_{K^*}^2 BW_{K^*}(s)\right)\left(2\lambda'+\frac{1}{\sqrt{2}}\lambda g_v\left(\frac{g_\omega}{3m_\omega^2}+\frac{g_\rho}{m_\rho^2}\right)\right) \tag{C.15}$$

$$D_2^{(s,d)} = -\frac{f_D}{f_\pi}g_{K^*}g_{K^{*\pm}K^\pm\gamma}BW_{K^{*-}}(t)-\frac{f_D}{f_K}g_\rho g_{\rho^\pm\pi^\pm\gamma}BW_{\rho^+}(u) \tag{C.16}$$

$$D_3^{(s,d)} = f_D f_K\frac{m_D^2}{m_D^2-m_K^2}\left(\frac{m_\rho^2}{g_\rho}g_{\rho^\pm\pi^\pm\gamma}BW_{\rho^+}(u)+\frac{m_{K^*}^2}{g_{K^*}}g_{K^{*\pm}K^\pm\gamma}BW_{K^{*-}}(t)\right) \tag{C.17}$$

$\underline{D^+\to\pi^+\overline{K}^0\gamma}$

$$A_1^{(s,d)} = -i\frac{f_D f_\pi}{f_K}\frac{v\cdot p_1+v\cdot k}{(v\cdot k)(p_1\cdot k)} \tag{C.18}$$

$$A_3^{(s,d)} = -i\sqrt{\frac{m_{D_s}}{m_D}}\frac{f_{D_s}f_\pi g}{f_K}\frac{p_1\cdot p_2-(v\cdot p_1)(v\cdot p_2)+(v\cdot k)(m_D-v\cdot p_2)}{(v\cdot p_2+\Delta)(v\cdot k)(p_1\cdot k)} \tag{C.19}$$

$$A_4^{(s,d)} = -i\sqrt{\frac{m_{D_s}}{m_D}}\frac{f_{D_s}f_\pi g(v\cdot k)}{f_K(v\cdot k+v\cdot p_2+\Delta)}\left[\frac{2\lambda'+\frac{1}{\sqrt{2}}g_v\lambda\left(\frac{g_\omega}{3m_\omega^2}-\frac{g_\rho}{m_\rho^2}\right)}{v\cdot k+\Delta}-\frac{2\lambda'-\frac{\sqrt{2}}{3}g_v\lambda\frac{g_\phi}{m_\phi^2}}{v\cdot p_2+\Delta}\right] \tag{C.20}$$

$$E_1^{(s,d)} = -i\frac{f_D f_K}{f_\pi}\frac{v\cdot p_2}{(v\cdot k)(p_1\cdot k)} \tag{C.21}$$

$$E_2^{(s,d)} = -i\frac{f_D f_K g}{f_\pi}\frac{p_1\cdot p_2-(v\cdot p_1)(v\cdot p_2)+(v\cdot k)(m_D-v\cdot p_2)}{(v\cdot k+v\cdot p_1+\Delta)(v\cdot k)(p_1\cdot k)} \tag{C.22}$$

$$E_3^{(s,d)} = -i\frac{f_D f_K g(v\cdot k)}{f_\pi(v\cdot k+v\cdot p_1+\Delta)}$$
$$\times\left[\frac{2\lambda'+\frac{1}{\sqrt{2}}g_v\lambda\left(\frac{g_\omega}{3m_\omega^2}+\frac{g_\rho}{m_\rho^2}\right)}{v\cdot p_1+\Delta}-\frac{2\lambda'+\frac{1}{\sqrt{2}}g_v\lambda\left(\frac{g_\omega}{3m_\omega^2}-\frac{g_\rho}{m_\rho^2}\right)}{v\cdot k+\Delta}\right] \tag{C.23}$$

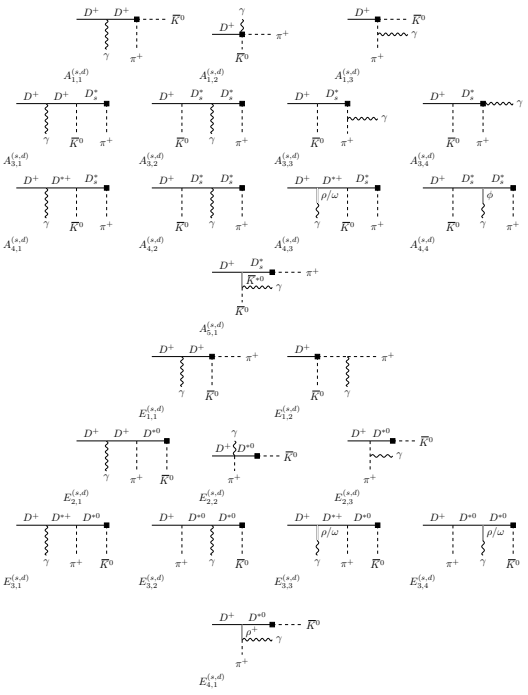

a) Contributions to the parity-even form factors A and E. For each of the diagrams $A_{1,2}$, $A_{1,3}$, $A_{3,3}$, $A_{3,4}$, $E_{1,2}$ nd $E_{2,3}$ there are additional diagrams where the photon is coupled to the pseudoscalar via a ρ^0-, ω-, ϕ-mesons.

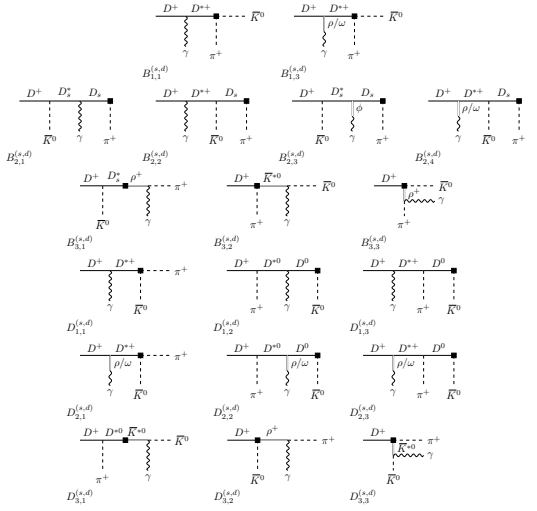

b) Contributions to the parity-odd form factors B and D.

Figure C.3: HHχPTFeynman diagrams for the decay $D^+ \to \pi^+ \overline{K}^0 \gamma$.

$$B_1^{(s,d)} = \frac{f_D f_\pi}{f_K(v\cdot k + \Delta)} \left[2\lambda' + \frac{1}{\sqrt{2}} g_v \lambda \left(\frac{g_\omega}{3m_\omega^2} - \frac{g_\rho}{m_\rho^2} \right) \right] \tag{C.24}$$

$$B_2^{(s,d)} = \sqrt{\frac{m_{D_s}}{m_D}} \frac{f_{D_s} f_\pi g(v\cdot p_1)}{f_K(v\cdot k + v\cdot p_2)} \left[\frac{2\lambda' - \frac{\sqrt{2}}{3} g_v \lambda \frac{g_\phi}{m_\phi^2}}{v\cdot p_2 + \Delta} + \frac{2\lambda' + \frac{1}{\sqrt{2}} g_v \lambda \left(\frac{g_\omega}{3m_\omega^2} - \frac{g_\rho}{m_\rho^2} \right)}{v\cdot k + \Delta} \right] \tag{C.25}$$

$$\begin{aligned} B_3^{(s,d)} = & -\frac{g_\rho g_{\rho^\pm \pi^\pm \gamma}}{f_K} \left(f_D + \sqrt{\frac{m_{D_s}}{m_D}} f_{D_s} g \frac{m_D - v\cdot p_2}{v\cdot p_2 + \Delta} \right) BW_{\rho^+}(u) \\ & + \frac{2 f_\pi (m_D \alpha_1 - \alpha_2 v\cdot p_1)}{\sqrt{m_D}} \frac{m_{K^*}^2}{g_{K^*}} g_{K^* K \gamma} BW_{\overline{K}^*}(t) \end{aligned} \tag{C.26}$$

$$D_1^{(s,d)} = -2\frac{f_D f_K}{f_\pi} \lambda' \left[\frac{1}{v\cdot k + \Delta} + \frac{g(v\cdot p_2)}{v\cdot k + v\cdot p_1} \left(\frac{1}{v\cdot k + \Delta} + \frac{1}{v\cdot p_1 + \Delta} \right) \right] \tag{C.27}$$

$$D_2^{(s,d)} = -\frac{f_D f_K g_v \lambda}{\sqrt{2} f_\pi} \left[\frac{\frac{g_\omega}{3m_\omega^2} - \frac{g_\rho}{m_\rho^2}}{v\cdot k + \Delta} + \frac{g(v\cdot p_2)}{v\cdot k + v\cdot p_1} \left(\frac{\frac{g_\omega}{3m_\omega^2} - \frac{g_\rho}{m_\rho^2}}{v\cdot k + \Delta} + \frac{\frac{g_\omega}{3m_\omega^2} + \frac{g_\rho}{m_\rho^2}}{v\cdot p_1 + \Delta} \right) \right] \tag{C.28}$$

$$
\begin{aligned}
D_3^{(s,d)} = & \frac{f_D g_{K^*} g_{K^* K\gamma}}{f_\pi} \left(1 + g \frac{m_D - v\cdot p_1}{v\cdot p_1 + \Delta}\right) BW_{\overline{K}^*}(t) \\
& - \frac{2 f_K \left(m_D \alpha_1 - \alpha_2 v\cdot p_2\right)}{\sqrt{m_D}} \frac{m_\rho^2}{g_\rho} g_{\rho^\pm \pi^\pm \gamma} BW_{\rho^+}(u)
\end{aligned}
\tag{C.29}
$$

$\underline{D_s \to \pi^+\pi^0\gamma}$

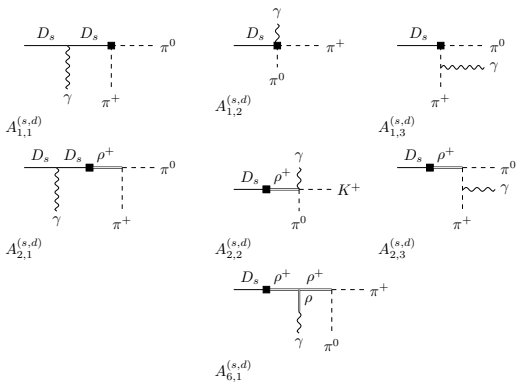

a) Contributions to the parity-even form factors A and E. Additionally, for each of the diagrams $A_{1,2}$, $A_{1,3}$ and $A_{2,3}$ there are additional diagrams where the photon is coupled to the pseudoscalar via a ρ^0-mesons.

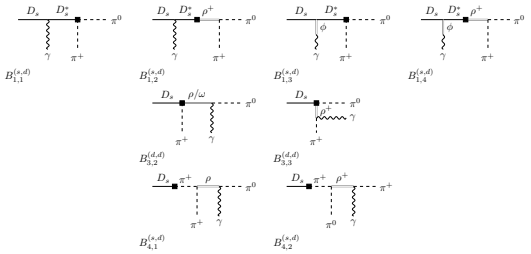

b) Contributions to the parity-odd form factors B and D.

Figure C.4: HHχPTFeynman diagrams for the decay $D_s \to \pi^+\pi^0\gamma$ within the SM.

$$A_{1+2}^{(s,d)} = i\sqrt{2} f_{D_s} \frac{v\cdot p_2 - v\cdot p_1 - v\cdot k}{(v\cdot k)(p_1\cdot k)} \tag{C.30}$$

$$A_6^{(s,d)} = i2\sqrt{2} f_{D_s} \frac{p_1\cdot p_2}{m_{D_s}(v\cdot k)} BW_{\rho^+}(s) \tag{C.31}$$

$$B_1^{(s,d)} = \frac{f_{D_s}}{v\cdot k + \Delta} \left[1 - m_\rho^2 BW_{\rho^+}(s)\right] \left[2\sqrt{2}\lambda' - g_v \lambda \frac{2 g_\phi}{3 m_\phi^2}\right] \tag{C.32}$$

$$B_3^{(s,d)} = -\frac{\sqrt{2} f_{D_s} g_\rho}{f_\pi} \left(g_{\rho\pi\gamma} BW_\rho(t) + g_{\rho^\pm\pi^\pm\gamma} BW_{\rho^+}(u)\right) \tag{C.33}$$

$$B_4^{(s,d)} = \frac{\sqrt{2} m_{D_s}^2 f_{D_s} f_\pi m_\rho^2}{g_\rho (m_{D_s}^2 - m_\pi^2)} \left(g_{\rho\pi\gamma} BW_\rho(t) + g_{\rho^\pm\pi^\pm\gamma} BW_{\rho^+}(u)\right) \tag{C.34}$$

$\underline{D_s \to K^+\overline{K}^0\gamma}$

$$A_{1+2}^{(s,d)} = -i f_{D_s} \frac{v\cdot p_2 - v\cdot p_1 - v\cdot k}{(v\cdot k)(p_1\cdot k)} \tag{C.35}$$

$$A_6^{(s,d)} = -i2 f_{D_s} \frac{p_1\cdot p_2}{m_{D_s}(v\cdot k)} BW_{\rho^+}(s) \tag{C.36}$$

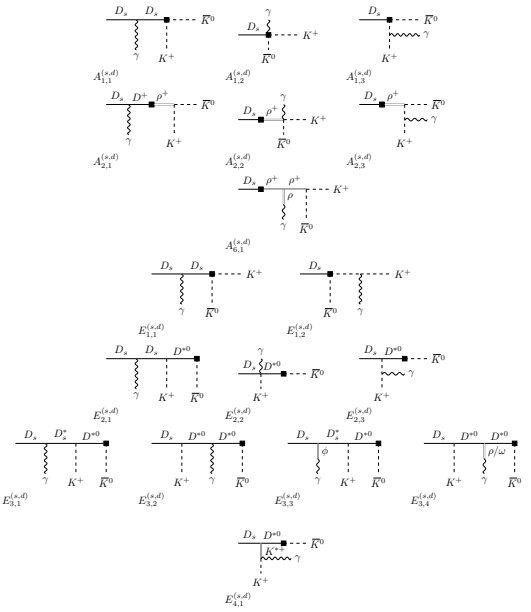

a) Contributions to the parity-even form factors A and E. Additionally, for each of the diagrams $A_{1,2}$, $A_{1,3}$, $A_{2,3}$, $E_{1,2}$ nd $E_{2,3}$ there are additional diagrams where the photon is coupled to the pseudoscalar via a ρ^0-, ω-, ϕ-mesons.

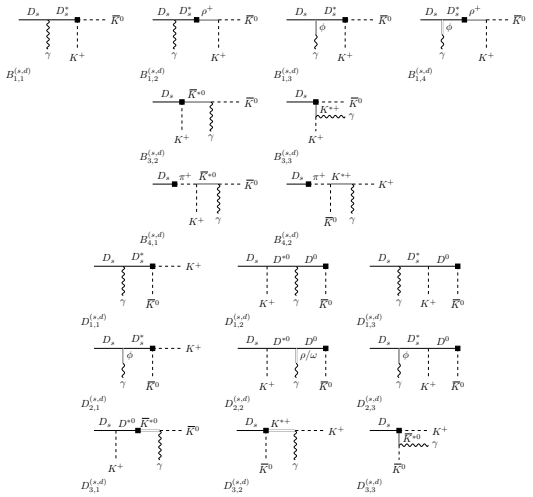

b) Contributions to the parity-odd form factors B and D.

Figure C.5: HHχPTFeynman diagrams for the decay $D_s \to K^+ \overline{K}^0 \gamma$ within the SM.

$$E_1^{(s,d)} = -if_{D_s} \frac{v \cdot p_2}{(v \cdot k)(p_1 \cdot k)} \tag{C.37}$$

$$E_2^{(s,d)} = -i\sqrt{\frac{m_D}{m_{D_s}}} f_D g \frac{p_1 \cdot p_2 - (v \cdot p_1)(v \cdot p_2) + (v \cdot k)(m_{D_s} - v \cdot p_2)}{(v \cdot k + v \cdot p_1 + \Delta)(v \cdot k)(p_1 \cdot k)} \tag{C.38}$$

$$\begin{aligned} E_3^{(s,d)} = &-i\sqrt{\frac{m_D}{m_{D_s}}} \frac{f_D g (v \cdot k)}{v \cdot k + v \cdot p_1 + \Delta} \\ &\times \left[\frac{2\lambda' + \frac{1}{\sqrt{2}} g_v \lambda \left(\frac{g_\omega}{3m_\omega^2} + \frac{g_\rho}{m_\rho^2} \right)}{v \cdot p_1 + \Delta} - \frac{2\lambda' - g_v \lambda \frac{\sqrt{2} g_\phi}{3m_\phi^2}}{v \cdot k + \Delta} \right] \end{aligned} \tag{C.39}$$

$$B_1^{(s,d)} = -\frac{f_{D_s}}{v \cdot k + \Delta} \left[1 - m_\rho^2 BW_{\rho^+}(s) \right] \left[2\lambda' - g_v \lambda \frac{\sqrt{2} g_\phi}{3m_\phi^2} \right] \tag{C.40}$$

$$B_3^{(s,d)} = \frac{f_{D_s} g_{K^*}}{f_K} \left(g_{K^* K \gamma} BW_{K^*}(t) + g_{K^{*\pm} K^\pm \gamma} BW_{K^{*+}}(u) \right) \tag{C.41}$$

$$B_4^{(s,d)} = -\frac{m_{D_s}^2 f_{D_s} f_\pi}{m_{D_s}^2 - m_\pi^2} \frac{m_{K^*}^2}{g_{K^*}} \left(g_{K^{*\pm} K^\pm \gamma} BW_{K^{*+}}(u) + g_{K^* K \gamma} BW_{K^*}(t) \right) \tag{C.42}$$

$$D_1^{(s,d)} = -2\lambda' \left[\frac{f_{D_s}}{v\cdot k + \Delta} + \frac{\sqrt{m_D} f_D g (v\cdot p_2)}{\sqrt{m_{D_s}}(v\cdot k + v\cdot p_1)} \left(\frac{1}{v\cdot k + \Delta} + \frac{1}{v\cdot p_1 + \Delta} \right) \right] \tag{C.43}$$

$$D_2^{(s,d)} = -g_v\lambda \left[\frac{-f_{D_s} \frac{\sqrt{2} g_\phi}{3m_\phi^2}}{v\cdot k + \Delta} + \frac{\sqrt{m_D} f_D g (v\cdot p_2)}{\sqrt{m_{D_s}}(v\cdot k + v\cdot p_1)} \left(\frac{-\frac{\sqrt{2} g_\phi}{3m_\phi^2}}{v\cdot k + \Delta} + \frac{\frac{1}{\sqrt{2}} \left(\frac{g_\omega}{3m_\omega^2} + \frac{g_\rho}{m_\rho^2} \right)}{v\cdot p_1 + \Delta} \right) \right] \tag{C.44}$$

$$\begin{aligned} D_3^{(s,d)} = {} & \frac{g_{K^*} g_{K^*K\gamma}}{f_K} \left(f_{D_s} + \sqrt{\frac{m_D}{m_{D_s}}} f_D g \frac{m_{D_s} - v\cdot p_1}{v\cdot p_1 + \Delta} \right) BW_{K^*}(t) \\ & - \frac{2 f_K \left(m_{D_s} \alpha_1 - \alpha_2 v\cdot p_2 \right)}{\sqrt{m_{D_s}}} \frac{m_{K^*}^2}{g_{K^*}} g_{K^{*\pm}K^\pm\gamma} BW_{K^{*+}}(u) \end{aligned} \tag{C.45}$$

C.1.2 Singly Cabibbo suppressed modes

$\underline{D^0 \to \pi^+\pi^-\gamma}$

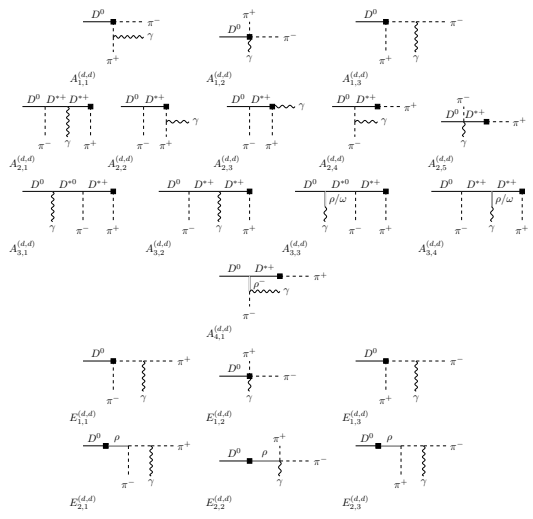

a) Contributions to the parity-even form factors A and E. For each of the diagrams $A_{1,1}$, $A_{1,2}$, $A_{1,3}$, $A_{2,2}$, $A_{2,3}$, $A_{2,4}$, $E_{1,1}$, $E_{1,2}$, $E_{1,3}$, $E_{2,1}$ and $E_{2,3}$ there are additional diagrams where the photon is coupled to the pseudoscalar via a ρ^0-mesons.

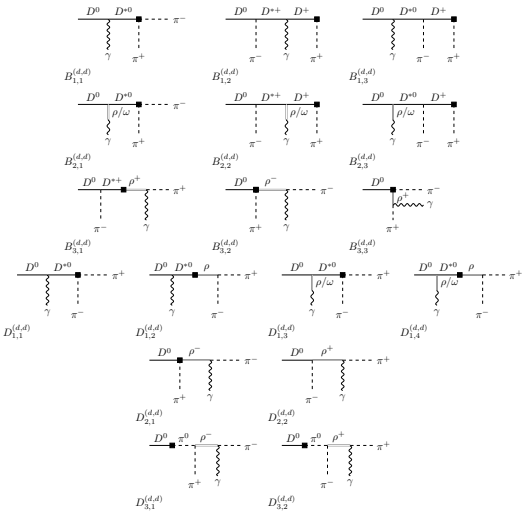

b) Contributions to the parity-odd form factors B and D.

Figure C.6: HHχPTFeynman diagrams for the decay $D^0 \to \pi^+\pi^-\gamma$ within the SM.

$$A_1^{(d,d)} = if_D \frac{p_1 \cdot k - m_D(v \cdot k + v \cdot p_1)}{(p_1 \cdot k)(p_2 \cdot k)} \tag{C.46}$$

$$\begin{aligned} A_2^{(d,d)} = &-im_D f_D \frac{g}{(p_1 \cdot k)(p_2 \cdot k)} \left(\frac{p_2 \cdot k(m_D - v \cdot p_2)}{m_D(v \cdot p_2 + \Delta)} \right. \\ &+ \frac{p_2 \cdot k\,[p_1 \cdot p_2 - (v \cdot p_1)(v \cdot p_2)]}{m_D(v \cdot p_2 + \Delta)(v \cdot p_2 + v \cdot k + \Delta)} \\ &\left. + \frac{(m_D - v \cdot p_1)p_1 \cdot k + m_D p_1 \cdot p_2 + m_D(v \cdot p_1)(v \cdot p_2)}{m_D(v \cdot p_2 + v \cdot k + \Delta)} \right) \end{aligned} \tag{C.47}$$

$$\begin{aligned} A_3^{(d,d)} = &\, if_D g \frac{v \cdot k}{v \cdot k + v \cdot p_2 + \Delta} \\ &\times \left(\frac{2\lambda' + \frac{1}{\sqrt{2}}\lambda g_v \left(\frac{g_\omega}{3m_\omega^2} - \frac{g_\rho}{m_\rho^2} \right)}{v \cdot p_2 + \Delta} - \frac{2\lambda' + \frac{1}{\sqrt{2}}\lambda g_v \left(\frac{g_\omega}{3m_\omega^2} + \frac{g_\rho}{m_\rho^2} \right)}{v \cdot k + \Delta} \right) \end{aligned} \tag{C.48}$$

$$B_1^{(d,d)} = 2f_D\lambda' \left(\frac{1}{v \cdot k + \Delta} + g \frac{v \cdot p_1}{(v \cdot p_2 + v \cdot k)} \left[\frac{1}{v \cdot k + \Delta} + \frac{1}{v \cdot p_2 + \Delta} \right] \right) \tag{C.49}$$

$$\begin{aligned} B_2^{(d,d)} = &\frac{1}{\sqrt{2}}\lambda g_v f_D \left(\frac{g_\omega}{3m_\omega^2} + \frac{g_\rho}{m_\rho^2} \right) \frac{1}{v \cdot k + \Delta} \left(1 + g \frac{v \cdot p_1}{(v \cdot p_2 + v \cdot k)} \right) \\ &+ \frac{1}{\sqrt{2}} g\lambda g_v f_D \left(\frac{g_\omega}{3m_\omega^2} - \frac{g_\rho}{m_\rho^2} \right) \frac{v \cdot p_1}{(v \cdot p_2 + v \cdot k)(v \cdot p_2 + \Delta)} \end{aligned} \tag{C.50}$$

$$\begin{aligned} B_3^{(d,d)} = &\frac{2}{\sqrt{m_D}} f_\pi \frac{m_\rho^2}{g_\rho} g_{\rho^\pm\pi^\pm\gamma}(\alpha_1 m_D - \alpha_2 v \cdot p_1) BW_{\rho^-}(t) \\ &- g_\rho g_{\rho^\pm\pi^\pm\gamma} \frac{f_D}{f_\pi} \left(1 + g \frac{m_D - v \cdot p_2}{v \cdot p_2 + \Delta} \right) BW_{\rho^+}(u) \end{aligned} \tag{C.51}$$

$$D_1^{(d,d)} = f_D \frac{1}{v \cdot k + \Delta} \left(1 - m_\rho^2 BW_\rho(s) \right) \left(2\lambda' + \frac{1}{\sqrt{2}}\lambda g_v \left(\frac{g_\omega}{3m_\omega^2} + \frac{g_\rho}{m_\rho^2} \right) \right) \tag{C.52}$$

$$D_2^{(d,d)} = -\frac{f_D}{f_\pi} g_\rho g_{\rho^\pm\pi^\pm\gamma} (BW_{\rho^-}(t) + BW_{\rho^+}(u)) \tag{C.53}$$

$$D_3^{(d,d)} = f_D f_\pi \frac{m_D^2}{m_D^2 - m_{\pi^0}^2} \frac{m_\rho^2}{g_\rho} g_{\rho^\pm\pi^\pm\gamma} \left(BW_{\rho^+}(u) + BW_{\rho^-}(t) \right) \tag{C.54}$$

$$\begin{aligned} a' = &-\frac{g^2 f_D \left(p_2 \cdot k - (v \cdot k)(v \cdot p_2) \right)}{f_\pi^2 (v \cdot p_2 + \Delta)(v \cdot p_1 + v \cdot p_2 + \Delta)} \\ &+ \frac{\alpha_1 (v \cdot k)}{f_\pi^2 \sqrt{m_D}} \left[1 + \frac{f_\pi^2 m_\rho^4}{g_\rho^2} BW_\rho(s) \right] \\ &- \frac{\sqrt{2}\lambda f_D g_v}{(v \cdot p_1 + v \cdot p_2 + \Delta)} \frac{m_\rho^2}{g_\rho} \left(p_2 \cdot k - (v \cdot k)(v \cdot p_2) \right) BW_\rho(s) \end{aligned} \tag{C.55}$$

$$
\begin{aligned}
b' &= \frac{g f_D}{f_\pi^2 (v\cdot p_2 + \Delta)} \left[v\cdot k + \frac{g\,(p_1\cdot k - (v\cdot k)(v\cdot p_1))}{(v\cdot p_1 + v\cdot p_2 + \Delta)} \right] \\
&- \frac{\alpha_1 (v\cdot k)}{f_\pi^2 \sqrt{m_D}} \left[1 + \frac{f_\pi^2 m_\rho^4}{g_\rho^2} BW_\rho(s) \right] \\
&+ \frac{\sqrt{2}\lambda f_D g_v}{(v\cdot p_1 + v\cdot p_2 + \Delta)} \frac{m_\rho^2}{g_\rho} \left(p_1\cdot k - (v\cdot k)(v\cdot p_1)\right) BW_\rho(s)
\end{aligned} \tag{C.56}
$$

$$
\begin{aligned}
c' &= \frac{g f_D}{f_\pi^2 m_D (v\cdot p_2 + \Delta)} \left[-p_2\cdot k + \frac{g\left((p_2\cdot k)(v\cdot p_1) - (p_1\cdot k)(v\cdot p_2)\right)}{(v\cdot p_1 + v\cdot p_2 + \Delta)} \right] \\
&+ \frac{\alpha_1}{f_\pi^2 m_D^{\frac{3}{2}}} (p_2\cdot k - p_1\cdot k) \left[1 + \frac{f_\pi^2 m_\rho^4}{g_\rho^2} BW_\rho(s) \right] \\
&- \frac{\sqrt{2}\lambda f_D g_v}{m_D (v\cdot p_1 + v\cdot p_2 + \Delta)} \frac{m_\rho^2}{g_\rho} \left((p_1\cdot k)(v\cdot p_2) - (p_2\cdot k)(v\cdot p_1)\right) BW_\rho(s)
\end{aligned} \tag{C.57}
$$

$$
\begin{aligned}
h' &= \frac{g f_D}{2 f_\pi^2 m_D (v\cdot p_2 + \Delta)} \left[1 + \frac{g v\cdot k}{(v\cdot p_1 + v\cdot p_2 + \Delta)} \right] \\
&+ \frac{\alpha_1}{f_\pi^2 m_D^{\frac{3}{2}}} \left[1 + \frac{f_\pi^2 m_\rho^4}{g_\rho^2} BW_\rho(s) \right] \\
&+ \frac{\lambda f_D g_v\,(v\cdot k)}{\sqrt{2} m_D (v\cdot p_1 + v\cdot p_2 + \Delta)} \frac{m_\rho^2}{g_\rho} BW_\rho(s)
\end{aligned} \tag{C.58}
$$

$\underline{D^0 \to \pi^0\pi^0\gamma}$

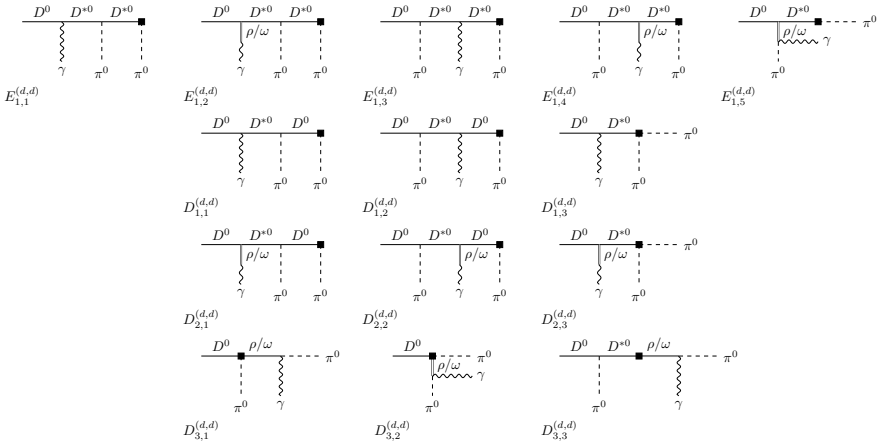

Figure C.7: HHχPTFeynman diagrams for the decay $D^0 \to \pi^0\pi^0\gamma$ within the SM.

$$E_1^{(d,d)} = igf_D \frac{(v\cdot k)(v\cdot p_1 - v\cdot p_2)}{(v\cdot k + v\cdot p_1 + \Delta)(v\cdot k + v\cdot p_2 + \Delta)} \left(\lambda' + \frac{1}{2\sqrt{2}}\lambda g_v \left(\frac{g_\omega}{3m_\omega^2} + \frac{g_\rho}{m_\rho^2}\right)\right) \cdot \left(\frac{1}{v\cdot k + \Delta} - \frac{m_D + 2\Delta}{(v\cdot p_1 + \Delta)(v\cdot p_2 + \Delta)}\right) \tag{C.59}$$

$$D_1^{(d,d)} = -f_D g\lambda' \left[\frac{m_D(v\cdot p_1 - v\cdot p_2)}{(v\cdot p_1 + v\cdot k)(v\cdot p_2 + v\cdot k)(v\cdot k + \Delta)} + \frac{v\cdot p_1}{(v\cdot p_2 + \Delta)(v\cdot p_2 + v\cdot k)} - \frac{v\cdot p_2}{(v\cdot p_1 + \Delta)(v\cdot p_1 + v\cdot k)}\right] \tag{C.60}$$

$$D_2^{(d,d)} = -\frac{1}{2\sqrt{2}} f_D g\lambda g_v \left(\frac{g_\omega}{3m_\omega^2} + \frac{g_\rho}{m_\rho^2}\right) \left[\frac{m_D(v\cdot p_1 - v\cdot p_2)}{(v\cdot p_1 + v\cdot k)(v\cdot p_2 + v\cdot k)(v\cdot k + \Delta)} + \frac{v\cdot p_1}{(v\cdot p_2 + \Delta)(v\cdot p_2 + v\cdot k)} - \frac{v\cdot p_2}{(v\cdot p_1 + \Delta)(v\cdot p_1 + v\cdot k)}\right] \tag{C.61}$$

$$\begin{aligned} D_3^{(d,d)} = {} & \sqrt{\frac{1}{m_D}} f_\pi(\alpha_1 m_D - \alpha_2 v\cdot p_2)\left(\frac{m_\rho^2 g_{\rho\pi\gamma}}{g_\rho} BW_\rho(u) + \frac{m_\omega^2 g_{\omega\pi\gamma}}{g_\omega} BW_\omega(u)\right) \\ & - \sqrt{\frac{1}{m_D}} f_\pi(\alpha_1 m_D - \alpha_2 v\cdot p_1)\left(\frac{m_\rho^2 g_{\rho\pi\gamma}}{g_\rho} BW_\rho(t) + \frac{m_\omega^2 g_{\omega\pi\gamma}}{g_\omega} BW_\omega(t)\right) \\ & + \frac{f_D}{2f_\pi}\left(1 + g\frac{m_D - v\cdot p_2}{v\cdot p_2 + \Delta}\right)\left(g_\rho g_{\rho\pi\gamma} BW_\rho(u) - g_\omega g_{\omega\pi\gamma} BW_\omega(u)\right) \\ & - \frac{f_D}{2f_\pi}\left(1 + g\frac{m_D - v\cdot p_1}{v\cdot p_1 + \Delta}\right)\left(g_\rho g_{\rho\pi\gamma} BW_\rho(t) - g_\omega g_{\omega\pi\gamma} BW_\omega(t)\right) \end{aligned} \tag{C.62}$$

$$a' = \frac{gf_D}{2f_\pi^2(v\cdot p_1 + \Delta)}\left[v\cdot k - \frac{g(v\cdot p_1 - v\cdot p_2)\,(p_2\cdot k - (v\cdot k)(v\cdot p_2))}{(v\cdot p_2 + \Delta)(v\cdot p_2 + v\cdot p_1 + \Delta)}\right] \tag{C.63}$$

$$b' = \frac{gf_D}{2f_\pi^2(v\cdot p_2 + \Delta)}\left[v\cdot k + \frac{g(v\cdot p_1 - v\cdot p_2)\,(p_1\cdot k - (v\cdot k)(v\cdot p_1))}{(v\cdot p_1 + \Delta)(v\cdot p_1 + v\cdot p_2 + \Delta)}\right] \tag{C.64}$$

$$\begin{aligned} c' = {} & -\frac{gf_D}{2f_\pi^2 m_D}\left[\frac{p_2\cdot k}{v\cdot p_2 + \Delta} + \frac{p_1\cdot k}{v\cdot p_1 + \Delta}\right] \\ & + \frac{g^2 f_D}{2f_\pi^2 m_D}\frac{(v\cdot p_1 - v\cdot p_2)\,((p_2\cdot k)(v\cdot p_1) - (p_1\cdot k)(v\cdot p_2))}{(v\cdot p_1 + \Delta)(v\cdot p_2 + \Delta)(v\cdot p_1 + v\cdot p_2 + \Delta)} \end{aligned} \tag{C.65}$$

$$h' = \frac{g^2 f_D}{4f_\pi^2 m_D}\frac{(v\cdot k)(v\cdot p_1 - v\cdot p_2)}{(v\cdot p_1 + \Delta)(v\cdot p_2 + \Delta)(v\cdot p_1 + v\cdot p_2 + \Delta)} \tag{C.66}$$

$D^0 \to K^+K^-\gamma$

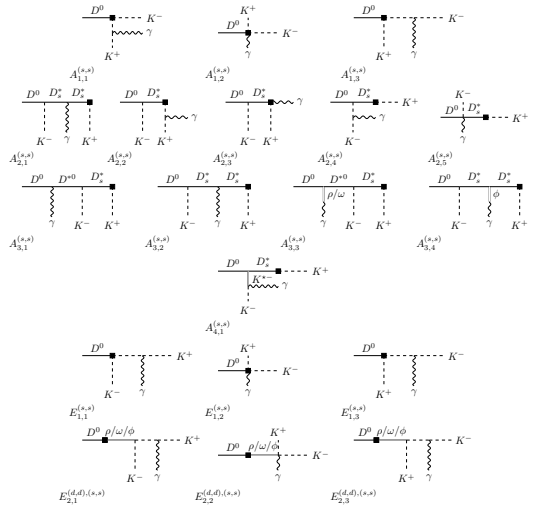

a) Contributions to the parity-even form factors A and E. For each of the diagrams $A_{1,1}$, $A_{1,2}$, $A_{1,3}$, $A_{2,2}$, $A_{2,3}$, $A_{2,4}$, $E_{1,1}$, $E_{1,2}$, $E_{1,3}$, $E_{2,1}$ and $E_{2,3}$ there are additional diagrams where the photon is coupled to the pseudoscalar via a ρ^0-, ω-, ϕ-mesons.

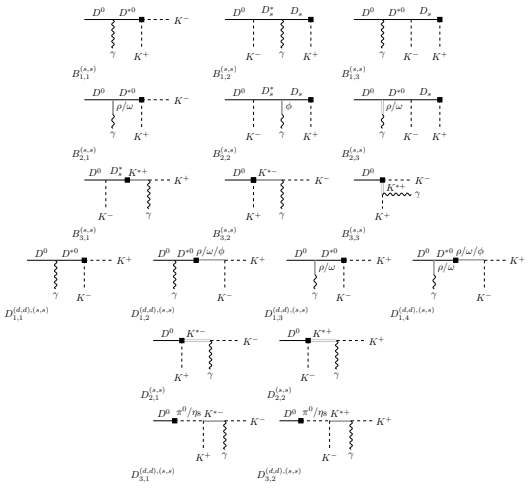

b) Contributions to the parity-odd form factors B and D.

Figure C.8: HHχPTFeynman diagrams for the decay $D^0 \to K^+K^-\gamma$ within the SM.

$$A_1^{(s,s)} = if_D \frac{p_1\cdot k - m_D(v\cdot k + v\cdot p_1)}{(p_1\cdot k)(p_2\cdot k)} \tag{C.67}$$

$$\begin{aligned} A_2^{(s,s)} = -i\sqrt{m_D m_{D_s}} f_{D_s} \frac{g}{(p_1\cdot k)(p_2\cdot k)} \Bigg(& \frac{p_2\cdot k(m_D - v\cdot p_2)}{m_D(v\cdot p_2 + \Delta)} \\ & + \frac{p_2\cdot k\,[p_1\cdot p_2 - (v\cdot p_1)(v\cdot p_2)]}{m_D(v\cdot p_2+\Delta)(v\cdot p_2 + v\cdot k + \Delta)} \\ & + \frac{(m_D - v\cdot p_1)p_1\cdot k + m_D p_1\cdot p_2 + m_D(v\cdot p_1)(v\cdot p_2)}{m_D(v\cdot p_2 + v\cdot k + \Delta)} \Bigg) \end{aligned} \tag{C.68}$$

$$A_3^{(s,s)} = i\sqrt{\frac{m_{D_s}}{m_D}} f_{D_s} g \frac{v\cdot k}{v\cdot k + v\cdot p_2 + \Delta} \left(\frac{2\lambda' - \frac{\sqrt{2}}{3}\lambda g_v \frac{g_\phi}{m_\phi^2}}{v\cdot p_2 + \Delta} - \frac{2\lambda' + \frac{1}{\sqrt{2}}\lambda g_v \left(\frac{g_\omega}{3m_\omega^2} + \frac{g_\rho}{m_\rho^2}\right)}{v\cdot k + \Delta} \right) \tag{C.69}$$

$$B_1^{(s,s)} = 2f_D\lambda' \left(\frac{1}{v\cdot k + \Delta} + g\frac{f_{D_s}}{f_D}\sqrt{\frac{m_{D_s}}{m_D}} \frac{v\cdot p_1}{(v\cdot p_2 + v\cdot k)} \left[\frac{1}{v\cdot k + \Delta} + \frac{1}{v\cdot p_2 + \Delta} \right] \right) \tag{C.70}$$

$$
\begin{aligned}
B_2^{(s,s)} &= \frac{1}{\sqrt{2}}\lambda g_v \left(\frac{g_\omega}{3m_\omega^2}+\frac{g_\rho}{m_\rho^2}\right)\frac{1}{v\cdot k+\Delta}\left(f_D + g f_{D_s}\sqrt{\frac{m_{D_s}}{m_D}}\frac{v\cdot p_1}{(v\cdot p_2+v\cdot k)}\right)\\
&\quad - g\lambda g_v\sqrt{\frac{m_{D_s}}{m_D}} f_{D_s}\frac{\sqrt{2}g_\phi}{3m_\phi^2}\frac{v\cdot p_1}{(v\cdot p_2+v\cdot k)(v\cdot p_2+\Delta)}
\end{aligned}
\tag{C.71}
$$

$$
\begin{aligned}
B_3^{(s,s)} &= \frac{2}{\sqrt{m_D}} f_K \frac{m_{K^*}^2}{g_{K^*}} g_{K^{*\pm}K^\pm\gamma}(\alpha_1 m_D - \alpha_2 v\cdot p_1) BW_{K^{*-}}(t)\\
&\quad - g_{K^*} g_{K^{*\pm}K^\pm\gamma}\frac{f_D}{f_K}\left(1+g\sqrt{\frac{m_{D_s}}{m_D}}\frac{f_{D_s}}{f_D}\frac{m_D - v\cdot p_2}{v\cdot p_2+\Delta}\right) BW_{K^{*+}}(u)
\end{aligned}
\tag{C.72}
$$

$$
D_1^{(s,s)} = f_D \frac{1}{v\cdot k+\Delta}\left(1-m_\phi^2 BW_\phi(s)\right)\left(2\lambda' + \frac{1}{\sqrt{2}}\lambda g_v\left(\frac{g_\omega}{3m_\omega^2}+\frac{g_\rho}{m_\rho^2}\right)\right) \tag{C.73}
$$

$$
\begin{aligned}
D_1^{(d,d)} &= f_D \frac{1}{v\cdot k+\Delta}\left(m_\omega^2 BW_\omega(s) - m_\rho^2 BW_\rho(s)\right)\\
&\quad \times\left(\lambda' + \frac{1}{2\sqrt{2}}\lambda g_v\left(\frac{g_\omega}{3m_\omega^2}+\frac{g_\rho}{m_\rho^2}\right)\right)
\end{aligned}
\tag{C.74}
$$

$$
D_2^{(s,s)} = -\frac{f_D}{f_K} g_{K^*} g_{K^{*\pm}K^\pm\gamma}\left(BW_{K^{*+}}(u) + BW_{K^{*-}}(t)\right) \tag{C.75}
$$

$$
D_3^{(s,s)} = \frac{f_D f_{\eta_8}}{2}\frac{m_D^2}{m_D^2-m_{\eta_8}^2}\frac{m_{K^*}^2}{g_{K^*}} g_{K^{*\pm}K^\pm\gamma}\left(BW_{K^{*+}}(u) + BW_{K^{*-}}(t)\right) \tag{C.76}
$$

$$
\begin{aligned}
D_3^{(d,d)} &= -\frac{f_D}{2} m_D^2\left(\frac{f_{\eta_8}}{m_D^2-m_{\eta_8}^2}+\frac{f_\pi}{m_D^2-m_\pi^2}\right)\\
&\quad \times \frac{m_{K^*}^2}{g_{K^*}} g_{K^{*\pm}K^\pm\gamma}\left(BW_{K^{*+}}(u) + BW_{K^{*-}}(t)\right)
\end{aligned}
\tag{C.77}
$$

$$
\begin{aligned}
a' &= -\frac{g^2 f_D\left(p_2\cdot k - (v\cdot k)(v\cdot p_2)\right)}{f_K^2(v\cdot p_2+\Delta)(v\cdot p_1+v\cdot p_2+\Delta)}\\
&\quad + \frac{\alpha_1(v\cdot k)}{f_K^2\sqrt{m_D}}\left[1+\frac{f_K^2}{2}\left(\frac{m_\rho^4}{g_\rho^2}BW_\rho(s)+\frac{m_\omega^4}{g_\omega^2}BW_\omega(s)\right)\right]\\
&\quad - \frac{\lambda f_D g_v\left(p_2\cdot k-(v\cdot k)(v\cdot p_2)\right)}{\sqrt{2}(v\cdot p_1+v\cdot p_2+\Delta)}\left(\frac{m_\rho^2}{g_\rho}BW_\rho(s)+\frac{m_\omega^2}{g_\omega}BW_\omega(s)\right)
\end{aligned}
\tag{C.78}
$$

$$
\begin{aligned}
b' &= \frac{g f_D}{f_K^2(v\cdot p_2+\Delta)}\left[\frac{f_{D_s}\sqrt{m_{D_s}}}{f_D\sqrt{m_D}}v\cdot k + \frac{g\left(p_1\cdot k-(v\cdot k)(v\cdot p_1)\right)}{(v\cdot p_1+v\cdot p_2+\Delta)}\right]\\
&\quad - \frac{\alpha_1(v\cdot k)}{f_K^2\sqrt{m_D}}\left[1+\frac{f_K^2}{2}\left(\frac{m_\rho^4}{g_\rho^2}BW_\rho(s)+\frac{m_\omega^4}{g_\omega^2}BW_\omega(s)\right)\right]\\
&\quad + \frac{\lambda f_D g_v\left(p_1\cdot k-(v\cdot k)(v\cdot p_1)\right)}{\sqrt{2}(v\cdot p_1+v\cdot p_2+\Delta)}\left(\frac{m_\rho^2}{g_\rho}BW_\rho(s)+\frac{m_\omega^2}{g_\omega}BW_\omega(s)\right)
\end{aligned}
\tag{C.79}
$$

$$
\begin{aligned}
c' = & \frac{g f_D}{f_K^2 m_D (v\cdot p_2 + \Delta)} \left[-\frac{f_{D_s}\sqrt{m_{D_s}}}{f_D \sqrt{m_D}} p_2 \cdot k + \frac{g\left((p_2\cdot k)(v\cdot p_1) - (p_1\cdot k)(v\cdot p_2)\right)}{(v\cdot p_1 + v\cdot p_2 + \Delta)} \right] \\
& + \frac{\alpha_1}{f_K^2 m_D^{\frac{3}{2}}} (p_2\cdot k - p_1\cdot k) \left[1 + \frac{f_K^2}{2} \left(\frac{m_\rho^4}{g_\rho^2} BW_\rho(s) + \frac{m_\omega^4}{g_\omega^2} BW_\omega(s) \right) \right] \\
& - \frac{\lambda f_D g_v \left((p_1\cdot k)(v\cdot p_2) - (p_2\cdot k)(v\cdot p_1)\right)}{\sqrt{2} m_D (v\cdot p_1 + v\cdot p_2 + \Delta)} \left(\frac{m_\rho^2}{g_\rho} BW_\rho(s) + \frac{m_\omega^2}{g_\omega} BW_\omega(s) \right)
\end{aligned}
\tag{C.80}
$$

$$
\begin{aligned}
h' = & \frac{g f_D}{2 f_K^2 m_D (v\cdot p_2 + \Delta)} \left[\frac{f_{D_s}\sqrt{m_{D_s}}}{f_D \sqrt{m_D}} + \frac{g v\cdot k}{(v\cdot p_1 + v\cdot p_2 + \Delta)} \right] \\
& + \frac{\alpha_1}{f_K^2 m_D^{\frac{3}{2}}} \left[1 + \frac{f_K^2}{2} \left(\frac{m_\rho^4}{g_\rho^2} BW_\rho(s) + \frac{m_\omega^4}{g_\omega^2} BW_\omega(s) \right) \right] \\
& + \frac{\lambda f_D g_v (v\cdot k)}{2\sqrt{2} m_D (v\cdot p_1 + v\cdot p_2 + \Delta)} \left(\frac{m_\rho^2}{g_\rho} BW_\rho(s) + \frac{m_\omega^2}{g_\omega} BW_\omega(s) \right)
\end{aligned}
\tag{C.81}
$$

$\underline{D^0 \to K^0 \overline{K}^0 \gamma}$

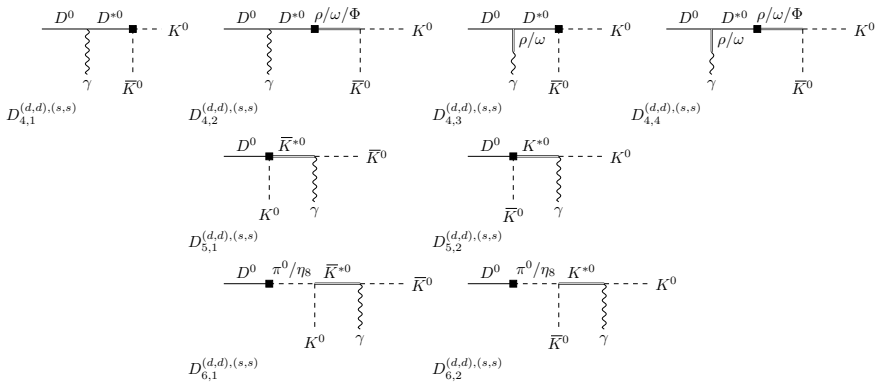

Figure C.9: HHχPTFeynman diagrams for the decay $D^0 \to K^0 \overline{K}^0 \gamma$ within the SM.

$$D_4^{(d,d)} = -f_D \frac{1}{v\cdot k + \Delta}\left(1 + \frac{m_\rho^2}{2} BW_\rho(s) + \frac{m_\omega^2}{2} BW_\omega(s)\right) \times \left(2\lambda' + \frac{1}{\sqrt{2}}\lambda g_v \left(\frac{g_\omega}{3m_\omega^2} + \frac{g_\rho}{m_\rho^2}\right)\right) \tag{C.82}$$

$$D_4^{(s,s)} = f_D \frac{1}{v\cdot k + \Delta}\left(1 + m_\phi^2 BW_\phi(s)\right)\left(2\lambda' + \frac{1}{\sqrt{2}}\lambda g_v \left(\frac{g_\omega}{3m_\omega^2} + \frac{g_\rho}{m_\rho^2}\right)\right) \tag{C.83}$$

$$D_5^{(d,d)} = \frac{f_D}{f_K} g_{K^*} g_{K^*K\gamma} \left(BW_{K^*}(u) + BW_{\overline{K}^*}(t)\right) \tag{C.84}$$

$$D_5^{(s,s)} = -\frac{f_D}{f_K} g_{K^*} g_{K^*K\gamma} \left(BW_{K^*}(u) + BW_{\overline{K}^*}(t)\right) \tag{C.85}$$

$$D_6^{(d,d)} = -\frac{f_D m_D^2}{2}\left(\frac{f_\pi}{m_D^2 - m_\pi^2} + \frac{f_{\eta_8}}{m_D^2 - m_{\eta_8}^2}\right) \times \frac{m_{K^*}^2}{g_{K^*}} g_{K^*K\gamma} \left(BW_{K^*}(u) + BW_{\overline{K}^*}(t)\right) \tag{C.86}$$

$$D_6^{(s,s)} = \frac{f_D m_D^2}{2} \frac{f_{\eta_8}}{m_D^2 - m_{\eta_8}^2} \frac{m_{K^*}^2}{g_{K^*}} g_{K^*K\gamma} \left(BW_{K^*}(u) + BW_{\overline{K}^*}(t)\right) \tag{C.87}$$

$$a' = \left(-\frac{\alpha_1 (v\cdot k)}{2\sqrt{m_D}} + \frac{\lambda f_D g_v \left(p_2\cdot k - (v\cdot k)(v\cdot p_2)\right)}{\sqrt{2}(v\cdot p_1 + v\cdot p_2 + \Delta)}\right) \times \left(\frac{m_\rho^2}{g_\rho} BW_\rho(s) - \frac{m_\omega^2}{g_\omega} BW_\omega(s)\right) \tag{C.88}$$

$$b' = \left(\frac{\alpha_1 (v\cdot k)}{2\sqrt{m_D}} - \frac{\lambda f_D g_v \left(p_1\cdot k - (v\cdot k)(v\cdot p_1)\right)}{\sqrt{2}(v\cdot p_1 + v\cdot p_2 + \Delta)}\right) \times \left(\frac{m_\rho^2}{g_\rho} BW_\rho(s) - \frac{m_\omega^2}{g_\omega} BW_\omega(s)\right) \tag{C.89}$$

$$c' = \left(\frac{\alpha_1}{2m_D^{\frac{3}{2}}}(p_1\cdot k - p_2\cdot k) + \frac{\lambda f_D g_v \left((p_1\cdot k)(v\cdot p_2) - (p_2\cdot k)(v\cdot p_1)\right)}{\sqrt{2} m_D (v\cdot p_1 + v\cdot p_2 + \Delta)}\right) \times \left(\frac{m_\rho^2}{g_\rho} BW_\rho(s) - \frac{m_\omega^2}{g_\omega} BW_\omega(s)\right) \tag{C.90}$$

$$h' = \left(-\frac{\alpha_1}{2m_D^{\frac{3}{2}}} - \frac{\lambda f_D g_v (v\cdot k)}{2\sqrt{2} m_D (v\cdot p_1 + v\cdot p_2 + \Delta)}\right) \times \left(\frac{m_\rho^2}{g_\rho} BW_\rho(s) - \frac{m_\omega^2}{g_\omega} BW_\omega(s)\right) \tag{C.91}$$

$\underline{D^+ \to \pi^+\pi^0\gamma}$

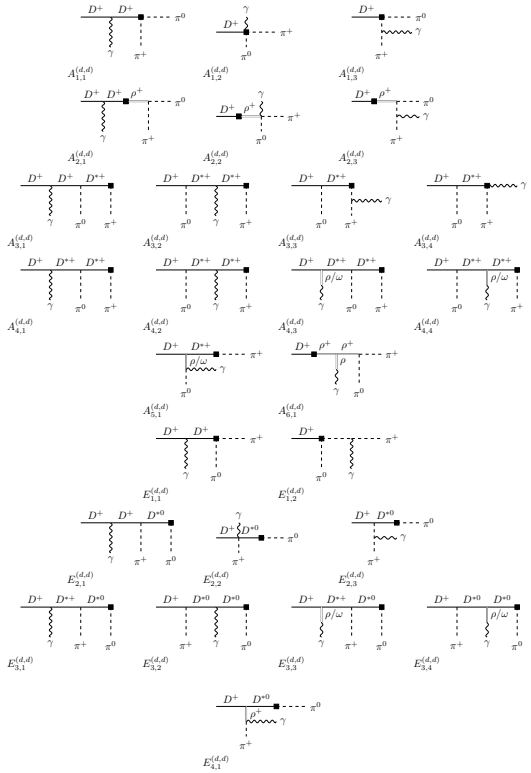

a) Contributions to the parity-even form factors A and E. Note that the diagrams A_1 have two different factorizations. Additionally, for each of the diagrams $A_{1,2}$, $A_{1,3}$, $A_{2,3}$, $A_{3,3}$, $A_{3,4}$, $E_{1,2}$ nd $E_{2,3}$ there are additional diagrams where the photon is coupled to the pseudoscalar via a ρ^0-mesons.

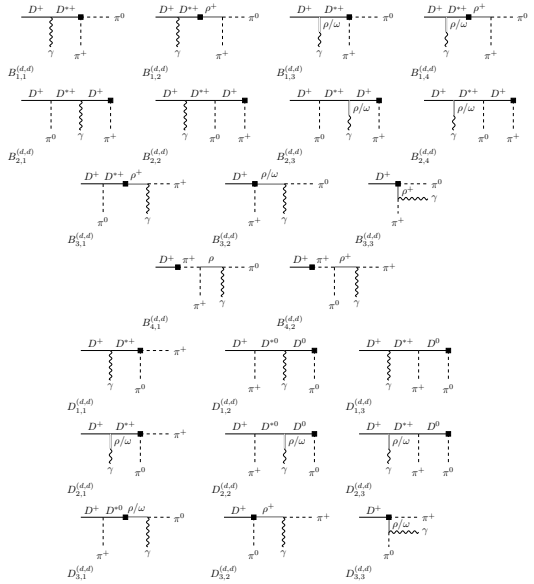

b) Contributions to the parity-odd form factors B and D. Note that the diagrams $B_{1,1/3}$ and $B_{3,2/3}$ have two different factorizations.

Figure C.10: HHχPTFeynman diagrams for the decay $D^+ \to \pi^+\pi^0\gamma$ within the SM.

$$A_{1+2}^{(d,d)} = i\sqrt{2}f_D \frac{v\cdot p_2 - v\cdot p_1 - v\cdot k}{(v\cdot k)(p_1\cdot k)} + i\frac{f_D}{\sqrt{2}}\frac{v\cdot p_1 + v\cdot k}{(v\cdot k)(p_1\cdot k)} \tag{C.92}$$

$$A_3^{(d,d)} = i\frac{f_D g}{\sqrt{2}}\frac{p_1\cdot p_2 - (v\cdot p_1)(v\cdot p_2) + (v\cdot k)(m_D - v\cdot p_2)}{(v\cdot p_2 + \Delta)(v\cdot k)(p_1\cdot k)} \tag{C.93}$$

$$A_4^{(d,d)} = i\frac{f_D g(v\cdot k)}{v\cdot k + v\cdot p_2 + \Delta}\left[\frac{\sqrt{2}\lambda' + \frac{1}{2}g_v\lambda\left(\frac{g_\omega}{3m_\omega^2} - \frac{g_\rho}{m_\rho^2}\right)}{v\cdot k + \Delta} - \frac{\sqrt{2}\lambda' + \frac{1}{2}g_v\lambda\left(\frac{g_\omega}{3m_\omega^2} - \frac{g_\rho}{m_\rho^2}\right)}{v\cdot p_2 + \Delta}\right] \tag{C.94}$$

$$A_6^{(d,d)} = i2\sqrt{2}f_D\frac{p_1\cdot p_2}{m_D(v\cdot k)}BW_{\rho^+}(s) \tag{C.95}$$

$$E_1^{(d,d)} = i\frac{f_D}{\sqrt{2}}\frac{v\cdot p_2}{(v\cdot k)(p_1\cdot k)} \tag{C.96}$$

$$E_2^{(d,d)} = i\frac{f_D g}{\sqrt{2}}\frac{p_1\cdot p_2 - (v\cdot p_1)(v\cdot p_2) + (v\cdot k)(m_D - v\cdot p_2)}{(v\cdot k + v\cdot p_1 + \Delta)(v\cdot k)(p_1\cdot k)} \tag{C.97}$$

$$E_3^{(d,d)} = i\frac{f_D g(v\cdot k)}{v\cdot k + v\cdot p_1 + \Delta}\left[\frac{\sqrt{2}\lambda' + \frac{1}{2}g_v\lambda\left(\frac{g_\omega}{3m_\omega^2} + \frac{g_\rho}{m_\rho^2}\right)}{v\cdot p_1 + \Delta} - \frac{\sqrt{2}\lambda' + \frac{1}{2}g_v\lambda\left(\frac{g_\omega}{3m_\omega^2} - \frac{g_\rho}{m_\rho^2}\right)}{v\cdot k + \Delta}\right] \tag{C.98}$$

$$B_1^{(d,d)} = \frac{f_D}{v\cdot k + \Delta}\left[\frac{1}{2} - m_\rho^2 BW_{\rho^+}(s)\right]\left[2\sqrt{2}\lambda' + g_v\lambda\left(\frac{g_\omega}{3m_\omega^2} - \frac{g_\rho}{m_\rho^2}\right)\right] \tag{C.99}$$

$$B_2^{(d,d)} = -\frac{f_D g(v\cdot p_1)}{v\cdot k + v\cdot p_2}\left[\frac{\sqrt{2}\lambda' + \frac{1}{2}g_v\lambda\left(\frac{g_\omega}{3m_\omega^2} - \frac{g_\rho}{m_\rho^2}\right)}{v\cdot p_2 + \Delta} + \frac{\sqrt{2}\lambda' + \frac{1}{2}g_v\lambda\left(\frac{g_\omega}{3m_\omega^2} - \frac{g_\rho}{m_\rho^2}\right)}{v\cdot k + \Delta}\right] \tag{C.100}$$

$$\begin{aligned} B_3^{(d,d)} = {} & \frac{f_D g_\rho g_{\rho^\pm\pi^\pm\gamma}}{\sqrt{2}f_\pi}\left(1 + g\frac{m_D - v\cdot p_2}{v\cdot p_2 + \Delta}\right)BW_{\rho^+}(u) \\ & + \frac{\sqrt{2}f_\pi(m_D\alpha_1 - \alpha_2 v\cdot p_1)}{\sqrt{m_D}}\left(\frac{m_\omega^2}{g_\omega}g_{\omega\pi\gamma}BW_\omega(t) - \frac{m_\rho^2}{g_\rho}g_{\rho\pi\gamma}BW_\rho(t)\right) \\ & - \frac{\sqrt{2}f_D g_\rho}{f_\pi}\left(g_{\rho\pi\gamma}BW_\rho(t) + g_{\rho^\pm\pi^\pm\gamma}BW_{\rho^+}(u)\right) \end{aligned} \tag{C.101}$$

$$B_4^{(d,d)} = \frac{\sqrt{2}m_D^2 f_D f_\pi m_\rho^2}{g_\rho(m_D^2 - m_\pi^2)}\left(g_{\rho\pi\gamma}BW_\rho(t) + g_{\rho^\pm\pi^\pm\gamma}BW_{\rho^+}(u)\right) \tag{C.102}$$

$$D_1^{(d,d)} = \sqrt{2}f_D\lambda'\left[\frac{1}{v\cdot k + \Delta} + \frac{g(v\cdot p_2)}{v\cdot k + v\cdot p_1}\left(\frac{1}{v\cdot k + \Delta} + \frac{1}{v\cdot p_1 + \Delta}\right)\right] \tag{C.103}$$

$$D_2^{(d,d)} = \frac{f_D g_v\lambda}{2}\left[\frac{\frac{g_\omega}{3m_\omega^2} - \frac{g_\rho}{m_\rho^2}}{v\cdot k + \Delta} + \frac{g(v\cdot p_2)}{v\cdot k + v\cdot p_1}\left(\frac{\frac{g_\omega}{3m_\omega^2} - \frac{g_\rho}{m_\rho^2}}{v\cdot k + \Delta} + \frac{\frac{g_\omega}{3m_\omega^2} + \frac{g_\rho}{m_\rho^2}}{v\cdot p_1 + \Delta}\right)\right] \tag{C.104}$$

$$\begin{aligned} D_3^{(d,d)} = {} & \frac{f_D}{\sqrt{2}f_\pi}\left(1 + g\frac{m_D - v\cdot p_1}{v\cdot p_1 + \Delta}\right)\left(g_\omega g_{\omega\pi\gamma}BW_\omega(t) - g_\rho g_{\rho\pi\gamma}BW_\rho(t)\right) \\ & + \frac{\sqrt{2}f_\pi\left(m_D\alpha_1 - \alpha_2 v\cdot p_2\right)}{\sqrt{m_D}}\frac{m_\rho^2}{g_\rho}g_{\rho^\pm\pi^\pm\gamma}BW_{\rho^+}(u) \end{aligned} \tag{C.105}$$

$$\begin{aligned} a' = {} & \frac{f_D g(v\cdot k)}{\sqrt{2}f_\pi^2(v\cdot p_1 + \Delta)} + \frac{f_D g^2\left(p_2\cdot k - (v\cdot k)(v\cdot p_2)\right)}{\sqrt{2}f_\pi^2(v\cdot p_1 + v\cdot p_2 + \Delta)}\left[\frac{1}{v\cdot p_1 + \Delta} + \frac{1}{v\cdot p_2 + \Delta}\right] \\ & - \frac{\sqrt{2}\alpha_1(v\cdot k)}{f_\pi^2\sqrt{m_D}}\left(1 + \frac{f_\pi^2 m_\rho^4}{g_\rho^2}BW_{\rho^+}(s)\right) \\ & + \frac{2f_D\lambda g_v m_\rho^2\left(p_2\cdot k - (v\cdot k)(v\cdot p_2)\right)}{g_\rho(v\cdot p_1 + v\cdot p_2 + \Delta)}BW_{\rho^+}(s) \end{aligned} \tag{C.106}$$

$$
\begin{aligned}
b' = &-\frac{f_D g(v\cdot k)}{\sqrt{2}f_\pi^2(v\cdot p_2+\Delta)} - \frac{f_D g^2\,(p_1\cdot k-(v\cdot k)(v\cdot p_1))}{\sqrt{2}f_\pi^2(v\cdot p_1+v\cdot p_2+\Delta)}\left[\frac{1}{v\cdot p_1+\Delta}+\frac{1}{v\cdot p_2+\Delta}\right]\\
&+\frac{\sqrt{2}\alpha_1(v\cdot k)}{f_\pi^2\sqrt{m_D}}\left(1+\frac{f_\pi^2 m_\rho^4}{g_\rho^2}BW_{\rho^+}(s)\right)\\
&-\frac{2f_D\lambda g_v m_\rho^2\,(p_1\cdot k-(v\cdot k)(v\cdot p_1))}{g_\rho(v\cdot p_1+v\cdot p_2+\Delta)}BW_{\rho^+}(s)
\end{aligned}
\tag{C.107}
$$

$$
\begin{aligned}
c' = &\frac{f_D g}{\sqrt{2}m_D f_\pi^2}\left(\frac{p_2\cdot k}{v\cdot p_2+\Delta}-\frac{p_1\cdot k}{v\cdot p_1+\Delta}\right)\\
&-\frac{f_D g^2\,((p_2\cdot k)(v\cdot p_1)-(p_1\cdot k)(v\cdot p_2))}{\sqrt{2}m_D f_\pi^2(v\cdot p_1+v\cdot p_2+\Delta)}\left(\frac{1}{v\cdot p_1+\Delta}+\frac{1}{v\cdot p_2+\Delta}\right)\\
&+\frac{\sqrt{2}\alpha_1(p_1\cdot k-p_2\cdot k)}{\sqrt{m_D^3}f_\pi^2}\left(1+\frac{f_\pi^2 m_\rho^4}{g_\rho^2}BW_{\rho^+}(s)\right)\\
&-\frac{2f_D\lambda g_v m_\rho^2\,((p_2\cdot k)(v\cdot p_1)-(p_1\cdot k)(v\cdot p_2))}{g_\rho m_D(v\cdot p_1+v\cdot p_2+\Delta)}BW_{\rho^+}(s)
\end{aligned}
\tag{C.108}
$$

$$
\begin{aligned}
h' = &-\frac{f_D g}{2\sqrt{2}m_D f_\pi^2}\left(\frac{1}{v\cdot p_1+\Delta}+\frac{1}{v\cdot p_2+\Delta}\right)\left(1+g\frac{v\cdot k}{v\cdot p_1+v\cdot p_2+\Delta}\right)\\
&-\frac{\sqrt{2}\alpha_1}{\sqrt{m_D^3}f_\pi^2}\left(1+\frac{f_\pi^2 m_\rho^4}{g_\rho^2}BW_{\rho^+}(s)\right)\\
&-\frac{f_D\lambda g_v m_\rho^2(v\cdot k)}{g_\rho m_D(v\cdot p_1+v\cdot p_2+\Delta)}BW_{\rho^+}(s)
\end{aligned}
\tag{C.109}
$$

$\underline{D^+\to K^+\overline{K}^0\gamma}$

$$A_1^{(s,s)} = -if_D\frac{v\cdot p_1+v\cdot k}{(v\cdot k)(p_1\cdot k)} \tag{C.110}$$

$$A_{1+2}^{(d,d)} = -if_D\frac{v\cdot p_2-v\cdot p_1-v\cdot k}{(v\cdot k)(p_1\cdot k)} \tag{C.111}$$

$$A_3^{(s,s)} = -i\sqrt{\frac{m_{D_s}}{m_D}}f_{D_s}g\frac{p_1\cdot p_2-(v\cdot p_1)(v\cdot p_2)+(v\cdot k)(M-v\cdot p_2)}{(v\cdot p_2+\Delta)(v\cdot k)(p_1\cdot k)} \tag{C.112}$$

$$A_4^{(s,s)} = -i\frac{\sqrt{m_{D_s}}f_{D_s}g(v\cdot k)}{\sqrt{m_D}(v\cdot k+v\cdot p_2+\Delta)}\left[\frac{2\lambda'+\frac{1}{\sqrt{2}}g_v\lambda\left(\frac{g_\omega}{3m_\omega^2}-\frac{g_\rho}{m_\rho^2}\right)}{v\cdot k+\Delta}-\frac{2\lambda'-\frac{\sqrt{2}}{3}g_v\lambda\frac{g_\phi}{m_\phi^2}}{v\cdot p_2+\Delta}\right] \tag{C.113}$$

$$A_6^{(d,d)} = -i2f_D\frac{p_1\cdot p_2}{m_D(v\cdot k)}BW_{\rho^+}(s) \tag{C.114}$$

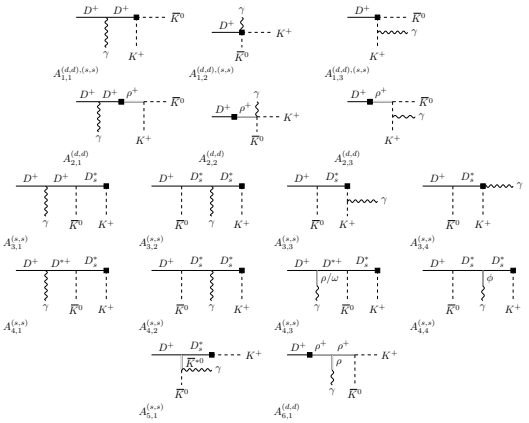

a) Contributions to the parity-even form factors A and E. Note that the diagrams A_1 have two different factorizations. Additionally, for each of the diagrams $A_{1,2}$, $A_{1,3}$, $A_{2,3}$, $A_{3,3}$ and $A_{3,4}$ there are additional diagrams where the photon is coupled to the pseudoscalar via a ρ^0-, ω-, ϕ-mesons.

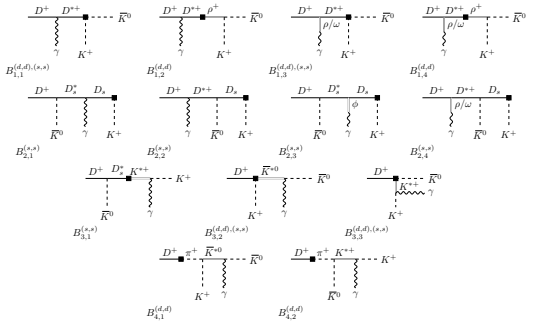

b) Contributions to the parity-odd form factors B and D. Note that the diagrams $B_{1,1/3}$ and $B_{3,2/3}$ have two different factorizations.

Figure C.11: HHχPTFeynman diagrams for the decay $D^+ \to K^+ \overline{K}^0 \gamma$ within the SM.

$$B_1^{(s,s)} = \frac{f_D}{(v\cdot k + \Delta)} \left[2\lambda' + \frac{1}{\sqrt{2}} g_v \lambda \left(\frac{g_\omega}{3m_\omega^2} - \frac{g_\rho}{m_\rho^2} \right) \right] \tag{C.115}$$

$$B_1^{(d,d)} = -\frac{f_D}{v\cdot k + \Delta} \left[1 - m_\rho^2 BW_{\rho^+}(s) \right] \left[2\lambda' + \frac{1}{\sqrt{2}} g_v \lambda \left(\frac{g_\omega}{3m_\omega^2} - \frac{g_\rho}{m_\rho^2} \right) \right] \tag{C.116}$$

$$B_2^{(s,s)} = \frac{\sqrt{m_{D_s}} f_{D_s} g(v\cdot p_1)}{\sqrt{m_D}(v\cdot k + v\cdot p_2)} \left[\frac{2\lambda' - \frac{\sqrt{2}}{3} g_v \lambda \frac{g_\phi}{m_\phi^2}}{v\cdot p_2 + \Delta} + \frac{2\lambda' + \frac{1}{\sqrt{2}} g_v \lambda \left(\frac{g_\omega}{3m_\omega^2} - \frac{g_\rho}{m_\rho^2} \right)}{v\cdot k + \Delta} \right] \tag{C.117}$$

$$\begin{aligned} B_3^{(s,s)} = &-\frac{g_{K^*} g_{K^{*\pm}K^\pm\gamma}}{f_K} \left(f_D + g f_{D_s} \sqrt{\frac{m_{D_s}}{m_D}} \frac{m_D - v\cdot p_2}{v\cdot p_2 + \Delta} \right) BW_{K^{*+}}(u) \\ &+ \frac{2 f_K (m_D \alpha_1 - \alpha_2 v\cdot p_1)}{\sqrt{m_D}} \frac{m_{K^*}^2}{g_{K^*}} g_{K^*K\gamma} BW_{K^*}(t)) \end{aligned} \tag{C.118}$$

$$B_3^{(d,d)} = \frac{f_D g_{K^*}}{f_K} \left(g_{K^*K\gamma} BW_{K^*}(t) + g_{K^{*\pm}K^\pm\gamma} BW_{K^{*+}}(u) \right) \tag{C.119}$$

$$B_4^{(d,d)} = -\frac{m_D^2 f_D f_\pi}{(m_D^2 - m_\pi^2)} \frac{m_{K^*}^2}{g_{K^*}} \left(g_{K^*K\gamma} BW_{K^*}(t) + g_{K^{*\pm}K^\pm\gamma} BW_{K^{*+}}(u) \right) \tag{C.120}$$

$$
\begin{aligned}
a' = & -\frac{f_D g^2 \left(p_2\cdot k-(v\cdot k)(v\cdot p_2)\right)}{f_K^2(v\cdot p_1+v\cdot p_2+\Delta)(v\cdot p_2+\Delta)} \\
& + \frac{\alpha_1(v\cdot k)}{f_K^2\sqrt{m_D}}\left(1+\frac{f_K^2 m_\rho^4}{g_\rho^2}BW_{\rho^+}(s)\right) \\
& - \frac{\sqrt{2}f_D\lambda g_v m_\rho^2\left(p_2\cdot k-(v\cdot k)(v\cdot p_2)\right)}{g_\rho(v\cdot p_1+v\cdot p_2+\Delta)}BW_{\rho^+}(s)
\end{aligned}
\tag{C.121}
$$

$$
\begin{aligned}
b' = & \frac{g}{f_K^2(v\cdot p_2+\Delta)}\left[\sqrt{\frac{m_{D_s}}{m_D}}f_{D_s}(v\cdot k)+f_D g\frac{p_1\cdot k-(v\cdot k)(v\cdot p_1)}{v\cdot p_1+v\cdot p_2+\Delta}\right] \\
& - \frac{\alpha_1(v\cdot k)}{f_K^2\sqrt{m_D}}\left(1+\frac{f_K^2 m_\rho^4}{g_\rho^2}BW_{\rho^+}(s)\right) \\
& + \frac{\sqrt{2}f_D\lambda g_v m_\rho^2\left(p_1\cdot k-(v\cdot k)(v\cdot p_1)\right)}{g_\rho(v\cdot p_1+v\cdot p_2+\Delta)}BW_{\rho^+}(s)
\end{aligned}
\tag{C.122}
$$

$$
\begin{aligned}
c' = & -\frac{g}{f_K^2 m_D(v\cdot p_2+\Delta)}\left[\sqrt{\frac{m_{D_s}}{m_D}}f_{D_s}(p_2\cdot k)-f_D g\frac{(p_2\cdot k)(v\cdot p_1)-(p_1\cdot k)(v\cdot p_2)}{v\cdot p_1+v\cdot p_2+\Delta}\right] \\
& - \frac{\alpha_1(p_1\cdot k-p_2\cdot k)}{\sqrt{m_D^3}f_K^2}\left(1+\frac{f_K^2 m_\rho^4}{g_\rho^2}BW_{\rho^+}(s)\right) \\
& + \frac{\sqrt{2}f_D\lambda g_v m_\rho^2\left((p_2\cdot k)(v\cdot p_1)-(p_1\cdot k)(v\cdot p_2)\right)}{g_\rho m_D(v\cdot p_1+v\cdot p_2+\Delta)}BW_{\rho^+}(s)
\end{aligned}
\tag{C.123}
$$

$$
\begin{aligned}
h' = & \frac{g}{2f_K^2 m_D(v\cdot p_2+\Delta)}\left(\sqrt{\frac{m_{D_s}}{m_D}}f_{D_s}+f_D g\frac{v\cdot k}{v\cdot p_1+v\cdot p_2+\Delta}\right) \\
& + \frac{\alpha_1}{\sqrt{m_D^3}f_K^2}\left(1+\frac{f_K^2 m_\rho^4}{g_\rho^2}BW_{\rho^+}(s)\right) \\
& + \frac{f_D\lambda g_v m_\rho^2(v\cdot k)}{\sqrt{2}g_\rho m_D(v\cdot p_1+v\cdot p_2+\Delta)}BW_{\rho^+}(s)
\end{aligned}
\tag{C.124}
$$

$\underline{D_s \to \pi^+ K^0 \gamma}$

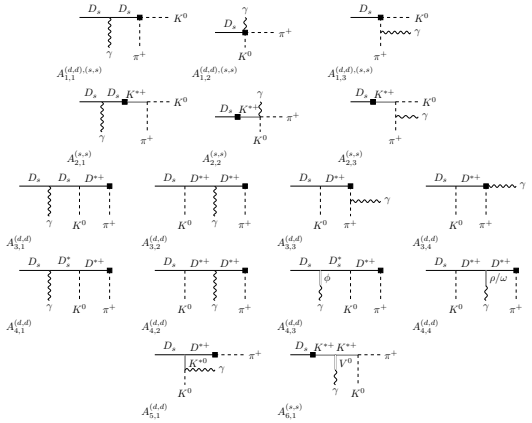

a) Contributions to the parity-even form factors A and E. Note that the diagrams A_1 have two different factorizations. Additionally, for each of the diagrams $A_{1,2}$, $A_{1,3}$, $A_{2,3}$, $A_{3,3}$ and $A_{3,4}$ there are additional diagrams where the photon is coupled to the pseudoscalar via a ρ^0-, ω-, ϕ-mesons.

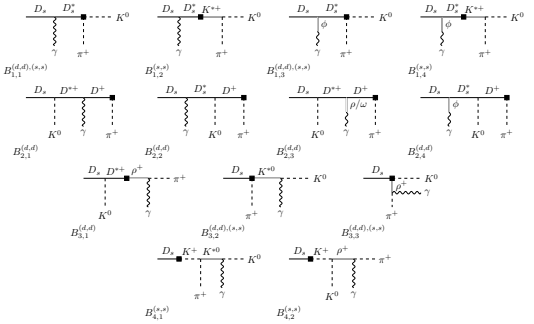

b) Contributions to the parity-odd form factors B and D. Note that the diagrams $B_{1,1/3}$ and $B_{3,2/3}$ have two different factorizations.

Figure C.12: HHχPTFeynman diagrams for the decay $D_s \to \pi^+ K^0 \gamma$ within the SM.

$$A_1^{(d,d)} = -i\frac{f_{D_s} f_\pi}{f_K} \frac{v\cdot p_1 + v\cdot k}{(v\cdot k)(p_1\cdot k)} \tag{C.125}$$

$$A_{1+2}^{(s,s)} = -i f_{D_s} \frac{v\cdot p_2 - v\cdot p_1 - v\cdot k}{(v\cdot k)(p_1\cdot k)} \tag{C.126}$$

$$A_3^{(d,d)} = -i\frac{f_{D_s} f_\pi g}{f_K} \frac{p_1\cdot p_2 - (v\cdot p_1)(v\cdot p_2) + (v\cdot k)(M - v\cdot p_2)}{(v\cdot p_2 + \Delta)(v\cdot k)(p_1\cdot k)} \tag{C.127}$$

$$A_4^{(d,d)} = -i\frac{\sqrt{m_D} f_D f_\pi g (v\cdot k)}{\sqrt{m_{D_s}} f_K (v\cdot k + v\cdot p_2 + \Delta)} \left[\frac{2\lambda' - \frac{\sqrt{2}}{3} g_v \lambda \frac{g_\phi}{m_\phi^2}}{v\cdot k + \Delta} - \frac{2\lambda' + \frac{1}{\sqrt{2}} g_v \lambda \left(\frac{g_\omega}{3m_\omega^2} - \frac{g_\rho}{m_\rho^2} \right)}{v\cdot p_2 + \Delta} \right] \tag{C.128}$$

$$A_6^{(s,s)} = -i2 f_{D_s} \frac{p_1\cdot p_2}{m_{D_s}(v\cdot k)} BW_{K^{*+}}(s) \tag{C.129}$$

$$B_1^{(d,d)} = \frac{f_{D_s} f_\pi}{f_K (v\cdot k + \Delta)} \left[2\lambda' - \frac{\sqrt{2}}{3} g_v \lambda \frac{g_\phi}{m_\phi^2} \right] \tag{C.130}$$

$$B_1^{(s,s)} = -\frac{f_{D_s}}{v\cdot k + \Delta} \left[1 - m_{K^*}^2 BW_{K^{*+}}(s) \right] \left[2\lambda' - \frac{\sqrt{2}}{3} g_v \lambda \frac{g_\phi}{m_\phi} \right] \tag{C.131}$$

$$
\begin{aligned}
B_2^{(d,d)} &= \frac{\sqrt{m_D} f_D f_\pi g (v\cdot p_1)}{\sqrt{m_{D_s}} f_K (v\cdot k + v\cdot p_2)} \\
&\times \left[\frac{2\lambda' + \frac{1}{\sqrt{2}} g_v \lambda \left(\frac{g_\omega}{3 m_\omega^2} - \frac{g_\rho}{m_\rho^2} \right)}{v\cdot p_2 + \Delta} + \frac{2\lambda' - \frac{\sqrt{2}}{3} g_v \lambda \frac{g_\phi}{m_\phi^2}}{v\cdot k + \Delta} \right]
\end{aligned} \tag{C.132}
$$

$$
\begin{aligned}
B_3^{(d,d)} &= -\frac{g_\rho g_{\rho^\pm \pi^\pm \gamma}}{f_K} \left(f_{D_s} + g f_D \sqrt{\frac{m_D}{m_{D_s}}} \frac{m_{D_s} - v\cdot p_2}{v\cdot p_2 + \Delta} \right) BW_{\rho^+}(u) \\
&+ \frac{2 f_\pi (m_{D_s} \alpha_1 - \alpha_2 v\cdot p_1)}{\sqrt{m_{D_s}}} \frac{m_{K^*}^2}{g_{K^*}} g_{K^* K \gamma} BW_{K^*}(t))
\end{aligned} \tag{C.133}
$$

$$
B_3^{(s,s)} = \frac{f_{D_s} g_{K^*}}{f_\pi} g_{K^* K \gamma} BW_{K^*}(t) + \frac{f_{D_s} g_\rho}{f_K} g_{\rho^\pm \pi^\pm \gamma} BW_{\rho^+}(u) \tag{C.134}
$$

$$
B_4^{(s,s)} = -\frac{m_{D_s}^2 f_{D_s} f_K}{(m_{D_s}^2 - m_K^2)} \left(\frac{m_{K^*}^2}{g_{K^*}} g_{K^* K \gamma} BW_{K^*}(t) + \frac{m_\rho^2}{g_\rho} g_{\rho^\pm \pi^\pm \gamma} BW_{\rho^+}(u) \right) \tag{C.135}
$$

$$
\begin{aligned}
a' &= -\frac{\sqrt{m_D} f_D g^2 \left(p_2\cdot k - (v\cdot k)(v\cdot p_2) \right)}{f_\pi f_K \sqrt{m_{D_s}} (v\cdot p_1 + v\cdot p_2 + \Delta)(v\cdot p_2 + \Delta)} \\
&+ \frac{\alpha_1 (v\cdot k)}{f_\pi f_K \sqrt{m_{D_s}}} \left(1 + \frac{f_\pi f_K m_{K^*}^4}{g_{K^*}^2} BW_{K^{*+}}(s) \right) \\
&- \frac{\sqrt{2 m_D} f_D \lambda g_v m_{K^*}^2 \left(p_2\cdot k - (v\cdot k)(v\cdot p_2) \right)}{g_{K^*} \sqrt{m_{D_s}} (v\cdot p_1 + v\cdot p_2 + \Delta)} BW_{K^{*+}}(s)
\end{aligned} \tag{C.136}
$$

$$
\begin{aligned}
b' &= \frac{\sqrt{m_D} f_D g}{f_\pi f_K \sqrt{m_{D_s}} (v\cdot p_2 + \Delta)} \left[v\cdot k + g \frac{p_1\cdot k - (v\cdot k)(v\cdot p_1)}{v\cdot p_1 + v\cdot p_2 + \Delta} \right] \\
&- \frac{\alpha_1 (v\cdot k)}{f_\pi f_K \sqrt{m_{D_s}}} \left(1 + \frac{f_\pi f_K m_{K^*}^4}{g_{K^*}^2} BW_{K^{*+}}(s) \right) \\
&+ \frac{\sqrt{2 m_D} f_D \lambda g_v m_{K^*}^2 \left(p_1\cdot k - (v\cdot k)(v\cdot p_1) \right)}{g_{K^*} \sqrt{m_{D_s}} (v\cdot p_1 + v\cdot p_2 + \Delta)} BW_{K^{*+}}(s)
\end{aligned} \tag{C.137}
$$

$$
\begin{aligned}
c' &= -\frac{\sqrt{m_D} f_D g}{\sqrt{m_{D_s}^3} f_\pi f_K (v\cdot p_2 + \Delta)} \left[p_2\cdot k - g \frac{(p_2\cdot k)(v\cdot p_1) - (p_1\cdot k)(v\cdot p_2)}{v\cdot p_1 + v\cdot p_2 + \Delta} \right] \\
&- \frac{\alpha_1 (p_1\cdot k - p_2\cdot k)}{\sqrt{m_{D_s}^3} f_\pi f_K} \left(1 + \frac{f_\pi f_K m_{K^*}^4}{g_{K^*}^2} BW_{K^{*+}}(s) \right) \\
&+ \frac{\sqrt{2 m_D} f_D \lambda g_v m_{K^*}^2 \left((p_2\cdot k)(v\cdot p_1) - (p_1\cdot k)(v\cdot p_2) \right)}{\sqrt{m_{D_s}^3} g_{K^*} (v\cdot p_1 + v\cdot p_2 + \Delta)} BW_{K^{*+}}(s)
\end{aligned} \tag{C.138}
$$

$$
\begin{aligned}
h' = & \frac{\sqrt{m_D} f_D g}{2\sqrt{m_{D_s}^3} f_\pi f_K (v\cdot p_2 + \Delta)} \left(1 + g \frac{v\cdot k}{v\cdot p_1 + v\cdot p_2 + \Delta}\right) \\
& + \frac{\alpha_1}{\sqrt{m_{D_s}^3} f_\pi f_K} \left(1 + \frac{f_\pi f_K m_{K^*}^4}{g_{K^*}^2} BW_{K^{*+}}(s)\right) \\
& + \frac{\sqrt{m_D} f_D \lambda g_v m_{K^*}^2 (v\cdot k)}{\sqrt{2 m_{D_s}^3} g_{K^*} (v\cdot p_1 + v\cdot p_2 + \Delta)} BW_{K^{*+}}(s)
\end{aligned}
\tag{C.139}
$$

$\underline{D_s \to K^+\pi^0\gamma}$

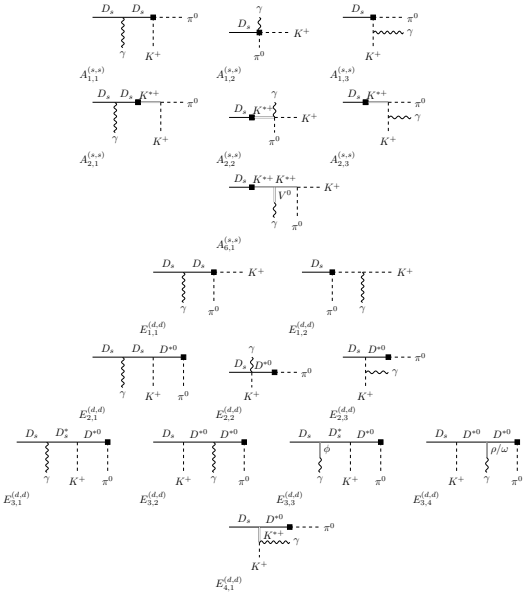

a) Contributions to the parity-even form factors A and E. Additionally, for each of the diagrams $A_{1,2}$, $A_{1,3}$, $A_{2,3}$, $E_{1,2}$ nd $E_{2,3}$ there are additional diagrams where the photon is coupled to the pseudoscalar via a ρ^0-, ω-, ϕ-mesons.

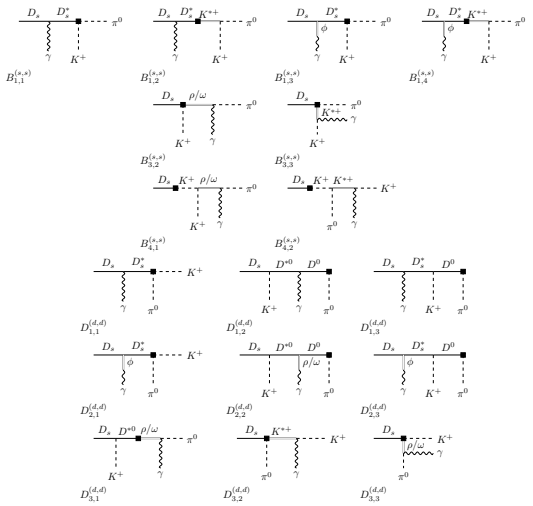

b) Contributions to the parity-odd form factors B and D.

Figure C.13: HHχPTFeynman diagrams for the decay $D_s \to K^+\pi^0\gamma$ within the SM.

$$
A_{1+2}^{(s,s)} = i \frac{f_{D_s}}{\sqrt{2}} \frac{v\cdot p_2 - v\cdot p_1 - v\cdot k}{(v\cdot k)(p_1\cdot k)} \tag{C.140}
$$

$$
A_6^{(s,s)} = i\sqrt{2} f_{D_s} \frac{p_1\cdot p_2}{m_{D_s}(v\cdot k)} BW_{K^{*+}}(s) \tag{C.141}
$$

$$E_1^{(d,d)} = i\frac{f_{D_s} f_\pi}{\sqrt{2} f_K} \frac{v\cdot p_2}{(v\cdot k)(p_1\cdot k)} \tag{C.142}$$

$$E_2^{(d,d)} = i\sqrt{\frac{m_D}{m_{D_s}}} \frac{f_D f_\pi g}{\sqrt{2} f_K} \frac{p_1\cdot p_2 - (v\cdot p_1)(v\cdot p_2) + (v\cdot k)(m_{D_s} - v\cdot p_2)}{(v\cdot k + v\cdot p_1 + \Delta)(v\cdot k)(p_1\cdot k)} \tag{C.143}$$

$$E_3^{(d,d)} = i\sqrt{\frac{m_D}{m_{D_s}}} \frac{f_D f_\pi g (v\cdot k)}{f_K (v\cdot k + v\cdot p_1 + \Delta)} \left[\frac{\sqrt{2}\lambda' + \frac{1}{2} g_v \lambda \left(\frac{g_\omega}{3m_\omega^2} + \frac{g_\rho}{m_\rho^2} \right)}{v\cdot p_1 + \Delta} - \frac{\sqrt{2}\lambda' - g_v \lambda \frac{g_\phi}{3m_\phi^2}}{v\cdot k + \Delta} \right] \tag{C.144}$$

$$B_1^{(s,s)} = \frac{f_{D_s}}{v\cdot k + \Delta} \left[1 - m_{K^*}^2 BW_{K^{*+}}(s) \right] \left[\sqrt{2}\lambda' - g_v \lambda \frac{g_\phi}{3m_\phi^2} \right] \tag{C.145}$$

$$\begin{aligned} B_3^{(s,s)} = &-\frac{f_{D_s} g_\rho}{\sqrt{2} f_K} g_{\rho\pi\gamma} BW_\rho(t) - \frac{f_{D_s} g_\omega}{\sqrt{2} f_K} g_{\omega\pi\gamma} BW_\omega(t) \\ &- \frac{f_{D_s} g_{K^*}}{\sqrt{2} f_\pi} g_{K^{*\pm}K^\pm\gamma} BW_{K^{*+}}(u) \end{aligned} \tag{C.146}$$

$$\begin{aligned} B_4^{(s,s)} = &\frac{m_{D_s}^2 f_{D_s} f_K}{\sqrt{2}(m_{D_s}^2 - m_K^2)} \left(\frac{2m_{K^*}^2}{g_{K^*}} g_{K^{*\pm}K^\pm\gamma} BW_{K^{*+}}(u) \right. \\ &\left. + \frac{m_\rho^2}{g_\rho} g_{\rho\pi\gamma} BW_\rho(t) + \frac{m_\omega^2}{g_\omega} g_{\omega\pi\gamma} BW_\omega(t) \right) \end{aligned} \tag{C.147}$$

$$D_1^{(d,d)} = \sqrt{2}\frac{f_\pi}{f_K}\lambda' \left[\frac{f_{D_s}}{v\cdot k + \Delta} + \frac{\sqrt{m_D} f_D g (v\cdot p_2)}{\sqrt{m_{D_s}}(v\cdot k + v\cdot p_1)} \left(\frac{1}{v\cdot k + \Delta} + \frac{1}{v\cdot p_1 + \Delta} \right) \right] \tag{C.148}$$

$$D_2^{(d,d)} = \frac{f_\pi g_v \lambda}{f_K} \left[\frac{-f_{D_s} \frac{g_\phi}{3m_\phi^2}}{v\cdot k + \Delta} + \frac{\sqrt{m_D} f_D g (v\cdot p_2)}{\sqrt{m_{D_s}}(v\cdot k + v\cdot p_1)} \left(\frac{-\frac{g_\phi}{3m_\phi^2}}{v\cdot k + \Delta} + \frac{\frac{1}{2}\left(\frac{g_\omega}{3m_\omega^2} + \frac{g_\rho}{m_\rho^2} \right)}{v\cdot p_1 + \Delta} \right) \right] \tag{C.149}$$

$$\begin{aligned} D_3^{(d,d)} = &\frac{1}{\sqrt{2} f_K} \left(f_{D_s} + \sqrt{\frac{m_D}{m_{D_s}}} f_D g \frac{m_{D_s} - v\cdot p_1}{v\cdot p_1 + \Delta} \right) \\ &\times \left(g_\omega g_{\omega\pi\gamma} BW_\omega(t) - g_\rho g_{\rho\pi\gamma} BW_\rho(t) \right) \\ &+ \frac{\sqrt{2} f_\pi \left(m_{D_s}\alpha_1 - \alpha_2 v\cdot p_2 \right)}{\sqrt{m_{D_s}}} \frac{m_{K^*}^2}{g_{K^*}} g_{K^{*\pm}K^\pm\gamma} BW_{K^{*+}}(u) \end{aligned} \tag{C.150}$$

$$
\begin{aligned}
a' = & \frac{\sqrt{m_D} f_D g}{\sqrt{2} f_\pi f_K \sqrt{m_{D_s}} (v\cdot p_1 + \Delta)} \left[v\cdot k + g \frac{p_2\cdot k - (v\cdot k)(v\cdot p_2)}{v\cdot p_1 + v\cdot p_2 + \Delta} \right] \\
& - \frac{\alpha_1 (v\cdot k)}{\sqrt{2} f_\pi f_K \sqrt{m_{D_s}}} \left(1 + \frac{f_\pi f_K m_{K^*}^4}{g_{K^*}^2} BW_{K^{*+}}(s) \right) \\
& + \frac{\sqrt{m_D} f_D \lambda g_v m_{K^*}^2 \left(p_2\cdot k - (v\cdot k)(v\cdot p_2) \right)}{g_{K^*} \sqrt{m_{D_s}} (v\cdot p_1 + v\cdot p_2 + \Delta)} BW_{K^{*+}}(s)
\end{aligned}
\tag{C.151}
$$

$$
\begin{aligned}
b' = & - \frac{\sqrt{m_D} f_D g^2 \left(p_1\cdot k - (v\cdot k)(v\cdot p_1) \right)}{\sqrt{2} f_\pi f_K \sqrt{m_{D_s}} (v\cdot p_1 + \Delta)(v\cdot p_1 + v\cdot p_2 + \Delta)} \\
& + \frac{\alpha_1 (v\cdot k)}{\sqrt{2} f_\pi f_K \sqrt{m_{D_s}}} \left(1 + \frac{f_\pi f_K m_{K^*}^4}{g_{K^*}^2} BW_{K^{*+}}(s) \right) \\
& - \frac{\sqrt{m_D} f_D \lambda g_v m_{K^*}^2 \left(p_1\cdot k - (v\cdot k)(v\cdot p_1) \right)}{g_{K^*} \sqrt{m_{D_s}} (v\cdot p_1 + v\cdot p_2 + \Delta)} BW_{K^{*+}}(s)
\end{aligned}
\tag{C.152}
$$

$$
\begin{aligned}
c' = & - \frac{\sqrt{m_D} f_D g}{\sqrt{2 m_{D_s}^3} f_\pi f_K (v\cdot p_1 + \Delta)} \left[p_1\cdot k + g \frac{(p_2\cdot k)(v\cdot p_1) - (p_1\cdot k)(v\cdot p_2)}{v\cdot p_1 + v\cdot p_2 + \Delta} \right] \\
& + \frac{\alpha_1 (p_1\cdot k - p_2\cdot k)}{\sqrt{2 m_{D_s}^3} f_\pi f_K} \left(1 + \frac{f_\pi f_K m_{K^*}^4}{g_{K^*}^2} BW_{K^{*+}}(s) \right) \\
& - \frac{\sqrt{m_D} f_D \lambda g_v m_{K^*}^2 \left((p_2\cdot k)(v\cdot p_1) - (p_1\cdot k)(v\cdot p_2) \right)}{\sqrt{m_{D_s}^3} g_{K^*} (v\cdot p_1 + v\cdot p_2 + \Delta)} BW_{K^{*+}}(s)
\end{aligned}
\tag{C.153}
$$

$$
\begin{aligned}
h' = & - \frac{\sqrt{m_D} f_D g}{2\sqrt{2 m_{D_s}^3} f_\pi f_K (v\cdot p_1 + \Delta)} \left(1 + g \frac{v\cdot k}{v\cdot p_1 + v\cdot p_2 + \Delta} \right) \\
& - \frac{\alpha_1}{\sqrt{2 m_{D_s}^3} f_\pi f_K} \left(1 + \frac{f_\pi f_K m_{K^*}^4}{g_{K^*}^2} BW_{K^{*+}}(s) \right) \\
& - \frac{\sqrt{m_D} f_D \lambda g_v m_{K^*}^2 (v\cdot k)}{2\sqrt{m_{D_s}^3} g_{K^*} (v\cdot p_1 + v\cdot p_2 + \Delta)} BW_{K^{*+}}(s)
\end{aligned}
\tag{C.154}
$$

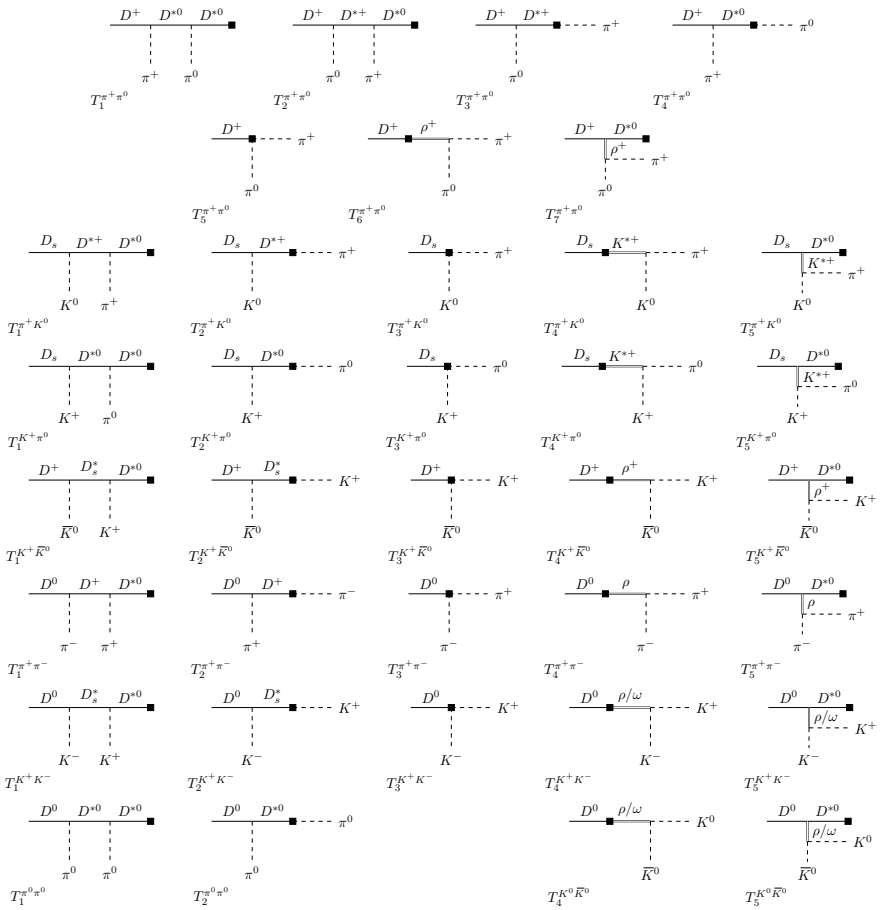

Figure C.14: HHχPTFeynman diagrams related to the tensor current matrix elements.

C.1.3 Doubly Cabibbo suppressed modes

$\underline{D^0 \to \pi^0 K^0 \gamma}$

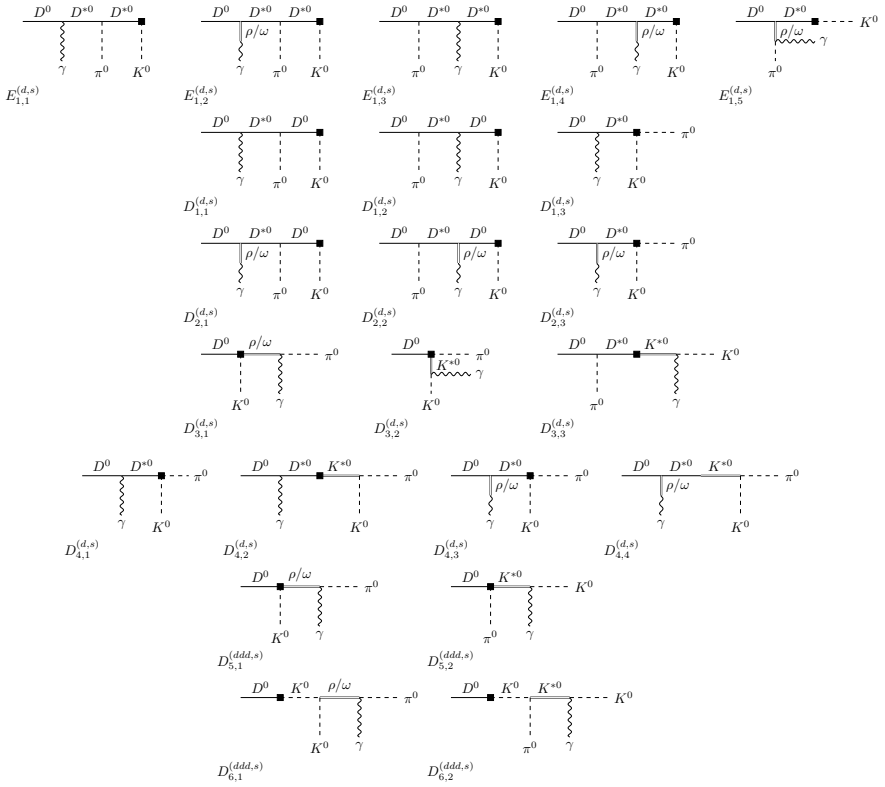

Figure C.15: HHχPTFeynman diagrams for the decay $D^0 \to \pi^0 K^0 \gamma$.

$$E_1^{(s,d)} = ig\frac{f_D f_K}{f_\pi}\frac{v\cdot k}{v\cdot k + v\cdot p_1 + \Delta}\left(\frac{1}{v\cdot k+\Delta} - \frac{1}{v\cdot p_1+\Delta}\right) \times \left(\sqrt{2}\lambda' + \frac{1}{2}\lambda g_v\left(\frac{g_\omega}{3m_\omega^2} + \frac{g_\rho}{m_\rho^2}\right)\right) \tag{C.155}$$

$$D_1^{(s,d)} = -\sqrt{2}\frac{f_D f_K}{f_\pi}\lambda'\left(\frac{1}{v\cdot k+\Delta} + g\frac{v\cdot p_2}{v\cdot p_1 + v\cdot k}\left[\frac{1}{v\cdot k+\Delta} + \frac{1}{v\cdot p_1+\Delta}\right]\right) \tag{C.156}$$

$$D_2^{(s,d)} = -\frac{1}{2}\frac{f_D f_K}{f_\pi}\lambda g_v\left(\frac{g_\omega}{3m_\omega^2} + \frac{g_\rho}{m_\rho^2}\right) \times \left(\frac{1}{v\cdot k+\Delta} + g\frac{v\cdot p_2}{v\cdot p_1 + v\cdot k}\left[\frac{1}{v\cdot k+\Delta} + \frac{1}{v\cdot p_1+\Delta}\right]\right) \tag{C.157}$$

$$
\begin{aligned}
D_3^{(s,d)} &= -\sqrt{\frac{2}{m_D}} f_K(\alpha_1 m_D - \alpha_2 v\cdot p_2) \\
&\times \left(\frac{m_\rho^2 g_{\rho\pi\gamma}}{g_\rho} BW_\rho(u) + \frac{m_\omega^2 g_{\omega\pi\gamma}}{g_\omega} BW_\omega(u)\right) \\
&+ \frac{1}{\sqrt{2}} g_{K^*} g_{K^*K\gamma} \frac{f_D}{f_\pi}\left(1 + g\frac{m_D - v\cdot p_1}{v\cdot p_1 + \Delta}\right) BW_{K^*}(t)
\end{aligned} \tag{C.158}
$$

$$
D_4^{(s,d)} = -f_D \frac{1}{v\cdot k + \Delta}\left(1 + m_{K^*}^2 BW_{K^*}(s)\right)\left(\sqrt{2}\lambda' + \frac{1}{2}\lambda g_v\left(\frac{g_\omega}{3m_\omega^2} + \frac{g_\rho}{m_\rho^2}\right)\right) \tag{C.159}
$$

$$
\begin{aligned}
D_5^{(s,d)} &= -\frac{1}{\sqrt{2}}\frac{f_D}{f_K}(g_\rho g_{\rho\pi\gamma} BW_\rho(u) - g_\omega g_{\omega\pi\gamma} BW_\omega(u)) \\
&- \frac{1}{\sqrt{2}}\frac{f_D}{f_\pi} g_{K^*} g_{K^*K\gamma} BW_{K^*}(t)
\end{aligned} \tag{C.160}
$$

$$
\begin{aligned}
D_6^{(s,d)} &= -\frac{1}{\sqrt{2}} f_D f_K \frac{m_D^2}{m_D^2 - m_K^2}\left(\frac{m_\rho^2}{g_\rho} g_{\rho\pi\gamma} BW_\rho(u)\right. \\
&\left. - \frac{m_\omega^2}{g_\omega} g_{\omega\pi\gamma} BW_\omega(u) + \frac{m_{K^*}^2}{g_{K^*}} g_{K^*K\gamma} BW_{K^*}(t)\right)
\end{aligned} \tag{C.161}
$$

$\underline{D^0 \to K^+\pi^-\gamma}$

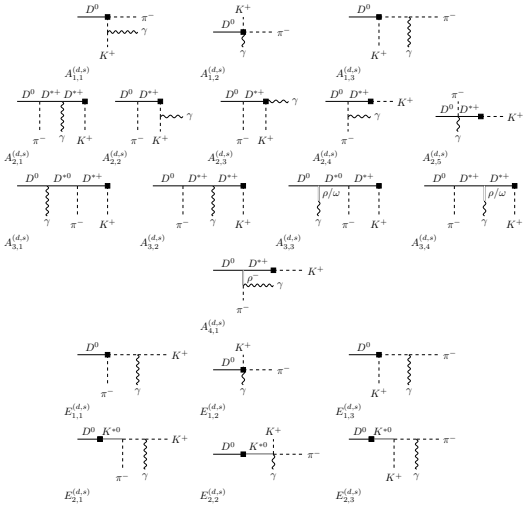

a) Contributions to the parity-even form factors A and E. For each of the diagrams $A_{1,1}$, $A_{1,2}$, $A_{1,3}$, $A_{2,2}$, $A_{2,3}$, $A_{2,4}$, $E_{1,1}$, $E_{1,2}$, $E_{1,3}$, $E_{2,1}$ and $E_{2,3}$ there are additional diagrams where the photon is coupled to the pseudoscalar via a ρ^0-, ω-, ϕ-mesons.

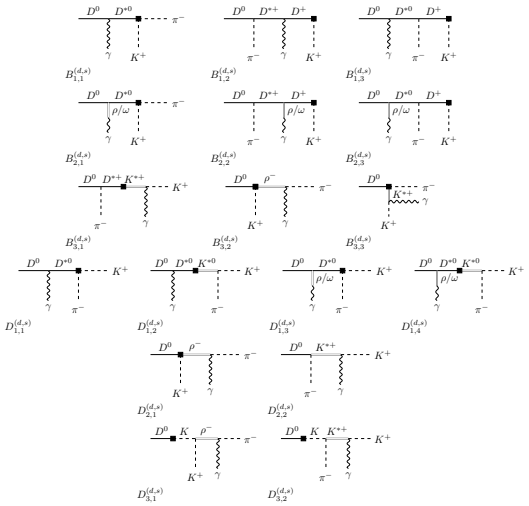

b) Contributions to the parity-odd form factors B and D.

Figure C.16: HHχPTFeynman diagrams for the decay $D^0 \to K^+\pi^-\gamma$.

$$A_1^{(s,d)} = i\frac{f_D f_K}{f_\pi}\frac{p_1\cdot k - m_D(v\cdot k + v\cdot p_1)}{(p_1\cdot k)(p_2\cdot k)} \tag{C.162}$$

$$\begin{aligned} A_2^{(s,d)} = &-im_D\frac{f_D f_K}{f_\pi}\frac{g}{(p_1\cdot k)(p_2\cdot k)}\left(\frac{p_2\cdot k(m_D - v\cdot p_2)}{m_D(v\cdot p_2 + \Delta)}\right.\\ &+\frac{p_2\cdot k\,[p_1\cdot p_2 - (v\cdot p_1)(v\cdot p_2)]}{m_D(v\cdot p_2+\Delta)(v\cdot p_2 + v\cdot k + \Delta)}\\ &\left.+\frac{(m_D - v\cdot p_1)p_1\cdot k + m_D p_1\cdot p_2 + m_D(v\cdot p_1)(v\cdot p_2)}{m_D(v\cdot p_2 + v\cdot k + \Delta)}\right) \end{aligned} \tag{C.163}$$

$$\begin{aligned} A_3^{(s,d)} = &\, i\frac{f_D f_K}{f_\pi} g\frac{v\cdot k}{v\cdot k + v\cdot p_2 + \Delta}\\ &\times\left(\frac{2\lambda' + \frac{1}{\sqrt{2}}\lambda g_v\left(\frac{g_\omega}{3m_\omega^2} - \frac{g_\rho}{m_\rho^2}\right)}{v\cdot p_2 + \Delta} - \frac{2\lambda' + \frac{1}{\sqrt{2}}\lambda g_v\left(\frac{g_\omega}{3m_\omega^2} + \frac{g_\rho}{m_\rho^2}\right)}{v\cdot k + \Delta}\right) \end{aligned} \tag{C.164}$$

$$B_1^{(s,d)} = 2\frac{f_D f_K}{f_\pi}\lambda'\left(\frac{1}{v\cdot k + \Delta} + g\frac{v\cdot p_1}{(v\cdot p_2 + v\cdot k)}\left[\frac{1}{v\cdot k + \Delta} + \frac{1}{v\cdot p_2 + \Delta}\right]\right) \tag{C.165}$$

$$\begin{aligned} B_2^{(s,d)} = &\frac{1}{\sqrt{2}}\frac{f_D f_K}{f_\pi}\lambda g_v\left(\frac{g_\omega}{3m_\omega^2} + \frac{g_\rho}{m_\rho^2}\right)\frac{1}{v\cdot k + \Delta}\left(1 + g\frac{v\cdot p_1}{(v\cdot p_2 + v\cdot k)}\right)\\ &-\frac{1}{\sqrt{2}}\frac{f_D f_K}{f_\pi} g\lambda g_v\left(\frac{g_\omega}{3m_\omega^2} - \frac{g_\rho}{m_\rho^2}\right)\frac{v\cdot p_1}{(v\cdot p_2 + v\cdot k)(v\cdot p_2 + \Delta)} \end{aligned} \tag{C.166}$$

$$\begin{aligned} B_3^{(s,d)} = &\frac{2}{\sqrt{m_D}} f_\pi\frac{m_\rho^2 g_{\rho^\pm\pi^\pm\gamma}}{g_\rho}(\alpha_1 m_D - \alpha_2 v\cdot p_1)BW_{\rho^-}(t)\\ &- g_{K^*} g_{K^{*\pm}K^\pm\gamma}\frac{f_D}{f_\pi}\left(1 + g\frac{m_D - v\cdot p_2}{v\cdot p_2 + \Delta}\right)BW_{K^{*+}}(u) \end{aligned} \tag{C.167}$$

$$D_1^{(s,d)} = -\frac{f_D}{v\cdot k + \Delta}\left(1 + m_{K^*}^2 BW_{K^*}(s)\right)\left(2\lambda' + \frac{1}{\sqrt{2}}\lambda g_v\left(\frac{g_\omega}{3m_\omega^2} + \frac{g_\rho}{m_\rho^2}\right)\right) \tag{C.168}$$

$$D_2^{(s,d)} = -\frac{f_D}{f_\pi} g_{K^*} g_{K^{*\pm}K^\pm\gamma} BW_{K^{*+}}(u) - \frac{f_D}{f_K} g_\rho g_{\rho^\pm\pi^\pm\gamma} BW_{\rho^-}(t) \tag{C.169}$$

$$D_3^{(s,d)} = f_D f_K\frac{m_D^2}{m_D^2 - m_K^2}\left(\frac{m_\rho^2}{g_\rho} g_{\rho^\pm\pi^\pm\gamma} BW_{\rho^-}(t) + \frac{m_{K^*}^2}{g_{K^*}} g_{K^{*\pm}K^\pm\gamma} BW_{K^{*+}}(u)\right) \tag{C.170}$$

<u>$D^+ \to \pi^+ K^0\gamma$</u>

$$\begin{aligned} A_{1+2}^{(d,s)} &= -if_D\frac{v\cdot p_2 - v\cdot p_1 - v\cdot k}{(v\cdot k)(p_1\cdot k)}\\ A_6^{(d,s)} &= -i2f_D\frac{p_1\cdot p_2}{m_D(v\cdot k)}BW_{K^{*+}}(s) \end{aligned} \tag{C.171}$$

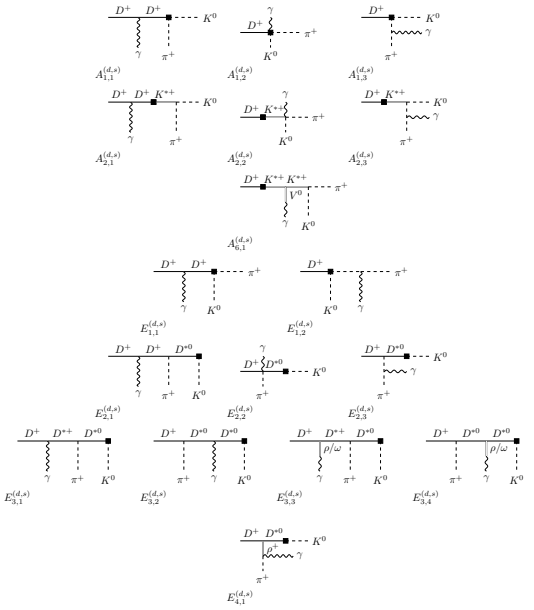

a) Contributions to the parity-even form factors A and E. Additionally, for each of the diagrams $A_{1,2}$, $A_{1,3}$, $A_{2,3}$, $E_{1,2}$ nd $E_{2,3}$ there are additional diagrams where the photon is coupled to the pseudoscalar via a ρ^0-, ω-, ϕ-mesons.

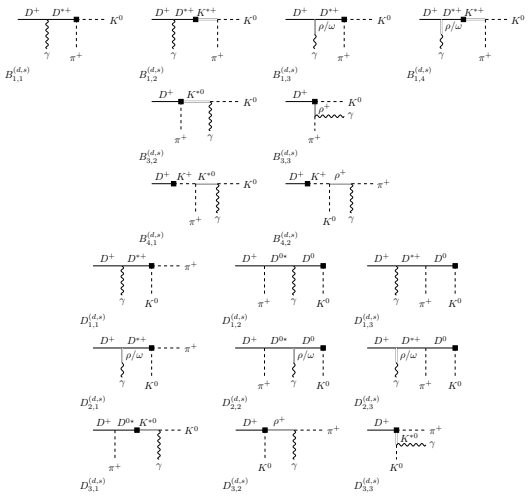

b) Contributions to the parity-odd form factors B and D.

Figure C.17: HHχPTFeynman diagrams for the decay $D^+ \to \pi^+ K^0 \gamma$.

$$E_1^{(d,s)} = -i\frac{f_D f_K}{f_\pi}\frac{v\cdot p_2}{(v\cdot k)(p_1\cdot k)} \tag{C.172}$$

$$E_2^{(d,s)} = -i\frac{f_D f_K g}{f_\pi}\frac{p_1\cdot p_2 - (v\cdot p_1)(v\cdot p_2) + (v\cdot k)(m_D - v\cdot p_2)}{(v\cdot k + v\cdot p_1 + \Delta)(v\cdot k)(p_1\cdot k)} \tag{C.173}$$

$$\begin{aligned} E_3^{(d,s)} &= -i\frac{f_D f_K g (v\cdot k)}{f_\pi (v\cdot k + v\cdot p_1 + \Delta)} \\ &\quad\times\left[\frac{2\lambda' + \frac{1}{\sqrt{2}} g_v \lambda\left(\frac{g_\omega}{3m_\omega^2} + \frac{g_\rho}{m_\rho^2}\right)}{v\cdot p_1 + \Delta} - \frac{2\lambda' + \frac{1}{\sqrt{2}} g_v \lambda\left(\frac{g_\omega}{3m_\omega^2} - \frac{g_\rho}{m_\rho^2}\right)}{v\cdot k + \Delta}\right] \end{aligned} \tag{C.174}$$

$$B_1^{(d,s)} = -\frac{f_D}{v\cdot k + \Delta}\left[1 - m_{K^*}^2 BW_{K^{*+}}(s)\right]\left[2\lambda' + \frac{g_v\lambda}{\sqrt{2}}\left(\frac{g_\omega}{3m_\omega^2} - \frac{g_\rho}{m_\rho^2}\right)\right] \tag{C.175}$$

$$B_3^{(d,s)} = \frac{f_D g_{K^*}}{f_\pi} g_{K^* K\gamma} BW_{K^*}(t) + \frac{f_D g_\rho}{f_K} g_{\rho^\pm\pi^\pm\gamma} BW_{\rho^+}(u) \tag{C.176}$$

$$B_4^{(d,s)} = -\frac{m_D^2 f_D f_K}{(m_D^2 - m_K^2)}\left(\frac{m_{K^*}^2}{g_{K^*}} g_{K^* K\gamma} BW_{K^*}(t) + \frac{m_\rho^2}{g_\rho} g_{\rho^\pm\pi^\pm\gamma} BW_{\rho^+}(u)\right) \tag{C.177}$$

$$D_1^{(d,s)} = -2\frac{f_D f_K}{f_\pi}\lambda' \left[\frac{1}{v\cdot k+\Delta} + \frac{g(v\cdot p_2)}{v\cdot k + v\cdot p_1}\left(\frac{1}{v\cdot k+\Delta}+\frac{1}{v\cdot p_1+\Delta}\right)\right] \tag{C.178}$$

$$D_2^{(d,s)} = -\frac{f_D f_K g_v \lambda}{\sqrt{2}f_\pi}\left[\frac{\frac{g_\omega}{3m_\omega^2}-\frac{g_\rho}{m_\rho^2}}{v\cdot k+\Delta} + \frac{g(v\cdot p_2)}{v\cdot k + v\cdot p_1}\left(\frac{\frac{g_\omega}{3m_\omega^2}-\frac{g_\rho}{m_\rho^2}}{v\cdot k+\Delta}+\frac{\frac{g_\omega}{3m_\omega^2}+\frac{g_\rho}{m_\rho^2}}{v\cdot p_1+\Delta}\right)\right] \tag{C.179}$$

$$\begin{aligned} D_3^{(d,s)} &= \frac{f_D g_{K^*} g_{K^*K\gamma}}{f_\pi}\left(1+g\frac{m_D - v\cdot p_1}{v\cdot p_1+\Delta}\right) BW_{K^*}(t) \\ &- \frac{2f_K\left(m_D\alpha_1-\alpha_2 v\cdot p_2\right)}{\sqrt{m_D}}\frac{m_\rho^2}{g_\rho} g_{\rho^\pm\pi^\pm\gamma} BW_{\rho^+}(u) \end{aligned} \tag{C.180}$$

$\underline{D^+ \to K^+\pi^0\gamma}$

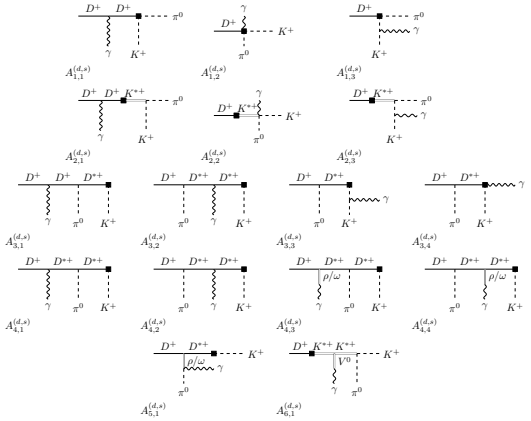

a) Contributions to the parity-even form factors A and E. Note that the diagrams A_1 have two different factorizations. Additionally, for each of the diagrams $A_{1,2}$, $A_{1,3}$, $A_{2,3}$, $A_{3,3}$ and $A_{3,4}$ there are additional diagrams where the photon is coupled to the pseudoscalar via a ρ^0-, ω-, ϕ-mesons.

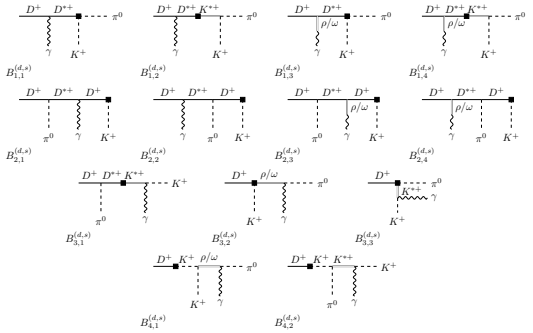

b) Contributions to the parity-odd form factors B and D. Note that the diagrams $B_{1,1/3}$ and $B_{3,2/3}$ have two different factorizations.

Figure C.18: HHχPTFeynman diagrams for the decay $D^+ \to K^+\pi^0\gamma$.

$$A_{1+2}^{(d,s)} = i\frac{f_D}{\sqrt{2}}\frac{v\cdot p_2 - v\cdot p_1 - v\cdot k}{(v\cdot k)(p_1\cdot k)} + i\frac{f_D f_K}{\sqrt{2}f_\pi}\frac{v\cdot p_1 + v\cdot k}{(v\cdot k)(p_1\cdot k)} \tag{C.181}$$

$$A_3^{(d,s)} = i\frac{f_D f_K g}{\sqrt{2}f_\pi}\frac{p_1\cdot p_2 - (v\cdot p_1)(v\cdot p_2) + (v\cdot k)(M - v\cdot p_2)}{(v\cdot p_2+\Delta)(v\cdot k)(p_1\cdot k)} \tag{C.182}$$

$$\begin{aligned} A_4^{(d,s)} &= i\frac{f_D f_K g (v\cdot k)}{f_\pi(v\cdot k + v\cdot p_2 + \Delta)} \\ &\times \left[\frac{\sqrt{2}\lambda' + \frac{1}{2}g_v\lambda\left(\frac{g_\omega}{3m_\omega^2}-\frac{g_\rho}{m_\rho^2}\right)}{v\cdot k+\Delta} - \frac{\sqrt{2}\lambda' + \frac{1}{2}g_v\lambda\left(\frac{g_\omega}{3m_\omega^2}-\frac{g_\rho}{m_\rho^2}\right)}{v\cdot p_2+\Delta}\right] \end{aligned} \tag{C.183}$$

$$A_6^{(d,s)} = i\sqrt{2} f_D \frac{p_1 \cdot p_2}{m_D (v \cdot k)} BW_{K^{*+}}(s) \tag{C.184}$$

$$B_1^{(d,s)} = \frac{f_D}{v \cdot k + \Delta} \left[1 - \frac{f_K}{f_\pi} - m_{K^*}^2 BW_{K^{*+}}(s) \right] \left[\sqrt{2}\lambda' + \frac{1}{2} g_v \lambda \left(\frac{g_\omega}{3m_\omega^2} - \frac{g_\rho}{m_\rho^2} \right) \right] \tag{C.185}$$

$$B_2^{(d,s)} = -\frac{f_D f_K g (v \cdot p_1)}{f_\pi (v \cdot k + v \cdot p_2)} \left[\frac{\sqrt{2}\lambda' + \frac{1}{2} g_v \lambda \left(\frac{g_\omega}{3m_\omega^2} - \frac{g_\rho}{m_\rho^2} \right)}{v \cdot p_2 + \Delta} + \frac{\sqrt{2}\lambda' + \frac{1}{2} g_v \lambda \left(\frac{g_\omega}{3m_\omega^2} - \frac{g_\rho}{m_\rho^2} \right)}{v \cdot k + \Delta} \right] \tag{C.186}$$

$$\begin{aligned} B_3^{(d,s)} = {} & \frac{f_D g_{K^*} g_{K^{*\pm} K^\pm \gamma} g (m_D - v \cdot p_2)}{\sqrt{2} f_\pi (v \cdot p_2 + \Delta)} BW_{K^{*+}}(u) \\ & + \frac{\sqrt{2} f_K (m_D \alpha_1 - \alpha_2 v \cdot p_1)}{\sqrt{m_D}} \left(\frac{m_\omega^2}{g_\omega} g_{\omega\pi\gamma} BW_\omega(t) - \frac{m_\rho^2}{g_\rho} g_{\rho\pi\gamma} BW_\rho(t) \right) \\ & - \frac{f_D}{\sqrt{2}} \left(\frac{g_\rho}{f_K} g_{\rho\pi\gamma} BW_\rho(t) + \frac{g_\omega}{f_K} g_{\omega\pi\gamma} BW_\omega(t) \right) \end{aligned} \tag{C.187}$$

$$\begin{aligned} B_4^{(d,s)} = {} & \frac{m_D^2 f_D f_K}{\sqrt{2}(m_D^2 - m_K^2)} \left(\frac{m_\rho^2}{g_\rho} g_{\rho\pi\gamma} BW_\rho(t) \right. \\ & \left. + \frac{m_\omega^2}{g_\omega} g_{\omega\pi\gamma} BW_\omega(t) + \frac{2m_{K^*}^2}{g_{K^*}} g_{K^{*\pm} K^\pm \gamma} BW_{K^{*+}}(u) \right) \end{aligned} \tag{C.188}$$

<u>$D_s \to K^+ K^0 \gamma$</u>

$$A_1^{(d,s)} = -i f_{D_s} \frac{v \cdot p_1 + v \cdot k}{(v \cdot k)(p_1 \cdot k)} \tag{C.189}$$

$$A_3^{(d,s)} = -i \sqrt{\frac{m_D}{m_{D_s}}} f_D g \frac{p_1 \cdot p_2 - (v \cdot p_1)(v \cdot p_2) + (v \cdot k)(m_D - v \cdot p_2)}{(v \cdot p_2 + \Delta)(v \cdot k)(p_1 \cdot k)} \tag{C.190}$$

$$A_4^{(d,s)} = -i \sqrt{\frac{m_D}{m_{D_s}}} \frac{f_D g (v \cdot k)}{v \cdot k + v \cdot p_2 + \Delta} \left[\frac{2\lambda' - \frac{\sqrt{2}}{3} g_v \lambda \frac{g_\phi}{m_\phi^2}}{v \cdot k + \Delta} - \frac{2\lambda' + \frac{1}{\sqrt{2}} g_v \lambda \left(\frac{g_\omega}{3m_\omega^2} - \frac{g_\rho}{m_\rho^2} \right)}{v \cdot p_2 + \Delta} \right] \tag{C.191}$$

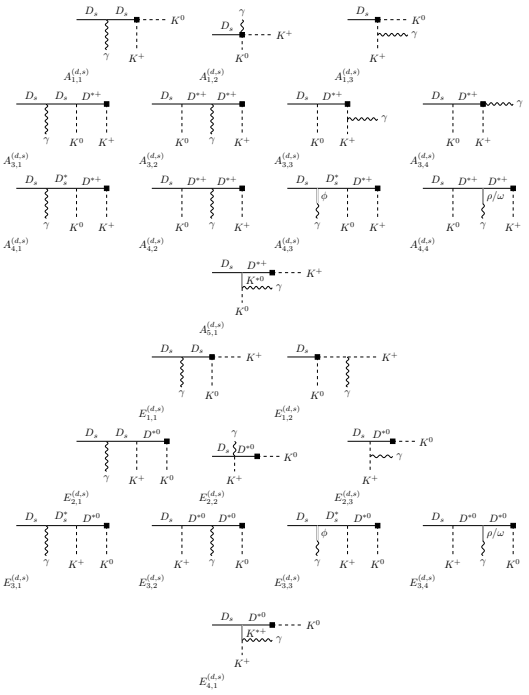

a) Contributions to the parity-even form factors A and E. For each of the diagrams $A_{1,2}$, $A_{1,3}$, $A_{3,3}$, $A_{3,4}$, $E_{1,2}$ nd $E_{2,3}$ there are additional diagrams where the photon is coupled to the pseudoscalar via a ρ^0-, ω-, ϕ-mesons.

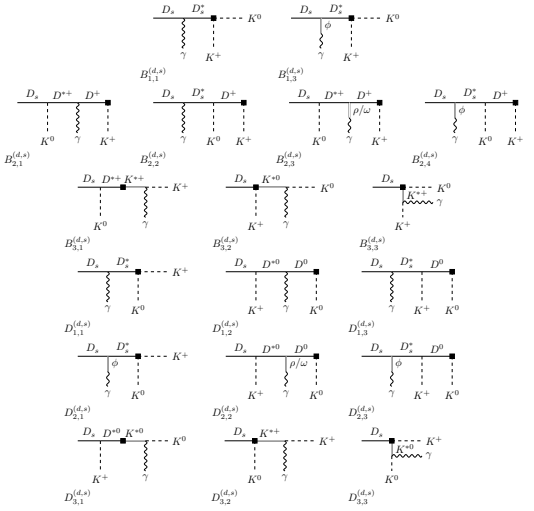

b) Contributions to the parity-odd form factors B and D.

Figure C.19: HHχPTFeynman diagrams for the decay $D_s \to K^+K^0\gamma$.

$$E_1^{(d,s)} = -if_{D_s}\frac{v\cdot p_2}{(v\cdot k)(p_1\cdot k)} \tag{C.192}$$

$$E_2^{(d,s)} = -i\sqrt{\frac{m_D}{m_{D_s}}}f_D g\frac{p_1\cdot p_2-(v\cdot p_1)(v\cdot p_2)+(v\cdot k)(m_D-v\cdot p_2)}{(v\cdot k+v\cdot p_1+\Delta)(v\cdot k)(p_1\cdot k)} \tag{C.193}$$

$$E_3^{(d,s)} = -i\sqrt{\frac{m_D}{m_{D_s}}}\frac{f_D g(v\cdot k)}{v\cdot k+v\cdot p_1+\Delta}\left[\frac{2\lambda'+\frac{1}{\sqrt{2}}g_v\lambda\left(\frac{g_\omega}{3m_\omega^2}+\frac{g_\rho}{m_\rho^2}\right)}{v\cdot p_1+\Delta}-\frac{2\lambda'-\frac{\sqrt{2}}{3}g_v\lambda\frac{g_\phi}{m_\phi^2}}{v\cdot k+\Delta}\right] \tag{C.194}$$

$$B_1^{(d,s)} = \frac{f_{D_s}}{v\cdot k+\Delta}\left[2\lambda'-\frac{\sqrt{2}}{3}g_v\lambda\frac{g_\phi}{m_\phi^2}\right] \tag{C.195}$$

$$B_2^{(d,s)} = \sqrt{\frac{m_D}{m_{D_s}}}\frac{f_D g(v\cdot p_1)}{v\cdot k+v\cdot p_2}\left[\frac{2\lambda'+\frac{1}{\sqrt{2}}g_v\lambda\left(\frac{g_\omega}{3m_\omega^2}-\frac{g_\rho}{m_\rho^2}\right)}{v\cdot p_2+\Delta}+\frac{2\lambda'-\frac{\sqrt{2}}{3}g_v\lambda\frac{g_\phi}{m_\phi^2}}{v\cdot k+\Delta}\right] \tag{C.196}$$

$$B_3^{(d,s)} = -\frac{g_{K^*} g_{K^{*\pm}K^\pm\gamma}}{f_K}\left(f_{D_s} + \sqrt{\frac{m_D}{m_{D_s}}} f_D g \frac{m_{D_s} - v\cdot p_2}{v\cdot p_2 + \Delta}\right) BW_{K^{*+}}(u) + \frac{2 f_K (m_{D_s}\alpha_1 - \alpha_2 v\cdot p_1)}{\sqrt{m_{D_s}}} \frac{m_{K^*}^2}{g_{K^*}} g_{K^*K\gamma} BW_{K^*}(t) \tag{C.197}$$

$$D_1^{(d,s)} = -2\lambda' \left[\frac{f_{D_s}}{v\cdot k + \Delta} + \sqrt{\frac{m_D}{m_{D_s}}} \frac{f_D g (v\cdot p_2)}{v\cdot k + v\cdot p_1}\left(\frac{1}{v\cdot k + \Delta} + \frac{1}{v\cdot p_1 + \Delta}\right)\right] \tag{C.198}$$

$$D_2^{(d,s)} = -g_v \lambda \left[\frac{-f_{D_s}\frac{\sqrt{2}}{3}\frac{g_\phi}{m_\phi^2}}{v\cdot k + \Delta} + \sqrt{\frac{m_D}{m_{D_s}}} \frac{f_D g (v\cdot p_2)}{v\cdot k + v\cdot p_1}\left(\frac{-\frac{\sqrt{2}}{3}\frac{g_\phi}{m_\phi^2}}{v\cdot k + \Delta} + \frac{\frac{1}{\sqrt{2}}\left(\frac{g_\omega}{3m_\omega^2} + \frac{g_\rho}{m_\rho^2}\right)}{v\cdot p_1 + \Delta}\right)\right] \tag{C.199}$$

$$D_3^{(d,s)} = \frac{g_{K^*} g_{K^*K\gamma}}{f_K}\left(f_{D_s} + \sqrt{\frac{m_D}{m_{D_s}}} f_D g \frac{m_{D_s} - v\cdot p_1}{v\cdot p_1 + \Delta}\right) BW_{K^*}(t) - \frac{2 f_K \left(m_{D_s}\alpha_1 - \alpha_2 v\cdot p_2\right)}{\sqrt{m_{D_s}}} \frac{m_{K^*}^2}{g_{K^*}} g_{K^{*\pm}K^\pm\gamma} BW_{K^{*\pm}}(u) \tag{C.200}$$

C.2 hadronic two body decays

Furthermore, we use the framework of HHχPT to estimate the phase of the $D(v) \to P_1(p_1)P_2(p_2)$ decay amplitudes which we extract from data in section 4.2.1. Within HHχPT the amplitude can be written as

$$A^{\mathrm{HH}\chi\mathrm{PT}} = \frac{G_F}{\sqrt{2}} \sum_{q,q'\in\{d,s\}} V_{\mathrm{cq}}^* V_{\mathrm{uq'}} \left[(C_2 - \frac{1}{6}C_1)F^{(q,q')} + \frac{1}{2}C_1 G^{(q,q')}\right], \tag{C.201}$$

where the Form factors F and G belong to the charged current and neutral current operator, respectively. The corresponding Feynman diagramms are shown in Fig. C.20.

C.2.1 Cabibbo favored (CF) modes

$\underline{D^0 \to \pi^+ K^-}$

$$F^{(s,d)} = i\frac{m_D f_D f_\pi}{f_K} v\cdot p_1 + i\frac{g\sqrt{m_D m_{D_s}} f_{D_s} f_\pi}{f_K} \frac{p_1\cdot p_2 - (v\cdot p_1)(v\cdot p_2)}{v\cdot p_2 + \Delta} \tag{C.202}$$

$$G^{(s,d)} = i m_D f_D (v\cdot p_1 - v\cdot p_2) \tag{C.203}$$

$\underline{D^+ \to \pi^+ \overline{K}^0}$

$$F^{(s,d)} = i\frac{m_D f_D f_\pi}{f_K} v\cdot p_1 + i\frac{g m_D f_D f_\pi}{f_K} \frac{p_1\cdot p_2 - (v\cdot p_1)(v\cdot p_2)}{v\cdot p_2 + \Delta} \tag{C.204}$$

$$G^{(s,d)} = i\frac{m_D f_D f_K}{f_\pi} v\cdot p_2 + i\frac{g m_D f_D f_K}{f_\pi} \frac{p_1\cdot p_2 - (v\cdot p_1)(v\cdot p_2)}{v\cdot p_1 + \Delta} \tag{C.205}$$

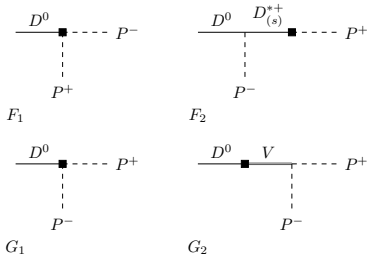

a) Contributions of the charged current operator F and neutral current operator G to the $D^0 \to P^+P^-$ decay amplitude.

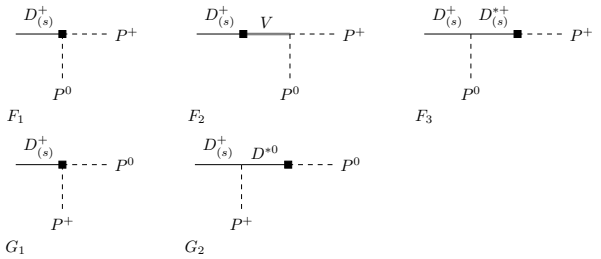

b) Contributions of the charged current operator F and neutral current operator G to $D^+_{(s)} \to P^+P^0$ decay amplitude. Note that the diagrams F_1 canhave two different factorizations.

Figure C.20: HHχPTFeynman diagrams for the hadronic two body decays $D \to PP$.

$\underline{D_s \to \pi^+\pi^0}$

$$F^{(s,d)} = i\sqrt{2}m_{D_s}f_{D_s}(v\cdot p_1 - v\cdot p_2) \tag{C.206}$$

$\underline{D_s \to K^+\overline{K}^0}$

$$F^{(s,d)} = -im_{D_s}f_{D_s}(v\cdot p_1 - v\cdot p_2) \tag{C.207}$$

$$G^{(s,d)} = im_{D_s}f_{D_s}v\cdot p_2 + ig\sqrt{m_D m_{D_s}}f_D\frac{p_1\cdot p_2 - (v\cdot p_1)(v\cdot p_2)}{v\cdot p_1 + \Delta} \tag{C.208}$$

C.2.2 Singly Cabibbo suppressed (SCS) modes

$\underline{D^0 \to \pi^+\pi^-}$

$$F^{(d,d)} = im_D f_D v\cdot p_1 + igm_D f_D\frac{p_1\cdot p_2 - (v\cdot p_1)(v\cdot p_2)}{v\cdot p_2 + \Delta} \tag{C.209}$$

$$G^{(d,d)} = im_D f_D(v\cdot p_1 - v\cdot p_2) \tag{C.210}$$

$\underline{D^0 \to K^+K^-}$

$$F^{(s,s)} = im_D f_D v\cdot p_1 + ig\sqrt{m_D m_{D_s}} f_{D_s} \frac{p_1\cdot p_2 - (v\cdot p_1)(v\cdot p_2)}{v\cdot p_2 + \Delta} \tag{C.211}$$

$$G^{(s,s)} = im_D f_D (v\cdot p_1 - v\cdot p_2) \tag{C.212}$$

$\underline{D^+ \to \pi^+\pi^0}$

$$\begin{aligned} F^{(d,d)} &= i\sqrt{2} m_D f_D (v\cdot p_1 - v\cdot p_2) \\ &- i\frac{f_D m_D}{\sqrt{2}} v\cdot p_1 - i\frac{g m_D f_D}{\sqrt{2}} \frac{p_1\cdot p_2 - (v\cdot p_1)(v\cdot p_2)}{v\cdot p_2 + \Delta} \end{aligned} \tag{C.213}$$

$$G^{(d,d)} = -i\frac{m_D f_D}{\sqrt{2}} v\cdot p_2 - i\frac{g m_D f_D}{\sqrt{2}} \frac{p_1\cdot p_2 - (v\cdot p_1)(v\cdot p_2)}{v\cdot p_1 + \Delta} \tag{C.214}$$

$\underline{D^+ \to K^+\overline{K}^0}$

$$F^{(d,d)} = -im_D f_D (v\cdot p_1 - v\cdot p_2) \tag{C.215}$$

$$F^{(s,s)} = im_D f_D v\cdot p_1 + igm_D f_D \frac{p_1\cdot p_2 - (v\cdot p_1)(v\cdot p_2)}{v\cdot p_2 + \Delta} \tag{C.216}$$

$\underline{D_s \to \pi^+K^0}$

$$F^{(s,s)} = -im_{D_s} f_{D_s} (v\cdot p_1 - v\cdot p_2) \tag{C.217}$$

$$F^{(d,d)} = i\frac{m_{D_s} f_{D_s} f_\pi}{f_K} v\cdot p_1 + i\frac{g\sqrt{m_D m_{D_s}} f_D f_\pi}{f_K} \frac{p_1\cdot p_2 - (v\cdot p_1)(v\cdot p_2)}{v\cdot p_2 + \Delta} \tag{C.218}$$

$\underline{D_s \to K^+\pi^0}$

$$F^{(s,s)} = i\frac{m_{D_s} f_{D_s}}{\sqrt{2}} (v\cdot p_1 - v\cdot p_2) \tag{C.219}$$

$$G^{(d,d)} = -i\frac{m_{D_s} f_{D_s} f_\pi}{\sqrt{2} f_K} v\cdot p_2 - i\frac{g\sqrt{m_D m_{D_s}} f_D f_\pi}{\sqrt{2} f_K} \frac{p_1\cdot p_2 - (v\cdot p_1)(v\cdot p_2)}{v\cdot p_1 + \Delta} \tag{C.220}$$

C.2.3 Doubly Cabibbo suppressed (DCS) modes

$\underline{D^0 \to K^+\pi^-}$

$$F^{(d,s)} = i\frac{m_D f_D f_K}{f_\pi} v\cdot p_1 + i\frac{g m_D f_D f_K}{f_\pi} \frac{p_1\cdot p_2 - (v\cdot p_1)(v\cdot p_2)}{v\cdot p_2 + \Delta} \tag{C.221}$$

$$G^{(d,s)} = im_D f_D (v\cdot p_1 - v\cdot p_2) \tag{C.222}$$

$\underline{D^+ \to \pi^+ K^0}$

$$F^{(d,s)} = -im_D f_D (v \cdot p_1 - v \cdot p_2) \tag{C.223}$$

$$G^{(d,s)} = i\frac{m_D f_D f_K}{f_\pi} v \cdot p_2 + i\frac{g m_D f_D f_K}{f_\pi} \frac{p_1 \cdot p_2 - (v \cdot p_1)(v \cdot p_2)}{v \cdot p_1 + \Delta} \tag{C.224}$$

$\underline{D^+ \to K^+ \pi^0}$

$$\begin{aligned} F^{(d,s)} = {} & i\frac{m_D f_D}{\sqrt{2}} (v \cdot p_1 - v \cdot p_2) - i\frac{f_D m_D f_K}{\sqrt{2} f_\pi} v \cdot p_1 \\ & - i\frac{g m_D f_D f_K}{\sqrt{2} f_\pi} \frac{p_1 \cdot p_2 - (v \cdot p_1)(v \cdot p_2)}{v \cdot p_2 + \Delta} \end{aligned} \tag{C.225}$$

$\underline{D_s \to K^+ K^0}$

$$F^{(d,s)} = im_{D_s} f_{D_s} v \cdot p_1 + ig\sqrt{m_D m_{D_s}} f_D \frac{p_1 \cdot p_2 - (v \cdot p_1)(v \cdot p_2)}{v \cdot p_2 + \Delta} \tag{C.226}$$

$$G^{(d,s)} = im_{D_s} f_{D_s} v \cdot p_2 + ig\sqrt{m_D m_{D_s}} f_D \frac{p_1 \cdot p_2 - (v \cdot p_1)(v \cdot p_2)}{v \cdot p_1 + \Delta} \tag{C.227}$$

D Auxiliary information on the helicity amplitude

The hadronic form factors f^V and h^V are defined by the $K_1 \to VP$ decay amplitude

$$\mathcal{A}(K_1 \to VP) = \varepsilon^{\mu}_{K_1}(f^V g_{\mu\nu} + h^V p_{V\mu} p_{K_1\nu})\varepsilon^{\nu *}_V \tag{D.1}$$

and can be related to partial S, and D wave amplitudes as

$$\begin{aligned} f^V &= -A^V_S - \frac{1}{\sqrt{2}} A^V_D \,, \\ h^V &= \frac{E_V}{\sqrt{s}|\vec{p}_V|^2}\left[\left(1 - \frac{\sqrt{s_V}}{E_V}\right) A^V_S + \left(1 + 2\frac{\sqrt{s_V}}{E_V}\right)\frac{1}{\sqrt{2}} A^V_D\right] . \end{aligned} \tag{D.2}$$

They have been calculated in [175] using the $^3P_0$ QPCM [177]

$$\begin{aligned} A_S(K_1(1270) \to K^*\pi/K\rho) &= S^{(K_1 K^*\pi/K_1 K\rho)}(\sqrt{2}\sin(\theta_{K1}) \mp \cos(\theta_{K1}))\,, \\ A_D(K_1(1270) \to K^*\pi/K\rho) &= D^{(K_1 K^*\pi/K_1 K\rho)}(-\sin(\theta_{K1}) \mp \sqrt{2}\cos(\theta_{K1}))\,, \\ A_S(K_1(1400) \to K^*\pi/K\rho) &= S^{(K_1 K^*\pi/K_1 K\rho)}(\sqrt{2}\cos(\theta_{K1}) \pm \sin(\theta_{K1}))\,, \\ A_D(K_1(1400) \to K^*\pi/K\rho) &= D^{(K_1 K^*\pi/K_1 K\rho)}(-\cos(\theta_{K1}) \pm \sqrt{2}\sin(\theta_{K1}))\,, \end{aligned} \tag{D.3}$$

with

$$\begin{aligned} S^{(ABC)} &= \gamma\sqrt{\frac{3}{2}}\frac{2I_1^{(ABC)} - I_0^{(ABC)}}{18}\exp(-\beta'(p^2 - p_0^2))\,, \\ D^{(ABC)} &= \gamma\sqrt{\frac{3}{2}}\frac{I_1^{(ABC)} + I_0^{(ABC)}}{18}\exp(-\beta'(p^2 - p_0^2))\,. \end{aligned} \tag{D.4}$$

Here, p_0 is the decay momentum when all particles are on-shell and $\beta' \approx 3\,\mathrm{GeV}^{-2}$. For $K_1(1270) \to K\rho$, an on-shell decay is not possible since the mass of the $K_1(1270)$ is too small. Therefore, the momentum p_0 is set to zero. Note, that the amplitudes $A_{S/D}$ in (D.3) are given in non-relativistic phase space conventions. Therefore, one has to add a phase space correction

$$A^R_{S/D} = 4\pi^{3/2}\sqrt{\frac{s^2 - (s_V^2 - m_P^2)^2}{\sqrt{s}}}A^{NR}_{S/D} \tag{D.5}$$

to obtain the relativistic decay amplitudes. $\gamma = 4.0 \pm 0.5$ is a dimensionless constant and $\theta_{K1} = 59^\circ \pm 10^\circ$ [175] is the mixing angle of the spin singlet and triplet states

$$\begin{aligned} |K_1(1270)\rangle &= |K_{1A}\rangle \sin\theta_{K_1} + |K_{1B}\rangle \cos\theta_{K_1}\,, \\ |K_1(1400)\rangle &= |K_{1A}\rangle \cos\theta_{K_1} - |K_{1B}\rangle \sin\theta_{K_1}\,, \end{aligned} \tag{D.6}$$

Finally, the functions $I_{0,1}^{(ABC)}$ are given by

$$\begin{aligned} I_0^{(ABC)} &= -\frac{4\sqrt{3}}{\pi^{5/4}} \frac{R_A^{5/2}(R_B R_C)^{3/2}}{(R_A^2+R_B^2+R_C^2)^{5/2}} \left(1 - \vec{p}_B^{\,2} \frac{(2R_A^2+R_B^2+R_C^2)(R_B^2+R_C^2)}{4(R_A^2+R_B^2+R_C^2)}\right) \\ &\quad \times \exp\left(-\vec{p}_B^{\,2} \frac{R_A^2(R_B^2+R_C^2)}{8(R_A^2+R_B^2+R_C^2)}\right), \\ I_1^{(ABC)} &= \frac{4\sqrt{3}}{\pi^{5/4}} \frac{R_A^{5/2}(R_B R_C)^{3/2}}{(R_A^2+R_B^2+R_C^2)^{5/2}} \exp\left(-\vec{p}_B^{\,2} \frac{R_A^2(R_B^2+R_C^2)}{8(R_A^2+R_B^2+R_C^2)}\right), \end{aligned} \tag{D.7}$$

where R_i is the meson wave function radius. For the numerical evaluation the common harmonic oscillator radius $R = 2.5\,\mathrm{GeV}^{-1}$ was used [175, 222]. In this case, the functions simplify to

$$\begin{aligned} I_0^{(ABC)} &= -\frac{4\sqrt{R}}{9\pi^{5/4}} \left(1 - \frac{2}{3}\vec{p}_B^{\,2} R^2\right) \exp\left(-\frac{\vec{p}_B^{\,2} R^2}{12}\right), \\ I_1^{(ABC)} &= \frac{4\sqrt{R}}{9\pi^{5/4}} \exp\left(-\frac{\vec{p}_B^{\,2} R^2}{12}\right), \end{aligned} \tag{D.8}$$

E Approximate flavor symmetries

We use the approximate $SU(3)_F$ symmetry of QCD, as well as its three $SU(2)$ subgroups, to determine relations between form factors and decay amplitudes $\mathcal{A}(B_c \to B\gamma)$.

E.1 Relations between vacuum $\to PP$ form factors

The form factors required in section 4.2.3 are mostly unknown. However, all required $f^{P_1P_2}$ can be determined from the form factors given in section B.1 as well as isospin relations. The isospin states of the pseudoscalar octet are given in Table E.1. In subsection E.1.1, the relations of the Pion and Kaon form factors are addressed. Subsequently, the relations between the $K\pi$ form factors are discussed in subsection E.1.2.

E.1.1 Relations for Pion and Kaon form factors

The isotriplet partner of the neutral current

$$j_\mu^{(I=1)} = \frac{1}{\sqrt{2}}\left(\bar{u}\gamma_\mu u - \bar{d}\gamma_\mu d\right) \tag{E.1}$$

are the charged currents

$$j_\mu^- = \bar{u}\gamma_\mu d\,, \qquad \text{and} \qquad j_\mu^+ = \bar{d}\gamma_\mu u\,. \tag{E.2}$$

They change the isospin and its third component, $\left|j_\mu^-\right\rangle = -\left|1,1\right\rangle_I$ and $\left|j_\mu^+\right\rangle = \left|1,-1\right\rangle_I$. The isospin representations of the two particle final states are given by

$$\begin{aligned}
|K^+K^-\rangle &= \left|\frac{1}{2},\frac{1}{2}\right\rangle_I \left|\frac{1}{2},-\frac{1}{2}\right\rangle_I = \frac{1}{\sqrt{2}}\left|1,0\right\rangle_I + \frac{1}{\sqrt{2}}\left|0,0\right\rangle_I\,,\\
\left|K^0\overline{K}^0\right\rangle &= -\left|\frac{1}{2},-\frac{1}{2}\right\rangle_I \left|\frac{1}{2},\frac{1}{2}\right\rangle_I = -\frac{1}{\sqrt{2}}\left|1,0\right\rangle_I + \frac{1}{\sqrt{2}}\left|0,0\right\rangle_I\,,\\
\left|K^+\overline{K}^0\right\rangle &= -\left|\frac{1}{2},\frac{1}{2}\right\rangle_I \left|\frac{1}{2},\frac{1}{2}\right\rangle_I = -\left|1,1\right\rangle_I\,,\\
|\pi^+\pi^-\rangle &= -\left|1,1\right\rangle_I\left|1,-1\right\rangle_I = -\frac{1}{\sqrt{6}}\left|2,0\right\rangle_I - \frac{1}{\sqrt{2}}\left|1,0\right\rangle_I - \frac{1}{\sqrt{3}}\left|0,0\right\rangle_I\,,\\
\left|\pi^+\pi^0\right\rangle &= -\left|1,1\right\rangle_I\left|1,0\right\rangle_I = -\frac{1}{\sqrt{2}}\left|2,1\right\rangle_I - \frac{1}{\sqrt{2}}\left|1,1\right\rangle_I\,.
\end{aligned} \tag{E.3}$$

Particle	Quarks	$SU(3)_F$	Isospin	U-Spin	V-spin
$\lvert u\rangle$	u	$\lvert\mathbf{3},\frac{1}{3},\frac{1}{2},\frac{1}{2}\rangle$	$\lvert\frac{1}{2},\frac{1}{2}\rangle_I$	$\lvert0,0\rangle_U$	$\lvert\frac{1}{2},\frac{1}{2}\rangle_V$
$\lvert d\rangle$	d	$\lvert\mathbf{3},\frac{1}{3},\frac{1}{2},-\frac{1}{2}\rangle$	$\lvert\frac{1}{2},-\frac{1}{2}\rangle_I$	$\lvert\frac{1}{2},\frac{1}{2}\rangle_U$	$\lvert0,0\rangle_V$
$\lvert s\rangle$	s	$\lvert\mathbf{3},-\frac{2}{3},0,0\rangle$	$\lvert0,0\rangle_I$	$\lvert\frac{1}{2},-\frac{1}{2}\rangle_U$	$\lvert\frac{1}{2},-\frac{1}{2}\rangle_V$
$\lvert\overline{u}\rangle$	$\overline{u}$	$\lvert\overline{\mathbf{3}},-\frac{1}{3},\frac{1}{2},-\frac{1}{2}\rangle$	$\lvert\frac{1}{2},-\frac{1}{2}\rangle_I$	$\lvert0,0\rangle_U$	$\lvert\frac{1}{2},-\frac{1}{2}\rangle_V$
$\lvert\overline{d}\rangle$	$\overline{d}$	$\lvert\overline{\mathbf{3}},-\frac{1}{3},\frac{1}{2},\frac{1}{2}\rangle$	$-\lvert\frac{1}{2},\frac{1}{2}\rangle_I$	$\lvert\frac{1}{2},-\frac{1}{2}\rangle_U$	$\lvert0,0\rangle_V$
$\lvert\overline{s}\rangle$	$\overline{s}$	$\lvert\overline{\mathbf{3}},\frac{2}{3},0,0\rangle$	$\lvert0,0\rangle_I$	$-\lvert\frac{1}{2},\frac{1}{2}\rangle_U$	$-\lvert\frac{1}{2},\frac{1}{2}\rangle_V$
$\lvert D^0\rangle$	$c\overline{u}$	$\lvert\overline{\mathbf{3}},-\frac{1}{3},\frac{1}{2},-\frac{1}{2}\rangle$	$\lvert\frac{1}{2},-\frac{1}{2}\rangle_I$	$\lvert0,0\rangle_U$	$\lvert\frac{1}{2},-\frac{1}{2}\rangle_V$
$\lvert D^+\rangle$	$c\overline{d}$	$\lvert\overline{\mathbf{3}},-\frac{1}{3},\frac{1}{2},\frac{1}{2}\rangle$	$-\lvert\frac{1}{2},\frac{1}{2}\rangle_I$	$\lvert\frac{1}{2},-\frac{1}{2}\rangle_U$	$\lvert0,0\rangle_V$
$\lvert D_s\rangle$	$c\overline{s}$	$\lvert\overline{\mathbf{3}},\frac{2}{3},0,0\rangle$	$\lvert0,0\rangle_I$	$-\lvert\frac{1}{2},\frac{1}{2}\rangle_U$	$-\lvert\frac{1}{2},\frac{1}{2}\rangle_V$
$\lvert\eta_8\rangle$	$\frac{1}{\sqrt{6}}(u\overline{u}+d\overline{d}-2s\overline{s})$	$\lvert\mathbf{8},0,0,0\rangle$	$\lvert0,0\rangle_I$	$\frac{\sqrt{3}}{2}\lvert1,0\rangle_U-\frac{1}{2}\lvert0,0\rangle_U$	$\frac{\sqrt{3}}{2}\lvert1,0\rangle_V-\frac{1}{2}\lvert0,0\rangle_V$
$\lvert\pi^+\rangle$	$u\overline{d}$	$\lvert\mathbf{8},0,1,1\rangle$	$-\lvert1,1\rangle_I$	$\lvert\frac{1}{2},-\frac{1}{2}\rangle_U^1$	$\lvert\frac{1}{2},\frac{1}{2}\rangle_V^1$
$\lvert\pi^0\rangle$	$\frac{1}{\sqrt{2}}(u\overline{u}-d\overline{d})$	$\lvert\mathbf{8},0,1,0\rangle$	$\lvert1,0\rangle_I$	$-\frac{1}{2}\lvert1,0\rangle_U-\frac{\sqrt{3}}{2}\lvert0,0\rangle_U$	$\frac{1}{2}\lvert1,0\rangle_V+\frac{\sqrt{3}}{2}\lvert0,0\rangle_V$
$\lvert\pi^-\rangle$	$d\overline{u}$	$\lvert\mathbf{8},0,1,-1\rangle$	$\lvert1,-1\rangle_I$	$\lvert\frac{1}{2},\frac{1}{2}\rangle_U^2$	$\lvert\frac{1}{2},-\frac{1}{2}\rangle_V^2$
$\lvert K^+\rangle$	$u\overline{s}$	$\lvert\mathbf{8},1,\frac{1}{2},\frac{1}{2}\rangle$	$\lvert\frac{1}{2},\frac{1}{2}\rangle_I$	$-\lvert\frac{1}{2},\frac{1}{2}\rangle_U^1$	$-\lvert1,1\rangle_V$
$\lvert K^0\rangle$	$d\overline{s}$	$\lvert\mathbf{8},1,\frac{1}{2},-\frac{1}{2}\rangle$	$\lvert\frac{1}{2},-\frac{1}{2}\rangle_I$	$-\lvert1,1\rangle_U$	$-\lvert\frac{1}{2},\frac{1}{2}\rangle_V^2$
$\lvert\overline{K}^0\rangle$	$s\overline{d}$	$\lvert\mathbf{8},-1,\frac{1}{2},\frac{1}{2}\rangle$	$-\lvert\frac{1}{2},\frac{1}{2}\rangle_I$	$\lvert1,-1\rangle_U$	$\lvert\frac{1}{2},-\frac{1}{2}\rangle_V^1$
$\lvert K^-\rangle$	$s\overline{u}$	$\lvert\mathbf{8},-1,\frac{1}{2},-\frac{1}{2}\rangle$	$\lvert\frac{1}{2},-\frac{1}{2}\rangle_I$	$\lvert\frac{1}{2},-\frac{1}{2}\rangle_U^2$	$\lvert1,-1\rangle_V$

Table E.1: Isospin, U-spin and V-spin wave functions of quarks and (charmed) mesons, analogously to [223]. The superscript $1,2$ refer to different doublets within the baryon and meson octet.

Thus, the matrix elements can be decomposed into one isotriplet and two isosinglet contributions as follows

$$\begin{aligned}
\left\langle K^+K^-|j_\mu^{\text{em}}|0\right\rangle &= \frac{1}{2}A_\mu^{(I=1)}+\frac{1}{6}A_\mu^{(I=0)}-\frac{1}{3}A_\mu^s\,,\\
\left\langle K^0\overline{K}^0|j_\mu^{\text{em}}|0\right\rangle &= -\frac{1}{2}A_\mu^{(I=1)}+\frac{1}{6}A_\mu^{(I=0)}-\frac{1}{3}A_\mu^s\,,\\
\left\langle K^+\overline{K}^0|j_\mu^-|0\right\rangle &= A_\mu^{(I=1)}\,,\\
\left\langle \pi^+\pi^-|j_\mu^{\text{em}}|0\right\rangle &= -\frac{1}{2}A_\mu^{(I=1)}\,,\\
\left\langle \pi^+\pi^0|j_\mu^-|0\right\rangle &= \frac{1}{\sqrt{2}}A_\mu^{(I=1)}\,.
\end{aligned}\tag{E.4}$$

E.1.2 Relations for πK form factors

There are four relevant vector currents that contain a strange quark field, which form two isospin doublets

$$\begin{aligned}
j_\mu^0 &= \bar{s}\gamma_\mu d\,,\\
j_\mu^+ &= \bar{s}\gamma_\mu u\,,
\end{aligned}\qquad\text{and}\qquad
\begin{aligned}
j_\mu^- &= \bar{u}\gamma_\mu s\,,\\
j_\mu^0 &= \bar{d}\gamma_\mu s\,.
\end{aligned}\tag{E.5}$$

The isospin representations of these currents read $\left|j_\mu^0\right\rangle = -\left|\frac{1}{2},\frac{1}{2}\right\rangle_I$, $\left|j_\mu^+\right\rangle = \left|\frac{1}{2},-\frac{1}{2}\right\rangle_I$, $\left|j_\mu^-\right\rangle = \left|\frac{1}{2},\frac{1}{2}\right\rangle_I$ and $\left|j_\mu^{\overline{0}}\right\rangle = \left|\frac{1}{2},-\frac{1}{2}\right\rangle_I$. The two particle final states are given by

$$\begin{aligned}
\left|\overline{K}\pi^-\right\rangle &= -\left|\frac{1}{2},\frac{1}{2}\right\rangle|1,-1\rangle = -\sqrt{\frac{1}{3}}\left|\frac{3}{2},-\frac{1}{2}\right\rangle + \sqrt{\frac{2}{3}}\left|\frac{1}{2},-\frac{1}{2}\right\rangle\,,\\
\left|K^-\pi^+\right\rangle &= -\left|\frac{1}{2},-\frac{1}{2}\right\rangle|1,1\rangle = -\sqrt{\frac{1}{3}}\left|\frac{3}{2},\frac{1}{2}\right\rangle - \sqrt{\frac{2}{3}}\left|\frac{1}{2},\frac{1}{2}\right\rangle\,,\\
\left|\overline{K}\pi^0\right\rangle &= -\left|\frac{1}{2},\frac{1}{2}\right\rangle|1,0\rangle = -\sqrt{\frac{2}{3}}\left|\frac{3}{2},\frac{1}{2}\right\rangle + \sqrt{\frac{1}{3}}\left|\frac{1}{2},\frac{1}{2}\right\rangle\,,\\
\left|K^0\pi^+\right\rangle &= -\left|\frac{1}{2},-\frac{1}{2}\right\rangle|1,1\rangle = -\sqrt{\frac{1}{3}}\left|\frac{3}{2},\frac{1}{2}\right\rangle - \sqrt{\frac{2}{3}}\left|\frac{1}{2},\frac{1}{2}\right\rangle\,,\\
\left|K^+\pi^0\right\rangle &= \left|\frac{1}{2},\frac{1}{2}\right\rangle|1,0\rangle = \sqrt{\frac{2}{3}}\left|\frac{3}{2},\frac{1}{2}\right\rangle - \sqrt{\frac{1}{3}}\left|\frac{1}{2},\frac{1}{2}\right\rangle\,,\\
\left|K^0\pi^0\right\rangle &= \left|\frac{1}{2},-\frac{1}{2}\right\rangle|1,0\rangle = \sqrt{\frac{2}{3}}\left|\frac{3}{2},-\frac{1}{2}\right\rangle + \sqrt{\frac{1}{3}}\left|\frac{1}{2},-\frac{1}{2}\right\rangle\,,\\
\left|K^+\pi^-\right\rangle &= \left|\frac{1}{2},\frac{1}{2}\right\rangle|1,-1\rangle = \sqrt{\frac{1}{3}}\left|\frac{3}{2},-\frac{1}{2}\right\rangle - \sqrt{\frac{2}{3}}\left|\frac{1}{2},-\frac{1}{2}\right\rangle\,.
\end{aligned} \tag{E.6}$$

The isospin symmetry allows to determine relations between form factors if the currents are in the same doublet. We start with the isospin decomposition of all matrix elements from the first doublet

$$\begin{aligned}
\left\langle\overline{K}^0\pi^-|j_\mu^+|0\right\rangle &= +\sqrt{\frac{2}{3}}A_\mu^1\,,\\
\left\langle K^-\pi^+|j_\mu^0|0\right\rangle &= +\sqrt{\frac{2}{3}}A_\mu^1\,,\\
\left\langle\overline{K}^0\pi^0|j_\mu^0|0\right\rangle &= -\sqrt{\frac{1}{3}}A_\mu^1\,,
\end{aligned} \tag{E.7}$$

which yields $f_+^{\overline{K}^0\pi^-} = -f_+^{\pi^+K^-} = \frac{1}{\sqrt{2}}f_+^{\pi^0\overline{K}^0}$. Analogously, for the second doublet we get

$$\begin{aligned}
\left\langle K^0\pi^+|j_\mu^-|0\right\rangle &= -\sqrt{\frac{2}{3}}A_\mu^2\,,\\
\left\langle K^+\pi^0|j_\mu^-|0\right\rangle &= -\sqrt{\frac{1}{3}}A_\mu^2\,,\\
\left\langle K^0\pi^0|j_\mu^{\overline{0}}|0\right\rangle &= +\sqrt{\frac{1}{3}}A_\mu^2\,,\\
\left\langle K^+\pi^-|j_\mu^{\overline{0}}|0\right\rangle &= -\sqrt{\frac{2}{3}}A_\mu^2\,,
\end{aligned} \tag{E.8}$$

which gives rise to $f_+^{\pi^+K^0} = -\frac{1}{\sqrt{2}}f_+^{K^+\pi^0} = -\frac{1}{\sqrt{2}}f_+^{\pi^0K^0} = -f_+^{K^+\pi^-}$. The two different currents are connected due to C-parity $f_+^{\overline{K}^0\pi^-} = f_+^{\pi^+K^0}$. These relations are in agreement with results from χPT.

E.2 Baryonic decays

In this section, we provide additional information on flavor relations for $B_c \to B\gamma$ decay amplitudes. $SU(3)_F$ and $SU(2)_{I,U,V}$ wave functions of baryons are listed in Table E.2. In subsection E.2.1 we show the U-spin decompositions of $B_{c\bar{3}/c6} \to B_8\gamma$ decays. Subsequently, we provide analogous information for $SU(3)_F$ on the same decay modes in subsection E.2.2. Furthermore, we list the relevant decompositions of products of $SU(3)_F$ operators and charm baryons wave functions in irreducible representations. $B_{c6} \to B_{10}\gamma$ decays are covered in subsection E.2.3.

Particle	Quarks	$SU(3)_F$	Isospin	U-Spin	V-spin
$\lvert\Lambda_c\rangle$	cud	$\lvert\overline{\mathbf{3}}, \frac{2}{3}, 0, 0\rangle$	$\lvert 0,0\rangle_I$	$\lvert\frac{1}{2}, \frac{1}{2}\rangle_U$	$\lvert\frac{1}{2}, \frac{1}{2}\rangle_V$
$\lvert\Xi_c^0\rangle$	cds	$\lvert\overline{\mathbf{3}}, -\frac{1}{3}, \frac{1}{2}, -\frac{1}{2}\rangle$	$\lvert\frac{1}{2}, -\frac{1}{2}\rangle_I$	$\lvert 0,0\rangle_U$	$\lvert\frac{1}{2}, -\frac{1}{2}\rangle_V$
$\lvert\Xi_c^+\rangle$	cus	$\lvert\overline{\mathbf{3}}, -\frac{1}{3}, \frac{1}{2}, \frac{1}{2}\rangle$	$\lvert\frac{1}{2}, \frac{1}{2}\rangle_I$	$\lvert\frac{1}{2}, -\frac{1}{2}\rangle_U$	$\lvert 0,0\rangle_V$
$\lvert\Omega_c\rangle$	css	$\lvert\mathbf{6}, -\frac{4}{3}, 0, 0\rangle$	$\lvert 0,0\rangle_I$	$\lvert 1,-1\rangle_U$	$\lvert 1,-1\rangle_V$
$\lvert\Xi_c'^0\rangle$	cds	$\lvert\mathbf{6}, -\frac{1}{3}, \frac{1}{2}, -\frac{1}{2}\rangle$	$\lvert\frac{1}{2}, -\frac{1}{2}\rangle_I$	$\lvert 1,0\rangle_U$	$\lvert\frac{1}{2}, -\frac{1}{2}\rangle_V$
$\lvert\Xi_c'^+\rangle$	cus	$\lvert\mathbf{6}, -\frac{1}{3}, \frac{1}{2}, \frac{1}{2}\rangle$	$\lvert\frac{1}{2}, \frac{1}{2}\rangle_I$	$\lvert\frac{1}{2}, -\frac{1}{2}\rangle_U$	$\lvert 1,0\rangle_V$
$\lvert\Sigma_c^0\rangle$	cdd	$\lvert\mathbf{6}, \frac{2}{3}, 1, -1\rangle$	$\lvert 1,-1\rangle_I$	$\lvert 1,1\rangle_U$	$\lvert 0,0\rangle_V$
$\lvert\Sigma_c^+\rangle$	cud	$\lvert\mathbf{6}, \frac{2}{3}, 1, 0\rangle$	$\lvert 1,0\rangle_I$	$\lvert\frac{1}{2}, \frac{1}{2}\rangle_U$	$\lvert\frac{1}{2}, \frac{1}{2}\rangle_V$
$\lvert\Sigma_c^{++}\rangle$	cuu	$\lvert\mathbf{6}, \frac{2}{3}, 1, 1\rangle$	$\lvert 1,1\rangle_I$	$\lvert 0,0\rangle_U$	$\lvert 1,1\rangle_V$
$\lvert\Lambda\rangle$	uds	$\lvert\mathbf{8}, 0, 0, 0\rangle$	$\lvert 0,0\rangle_I$	$\frac{\sqrt{3}}{2}\lvert 1,0\rangle_U - \frac{1}{2}\lvert 0,0\rangle_U$	$-\frac{\sqrt{3}}{2}\lvert 1,0\rangle_V + \frac{1}{2}\lvert 0,0\rangle_V$
$\lvert\Sigma^0\rangle$	uds	$\lvert\mathbf{8}, 0, 1, 0\rangle$	$\lvert 1,0\rangle_I$	$\frac{1}{2}\lvert 1,0\rangle_U + \frac{\sqrt{3}}{2}\lvert 0,0\rangle_U$	$\frac{1}{2}\lvert 1,0\rangle_V + \frac{\sqrt{3}}{2}\lvert 0,0\rangle_V$
$\lvert\Sigma^-\rangle$	dds	$\lvert\mathbf{8}, 0, 1, -1\rangle$	$\lvert 1,-1\rangle_I$	$\lvert\frac{1}{2}, \frac{1}{2}\rangle_U^1$	$\lvert\frac{1}{2}, -\frac{1}{2}\rangle_V^1$
$\lvert\Sigma^+\rangle$	uus	$\lvert\mathbf{8}, 0, 1, 1\rangle$	$\lvert 1,1\rangle_I$	$\lvert\frac{1}{2}, -\frac{1}{2}\rangle_U^2$	$\lvert\frac{1}{2}, \frac{1}{2}\rangle_V^2$
$\lvert\Xi^0\rangle$	uss	$\lvert\mathbf{8}, -1, \frac{1}{2}, \frac{1}{2}\rangle$	$\lvert\frac{1}{2}, \frac{1}{2}\rangle_I^1$	$\lvert 1,-1\rangle_U$	$\lvert\frac{1}{2}, -\frac{1}{2}\rangle_V^2$
$\lvert\Xi^-\rangle$	dss	$\lvert\mathbf{8}, -1, \frac{1}{2}, -\frac{1}{2}\rangle$	$\lvert\frac{1}{2}, -\frac{1}{2}\rangle_I^1$	$\lvert\frac{1}{2}, -\frac{1}{2}\rangle_U^1$	$\lvert 1,-1\rangle_V$
$\lvert n\rangle$	udd	$\lvert\mathbf{8}, 1, \frac{1}{2}, -\frac{1}{2}\rangle$	$\lvert\frac{1}{2}, -\frac{1}{2}\rangle_I^2$	$\lvert 1,1\rangle_U$	$\lvert\frac{1}{2}, \frac{1}{2}\rangle_V^1$
$\lvert p\rangle$	uud	$\lvert\mathbf{8}, 1, \frac{1}{2}, \frac{1}{2}\rangle$	$\lvert\frac{1}{2}, \frac{1}{2}\rangle_I^2$	$\lvert\frac{1}{2}, \frac{1}{2}\rangle_U^2$	$\lvert 1,1\rangle_V$
$\lvert\Delta^{++}\rangle$	uuu	$\lvert\mathbf{10}, 1, \frac{3}{2}, \frac{3}{2}\rangle$	$\lvert\frac{3}{2}, \frac{3}{2}\rangle_I$	$\lvert 0,0\rangle_U$	$\lvert\frac{3}{2}, \frac{3}{2}\rangle_V$
$\lvert\Delta^+\rangle$	uud	$\lvert\mathbf{10}, 1, \frac{3}{2}, \frac{1}{2}\rangle$	$\lvert\frac{3}{2}, \frac{1}{2}\rangle_I$	$\lvert\frac{1}{2}, \frac{1}{2}\rangle_U$	$\lvert 1,1\rangle_V$
$\lvert\Delta^0\rangle$	udd	$\lvert\mathbf{10}, 1, \frac{3}{2}, -\frac{1}{2}\rangle$	$\lvert\frac{3}{2}, -\frac{1}{2}\rangle_I$	$\lvert 1,1\rangle_U$	$\lvert\frac{1}{2}, \frac{1}{2}\rangle_V$
$\lvert\Delta^-\rangle$	ddd	$\lvert\mathbf{10}, 1, \frac{3}{2}, -\frac{3}{2}\rangle$	$\lvert\frac{3}{2}, -\frac{3}{2}\rangle_I$	$\lvert\frac{3}{2}, \frac{3}{2}\rangle_U$	$\lvert 0,0\rangle_V$
$\lvert\Sigma^{*+}\rangle$	uus	$\lvert\mathbf{10}, 0, 1, 1\rangle$	$\lvert 1,1\rangle_I$	$\lvert\frac{1}{2}, -\frac{1}{2}\rangle_U$	$\lvert\frac{3}{2}, \frac{1}{2}\rangle_V$
$\lvert\Sigma^{*0}\rangle$	uds	$\lvert\mathbf{10}, 0, 1, 0\rangle$	$\lvert 1,0\rangle_I$	$\lvert 1,0\rangle_U$	$\lvert 1,0\rangle_V$
$\lvert\Sigma^{*-}\rangle$	dds	$\lvert\mathbf{10}, 0, 1, -1\rangle$	$\lvert 1,-1\rangle_I$	$\lvert\frac{3}{2}, \frac{1}{2}\rangle_U$	$\lvert\frac{1}{2}, -\frac{1}{2}\rangle_V$
$\lvert\Xi^{*0}\rangle$	uss	$\lvert\mathbf{10}, -1, \frac{1}{2}, \frac{1}{2}\rangle$	$\lvert\frac{1}{2}, \frac{1}{2}\rangle_I$	$\lvert 1,-1\rangle_U$	$\lvert\frac{3}{2}, -\frac{1}{2}\rangle_V$
$\lvert\Xi^{*-}\rangle$	dss	$\lvert\mathbf{10}, -1, \frac{1}{2}, -\frac{1}{2}\rangle$	$\lvert\frac{1}{2}, -\frac{1}{2}\rangle_I$	$\lvert\frac{3}{2}, -\frac{1}{2}\rangle_U$	$\lvert 1,-1\rangle_V$
$\lvert\Omega^-\rangle$	sss	$\lvert\mathbf{10}, -2, 0, 0\rangle$	$\lvert 0,0\rangle_I$	$\lvert\frac{3}{2}, -\frac{3}{2}\rangle_U$	$\lvert\frac{3}{2}, -\frac{3}{2}\rangle_V$

Table E.2: $SU(3)_F$, isospin, U-spin and V-spin wave functions of charmed anti-triplet/sextet baryons and the light baryon octet and decuplet, analogously to [223]. For the $SU(3)_F$ states we use the convention $\lvert R, Y, I, I_3\rangle$. The superscript $1, 2$ refer to different doublets within the baryon octet.

E.2.1 U-spin decomposition

In Table E.3 and E.5, we show the U-spin decompositions of the SM decay amplitudes for $B_{c\bar{3}} \to B_8\gamma$ and $B_{c6} \to B_8\gamma$, respectively. In Table E.4 and E.6, we show the Iso- and U-spin decomposition of the $c \to u\gamma$ contributions. Note that the $c \to u\gamma$ contributions have the same U-spin structure as the SM singlet operator. On the one hand, we distinguish between them as we study possible BSM effects in the electromagnetic dipole operators. On the other hand, differentiation enables us to use the additional simple isospin relations between the amplitudes of the dipole operators.

Decay	$\langle\frac{1}{2}\vert 1\vert\frac{1}{2}\rangle$	$\langle 1\vert 1\vert 0\rangle$	$\langle\frac{1}{2}\vert 0\vert\frac{1}{2}\rangle$	$\langle 0\vert 0\vert 0\rangle$
$\Lambda_c \to \Sigma^+\gamma$	$\sqrt{\frac{2}{3}}V_{cs}^*V_{ud}$	0	-	-
$\Xi_c^0 \to \Xi^0\gamma$	0	$-V_{cs}^*V_{ud}$	-	-
$\Lambda_c \to p\gamma$	$-\sqrt{\frac{2}{3}}\Sigma$	0	$\sqrt{2}\Delta$	0
$\Xi_c^+ \to \Sigma^+\gamma$	$\sqrt{\frac{2}{3}}\Sigma$	0	$\sqrt{2}\Delta$	0
$\Xi_c^0 \to \Lambda\gamma$	0	$\sqrt{\frac{3}{2}}\Sigma$	0	$-\frac{1}{\sqrt{2}}\Delta$
$\Xi_c^0 \to \Sigma^0\gamma$	0	$\frac{1}{\sqrt{2}}\Sigma$	0	$\frac{\sqrt{3}}{\sqrt{2}}\Delta$
$\Xi_c^+ \to p\gamma$	$\sqrt{\frac{2}{3}}V_{cd}^*V_{us}$	0	-	-
$\Xi_c^0 \to n\gamma$	0	$V_{cd}^*V_{us}$	-	-

Table E.3: U-Spin decomposition of the SM decay amplitudes for the charmed anti-triplet baryons. In the matrix element $\langle U(f)\vert U(O)\vert U(i)\rangle$, $U(f)$, $U(O)$ and $U(i)$ denote the U-spin of the final state, the U-spin changing operators and the initial state, respectively. The matrix elements are related to the amplitudes in Table 6.1 as follows: $A_\Sigma \sim \sqrt{\frac{2}{3}}\,\langle\frac{1}{2}\vert 1\vert\frac{1}{2}\rangle$, $A'_\Sigma \sim -\langle 1\vert 1\vert 0\rangle$, $A_\Delta \sim \sqrt{2}\,\langle\frac{1}{2}\vert 0\vert\frac{1}{2}\rangle$ and $A'_\Delta \sim \sqrt{2}\,\langle 0\vert 0\vert 0\rangle$.

Decay	$\langle 1\vert\frac{1}{2}\vert\frac{1}{2}\rangle_I$	$\langle\frac{1}{2}\vert 0\vert\frac{1}{2}\rangle_U$	$\langle 0\vert 0\vert 0\rangle_U$
$\Lambda_c \to p\gamma$	1	1	0
$\Xi_c^+ \to \Sigma^+\gamma$	0	1	0
$\Xi_c^0 \to \Lambda\gamma$	0	0	$-\frac{1}{2}$
$\Xi_c^0 \to \Sigma^0\gamma$	$\sqrt{\frac{1}{2}}$	0	$\frac{\sqrt{3}}{2}$

Table E.4: Iso- and U-spin decomposition of the BSM contribution for the charm anti-triplet baryons. The matrix elements are related to the amplitudes in Table 6.1 as follows: $A'_7 \sim \langle\frac{1}{2}\vert 0\vert\frac{1}{2}\rangle_U$ and $A_7 \sim \langle 0\vert 0\vert 0\rangle_U$

Decay	$\langle\frac{1}{2}\vert 1\vert\frac{1}{2}\rangle$	$\langle 1\vert 1\vert 1\rangle$	$\langle 0\vert 1\vert 1\rangle$	$\langle\frac{1}{2}\vert 0\vert\frac{1}{2}\rangle$	$\langle 1\vert 0\vert 1\rangle$
$\Sigma_c^+ \to \Sigma^+\gamma$	$\sqrt{\frac{2}{3}}V_{cs}^*V_{ud}$	0	0	-	-
$\Sigma_c^0 \to \Lambda\gamma$	0	$\frac{\sqrt{3}}{2\sqrt{2}}V_{cs}^*V_{ud}$	$\frac{1}{2\sqrt{3}}V_{cs}^*V_{ud}$	-	-
$\Sigma_c^0 \to \Sigma^0\gamma$	0	$\frac{1}{2\sqrt{2}}V_{cs}^*V_{ud}$	$-\frac{1}{2}V_{cs}^*V_{ud}$	-	-
$\Xi_c'^0 \to \Xi^0\gamma$	0	$\frac{1}{\sqrt{2}}V_{cs}^*V_{ud}$	0	-	-
$\Sigma_c^+ \to p\gamma$	$-\sqrt{\frac{2}{3}}\Sigma$	0	0	$\sqrt{2}\Delta$	0
$\Sigma_c^0 \to n\gamma$	0	$-\Sigma$	0	0	$\sqrt{2}\Delta$
$\Xi_c'^+ \to \Sigma^+\gamma$	$\sqrt{\frac{2}{3}}\Sigma$	0	0	$\sqrt{2}\Delta$	0
$\Xi_c'^0 \to \Lambda\gamma$	0	0	$\frac{1}{\sqrt{6}}\Sigma$	0	$\sqrt{\frac{3}{2}}\Delta$
$\Xi_c'^0 \to \Sigma^0\gamma$	0	0	$-\frac{1}{\sqrt{2}}\Sigma$	0	$\frac{1}{\sqrt{2}}\Delta$
$\Omega_c \to \Xi^0\gamma$	0	Σ	0	0	$\sqrt{2}\Delta$
$\Xi_c'^+ \to p\gamma$	$\sqrt{\frac{2}{3}}V_{cd}^*V_{us}$	0	0	-	-
$\Xi_c'^0 \to n\gamma$	0	$\frac{1}{\sqrt{2}}V_{cd}^*V_{us}$	0	-	-
$\Omega_c \to \Lambda\gamma$	0	$\frac{\sqrt{3}}{2\sqrt{2}}V_{cd}^*V_{us}$	$-\frac{1}{2\sqrt{3}}V_{cd}^*V_{us}$	-	-
$\Omega_c \to \Sigma^0\gamma$	0	$\frac{1}{2\sqrt{2}}V_{cd}^*V_{us}$	$\frac{1}{2}V_{cd}^*V_{us}$	-	-

Table E.5: U-Spin decomposition of the SM decay amplitudes for the charmed sextet baryons. In the matrix element $\langle U(f)\vert U(O)\vert U(i)\rangle$, $U(f)$, $U(O)$ and $U(i)$ denote the U-spin of the final state, the U-spin changing operators and the initial state, respectively. The matrix elements are related to the amplitudes in Table 6.2 as follows: $E_\Sigma \sim \sqrt{\frac{2}{3}}\,\langle\frac{1}{2}\vert 1\vert\frac{1}{2}\rangle$, $E'_\Sigma \sim \langle 1\vert 1\vert 1\rangle$, $E''_\Sigma \sim \langle 0\vert 1\vert 1\rangle$, $E_\Delta \sim \sqrt{2}\,\langle\frac{1}{2}\vert 1\vert\frac{1}{2}\rangle$ and $E'_\Delta \sim \sqrt{2}\,\langle 0\vert 0\vert 0\rangle$.

Decay	$\langle\frac{1}{2}\vert\frac{1}{2}\vert 1\rangle_I$	$\langle\frac{1}{2}\vert 0\vert\frac{1}{2}\rangle_U$	$\langle 1\vert 0\vert 1\rangle_U$
$\Sigma_c^+ \to p\gamma$	$\sqrt{\frac{1}{3}}$	1	0
$\Sigma_c^0 \to n\gamma$	$\sqrt{\frac{2}{3}}$	0	1
$\Xi_c'^+ \to \Sigma^+\gamma$	0	1	0
$\Xi_c'^0 \to \Lambda\gamma$	0	0	$\frac{\sqrt{3}}{2}$
$\Xi_c'^0 \to \Sigma^0\gamma$	0	0	$\frac{1}{2}$
$\Omega_c \to \Xi^0\gamma$	0	0	1

Table E.6: Iso- and U-spin decomposition of the BSM contribution for the charm sextet baryons. The matrix elements are related to the amplitudes in Table 6.2 as follows: $E_7 \sim \langle\frac{1}{2}\vert 0\vert\frac{1}{2}\rangle_U$ and $E'_7 \sim \langle 1\vert 0\vert 1\rangle_U$

E.2.2 $SU(3)_F$ decomposition

In this subsection we show the decompositions of the relevant products of $SU(3)_F$ operators and charm baryon wave functions in irreducible representations. Subsequently, information in the $SU(3)_F$ decomposition of $B_{c\overline{3}} \to B_8\gamma$ and $B_{c6} \to B_8\gamma$ decay amplitudes are given in Table E.7 and E.8, respectively.

$\Lambda_c \to B_8\gamma$

$$\begin{aligned}
\overline{\mathbf{6}}_{-\frac{2}{3},1,1}\left|\overline{\mathbf{3}},\frac{2}{3},0,0\right\rangle &= \sqrt{\frac{2}{3}}\left|\mathbf{8},0,1,1\right\rangle + \sqrt{\frac{1}{3}}\left|\overline{\mathbf{10}},0,1,1\right\rangle \\
\overline{\mathbf{6}}_{\frac{1}{3},\frac{1}{2},\frac{1}{2}}\left|\overline{\mathbf{3}},\frac{2}{3},0,0\right\rangle &= \sqrt{\frac{1}{3}}\left|\mathbf{8},1,\frac{1}{2},\frac{1}{2}\right\rangle + \sqrt{\frac{2}{3}}\left|\overline{\mathbf{10}},1,\frac{1}{2},\frac{1}{2}\right\rangle
\end{aligned} \tag{E.9}$$

$$\begin{aligned}
\mathbf{15}_{-\frac{2}{3},1,1}\left|\overline{\mathbf{3}},\frac{2}{3},0,0\right\rangle &= -\frac{2}{\sqrt{15}}\left|\mathbf{8},0,1,1\right\rangle + \sqrt{\frac{1}{3}}\left|\mathbf{10},0,1,1\right\rangle + \sqrt{\frac{2}{5}}\left|\mathbf{27},0,1,1\right\rangle \\
\mathbf{15}_{\frac{1}{3},\frac{1}{2},\frac{1}{2}}\left|\overline{\mathbf{3}},\frac{2}{3},0,0\right\rangle &= -\sqrt{\frac{1}{5}}\left|\mathbf{8},1,\frac{1}{2},\frac{1}{2}\right\rangle + \frac{2}{\sqrt{5}}\left|\mathbf{27},1,\frac{1}{2},\frac{1}{2}\right\rangle \\
\mathbf{15}_{\frac{1}{3},\frac{3}{2},\frac{1}{2}}\left|\overline{\mathbf{3}},\frac{2}{3},0,0\right\rangle &= \sqrt{\frac{1}{2}}\left|\mathbf{10},1,\frac{3}{2},\frac{1}{2}\right\rangle + \sqrt{\frac{1}{2}}\left|\mathbf{27},1,\frac{3}{2},\frac{1}{2}\right\rangle
\end{aligned} \tag{E.10}$$

$$\mathbf{3}_{\frac{1}{3},\frac{1}{2},\frac{1}{2}}\left|\overline{\mathbf{3}},\frac{2}{3},0,0\right\rangle = \left|\mathbf{8},1,\frac{1}{2},\frac{1}{2}\right\rangle \tag{E.11}$$

$\Xi_c^+ \to B_8\gamma$

$$\begin{aligned}
\overline{\mathbf{6}}_{\frac{1}{3},\frac{1}{2},\frac{1}{2}}\left|\overline{\mathbf{3}},-\frac{1}{3},\frac{1}{2},\frac{1}{2}\right\rangle &= -\sqrt{\frac{1}{3}}\left|\mathbf{8},0,1,1\right\rangle + \sqrt{\frac{2}{3}}\left|\overline{\mathbf{10}},0,1,1\right\rangle \\
\overline{\mathbf{6}}_{\frac{4}{3},0,0}\left|\overline{\mathbf{3}},-\frac{1}{3},\frac{1}{2},\frac{1}{2}\right\rangle &= -\sqrt{\frac{2}{3}}\left|\mathbf{8},1,\frac{1}{2},\frac{1}{2}\right\rangle + \sqrt{\frac{1}{3}}\left|\overline{\mathbf{10}},1,\frac{1}{2},\frac{1}{2}\right\rangle
\end{aligned} \tag{E.12}$$

$$\begin{aligned}
\mathbf{15}_{\frac{1}{3},\frac{1}{2},\frac{1}{2}}\left|\overline{\mathbf{3}},-\frac{1}{3},\frac{1}{2},\frac{1}{2}\right\rangle &= \frac{1}{3\sqrt{5}}\left|\mathbf{8},0,1,1\right\rangle - \frac{2}{3}\left|\mathbf{10},0,1,1\right\rangle + \frac{2\sqrt{2}}{3\sqrt{5}}\left|\mathbf{27},0,1,1\right\rangle \\
\mathbf{15}_{\frac{1}{3},\frac{3}{2},\frac{1}{2}}\left|\overline{\mathbf{3}},-\frac{1}{3},\frac{1}{2},\frac{1}{2}\right\rangle &= -\frac{2\sqrt{2}}{3\sqrt{5}}\left|\mathbf{8},0,1,1\right\rangle - \frac{1}{3\sqrt{2}}\left|\mathbf{10},0,1,1\right\rangle \\
, \qquad &\quad - \frac{1}{2\sqrt{15}}\left|\mathbf{27},0,1,1\right\rangle + \frac{\sqrt{3}}{2}\left|\mathbf{27},0,2,1\right\rangle \\
\mathbf{15}_{\frac{4}{3},1,0}\left|\overline{\mathbf{3}},-\frac{1}{3},\frac{1}{2},\frac{1}{2}\right\rangle &= -\frac{2}{\sqrt{15}}\left|\mathbf{8},1,\frac{1}{2},\frac{1}{2}\right\rangle - \frac{1}{\sqrt{15}}\left|\mathbf{17},1,\frac{1}{2},\frac{1}{2}\right\rangle \\
&\quad - \sqrt{\frac{1}{3}}\left|\mathbf{10},1,\frac{3}{2},\frac{1}{2}\right\rangle + \sqrt{\frac{1}{3}}\left|\mathbf{27},1,\frac{3}{2},\frac{1}{2}\right\rangle
\end{aligned} \tag{E.13}$$

$$\mathbf{3}_{\frac{1}{3},\frac{1}{2},\frac{1}{2}}\left|\overline{\mathbf{3}},-\frac{1}{3},\frac{1}{2},\frac{1}{2}\right\rangle = \left|\mathbf{8},0,1,1\right\rangle \tag{E.14}$$

$\Xi_c^0 \to B_8\gamma$

$$
\begin{aligned}
\overline{\mathbf{6}}_{-\frac{2}{3},1,1}\left|\overline{\mathbf{3}},-\frac{1}{3},\frac{1}{2},-\frac{1}{2}\right\rangle &= \sqrt{\frac{2}{3}}\left|\mathbf{8},-1,\frac{1}{2},\frac{1}{2}\right\rangle + \sqrt{\frac{1}{3}}\left|\overline{\mathbf{10}},-1,\frac{3}{2},\frac{1}{2}\right\rangle \\
\overline{\mathbf{6}}_{\frac{1}{3},\frac{1}{2},\frac{1}{2}}\left|\overline{\mathbf{3}},-\frac{1}{3},\frac{1}{2},-\frac{1}{2}\right\rangle &= \sqrt{\frac{1}{2}}\left|\mathbf{8},0,0,0\right\rangle - \sqrt{\frac{1}{6}}\left|\mathbf{8},0,1,0\right\rangle + \sqrt{\frac{1}{3}}\left|\overline{\mathbf{10}},0,1,0\right\rangle \\
\overline{\mathbf{6}}_{\frac{4}{3},0,0}\left|\overline{\mathbf{3}},-\frac{1}{3},\frac{1}{2},-\frac{1}{2}\right\rangle &= -\sqrt{\frac{2}{3}}\left|\mathbf{8},1,\frac{1}{2},-\frac{1}{2}\right\rangle + \sqrt{\frac{1}{3}}\left|\overline{\mathbf{10}},1,\frac{1}{2},-\frac{1}{2}\right\rangle
\end{aligned}
\tag{E.15}
$$

$$
\begin{aligned}
\mathbf{15}_{-\frac{2}{3},1,1}\left|\overline{\mathbf{3}},-\frac{1}{3},\frac{1}{2},-\frac{1}{2}\right\rangle &= \frac{2}{\sqrt{15}}\left|\mathbf{8},-1,\frac{1}{2},\frac{1}{2}\right\rangle + \sqrt{\frac{1}{3}}\left|\mathbf{10},-1,\frac{1}{2},\frac{1}{2}\right\rangle \\
&\quad + \sqrt{\frac{1}{15}}\left|\mathbf{27},-1,\frac{1}{2},\frac{1}{2}\right\rangle + \sqrt{\frac{1}{3}}\left|\mathbf{27},-1,\frac{3}{2},\frac{1}{2}\right\rangle \\
\mathbf{15}_{\frac{1}{3},\frac{1}{2},\frac{1}{2}}\left|\overline{\mathbf{3}},-\frac{1}{3},\frac{1}{2},-\frac{1}{2}\right\rangle &= \sqrt{\frac{3}{10}}\left|\mathbf{8},0,0,0\right\rangle + \frac{1}{3\sqrt{10}}\left|\mathbf{8},0,1,0\right\rangle - \frac{\sqrt{2}}{3}\left|\mathbf{10},0,1,0\right\rangle \\
&\quad + \sqrt{\frac{1}{5}}\left|\mathbf{27},0,0,0\right\rangle + \frac{2}{\sqrt{15}}\left|\mathbf{27},0,1,0\right\rangle \\
\mathbf{15}_{\frac{1}{3},\frac{3}{2},\frac{1}{2}}\left|\overline{\mathbf{3}},-\frac{1}{3},\frac{1}{2},-\frac{1}{2}\right\rangle &= \frac{4}{3\sqrt{5}}\left|\mathbf{8},0,1,0\right\rangle + \frac{1}{3}\left|\mathbf{10},0,1,0\right\rangle \\
&\quad + \sqrt{\frac{1}{30}}\left|\mathbf{27},0,1,0\right\rangle + \sqrt{\frac{1}{2}}\left|\mathbf{27},0,2,0\right\rangle \\
\mathbf{15}_{\frac{4}{3},1,0}\left|\overline{\mathbf{3}},-\frac{1}{3},\frac{1}{2},-\frac{1}{2}\right\rangle &= \frac{2}{\sqrt{15}}\left|\mathbf{8},1,\frac{1}{2},-\frac{1}{2}\right\rangle + \sqrt{\frac{1}{15}}\left|\mathbf{27},1,\frac{1}{2},-\frac{1}{2}\right\rangle \\
&\quad - \sqrt{\frac{1}{3}}\left|\mathbf{10},1,\frac{3}{2},-\frac{1}{2}\right\rangle + \sqrt{\frac{1}{3}}\left|\mathbf{27},1,\frac{3}{2},-\frac{1}{2}\right\rangle
\end{aligned}
\tag{E.16}
$$

,

$$
\mathbf{3}_{\frac{1}{3},\frac{1}{2},\frac{1}{2}}\left|\overline{\mathbf{3}},-\frac{1}{3},\frac{1}{2},-\frac{1}{2}\right\rangle = \sqrt{\frac{1}{3}}\left|\mathbf{1},0,0,0\right\rangle - \sqrt{\frac{1}{6}}\left|\mathbf{8},0,0,0\right\rangle + \sqrt{\frac{1}{2}}\left|\mathbf{8},0,1,0\right\rangle \tag{E.17}
$$

$\Sigma_c^{++} \to B_{10}\gamma$

$$
\overline{\mathbf{6}}_{\frac{1}{3},\frac{1}{2},\frac{1}{2}}\left|\mathbf{6},\frac{2}{3},1,1\right\rangle = \left|\mathbf{27},1,\frac{3}{2},\frac{3}{2}\right\rangle \tag{E.18}
$$

$$
\begin{aligned}
\mathbf{15}_{\frac{1}{3},\frac{1}{2},\frac{1}{2}}\left|\mathbf{6},\frac{2}{3},1,1\right\rangle &= -\frac{1}{3}\left|\mathbf{10},1,\frac{3}{2},\frac{3}{2}\right\rangle - \sqrt{\frac{1}{3}}\left|\mathbf{27},1,\frac{3}{2},\frac{3}{2}\right\rangle + \frac{\sqrt{5}}{3}\left|\mathbf{35},1,\frac{3}{2},\frac{3}{2}\right\rangle \\
\mathbf{15}_{\frac{1}{3},\frac{3}{2},\frac{1}{2}}\left|\mathbf{6},\frac{2}{3},1,1\right\rangle &= -\frac{\sqrt{2}}{3}\left|\mathbf{10},1,\frac{3}{2},\frac{3}{2}\right\rangle + \sqrt{\frac{1}{6}}\left|\mathbf{27},1,\frac{3}{2},\frac{3}{2}\right\rangle \\
&\quad - \frac{1}{3\sqrt{10}}\left|\mathbf{35},1,\frac{3}{2},\frac{3}{2}\right\rangle + \sqrt{\frac{3}{5}}\left|\mathbf{35},1,\frac{5}{2},\frac{3}{2}\right\rangle
\end{aligned}
\tag{E.19}
$$

$$
\mathbf{3}_{\frac{1}{3},\frac{1}{2},\frac{1}{2}}\left|\mathbf{6},\frac{2}{3},1,1\right\rangle = \left|\mathbf{10},1,\frac{3}{2},\frac{3}{2}\right\rangle \tag{E.20}
$$

$\Sigma_c^+ \to B_{8/10}\gamma$

$$
\begin{aligned}
\overline{\mathbf{6}}_{-\frac{2}{3},1,1}\left|\mathbf{6},\frac{2}{3},1,0\right\rangle &= \sqrt{\frac{2}{5}}\left|\mathbf{8},0,1,1\right\rangle - \sqrt{\frac{1}{10}}\left|\mathbf{27},0,1,1\right\rangle + \sqrt{\frac{1}{2}}\left|\mathbf{27},0,2,1\right\rangle \\
\overline{\mathbf{6}}_{\frac{1}{3},\frac{1}{2},\frac{1}{2}}\left|\mathbf{6},\frac{2}{3},1,0\right\rangle &= \sqrt{\frac{1}{5}}\left|\mathbf{8},1,\frac{1}{2},\frac{1}{2}\right\rangle - \sqrt{\frac{2}{15}}\left|\mathbf{27},1,\frac{1}{2},\frac{1}{2}\right\rangle + \sqrt{\frac{2}{3}}\left|\mathbf{27},1,\frac{3}{2},\frac{1}{2}\right\rangle
\end{aligned}
\tag{E.21}
$$

$$
\begin{aligned}
\mathbf{15}_{-\frac{2}{3},1,1}\left|\mathbf{6},\frac{2}{3},1,0\right\rangle &= -\frac{2}{3\sqrt{5}}\left|\mathbf{8},0,1,1\right\rangle + \frac{\sqrt{2}}{3}\left|\mathbf{10},0,1,1\right\rangle + \frac{1}{3}\left|\overline{\mathbf{10}},0,1,1\right\rangle \\
&\quad - \sqrt{\frac{1}{10}}\left|\mathbf{27},0,1,1\right\rangle - \frac{1}{6}\left|\mathbf{35},0,1,1\right\rangle \\
&\quad - \frac{1}{2}\left|\mathbf{27},0,2,1\right\rangle + \frac{1}{2}\left|\mathbf{35},0,2,1\right\rangle \\
\mathbf{15}_{\frac{1}{3},\frac{1}{2},\frac{1}{2}}\left|\mathbf{6},\frac{2}{3},1,0\right\rangle &= \frac{1}{3\sqrt{15}}\left|\mathbf{8},1,\frac{1}{2},\frac{1}{2}\right\rangle + \frac{2}{3\sqrt{3}}\left|\overline{\mathbf{10}},1,\frac{1}{2},\frac{1}{2}\right\rangle - \frac{2\sqrt{2}}{3\sqrt{5}}\left|\mathbf{27},1,\frac{1}{2},\frac{1}{2}\right\rangle \\
&\quad - \frac{\sqrt{2}}{3\sqrt{3}}\left|\mathbf{10},1,\frac{3}{2},\frac{1}{2}\right\rangle - \frac{\sqrt{2}}{3}\left|\mathbf{27},1,\frac{3}{2},\frac{1}{2}\right\rangle + \frac{\sqrt{10}}{3\sqrt{3}}\left|\mathbf{35},1,\frac{3}{2},\frac{1}{2}\right\rangle \\
\mathbf{15}_{\frac{1}{3},\frac{3}{2},\frac{1}{2}}\left|\mathbf{6},\frac{2}{3},1,0\right\rangle &= \frac{4\sqrt{2}}{3\sqrt{15}}\left|\mathbf{8},1,\frac{1}{2},\frac{1}{2}\right\rangle - \frac{\sqrt{2}}{3\sqrt{3}}\left|\overline{\mathbf{10}},1,\frac{1}{2},\frac{1}{2}\right\rangle - \frac{1}{5\sqrt{3}}\left|\mathbf{27},1,\frac{1}{2},\frac{1}{2}\right\rangle \\
&\quad + \frac{1}{3\sqrt{3}}\left|\mathbf{10},1,\frac{3}{2},\frac{1}{2}\right\rangle - \frac{1}{6}\left|\mathbf{27},1,\frac{3}{2},\frac{1}{2}\right\rangle - \frac{1}{6\sqrt{15}}\left|\mathbf{35},1,\frac{3}{2},\frac{1}{3}\right\rangle \\
&\quad + \sqrt{\frac{3}{5}}\left|\mathbf{35},1,\frac{5}{2},\frac{1}{2}\right\rangle
\end{aligned}
\tag{E.22}
$$

$$
\mathbf{3}_{\frac{1}{3},\frac{1}{2},\frac{1}{2}}\left|\mathbf{6},\frac{2}{3},1,0\right\rangle = -\sqrt{\frac{1}{3}}\left|\mathbf{8},1,\frac{1}{2},\frac{1}{2}\right\rangle + \sqrt{\frac{2}{3}}\left|\mathbf{10},1,\frac{1}{2},\frac{1}{2}\right\rangle \tag{E.23}
$$

$\Sigma_c^0 \to B_{8/10}\gamma$

$$
\begin{aligned}
\overline{\mathbf{6}}_{-\frac{2}{3},1,1}\left|\mathbf{6},\frac{2}{3},1,-1\right\rangle &= \sqrt{\frac{1}{6}}\left|\mathbf{1},0,0,0\right\rangle - \sqrt{\frac{2}{15}}\left|\mathbf{8},0,0,0\right\rangle + \sqrt{\frac{1}{30}}\left|\mathbf{27},0,0,0\right\rangle \\
&\quad \sqrt{\frac{2}{5}}\left|\mathbf{8},0,1,0\right\rangle - \sqrt{\frac{1}{10}}\left|\mathbf{27},0,1,0\right\rangle + \sqrt{\frac{1}{6}}\left|\mathbf{27},0,2,0\right\rangle \\
\overline{\mathbf{6}}_{\frac{1}{3},\frac{1}{2},\frac{1}{2}}\left|\mathbf{6},\frac{2}{3},1,-1\right\rangle &= \sqrt{\frac{2}{5}}\left|\mathbf{8},1,\frac{1}{2},-\frac{1}{2}\right\rangle - \frac{2}{\sqrt{15}}\left|\mathbf{27},1,\frac{1}{2},-\frac{1}{2}\right\rangle + \sqrt{\frac{1}{3}}\left|\mathbf{27},1,\frac{3}{2},-\frac{1}{2}\right\rangle
\end{aligned}
\tag{E.24}
$$

$$
\begin{aligned}
\mathbf{15}_{-\frac{2}{3},1,1}\left|\mathbf{6},\frac{2}{3},1,-1\right\rangle &= -\sqrt{\frac{2}{15}}\,|\mathbf{8},0,0,0\rangle + \sqrt{\frac{1}{30}}\,|\mathbf{27},0,0,0\rangle - \frac{2}{3\sqrt{5}}\,|\mathbf{8},0,1,0\rangle \\
&\quad + \frac{\sqrt{2}}{3}\,|\mathbf{10},0,1,0\rangle + \sqrt{\frac{1}{3}}\,|\overline{\mathbf{10}},0,1,0\rangle - \sqrt{\frac{1}{20}}\,|\mathbf{27},0,1,0\rangle \\
&\quad - \frac{1}{6}\,|\mathbf{35},0,1,0\rangle - \sqrt{\frac{1}{6}}\,|\mathbf{27},0,2,0\rangle + \sqrt{\frac{1}{6}}\,|\mathbf{35},0,2,0\rangle \\
\mathbf{15}_{\frac{1}{3},\frac{1}{2},\frac{1}{2}}\left|\mathbf{6},\frac{2}{3},1,-1\right\rangle &= \frac{\sqrt{2}}{3\sqrt{15}}\left|\mathbf{8},1,\frac{1}{2},-\frac{1}{2}\right\rangle + \frac{2\sqrt{2}}{3\sqrt{3}}\left|\overline{\mathbf{10}},1,\frac{1}{2},-\frac{1}{2}\right\rangle - \frac{4}{3\sqrt{5}}\left|\mathbf{27},1,\frac{1}{2},-\frac{1}{2}\right\rangle \\
&\quad - \frac{1}{3\sqrt{3}}\left|\mathbf{10},1,\frac{3}{2},-\frac{1}{2}\right\rangle - \frac{1}{3}\left|\mathbf{27},1,\frac{3}{2},-\frac{1}{2}\right\rangle + \frac{\sqrt{5}}{3\sqrt{3}}\left|\mathbf{35},1,\frac{1}{2},-\frac{1}{2}\right\rangle \\
\mathbf{15}_{\frac{1}{3},\frac{3}{2},\frac{1}{2}}\left|\mathbf{6},\frac{2}{3},1,-1\right\rangle &= -\frac{4}{3\sqrt{15}}\left|\mathbf{8},1,\frac{1}{2},-\frac{1}{2}\right\rangle + \frac{1}{3\sqrt{3}}\left|\overline{\mathbf{10}},1,\frac{1}{2},-\frac{1}{2}\right\rangle - \frac{1}{3\sqrt{10}}\left|\mathbf{27},1,\frac{1}{2},-\frac{1}{2}\right\rangle \\
&\quad + \frac{2\sqrt{2}}{3\sqrt{3}}\left|\mathbf{10},1,\frac{3}{2},-\frac{1}{2}\right\rangle - \frac{2\sqrt{2}}{6}\left|\mathbf{27},1,\frac{3}{2},-\frac{1}{2}\right\rangle - \frac{1}{8\sqrt{3}}\left|\mathbf{35},1,\frac{3}{2},-\frac{1}{2}\right\rangle \\
&\quad + \sqrt{\frac{3}{10}}\left|\mathbf{35},1,\frac{5}{2},-\frac{1}{2}\right\rangle
\end{aligned}
\tag{E.25}
$$

$$
\mathbf{3}_{\frac{1}{3},\frac{1}{2},\frac{1}{2}}\left|\mathbf{6},\frac{2}{3},1,-1\right\rangle = -\sqrt{\frac{2}{3}}\left|\mathbf{8},1,\frac{1}{2},-\frac{1}{2}\right\rangle + \sqrt{\frac{1}{3}}\left|\mathbf{10},1,\frac{1}{2},-\frac{1}{2}\right\rangle \tag{E.26}
$$

$\Xi_c'^{+} \to B_{8/10}\gamma$

$$
\begin{aligned}
\overline{\mathbf{6}}_{\frac{1}{3},\frac{1}{2},\frac{1}{2}}\left|\mathbf{6},-\frac{1}{3},\frac{1}{2},\frac{1}{2}\right\rangle &= \sqrt{\frac{1}{5}}\,|\mathbf{8},0,1,1\rangle + \frac{2}{\sqrt{5}}\,|\mathbf{27},0,1,1\rangle \\
\overline{\mathbf{6}}_{\frac{4}{3},0,0}\left|\mathbf{6},-\frac{1}{3},\frac{1}{2},\frac{1}{2}\right\rangle &= \sqrt{\frac{2}{5}}\left|\mathbf{8},1,\frac{1}{2},\frac{1}{2}\right\rangle + \sqrt{\frac{3}{5}}\left|\mathbf{27},1,\frac{1}{2},\frac{1}{2}\right\rangle
\end{aligned}
\tag{E.27}
$$

$$
\begin{aligned}
\mathbf{15}_{\frac{1}{3},\frac{1}{2},\frac{1}{2}}\left|\mathbf{6},-\frac{1}{3},\frac{1}{2},\frac{1}{2}\right\rangle &= -\frac{\sqrt{5}}{3\sqrt{3}}\,|\mathbf{8},0,1,1\rangle + \frac{\sqrt{2}}{3\sqrt{3}}\,|\mathbf{10},0,1,1\rangle \\
&\quad - \frac{2}{3\sqrt{3}}\,|\overline{\mathbf{10}},0,1,1\rangle + \frac{4}{3\sqrt{3}}\,|\mathbf{35},0,1,1\rangle \\
\mathbf{15}_{\frac{1}{3},\frac{3}{2},\frac{1}{2}}\left|\mathbf{6},-\frac{1}{3},\frac{1}{2},\frac{1}{2}\right\rangle &= -\frac{2\sqrt{2}}{3\sqrt{15}}\,|\mathbf{8},0,1,1\rangle - \frac{1}{3\sqrt{3}}\,|\mathbf{10},0,1,1\rangle + \frac{\sqrt{2}}{3\sqrt{3}}\,|\overline{\mathbf{10}},0,1,1\rangle \\
&\quad + \frac{\sqrt{3}}{2\sqrt{10}}\,|\mathbf{27},0,1,1\rangle + \frac{1}{6\sqrt{3}}\,|\mathbf{35},0,1,1\rangle \\
&\quad + \frac{\sqrt{3}}{2\sqrt{2}}\,|\mathbf{27},0,2,1\rangle + \frac{\sqrt{3}}{2\sqrt{2}}\,|\mathbf{35},0,2,1\rangle
\end{aligned}
\tag{E.28}
$$

$$
\begin{aligned}
\mathbf{15}_{\frac{4}{3},1,0}\left|\mathbf{6},-\frac{1}{3},\frac{1}{2},\frac{1}{2}\right\rangle &= \frac{2}{3\sqrt{5}}\left|\mathbf{8},1,\frac{1}{2},\frac{1}{2}\right\rangle + \frac{1}{3}\left|\overline{\mathbf{10}},1,\frac{1}{2},\frac{1}{2}\right\rangle + \sqrt{\frac{2}{15}}\left|\mathbf{27},1,\frac{1}{2},\frac{1}{2}\right\rangle \\
&\quad + \frac{\sqrt{2}}{3}\left|\mathbf{10},1,\frac{3}{2},\frac{1}{2}\right\rangle + \sqrt{\frac{1}{6}}\left|\mathbf{27},1,\frac{3}{2},\frac{1}{2}\right\rangle + \frac{\sqrt{5}}{3\sqrt{2}}\left|\mathbf{35},1,\frac{3}{2},\frac{1}{2}\right\rangle
\end{aligned}
\tag{E.29}
$$

$$\mathbf{3}_{\frac{1}{3},\frac{1}{2},\frac{1}{2}}\left|\mathbf{6},-\frac{1}{3},\frac{1}{2},\frac{1}{2}\right\rangle = \sqrt{\frac{1}{3}}\left|\mathbf{8},0,1,1\right\rangle + \sqrt{\frac{2}{3}}\left|\mathbf{10},0,1,1\right\rangle \tag{E.30}$$

$\Xi_c'^0 \to B_{8/10}\gamma$

$$\begin{aligned}
\overline{\mathbf{6}}_{-\frac{2}{3},1,1}\left|\mathbf{6},-\frac{1}{3},\frac{1}{2},-\frac{1}{2}\right\rangle &= \sqrt{\frac{2}{5}}\left|\mathbf{8},-1,\frac{1}{2},\frac{1}{2}\right\rangle - \frac{2}{\sqrt{15}}\left|\mathbf{27},-1,\frac{1}{2},\frac{1}{2}\right\rangle + \sqrt{\frac{1}{3}}\left|\mathbf{27},-1,\frac{3}{2},\frac{1}{2}\right\rangle \\
\overline{\mathbf{6}}_{\frac{1}{3},\frac{1}{2},\frac{1}{2}}\left|\mathbf{6},-\frac{1}{3},\frac{1}{2},-\frac{1}{2}\right\rangle &= \sqrt{\frac{1}{6}}\left|\mathbf{1},0,0,0\right\rangle + \sqrt{\frac{1}{30}}\left|\mathbf{8},0,0,0\right\rangle - \sqrt{\frac{2}{5}}\left|\mathbf{27},0,0,0\right\rangle \\
&\quad + \sqrt{\frac{1}{10}}\left|\mathbf{8},0,1,0\right\rangle + \sqrt{\frac{2}{5}}\left|\mathbf{27},0,1,0\right\rangle \\
\overline{\mathbf{6}}_{\frac{4}{3},0,0}\left|\mathbf{6},-\frac{1}{3},\frac{1}{2},-\frac{1}{2}\right\rangle &= \sqrt{\frac{2}{5}}\left|\mathbf{8},1,\frac{1}{2},-\frac{1}{2}\right\rangle + \sqrt{\frac{3}{5}}\left|\mathbf{27},1,\frac{1}{2},-\frac{1}{2}\right\rangle
\end{aligned} \tag{E.31}$$

$$\begin{aligned}
\mathbf{15}_{-\frac{2}{3},1,1}\left|\mathbf{6},-\frac{1}{3},\frac{1}{2},-\frac{1}{2}\right\rangle &= \frac{2}{3\sqrt{5}}\left|\mathbf{8},-1,\frac{1}{2},-\frac{1}{2}\right\rangle + \frac{\sqrt{2}}{3}\left|\mathbf{10},-1,\frac{1}{2},-\frac{1}{2}\right\rangle \\
&\quad - \sqrt{\frac{3}{10}}\left|\mathbf{27},-1,\frac{1}{2},-\frac{1}{2}\right\rangle - \frac{1}{3\sqrt{2}}\left|\mathbf{35},-1,\frac{1}{2},-\frac{1}{2}\right\rangle \\
&\quad - \frac{1}{3}\left|\overline{\mathbf{10}},-1,\frac{3}{2},-\frac{1}{2}\right\rangle + \frac{\sqrt{2}}{3}\left|\mathbf{35},-1,\frac{3}{2},-\frac{1}{2}\right\rangle \\
\mathbf{15}_{\frac{1}{3},\frac{1}{2},\frac{1}{2}}\left|\mathbf{6},-\frac{1}{3},\frac{1}{2},-\frac{1}{2}\right\rangle &= -\sqrt{\frac{1}{10}}\left|\mathbf{8},0,0,0\right\rangle - \sqrt{\frac{2}{5}}\left|\mathbf{27},0,0,0\right\rangle - \frac{\sqrt{5}}{3\sqrt{6}}\left|\mathbf{8},0,1,0\right\rangle \\
&\quad \frac{1}{3\sqrt{3}}\left|\mathbf{10},0,1,0\right\rangle - \frac{\sqrt{2}}{3\sqrt{3}}\left|\overline{\mathbf{10}},0,1,0\right\rangle + \frac{\sqrt{5}}{3\sqrt{3}}\left|\mathbf{35},0,1,0\right\rangle \\
\mathbf{15}_{\frac{1}{3},\frac{3}{2},\frac{1}{2}}\left|\mathbf{6},-\frac{1}{3},\frac{1}{2},-\frac{1}{2}\right\rangle &= \frac{4}{3\sqrt{15}}\left|\mathbf{8},0,1,0\right\rangle + \frac{\sqrt{2}}{3\sqrt{3}}\left|\mathbf{10},0,1,0\right\rangle - \frac{2}{3\sqrt{3}}\left|\overline{\mathbf{10}},0,1,0\right\rangle \\
&\quad - \sqrt{\frac{3}{20}}\left|\mathbf{27},0,1,0\right\rangle - \frac{1}{6\sqrt{3}}\left|\mathbf{35},0,1,0\right\rangle \\
&\quad + \frac{1}{2}\left|\mathbf{27},0,1,0\right\rangle + \frac{1}{2}\left|\mathbf{35},0,1,0\right\rangle \\
\mathbf{15}_{\frac{4}{3},1,0}\left|\mathbf{6},-\frac{1}{3},\frac{1}{2},-\frac{1}{2}\right\rangle &= -\frac{2}{3\sqrt{5}}\left|\mathbf{8},1,\frac{1}{2},-\frac{1}{2}\right\rangle - \frac{1}{3}\left|\overline{\mathbf{10}},1,\frac{1}{2},-\frac{1}{2}\right\rangle - \sqrt{\frac{2}{15}}\left|\mathbf{27},1,\frac{1}{2},-\frac{1}{2}\right\rangle \\
&\quad + \frac{\sqrt{2}}{3}\left|\mathbf{10},1,\frac{3}{2},-\frac{1}{2}\right\rangle + \sqrt{\frac{1}{6}}\left|\mathbf{27},1,\frac{3}{2},-\frac{1}{2}\right\rangle + \frac{\sqrt{5}}{3\sqrt{2}}\left|\mathbf{35},1,\frac{3}{2},-\frac{1}{2}\right\rangle
\end{aligned} \tag{E.32}$$

$$\mathbf{3}_{\frac{1}{3},\frac{1}{2},\frac{1}{2}}\left|\mathbf{6},-\frac{1}{3},\frac{1}{2},-\frac{1}{2}\right\rangle = -\sqrt{\frac{1}{2}}\left|\mathbf{8},0,0,0\right\rangle + \sqrt{\frac{1}{6}}\left|\mathbf{8},0,1,0\right\rangle + \sqrt{\frac{1}{3}}\left|\mathbf{10},0,1,0\right\rangle \tag{E.33}$$

$\Omega_c \to B_{8/10}\gamma$

$$\begin{aligned}
\overline{\mathbf{6}}_{\frac{1}{3},\frac{1}{2},\frac{1}{2}}\left|\mathbf{6},-\frac{4}{3},0,0\right\rangle &= \sqrt{\frac{2}{5}}\left|\mathbf{8},-1,\frac{1}{2},\frac{1}{2}\right\rangle + \sqrt{\frac{3}{5}}\left|\mathbf{27},-1,\frac{1}{2},\frac{1}{2}\right\rangle \\
\overline{\mathbf{6}}_{\frac{4}{3},0,0}\left|\mathbf{6},-\frac{4}{3},0,0\right\rangle &= \sqrt{\frac{1}{6}}\left|\mathbf{1},0,0,0\right\rangle + \frac{2\sqrt{2}}{\sqrt{15}}\left|\mathbf{8},0,0,0\right\rangle + \sqrt{\frac{3}{10}}\left|\mathbf{27},0,0,0\right\rangle
\end{aligned} \tag{E.34}$$

$$\begin{aligned}
\mathbf{15}_{\frac{1}{3},\frac{1}{2},\frac{1}{2}}\left|\mathbf{6},-\frac{4}{3},0,0\right\rangle &= \sqrt{\frac{2}{15}}\left|\mathbf{8},-1,\frac{1}{2},\frac{1}{2}\right\rangle + \sqrt{\frac{1}{3}}\left|\mathbf{10},-1,\frac{1}{2},\frac{1}{2}\right\rangle \\
&\quad + \sqrt{\frac{1}{5}}\left|\mathbf{27},-1,\frac{1}{2},\frac{1}{2}\right\rangle + \sqrt{\frac{1}{3}}\left|\mathbf{35},-1,\frac{1}{2},\frac{1}{2}\right\rangle \\
\mathbf{15}_{\frac{1}{3},\frac{3}{2},\frac{1}{2}}\left|\mathbf{6},-\frac{4}{3},0,0\right\rangle &= \sqrt{\frac{1}{3}}\left|\overline{\mathbf{10}},-1,\frac{3}{2},\frac{1}{2}\right\rangle + \sqrt{\frac{1}{2}}\left|\mathbf{27},-1,\frac{1}{2},\frac{1}{2}\right\rangle + \sqrt{\frac{1}{6}}\left|\mathbf{35},-1,\frac{3}{2},\frac{1}{2}\right\rangle \\
\mathbf{15}_{\frac{4}{3},1,0}\left|\mathbf{6},-\frac{4}{3},0,0\right\rangle &= \frac{4}{3\sqrt{5}}\left|\mathbf{8},0,1,0\right\rangle + \frac{\sqrt{2}}{3}\left|\mathbf{10},0,1,0\right\rangle + \frac{1}{3}\left|\overline{\mathbf{10}},0,1,0\right\rangle \\
&\quad + \sqrt{\frac{1}{5}}\left|\mathbf{27},0,1,0\right\rangle + \frac{1}{3}\left|\mathbf{35},0,1,0\right\rangle
\end{aligned} \tag{E.35}$$

$$\mathbf{3}_{\frac{1}{3},\frac{1}{2},\frac{1}{2}}\left|\mathbf{6},-\frac{4}{3},0,0\right\rangle = \sqrt{\frac{2}{3}}\left|\mathbf{8},-1,\frac{1}{2},\frac{1}{2}\right\rangle + \sqrt{\frac{1}{3}}\left|\mathbf{10},-1,\frac{1}{2},\frac{1}{2}\right\rangle \tag{E.36}$$

Decay	A_3	$A_{\overline{6}}$	A_{15}
$\Lambda_c \to \Sigma^+\gamma$	-	$\sqrt{\frac{2}{3}}V_{cs}^*V_{ud}$	$-\frac{2}{\sqrt{15}}V_{cs}^*V_{ud}$
$\Xi_c^0 \to \Xi^0\gamma$	-	$\sqrt{\frac{2}{3}}V_{cs}^*V_{ud}$	$\frac{2}{\sqrt{15}}V_{cs}^*V_{ud}$
$\Lambda_c \to p\gamma$	Δ	$\sqrt{\frac{2}{3}}\Sigma$	$-\frac{2}{\sqrt{15}}\Sigma - \frac{1}{\sqrt{15}}\Delta$
$\Xi_c^+ \to \Sigma^+\gamma$	Δ	$-\sqrt{\frac{2}{3}}\Sigma$	$\frac{2}{\sqrt{15}}\Sigma - \frac{1}{\sqrt{15}}\Delta$
$\Xi_c^0 \to \Lambda\gamma$	$\sqrt{\frac{1}{6}}\Delta$	Σ	$\sqrt{\frac{2}{5}}\Sigma + \frac{1}{\sqrt{10}}\Delta$
$\Xi_c^0 \to \Sigma^0\gamma$	$\sqrt{\frac{1}{2}}\Delta$	$-\sqrt{\frac{1}{3}}\Sigma$	$-\sqrt{\frac{2}{15}}\Sigma + \sqrt{\frac{3}{10}}\Delta$
$\Xi_c^+ \to p\gamma$	-	$\sqrt{\frac{2}{3}}V_{cd}^*V_{us}$	$-\frac{2}{\sqrt{15}}V_{cd}^*V_{us}$
$\Xi_c^0 \to n\gamma$	-	$\sqrt{\frac{2}{3}}V_{cd}^*V_{us}$	$\frac{2}{\sqrt{15}}V_{cd}^*V_{us}$

Table E.7: $SU(3)_F$ decomposition of the SM decay amplitudes for the charmed anti-triplet baryons.

Decay	A'_3	$A'_{\overline{6}}$	A'_{15}
$\Sigma_c^+ \to \Sigma^+\gamma$	-	$\sqrt{\frac{2}{5}}V_{cs}^*V_{ud}$	$-\frac{2}{3\sqrt{5}}V_{cs}^*V_{ud}$
$\Sigma_c^0 \to \Lambda\gamma$	-	$-\sqrt{\frac{2}{15}}V_{cs}^*V_{ud}$	$-\sqrt{\frac{2}{15}}V_{cs}^*V_{ud}$
$\Sigma_c^0 \to \Sigma^0\gamma$	-	$\sqrt{\frac{2}{5}}V_{cs}^*V_{ud}$	$-\frac{2}{3\sqrt{5}}V_{cs}^*V_{ud}$
$\Xi_c'^0 \to \Xi^0\gamma$	-	$\sqrt{\frac{2}{5}}V_{cs}^*V_{ud}$	$\frac{2}{3\sqrt{5}}V_{cs}^*V_{ud}$
$\Sigma_c^+ \to p\gamma$	$-\sqrt{\frac{1}{3}}\Delta$	$\sqrt{\frac{2}{5}}\Sigma$	$-\frac{2}{3\sqrt{5}}\Sigma + \frac{1}{\sqrt{5}}\Delta$
$\Sigma_c^0 \to n\gamma$	$-\sqrt{\frac{2}{3}}\Delta$	$\sqrt{\frac{4}{5}}\Sigma$	$\frac{2\sqrt{2}}{3\sqrt{5}}\Sigma - \frac{\sqrt{2}}{3\sqrt{5}}\Delta$
$\Xi_c'^+ \to \Sigma^+\gamma$	$\sqrt{\frac{1}{3}}\Delta$	$\sqrt{\frac{2}{5}}\Sigma$	$-\frac{2}{3\sqrt{5}}\Sigma - \frac{1}{\sqrt{5}}\Delta$
$\Xi_c'^0 \to \Lambda\gamma$	$-\sqrt{\frac{1}{2}}\Delta$	$\sqrt{\frac{1}{15}}\Sigma$	$-\sqrt{\frac{2}{15}}\Sigma - \frac{1}{\sqrt{30}}\Delta$
$\Xi_c'^0 \to \Sigma^0\gamma$	$\sqrt{\frac{1}{6}}\Delta$	$\sqrt{\frac{1}{5}}\Sigma$	$-\sqrt{\frac{2}{5}}\Sigma + \frac{1}{3\sqrt{10}}\Delta$
$\Omega_c \to \Xi^0\gamma$	$\sqrt{\frac{2}{3}}\Delta$	$\sqrt{\frac{4}{5}}\Sigma$	$\frac{2\sqrt{2}}{3\sqrt{5}}\Sigma + \frac{\sqrt{2}}{3\sqrt{5}}\Delta$
$\Xi_c'^+ \to p\gamma$	-	$-\sqrt{\frac{2}{5}}V_{cd}^*V_{us}$	$\frac{2}{3\sqrt{5}}V_{cd}^*V_{us}$
$\Xi_c'^0 \to n\gamma$	-	$-\sqrt{\frac{2}{5}}V_{cd}^*V_{us}$	$-\frac{2}{3\sqrt{5}}V_{cd}^*V_{us}$
$\Omega_c \to \Lambda\gamma$	-	$-\frac{2\sqrt{2}}{\sqrt{15}}V_{cd}^*V_{us}$	0
$\Omega_c \to \Sigma^0\gamma$	-	0	$\frac{4}{3\sqrt{5}}V_{cd}^*V_{us}$

Table E.8: $SU(3)_F$ decomposition of the SM decay amplitudes for the charmed sextet baryons.

E.2.3 Flavor relations for $B_{c6} \to B_{10}\gamma$

We provide the flavor relations for $B_{c6} \to B_{10}\gamma$ decays in Table E.9, as well as the U-spin, isospin and $SU(3)_F$ decompositions in Table E.11, E.10 and E.12, respectively.

Decay	U-Spin	$SU(3)_F$	$SU(3)_F$ IRA
$\Sigma_c^+ \to \Sigma^{*+}\gamma$	$V_{cs}^* V_{ud} H_\Sigma$	$V_{cs}^* V_{ud} I$	$V_{cs}^* V_{ud} J$
$\Sigma_c^0 \to \Sigma^{*0}\gamma$	$V_{cs}^* V_{ud} H'_\Sigma$	$V_{cs}^* V_{ud} I$	$V_{cs}^* V_{ud} J$
$\Xi_c'^0 \to \Xi^{*0}\gamma$	$V_{cs}^* V_{ud} H'_\Sigma$	$V_{cs}^* V_{ud} I$	$V_{cs}^* V_{ud} J$
$\Sigma_c^{++} \to \Delta^{++}\gamma$	$\Delta H''_\Delta + H''_7$	$-\sqrt{\frac{3}{2}}\Delta I + \sqrt{3} I_7$	$-\sqrt{\frac{3}{2}}\Delta J + \sqrt{3} J_7$
$\Sigma_c^+ \to \Delta^+\gamma$	$-\Sigma H_\Sigma + \Delta H_\Delta + H_7$	$-\Sigma I + \sqrt{2} I_7$	$-\Sigma J + \sqrt{2} J_7$
$\Sigma_c^0 \to \Delta^0\gamma$	$-\sqrt{2}\Sigma H'_\Sigma + \Delta H'_\Delta + H'_7$	$-\sqrt{2}\Sigma I + \frac{1}{\sqrt{2}}\Delta I + J_7$	$-\sqrt{2}\Sigma J + \frac{1}{\sqrt{2}}\Delta J + J_7$
$\Xi_c'^+ \to \Sigma^{*+}\gamma$	$\Sigma H_\Sigma + \Delta H_\Delta + H_7$	$\Sigma I + \sqrt{2} I_7$	$\Sigma J + \sqrt{2} J_7$
$\Xi_c'^0 \to \Sigma^{*0}\gamma$	$\Delta H'_\Delta + H'_7$	$\frac{1}{\sqrt{2}}\Delta I + I_7$	$\frac{1}{\sqrt{2}}\Delta J + J_7$
$\Omega_c \to \Xi^{*0}\gamma$	$\sqrt{2}\Sigma H'_\Sigma + \Delta H'_\Delta + H'_7$	$\sqrt{2}\Sigma I + \frac{1}{\sqrt{2}}\Delta I + J_7$	$\sqrt{2}\Sigma J + \frac{1}{\sqrt{2}}\Delta J + J_7$
$\Xi_c'^+ \to \Delta^+\gamma$	$V_{cd}^* V_{us} H_\Sigma$	$V_{cd}^* V_{us} I$	$-V_{cd}^* V_{us} J$
$\Xi_c'^0 \to \Delta^0\gamma$	$V_{cd}^* V_{us} H'_\Sigma$	$V_{cd}^* V_{us} I$	$-V_{cd}^* V_{us} J$
$\Omega_c \to \Sigma^{*0}\gamma$	$V_{cd}^* V_{us} H'_\Sigma$	$V_{cd}^* V_{us} I$	$-V_{cd}^* V_{us} J$

Table E.9: Flavor symmetry relations of the decay amplitudes for the charmed sextet baryons into decuplet baryons. Analogously to Table 6.1, $H_\Sigma^{(\prime)}$, $H_\Delta^{(\prime,\prime\prime)}$ and $H_7^{(\prime,\prime\prime)}$ denote the U-spin triplet, U-spin singlet and the $c \to u\gamma$ contributions, respectively. Note that $\frac{1}{\sqrt{3}}H''_7 = \frac{1}{\sqrt{2}}H'_7 = H_7$ in the isospin limit. Furthermore, $I = \frac{\sqrt{2}}{3}A''_{15}$ and $I_7 = \sqrt{\frac{1}{3}}(I_{\text{NP}} + \Delta A''_3)$. $J = \sqrt{\frac{2}{3}}\tilde{b}''_1$ and $J_7 = \frac{1}{\sqrt{3}}b''_1$ denote the weak annihilation and $c \to u\gamma$ contributions in the $SU(3)_F$ IRA.

Decay	$\langle\frac{3}{2}\vert\frac{1}{2}\vert 1\rangle_I$	$\langle 1\vert\frac{1}{2}\vert\frac{1}{2}\rangle_I$	$\langle\frac{1}{2}\vert 0\vert\frac{1}{2}\rangle_U$	$\langle 1\vert 0\vert 1\rangle_U$	$\langle 0\vert 0\vert 0\rangle_U$
$\Sigma_c^{++}\to\Delta^{++}\gamma$	1	0	0	0	1
$\Sigma_c^{+}\to\Delta^{+}\gamma$	$\sqrt{\frac{2}{3}}$	0	1	0	0
$\Sigma_c^{0}\to\Delta^{0}\gamma$	$\sqrt{\frac{1}{3}}$	0	0	1	0
$\Xi_c^{\prime+}\to\Sigma^{*+}\gamma$	0	1	1	0	0
$\Xi_c^{\prime0}\to\Sigma^{*0}\gamma$	0	$\sqrt{\frac{1}{3}}$	0	1	0
$\Omega_c\to\Xi^{*0}\gamma$	0	0	0	1	0

Table E.10: Iso- and U-spin decomposition of the BSM contribution for decays of charm sextet baryons into decuplet baryons. The matrix elements are related to the amplitudes in Table E.9 as follows: $H_7\sim\langle\frac{1}{2}\vert 0\vert\frac{1}{2}\rangle_U$, $H_7'\sim\langle 1\vert 0\vert 1\rangle_U$ and $H_7''\sim\langle 0\vert 0\vert 0\rangle_U$

Decay	$\langle\frac{1}{2}\vert 1\vert\frac{1}{2}\rangle$	$\langle 1\vert 1\vert 1\rangle$	$\langle\frac{1}{2}\vert 0\vert\frac{1}{2}\rangle$	$\langle 1\vert 0\vert 1\rangle$	$\langle 0\vert 0\vert 0\rangle$
$\Sigma_c^{+}\to\Sigma^{*+}\gamma$	$\sqrt{\frac{2}{3}}V_{cs}^*V_{ud}$	0	-	-	-
$\Sigma_c^{0}\to\Sigma^{*0}\gamma$	0	$\frac{1}{\sqrt{2}}V_{cs}^*V_{ud}$	-	-	-
$\Xi_c^{\prime0}\to\Xi^{*0}\gamma$	0	$\frac{1}{\sqrt{2}}V_{cs}^*V_{ud}$	-	-	-
$\Sigma_c^{++}\to\Delta^{++}\gamma$	0	0	0	0	$\sqrt{2}\Delta$
$\Sigma_c^{+}\to\Delta^{+}\gamma$	$-\sqrt{\frac{2}{3}}\Sigma$	0	$\sqrt{2}\Delta$	0	0
$\Sigma_c^{0}\to\Delta^{0}\gamma$	0	$-\Sigma$	0	$\sqrt{2}\Delta$	0
$\Xi_c^{\prime+}\to\Sigma^{*+}\gamma$	$\sqrt{\frac{2}{3}}\Sigma$	0	$\sqrt{2}\Delta$	0	0
$\Xi_c^{\prime0}\to\Sigma^{*0}\gamma$	0	0	0	$\sqrt{2}\Delta$	0
$\Omega_c\to\Xi^{*0}\gamma$	0	Σ	0	$\sqrt{2}\Delta$	0
$\Xi_c^{\prime+}\to\Delta^{+}\gamma$	$\sqrt{\frac{2}{3}}V_{cd}^*V_{us}$	0	-	-	-
$\Xi_c^{\prime0}\to\Delta^{0}\gamma$	0	$\frac{1}{\sqrt{2}}V_{cd}^*V_{us}$	-	-	-
$\Omega_c\to\Sigma^{*0}\gamma$	0	$\frac{1}{\sqrt{2}}V_{cd}^*V_{us}$	-	-	-

Table E.11: U-Spin decomposition of the SM decay amplitudes for the decays of charmed sextet baryons into decuplet baryons. In the matrix element $\langle U(f)\vert U(O)\vert U(i)\rangle$, $U(f)$, $U(O)$ and $U(i)$ denote the U-spin of the final state, the U-spin changing operators and the initial state, respectively. The matrix elements are related to the amplitudes in Table E.9 as follows: $H_\Sigma\sim\sqrt{\frac{2}{3}}\langle\frac{1}{2}\vert 1\vert\frac{1}{2}\rangle$, $H_\Sigma'\sim\frac{1}{\sqrt{2}}\langle 1\vert 1\vert 1\rangle$, $H_\Delta\sim\sqrt{2}\langle\frac{1}{2}\vert 0\vert\frac{1}{2}\rangle$, $H_\Delta'\sim\sqrt{2}\langle 1\vert 0\vert 1\rangle$ and $H_\Delta''\sim\sqrt{2}\langle 0\vert 0\vert 0\rangle$.

Decay	A_3''	$A_{\overline{6}}''$	A_{15}''
$\Sigma_c^+ \to \Sigma^{*+}\gamma$	-	0	$\frac{\sqrt{2}}{3}V_{cs}^*V_{ud}$
$\Sigma_c^0 \to \Sigma^{*0}\gamma$	-	0	$\frac{\sqrt{2}}{3}V_{cs}^*V_{ud}$
$\Xi_c'^0 \to \Xi^{*0}\gamma$	-	0	$\frac{\sqrt{2}}{3}V_{cs}^*V_{ud}$
$\Sigma_c^{++} \to \Delta^{++}\gamma$	Δ	0	$-\sqrt{\frac{1}{3}}\Delta$
$\Sigma_c^+ \to \Delta^+\gamma$	$\sqrt{\frac{2}{3}}\Delta$	0	$-\frac{\sqrt{2}}{3}\Sigma$
$\Sigma_c^0 \to \Delta^0\gamma$	$\sqrt{\frac{1}{3}}\Delta$	0	$-\frac{2}{3}\Sigma + \frac{1}{3}\Delta$
$\Xi_c'^+ \to \Sigma^{*+}\gamma$	$\sqrt{\frac{2}{3}}\Delta$	0	$\frac{\sqrt{2}}{3}\Sigma$
$\Xi_c'^0 \to \Sigma^{*0}\gamma$	$\sqrt{\frac{1}{3}}\Delta$	0	$\frac{1}{3}\Delta$
$\Omega_c \to \Xi^{*0}\gamma$	$\sqrt{\frac{1}{3}}\Delta$	0	$\frac{2}{3}\Sigma + \frac{1}{3}\Delta$
$\Xi_c'^+ \to \Delta^+\gamma$	-	0	$\frac{\sqrt{2}}{3}V_{cs}^*V_{ud}$
$\Xi_c'^0 \to \Delta^0\gamma$	-	0	$\frac{\sqrt{2}}{3}V_{cs}^*V_{ud}$
$\Omega_c \to \Sigma^{*0}\gamma$	-	0	$\frac{\sqrt{2}}{3}V_{cs}^*V_{ud}$

Table E.12: $SU(3)_F$ decomposition of the SM decay amplitudes for the decays of charmed sextet baryons into decuplet baryons.

Acronyms

χPT chiral perturbation theory. 12, 15, 155

ADM anomalous dimension matrix. 21

BSM beyond the standard model. 1, 2, 10, 19, 23, 24, 26, 31, 34, 39–41, 45, 48, 51, 52, 55–57, 60, 61, 63, 66, 68, 74–78, 84, 91–94, 97, 98

CF Cabibbo favored. viii, 10, 22, 25, 35, 37, 39, 44, 46, 51, 60, 76, 78–80, 82, 84, 86, 87, 90–95, 113

CKM Cabibbo-Kobayashi-Maskawa. 9, 78, 82–84, 86, 88

CP charge parity. viii, 1, 25, 26, 39, 51–61, 63, 65, 74, 75, 78, 82, 84, 88, 90, 93, 94, 97, 98

DCS Doubly Cabibbo suppressed. viii, 10, 22, 25, 28, 35, 37, 44, 46, 51, 60, 63, 76, 78–80, 82, 86, 91, 93–95, 113, 139

EDM electric dipole moment. 5

EFT effective field theories. 15, 19, 21

FB forward-backward. 45, 48, 51, 60

FCNC flavor changing neutral current. 2, 11, 51, 63, 67, 74, 98

GIM Glashow-Iliopolus-Maiani. 11, 21, 22

GR general relativity. 1

HHχPT heavy hadron chiral perturbation theory. iii, 17, 25, 27, 28, 30, 31, 34–41, 44–48, 51, 52, 58–60, 97, 105, 110, 113, 146

HQET heavy quark effective theory. 12, 16

IRA irreducible representation approach. 79, 82

LHC Large Hadron Collider. 1

LLO leading logarithm order. 21

NLLO next to leading logarithm order. 21

NLO next-to leading order. 22

NNLLO next-to-next-to leading logarithmic order. 22, 23

NNLO next-to-next-to leading order. 22

NP new physics. 1, 2, 26, 28, 32, 39, 45, 51, 60, 68, 75, 77–79, 84, 88, 89, 91–94, 97, 98

QCD quantum chromodynamik. vii, 3–6, 10, 12–17, 20–23, 27, 77, 83, 97, 99, 105, 153

QCDF QCD factorization. 25, 27, 32–34, 37–39, 42–45, 48, 51, 53, 54, 60, 63, 66, 68, 74, 105

QED quantum electrodynamik. 10, 20, 22

QPCM quark pair creation model. 70–73, 151

RGE renormalization group equation. 21

SCS Singly Cabibbo suppressed. viii, 10, 22, 25, 36, 38, 44, 47, 51, 60, 63, 76, 78–80, 82–84, 86, 91–95, 113, 120

SM standard model of particle physics. iv, 1–5, 9–12, 19, 22, 23, 26, 31, 34, 39, 42, 43, 45–55, 60, 63, 65–68, 74–79, 82–84, 86–89, 91–95, 97–99

SSB spontaneous symmetry breaking. 7, 9

VEV vacuum expectation value. 7

VMD vector meson dominance. 29

WA weak annihilation. 26, 27, 31–33, 39, 45, 51, 76, 91

WET weak effective theory. 2

Bibliography

[1] Nico Adolph, Gudrun Hiller, and Andrey Tayduganov. "Testing the standard model with $D_{(s)} \to K_1(\to K\pi\pi)\gamma$ decays." In: *Phys. Rev. D* 99.7 (2019), p. 075023. DOI: 10.1103/PhysRevD.99.075023. arXiv: 1812.04679 [hep-ph].

[2] Nico Adolph, Joachim Brod, and Gudrun Hiller. "Radiative three-body D-meson decays in and beyond the standard model." In: *Eur. Phys. J. C* 81.1 (2021), p. 45. DOI: 10.1140/epjc/s10052-021-08832-3. arXiv: 2009.14212 [hep-ph].

[3] Nico Adolph and Gudrun Hiller. "Probing QCD dynamics and the standard model with $D^+_{(s)} \to P_1^+ P_2^0 \gamma$ decays." In: *JHEP* 06 (2021), p. 155. DOI: 10.1007/JHEP06(2021)155. arXiv: 2104.08287 [hep-ph].

[4] Nico Adolph and Gudrun Hiller. "Rare radiative decays of charm baryons." In: *Phys. Rev. D* 105.11 (2022), p. 116001. DOI: 10.1103/PhysRevD.105.116001. arXiv: 2203.14982 [hep-ph].

[5] B. P. Abbott et al. "Observation of Gravitational Waves from a Binary Black Hole Merger." In: *Phys. Rev. Lett.* 116 (6 Feb. 2016), p. 061102. DOI: 10.1103/PhysRevLett.116.061102. URL: https://link.aps.org/doi/10.1103/PhysRevLett.116.061102.

[6] F. Englert and R. Brout. "Broken Symmetry and the Mass of Gauge Vector Mesons." In: *Phys. Rev. Lett.* 13 (9 Aug. 1964), pp. 321–323. DOI: 10.1103/PhysRevLett.13.321. URL: https://link.aps.org/doi/10.1103/PhysRevLett.13.321.

[7] Peter W. Higgs. "Broken Symmetries and the Masses of Gauge Bosons." In: *Phys. Rev. Lett.* 13 (16 Oct. 1964), pp. 508–509. DOI: 10.1103/PhysRevLett.13.508. URL: https://link.aps.org/doi/10.1103/PhysRevLett.13.508.

[8] P.W. Higgs. "Broken symmetries, massless particles and gauge fields." In: *Physics Letters* 12.2 (1964), pp. 132–133. ISSN: 0031-9163. DOI: https://doi.org/10.1016/0031-9163(64)91136-9. URL: https://www.sciencedirect.com/science/article/pii/0031916364911369.

[9] Georges Aad et al. "Observation of a new particle in the search for the Standard Model Higgs boson with the ATLAS detector at the LHC." In: *Phys. Lett. B* 716 (2012), pp. 1–29. DOI: 10.1016/j.physletb.2012.08.020. arXiv: 1207.7214 [hep-ex].

[10] Serguei Chatrchyan et al. "Observation of a New Boson at a Mass of 125 GeV with the CMS Experiment at the LHC." In: *Phys. Lett. B* 716 (2012), pp. 30–61. DOI: 10.1016/j.physletb.2012.08.021. arXiv: 1207.7235 [hep-ex].

[11] Q. R. Ahmad et al. "Measurement of the rate of $\nu_e + d \to p + p + e^-$ interactions produced by ^{8}B solar neutrinos at the Sudbury Neutrino Observatory." In: *Phys. Rev. Lett.* 87 (2001), p. 071301. DOI: 10.1103/PhysRevLett.87.071301. arXiv: nucl-ex/0106015.

[12] Y. Fukuda et al. "Evidence for oscillation of atmospheric neutrinos." In: *Phys. Rev. Lett.* 81 (1998), pp. 1562–1567. DOI: 10.1103/PhysRevLett.81.1562. arXiv: hep-ex/9807003.

[13] M. B. Gavela et al. "Standard model CP violation and baryon asymmetry." In: *Mod. Phys. Lett. A* 9 (1994), pp. 795–810. DOI: 10.1142/S0217732394000629. arXiv: hep-ph/9312215.

[14] F. Zwicky. "Republication of: The redshift of extragalactic nebulae." In: 41.1 (Nov. 2008), pp. 207–224. DOI: 10.1007/s10714-008-0707-4. URL: https://doi.org/10.1007/s10714-008-0707-4.

[15] Fred Jegerlehner. "Muon g – 2 theory: The hadronic part." In: *EPJ Web Conf.* 166 (2018). Ed. by A. Di Domenico, p. 00022. DOI: 10.1051/epjconf/201816600022. arXiv: 1705.00263 [hep-ph].

[16] Michel Davier. "Update of the Hadronic Vacuum Polarisation Contribution to the muon g-2." In: *Nucl. Part. Phys. Proc.* 287-288 (2017). Ed. by Changzheng Yuan, Xiaohu Mo, and Liangliang Wang, pp. 70–75. DOI: 10.1016/j.nuclphysbps.2017.03.047. arXiv: 1612.02743 [hep-ph].

[17] T. Aoyama et al. "The anomalous magnetic moment of the muon in the Standard Model." In: *Phys. Rept.* 887 (2020), pp. 1–166. DOI: 10.1016/j.physrep.2020.07.006. arXiv: 2006.04822 [hep-ph].

[18] D. Hanneke, S. Fogwell, and G. Gabrielse. "New Measurement of the Electron Magnetic Moment and the Fine Structure Constant." In: *Physical Review Letters* 100.12 (Mar. 2008). ISSN: 1079-7114. DOI: 10.1103/physrevlett.100.120801. URL: http://dx.doi.org/10.1103/PhysRevLett.100.120801.

[19] Richard H. Parker et al. "Measurement of the fine-structure constant as a test of the Standard Model." In: *Science* 360.6385 (Apr. 2018), pp. 191–195. ISSN: 1095-9203. DOI: 10.1126/science.aap7706. URL: http://dx.doi.org/10.1126/science.aap7706.

[20] R. Aaij et al. "Differential branching fractions and isospin asymmetries of $B \to K^{(*)}\mu^+\mu^-$ decays." In: *JHEP* 06 (2014), p. 133. DOI: 10.1007/JHEP06(2014)133. arXiv: 1403.8044 [hep-ex].

[21] Roel Aaij et al. "Angular analysis and differential branching fraction of the decay $B_s^0 \to \phi\mu^+\mu^-$." In: *JHEP* 09 (2015), p. 179. DOI: 10.1007/JHEP09(2015)179. arXiv: 1506.08777 [hep-ex].

[22] Aoife Bharucha, David M. Straub, and Roman Zwicky. "$B \to V\ell^+\ell^-$ in the Standard Model from light-cone sum rules." In: *JHEP* 08 (2016), p. 098. DOI: 10.1007/JHEP08(2016)098. arXiv: 1503.05534 [hep-ph].

[23] R. R. Horgan et al. "Rare B decays using lattice QCD form factors." In: *PoS* LATTICE2014 (2015), p. 372. DOI: 10.22323/1.214.0372. arXiv: 1501.00367 [hep-lat].

[24] Nico Gubernari, Ahmet Kokulu, and Danny van Dyk. "$B \to P$ and $B \to V$ Form Factors from B-Meson Light-Cone Sum Rules beyond Leading Twist." In: *JHEP* 01 (2019), p. 150. DOI: 10.1007/JHEP01(2019)150. arXiv: 1811.00983 [hep-ph].

[25] Roel Aaij et al. "Angular analysis of the $B^0 \to K^{*0}\mu^+\mu^-$ decay using 3 fb^{-1} of integrated luminosity." In: *JHEP* 02 (2016), p. 104. DOI: 10.1007/JHEP02(2016)104. arXiv: 1512.04442 [hep-ex].

[26] Roel Aaij et al. "Measurement of CP-Averaged Observables in the $B^0 \to K^{*0}\mu^+\mu^-$ Decay." In: *Phys. Rev. Lett.* 125.1 (2020), p. 011802. DOI: 10.1103/PhysRevLett.125.011802. arXiv: 2003.04831 [hep-ex].

[27] Vardan Khachatryan et al. "Angular analysis of the decay $B^0 \to K^{*0}\mu^+\mu^-$ from pp collisions at $\sqrt{s} = 8$ TeV." In: *Phys. Lett. B* 753 (2016), pp. 424–448. DOI: 10.1016/j.physletb.2015.12.020. arXiv: 1507.08126 [hep-ex].

[28] A. Khodjamirian et al. "Charm-loop effect in $B \to K^{(*)}\ell^+\ell^-$ and $B \to K^*\gamma$." In: *JHEP* 09 (2010), p. 089. DOI: 10.1007/JHEP09(2010)089. arXiv: 1006.4945 [hep-ph].

[29] Christoph Bobeth et al. "Long-distance effects in $B \to K^*\ell\ell$ from analyticity." In: *Eur. Phys. J. C* 78.6 (2018), p. 451. DOI: 10.1140/epjc/s10052-018-5918-6. arXiv: 1707.07305 [hep-ph].

[30] Roel Aaij et al. "Test of lepton universality using $B^+ \to K^+\ell^+\ell^-$ decays." In: *Phys. Rev. Lett.* 113 (2014), p. 151601. DOI: 10.1103/PhysRevLett.113.151601. arXiv: 1406.6482 [hep-ex].

[31] R. Aaij et al. "Test of lepton universality with $B^0 \to K^{*0}\ell^+\ell^-$ decays." In: *JHEP* 08 (2017), p. 055. DOI: 10.1007/JHEP08(2017)055. arXiv: 1705.05802 [hep-ex].

[32] Roel Aaij et al. "Search for lepton-universality violation in $B^+ \to K^+\ell^+\ell^-$ decays." In: *Phys. Rev. Lett.* 122.19 (2019), p. 191801. DOI: 10.1103/PhysRevLett.122.191801. arXiv: 1903.09252 [hep-ex].

[33] Marzia Bordone, Gino Isidori, and Andrea Pattori. "On the Standard Model predictions for R_K and R_{K^*}." In: *Eur. Phys. J. C* 76.8 (2016), p. 440. DOI: 10.1140/epjc/s10052-016-4274-7. arXiv: 1605.07633 [hep-ph].

[34] A. Abdesselam et al. "Test of Lepton-Flavor Universality in $B \to K^*\ell^+\ell^-$ Decays at Belle." In: *Phys. Rev. Lett.* 126.16 (2021), p. 161801. DOI: 10.1103/PhysRevLett.126.161801. arXiv: 1904.02440 [hep-ex].

[35] Gudrun Hiller and Frank Kruger. "More model-independent analysis of $b \to s$ processes." In: *Phys. Rev. D* 69 (2004), p. 074020. DOI: 10.1103/PhysRevD.69.074020. arXiv: hep-ph/0310219.

[36] J. P. Lees et al. "Evidence for an excess of $\bar{B} \to D^{(*)}\tau^-\bar{\nu}_\tau$ decays." In: *Phys. Rev. Lett.* 109 (2012), p. 101802. DOI: 10.1103/PhysRevLett.109.101802. arXiv: 1205.5442 [hep-ex].

[37] J. P. Lees et al. "Measurement of an Excess of $\bar{B} \to D^{(*)}\tau^-\bar{\nu}_\tau$ Decays and Implications for Charged Higgs Bosons." In: *Phys. Rev. D* 88.7 (2013), p. 072012. DOI: 10.1103/PhysRevD.88.072012. arXiv: 1303.0571 [hep-ex].

[38] M. Huschle et al. "Measurement of the branching ratio of $\bar{B} \to D^{(*)}\tau^-\bar{\nu}_\tau$ relative to $\bar{B} \to D^{(*)}\ell^-\bar{\nu}_\ell$ decays with hadronic tagging at Belle." In: *Phys. Rev. D* 92.7 (2015), p. 072014. DOI: 10.1103/PhysRevD.92.072014. arXiv: 1507.03233 [hep-ex].

[39] Y. Sato et al. "Measurement of the branching ratio of $\bar{B}^0 \to D^{*+}\tau^-\bar{\nu}_\tau$ relative to $\bar{B}^0 \to D^{*+}\ell^-\bar{\nu}_\ell$ decays with a semileptonic tagging method." In: *Phys. Rev. D* 94.7 (2016), p. 072007. DOI: 10.1103/PhysRevD.94.072007. arXiv: 1607.07923 [hep-ex].

[40] S. Hirose et al. "Measurement of the τ lepton polarization and $R(D^*)$ in the decay $\bar{B} \to D^*\tau^-\bar{\nu}_\tau$." In: *Phys. Rev. Lett.* 118.21 (2017), p. 211801. DOI: 10.1103/PhysRevLett.118.211801. arXiv: 1612.00529 [hep-ex].

[41] Roel Aaij et al. "Measurement of the ratio of branching fractions $\mathcal{B}(\bar{B}^0 \to D^{*+}\tau^-\bar{\nu}_\tau)/\mathcal{B}(\bar{B}^0 \to D^{*+}\mu^-\bar{\nu}_\mu)$." In: *Phys. Rev. Lett.* 115.11 (2015). [Erratum: Phys.Rev.Lett. 115, 159901 (2015)], p. 111803. DOI: 10.1103/PhysRevLett.115.111803. arXiv: 1506.08614 [hep-ex].

[42] R. Aaij et al. "Measurement of the ratio of the $B^0 \to D^{*-}\tau^+\nu_\tau$ and $B^0 \to D^{*-}\mu^+\nu_\mu$ branching fractions using three-prong τ-lepton decays." In: *Phys. Rev. Lett.* 120.17 (2018), p. 171802. DOI: 10.1103/PhysRevLett.120.171802. arXiv: 1708.08856 [hep-ex].

[43] A. Abdesselam et al. "Precise determination of the CKM matrix element $|V_{cb}|$ with $\bar{B}^0 \to D^{*+}\,\ell^-\,\bar{\nu}_\ell$ decays with hadronic tagging at Belle." In: (Feb. 2017). arXiv: 1702.01521 [hep-ex].

[44] E. Waheed et al. "Measurement of the CKM matrix element $|V_{cb}|$ from $B^0 \to D^{*-}\ell^+\nu_\ell$ at Belle." In: *Phys. Rev. D* 100.5 (2019). [Erratum: Phys.Rev.D 103, 079901 (2021)], p. 052007. DOI: 10.1103/PhysRevD.100.052007. arXiv: 1809.03290 [hep-ex].

[45] Martin Jung and David M. Straub. "Constraining new physics in $b \to c\ell\nu$ transitions." In: *JHEP* 01 (2019), p. 009. DOI: 10.1007/JHEP01(2019)009. arXiv: 1801.01112 [hep-ph].

[46] Jon A. Bailey et al. "B→D$\ell\nu$ form factors at nonzero recoil and $|V_{cb}|$ from 2+1-flavor lattice QCD." In: *Phys. Rev. D* 92.3 (2015), p. 034506. DOI: 10.1103/PhysRevD.92.034506. arXiv: 1503.07237 [hep-lat].

[47] Heechang Na et al. "$B \to Dl\nu$ form factors at nonzero recoil and extraction of $|V_{cb}|$." In: *Phys. Rev. D* 92.5 (2015). [Erratum: Phys.Rev.D 93, 119906 (2016)], p. 054510. DOI: 10.1103/PhysRevD.93.119906. arXiv: 1505.03925 [hep-lat].

[48] Florian U. Bernlochner et al. "Combined analysis of semileptonic B decays to D and D^*: $R(D^{(*)})$, $|V_{cb}|$, and new physics." In: *Phys. Rev. D* 95.11 (2017). [Erratum: Phys.Rev.D 97, 059902 (2018)], p. 115008. DOI: 10.1103/PhysRevD.95.115008. arXiv: 1703.05330 [hep-ph].

[49] Dante Bigi, Paolo Gambino, and Stefan Schacht. "$R(D^*)$, $|V_{cb}|$, and the Heavy Quark Symmetry relations between form factors." In: *JHEP* 11 (2017), p. 061. DOI: 10.1007/JHEP11(2017)061. arXiv: 1707.09509 [hep-ph].

[50] R. Aaij et al. "Test of Lepton Flavor Universality by the measurement of the $B^0 \to D^{*-}\tau^+\nu_\tau$ branching fraction using three-prong τ decays." In: *Phys. Rev. D* 97.7 (2018), p. 072013. DOI: 10.1103/PhysRevD.97.072013. arXiv: 1711.02505 [hep-ex].

[51] S. Hirose et al. "Measurement of the τ lepton polarization and $R(D^*)$ in the decay $\bar{B} \to D^*\tau^-\bar{\nu}_\tau$ with one-prong hadronic τ decays at Belle." In: *Phys. Rev. D* 97.1 (2018), p. 012004. DOI: 10.1103/PhysRevD.97.012004. arXiv: 1709.00129 [hep-ex].

[52] A. Abdesselam et al. "Measurement of $\mathcal{R}(D)$ and $\mathcal{R}(D^*)$ with a semileptonic tagging method." In: (Apr. 2019). arXiv: 1904.08794 [hep-ex].

[53] Dante Bigi and Paolo Gambino. "Revisiting $B \to D\ell\nu$." In: *Phys. Rev. D* 94.9 (2016), p. 094008. DOI: 10.1103/PhysRevD.94.094008. arXiv: 1606.08030 [hep-ph].

[54] Sneha Jaiswal, Soumitra Nandi, and Sunando Kumar Patra. "Extraction of $|V_{cb}|$ from $B \to D^{(*)}\ell\nu_\ell$ and the Standard Model predictions of $R(D^{(*)})$." In: *JHEP* 12 (2017), p. 060. DOI: 10.1007/JHEP12(2017)060. arXiv: 1707.09977 [hep-ph].

[55] Rigo Bause et al. "Exploiting CP-asymmetries in rare charm decays." In: *Phys. Rev. D* 101.11 (2020), p. 115006. DOI: 10.1103/PhysRevD.101.115006. arXiv: 2004.01206 [hep-ph].

[56] Mikael Chala et al. "ΔA_{CP} within the Standard Model and beyond." In: *JHEP* 07 (2019), p. 161. DOI: 10.1007/JHEP07(2019)161. arXiv: 1903.10490 [hep-ph].

[57] Avital Dery and Yosef Nir. "Implications of the LHCb discovery of CP violation in charm decays." In: *JHEP* 12 (2019), p. 104. DOI: 10.1007/JHEP12(2019)104. arXiv: 1909.11242 [hep-ph].

[58] Franco Buccella, Ayan Paul, and Pietro Santorelli. "$SU(3)_F$ breaking through final state interactions and CP asymmetries in $D \to PP$ decays." In: *Phys. Rev. D* 99.11 (2019), p. 113001. DOI: 10.1103/PhysRevD.99.113001. arXiv: 1902.05564 [hep-ph].

[59] Hsiang-Nan Li, Cai-Dian Lü, and Fu-Sheng Yu. "Implications on the first observation of charm CPV at LHCb." In: (Mar. 2019). arXiv: 1903.10638 [hep-ph].

[60] Amarjit Soni. "Resonance enhancement of Charm CP." In: (May 2019). arXiv: 1905.00907 [hep-ph].

[61] Hai-Yang Cheng and Cheng-Wei Chiang. "Revisiting CP violation in $D \to PP$ and VP decays." In: *Phys. Rev. D* 100.9 (2019), p. 093002. DOI: 10.1103/PhysRevD.100.093002. arXiv: 1909.03063 [hep-ph].

[62] Alexander Khodjamirian and Alexey A. Petrov. "Direct CP asymmetry in $D \to \pi^-\pi^+$ and $D \to K^-K^+$ in QCD-based approach." In: *Phys. Lett. B* 774 (2017), pp. 235–242. DOI: 10.1016/j.physletb.2017.09.070. arXiv: 1706.07780 [hep-ph].

[63] Alexander L. Kagan and Luca Silvestrini. "Dispersive and absorptive CP violation in $D^0 - \overline{D^0}$ mixing." In: *Phys. Rev. D* 103.5 (2021), p. 053008. DOI: 10.1103/PhysRevD.103.053008. arXiv: 2001.07207 [hep-ph].

[64] Ulrich Nierste. "Charm decays." In: *PoS* Beauty2019 (2020), p. 048. DOI: 10.22323/1.377.0048. arXiv: 2002.06686 [hep-ph].

[65] Marcel Golz, Gudrun Hiller, and Tom Magorsch. "Probing for New Physics with Rare Charm Baryon (Λ_c, Ξ_c, Ω_c) Decays." In: *JHEP* 09 (2021), p. 208. DOI: 10.1007/jhep09(2021)208. arXiv: 2107.13010 [hep-ph].

[66] Rigo Bause et al. "Rare charm $c \to u\,\nu\bar{\nu}$ dineutrino null tests for e^+e^- machines." In: *Phys. Rev. D* 103.1 (2021), p. 015033. DOI: 10.1103/PhysRevD.103.015033. arXiv: 2010.02225 [hep-ph].

[67] Rigo Bause et al. "Lepton universality and lepton flavor conservation tests with dineutrino modes." In: (July 2020). arXiv: 2007.05001 [hep-ph].

[68] Rigo Bause et al. "The new physics reach of null tests with $D \to \pi\ell\ell$ and $D_s \to K\ell\ell$ decays." In: *Eur. Phys. J. C* 80.1 (2020). [Erratum: Eur.Phys.J.C 81, 219 (2021)], p. 65. DOI: 10.1140/epjc/s10052-020-7621-7. arXiv: 1909.11108 [hep-ph].

[69] Gustavo Burdman et al. "Rare charm decays in the standard model and beyond." In: *Phys. Rev. D* 66 (2002), p. 014009. DOI: 10.1103/PhysRevD.66.014009. arXiv: hep-ph/0112235.

[70] Ayan Paul, Ikaros I. Bigi, and Stefan Recksiegel. "On $D \to X_u l^+ l^-$ within the Standard Model and Frameworks like the Littlest Higgs Model with T Parity." In: *Phys. Rev. D* 83 (2011), p. 114006. DOI: 10.1103/PhysRevD.83.114006. arXiv: 1101.6053 [hep-ph].

[71] Svjetlana Fajfer and Nejc Košnik. "Resonance catalyzed CP asymmetries in D$\to$P$\ell^+\ell^-$." In: *Phys. Rev. D* 87.5 (2013), p. 054026. DOI: 10.1103/PhysRevD.87.054026. arXiv: 1208.0759 [hep-ph].

[72] Luigi Cappiello, Oscar Cata, and Giancarlo D'Ambrosio. "Standard Model prediction and new physics tests for $D^0 \to h^+h^-\ell^+\ell^-(h = \pi, K : \ell = e, \mu)$." In: *JHEP* 04 (2013), p. 135. DOI: 10.1007/JHEP04(2013)135. arXiv: 1209.4235 [hep-ph].

[73] Svjetlana Fajfer and Nejc Košnik. "Prospects of discovering new physics in rare charm decays." In: *Eur. Phys. J. C* 75.12 (2015), p. 567. DOI: 10.1140/epjc/s10052-015-3801-2. arXiv: 1510.00965 [hep-ph].

[74] V. Lubicz et al. "Tensor form factor of $D \to \pi(K)\ell\nu$ and $D \to \pi(K)\ell\ell$ decays with $N_f = 2 + 1 + 1$ twisted-mass fermions." In: *Phys. Rev. D* 98.1 (2018), p. 014516. DOI: 10.1103/PhysRevD.98.014516. arXiv: 1803.04807 [hep-lat].

[75] Stefan De Boer and Gudrun Hiller. "Null tests from angular distributions in $D \to P_1P_2l^+l^-$, $l = e, \mu$ decays on and off peak." In: *Phys. Rev. D* 98.3 (2018), p. 035041. DOI: 10.1103/PhysRevD.98.035041. arXiv: 1805.08516 [hep-ph].

[76] Stefan de Boer and Gudrun Hiller. "Flavor and new physics opportunities with rare charm decays into leptons." In: *Phys. Rev. D* 93.7 (2016), p. 074001. DOI: 10.1103/PhysRevD.93.074001. arXiv: 1510.00311 [hep-ph].

[77] A. Cerri et al. "Report from Working Group 4: Opportunities in Flavour Physics at the HL-LHC and HE-LHC." In: *CERN Yellow Rep. Monogr.* 7 (2019). Ed. by Andrea Dainese et al., pp. 867–1158. DOI: 10.23731/CYRM-2019-007.867. arXiv: 1812.07638 [hep-ph].

[78] W. Altmannshofer et al. "The Belle II Physics Book." In: *PTEP* 2019.12 (2019). Ed. by E. Kou and P. Urquijo. [Erratum: PTEP 2020, 029201 (2020)], p. 123C01. DOI: 10.1093/ptep/ptz106. arXiv: 1808.10567 [hep-ex].

[79] M. Ablikim et al. "Future Physics Programme of BESIII." In: *Chin. Phys. C* 44.4 (2020), p. 040001. DOI: 10.1088/1674-1137/44/4/040001. arXiv: 1912.05983 [hep-ex].

[80] A.E. Bondar. "Project of a Super Charm-Tau factory at the Budker Institute of Nuclear Physics in Novosibirsk." In: 76 (2013), pp. 1072–1085. DOI: 10.1134/S1063778813090032.

[81] A. Abada et al. "FCC Physics Opportunities." In: *The European Physical Journal C* 79.6 (June 2019). DOI: 10.1140/epjc/s10052-019-6904-3. URL: https://doi.org/10.1140/epjc/s10052-019-6904-3.

[82] David J. Gross and Frank Wilczek. "Ultraviolet Behavior of Non-Abelian Gauge Theories." In: *Phys. Rev. Lett.* 30 (26 June 1973), pp. 1343–1346. DOI: 10.1103/PhysRevLett.30.1343. URL: https://link.aps.org/doi/10.1103/PhysRevLett.30.1343.

[83] Steven Weinberg. "Non-Abelian Gauge Theories of the Strong Interactions." In: *Phys. Rev. Lett.* 31 (7 Aug. 1973), pp. 494–497. DOI: 10.1103/PhysRevLett.31.494. URL: https://link.aps.org/doi/10.1103/PhysRevLett.31.494.

[84] H. Fritzsch, M. Gell-Mann, and H. Leutwyler. "Advantages of the color octet gluon picture." In: *Physics Letters B* 47.4 (1973), pp. 365–368. ISSN: 0370-2693. DOI: https://doi.org/10.1016/0370-2693(73)90625-4. URL: https://www.sciencedirect.com/science/article/pii/0370269373906254.

[85] H. David Politzer. "Reliable Perturbative Results for Strong Interactions?" In: *Phys. Rev. Lett.* 30 (26 June 1973), pp. 1346–1349. DOI: 10.1103/PhysRevLett.30.1346. URL: https://link.aps.org/doi/10.1103/PhysRevLett.30.1346.

[86] Steven Weinberg. "A Model of Leptons." In: *Phys. Rev. Lett.* 19 (21 Nov. 1967), pp. 1264–1266. DOI: 10.1103/PhysRevLett.19.1264. URL: https://link.aps.org/doi/10.1103/PhysRevLett.19.1264.

[87] Sheldon L. Glashow. "Partial-symmetries of weak interactions." In: *Nuclear Physics* 22.4 (1961), pp. 579–588. ISSN: 0029-5582. DOI: https://doi.org/10.1016/0029-5582(61)90469-2. URL: https://www.sciencedirect.com/science/article/pii/0029558261904692.

[88] Abdus Salam. "Weak and electromagnetic interactions." In: *Selected Papers of Abdus Salam*. WORLD SCIENTIFIC, May 1994, pp. 244–254. DOI: 10.1142/9789812795915_0034. URL: https://doi.org/10.1142/9789812795915_0034.

[89] Matthew D. Schwartz. *Quantum Field Theory and the Standard Model* -. Cambridge: Cambridge University Press, 2014. ISBN: 978-1-107-03473-0.

[90] Shahida Dar. "The Neutron EDM in the SM: A Review." In: (Aug. 2000). arXiv: hep-ph/0008248.

[91] C. Abel et al. "Measurement of the permanent electric dipole moment of the neutron." In: *Phys. Rev. Lett.* 124.8 (2020), p. 081803. DOI: 10.1103/PhysRevLett.124.081803. arXiv: 2001.11966 [hep-ex].

[92] S. L. Glashow, J. Iliopoulos, and L. Maiani. "Weak Interactions with Lepton-Hadron Symmetry." In: *Phys. Rev. D* 2 (7 Oct. 1970), pp. 1285–1292. DOI: 10.1103/PhysRevD.2.1285. URL: https://link.aps.org/doi/10.1103/PhysRevD.2.1285.

[93] Nicola Cabibbo. "Unitary Symmetry and Leptonic Decays." In: *Phys. Rev. Lett.* 10 (12 June 1963), pp. 531–533. DOI: 10.1103/PhysRevLett.10.531. URL: https://link.aps.org/doi/10.1103/PhysRevLett.10.531.

[94] Makoto Kobayashi and Toshihide Maskawa. "CP-Violation in the Renormalizable Theory of Weak Interaction." In: *Progress of Theoretical Physics* 49.2 (Feb. 1973), pp. 652–657. ISSN: 0033-068X. DOI: 10.1143/PTP.49.652. eprint: https://academic.oup.com/ptp/article-pdf/49/2/652/5257692/49-2-652.pdf. URL: https://doi.org/10.1143/PTP.49.652.

[95] Ling-Lie Chau and Wai-Yee Keung. "Comments on the Parametrization of the Kobayashi-Maskawa Matrix." In: *Phys. Rev. Lett.* 53 (19 Nov. 1984), pp. 1802–1805. DOI: 10.1103/PhysRevLett.53.1802. URL: https://link.aps.org/doi/10.1103/PhysRevLett.53.1802.

[96] Lincoln Wolfenstein. "Parametrization of the Kobayashi-Maskawa Matrix." In: *Phys. Rev. Lett.* 51 (21 Nov. 1983), pp. 1945–1947. DOI: 10.1103/PhysRevLett.51.1945. URL: https://link.aps.org/doi/10.1103/PhysRevLett.51.1945.

[97] UTfit Collaboration. 2018. URL: http://www.utfit.org/UTfit/ResultsSummer2018SM.

[98] B Pontecorvo. "MESONIUM AND ANTIMESONIUM." In: *Zhur. Eksptl'. i Teoret. Fiz.* 33 (Aug. 1957). URL: https://www.osti.gov/biblio/4343073.

[99] B. Pontecorvo. "Inverse beta processes and nonconservation of lepton charge." In: *Zh. Eksp. Teor. Fiz.* 34 (1957), p. 247.

[100] Ziro Maki, Masami Nakagawa, and Shoichi Sakata. "Remarks on the unified model of elementary particles." In: *Prog. Theor. Phys.* 28 (1962), pp. 870–880. DOI: 10.1143/PTP.28.870.

[101] Andrei D Sakharov. "Violation ofCPin variance,Casymmetry, and baryon asymmetry of the universe." In: *Soviet Physics Uspekhi* 34.5 (May 1991), pp. 392–393. DOI: 10.1070/pu1991v034n05abeh002497. URL: https://doi.org/10.1070/pu1991v034n05abeh002497.

[102] C.D. Froggatt and H.B. Nielsen. "Hierarchy of quark masses, cabibbo angles and CP violation." In: *Nuclear Physics B* 147.3 (1979), pp. 277–298. ISSN: 0550-3213. DOI: https://doi.org/10.1016/0550-3213(79)90316-X. URL: https://www.sciencedirect.com/science/article/pii/055032137990316X.

[103] Particle Data Group et al. "Review of Particle Physics." In: *Progress of Theoretical and Experimental Physics* 2020.8 (Aug. 2020). 083C01. ISSN: 2050-3911. DOI: 10.1093/ptep/ptaa104. eprint: https://academic.oup.com/ptep/article-pdf/2020/8/083C01/34673722/ptaa104.pdf. URL: https://doi.org/10.1093/ptep/ptaa104.

[104] Murray Gell-Mann and Yuval Ne'eman. *The Eightfold Way*. New York, Amsterdam: W.A. Benjamin, 1964.

[105] Xiao-Gang He et al. "SU(3) symmetry and its breaking effects in semileptonic heavy baryon decays." In: (Oct. 2021). arXiv: 2110.04179 [hep-ph].

[106] A. Pich. "Chiral perturbation theory." In: *Rept. Prog. Phys.* 58 (1995), pp. 563–610. DOI: 10.1088/0034-4885/58/6/001. arXiv: hep-ph/9502366.

[107] Stefan Scherer. "Introduction to chiral perturbation theory." In: *Adv. Nucl. Phys.* 27 (2003). Ed. by John W. Negele and E. W. Vogt, p. 277. arXiv: hep-ph/0210398.

[108] Bugra Borasoy. "Introduction to Chiral Perturbation Theory." In: *Springer Proceedings in Physics*. Springer Berlin Heidelberg, 2008, pp. 1–26. DOI: 10.1007/978-3-540-73621-9_1. URL: https://doi.org/10.1007/978-3-540-73621-9_1.

[109] Jeffrey Goldstone. "Field Theories with Superconducter Solutions." In: *Nuovo Cim.* 19 (1961), pp. 154–164. DOI: 10.1007/BF02812722. URL: https://link.springer.com/article/10.1007/BF02812722#citeas.

[110] Jeffrey Goldstone, Abdus Salam, and Steven Weinberg. "Broken Symmetries." In: *Phys. Rev.* 127 (3 Aug. 1962), pp. 965–970. DOI: 10.1103/PhysRev.127.965. URL: https://link.aps.org/doi/10.1103/PhysRev.127.965.

[111] Aneesh V. Manohar and Mark B. Wise. *Heavy Quark Physics*. Cambridge University Press, Mar. 2000. DOI: 10.1017/cbo9780511529351. URL: https://doi.org/10.1017/cbo9780511529351.

[112] Matthias Neubert. "Heavy quark effective theory." In: *Subnucl. Ser.* 34 (1997). Ed. by A. Zichichi, pp. 98–165. arXiv: hep-ph/9610266.

[113] Andrey Grozin. *Heavy Quark Effective Theory*. Springer Berlin Heidelberg, 2004. DOI: 10.1007/b79301. URL: https://doi.org/10.1007/b79301.

[114] F. Hussain and G. Thompson. "An Introduction to the heavy quark effective theory." In: *ICTP Summer School in High-energy Physics and Cosmology*. June 1994, pp. 0045–115. arXiv: hep-ph/9502241.

[115] Thomas Appelquist and J. Carazzone. "Infrared singularities and massive fields." In: *Phys. Rev. D* 11 (10 May 1975), pp. 2856–2861. DOI: 10.1103/PhysRevD.11.2856. URL: https://link.aps.org/doi/10.1103/PhysRevD.11.2856.

[116] E. Fermi. "Versuch einer Theorie der ?-Strahlen. I." In: *Zeitschrift für Physik* 88.3-4 (Mar. 1934), pp. 161–177. DOI: 10.1007/bf01351864. URL: https://doi.org/10.1007/bf01351864.

[117] Andrzej J. Buras. "Operator product expansion, renormalization group and weak decays." In: *Lect. Notes Phys.* 558 (2000). Ed. by P. Breitenlohner and D. Maison, pp. 65–85. arXiv: hep-ph/9901409.

[118] Andrzej J. Buras. "Weak Hamiltonian, CP violation and rare decays." In: *Les Houches Summer School in Theoretical Physics, Session 68: Probing the Standard Model of Particle Interactions*. June 1998, pp. 281–539. arXiv: hep-ph/9806471.

[119] Gerhard Buchalla, Andrzej J. Buras, and Markus E. Lautenbacher. "Weak decays beyond leading logarithms." In: *Rev. Mod. Phys.* 68 (1996), pp. 1125–1144. DOI: 10.1103/RevModPhys.68.1125. arXiv: hep-ph/9512380.

[120] Antonio Pich. "Effective field theory: Course." In: *Les Houches Summer School in Theoretical Physics, Session 68: Probing the Standard Model of Particle Interactions*. June 1998, pp. 949–1049. arXiv: hep-ph/9806303.

[121] Matthias Neubert. "Effective field theory and heavy quark physics." In: *Theoretical Advanced Study Institute in Elementary Particle Physics: Physics in $D \geqq 4$*. Dec. 2005, pp. 149–194. DOI: 10.1142/9789812773579_0004. arXiv: hep-ph/0512222.

[122] Matthias Neubert. "Renormalization Theory and Effective Field Theories." In: (Jan. 2019). Ed. by Sacha Davidson et al. DOI: 10.1093/oso/9780198855743.003.0001. arXiv: 1901.06573 [hep-ph].

[123] A. V. Manohar. "Effective field theories." In: *Lect. Notes Phys.* 479 (1997). Ed. by H. Latal and W. Schweiger, pp. 311–362. DOI: 10.1007/BFb0104294. arXiv: hep-ph/9606222.

[124] Stefan de Boer and Gudrun Hiller. "Rare radiative charm decays within the standard model and beyond." In: *JHEP* 08 (2017), p. 091. DOI: 10.1007/JHEP08(2017)091. arXiv: 1701.06392 [hep-ph].

[125] Stefan de Boer. "Probing the standard model with rare charm decays." 2017. DOI: 10.17877/DE290R-18060. URL: https://eldorado.tu-dortmund.de/handle/2003/36043.

[126] Stefan de Boer, Bastian Müller, and Dirk Seidel. "Higher-order Wilson coefficients for $c \to u$ transitions in the standard model." In: *JHEP* 08 (2016), p. 091. DOI: 10.1007/JHEP08(2016)091. arXiv: 1606.05521 [hep-ph].

[127] Thomas Jubb, Matthew Kirk, and Alexander Lenz. "Charming Dark Matter." In: *JHEP* 12 (2017), p. 010. DOI: 10.1007/JHEP12(2017)010. arXiv: 1709.01930 [hep-ph].

[128] A. Abdesselam et al. "Observation of $D^0 \to \rho^0\gamma$ and search for CP violation in radiative charm decays." In: *Phys. Rev. Lett.* 118.5 (2017), p. 051801. DOI: 10.1103/PhysRevLett.118.051801. arXiv: 1603.03257 [hep-ex].

[129] Gino Isidori and Jernej F. Kamenik. "Shedding light on CP violation in the charm system via D to V gamma decays." In: *Phys. Rev. Lett.* 109 (2012), p. 171801. DOI: 10.1103/PhysRevLett.109.171801. arXiv: 1205.3164 [hep-ph].

[130] James Lyon and Roman Zwicky. "Anomalously large O_8 and long-distance chirality from $A_{CP}[D^0 \to (\rho^0, \omega)\gamma](t)$." In: (Oct. 2012). arXiv: 1210.6546 [hep-ph].

[131] Roel Aaij et al. "Observation of CP Violation in Charm Decays." In: *Phys. Rev. Lett.* 122.21 (2019), p. 211803. DOI: 10.1103/PhysRevLett.122.211803. arXiv: 1903.08726 [hep-ex].

[132] Stefan de Boer and Gudrun Hiller. "The photon polarization in radiative D decays, phenomenologically." In: *Eur. Phys. J. C* 78.3 (2018), p. 188. DOI: 10.1140/epjc/s10052-018-5682-7. arXiv: 1802.02769 [hep-ph].

[133] Yue-Long Shen and Gang Li. "Radiative D(D s) decays in the covariant light front approach." In: *The European Physical Journal C* 73.5 (May 2013). DOI: 10.1140/epjc/s10052-013-2441-7. URL: https://doi.org/10.1140/epjc/s10052-013-2441-7.

[134] S. Fajfer, Sasa Prelovsek, and P. Singer. "Long distance contributions in D —> V gamma decays." In: *Eur. Phys. J. C* 6 (1999), pp. 471–476. DOI: 10.1007/s100520050356. arXiv: hep-ph/9801279.

[135] B. Bajc, S. Fajfer, and Robert J. Oakes. "Vector and pseudoscalar charm meson radiative decays." In: *Phys. Rev. D* 51 (1995), pp. 2230–2236. DOI: 10.1103/PhysRevD.51.2230. arXiv: hep-ph/9407388.

[136] B. Bajc, S. Fajfer, and Robert J. Oakes. "Vector and pseudoscalar charm meson radiative decays." In: *Phys. Rev. D* 51 (5 Mar. 1995), pp. 2230–2236. DOI: 10.1103/PhysRevD.51.2230. URL: https://link.aps.org/doi/10.1103/PhysRevD.51.2230.

[137] S. Fajfer and P. Singer. "Long distance c —> u gamma effects in weak radiative decays of D mesons." In: *Phys. Rev. D* 56 (1997), pp. 4302–4310. DOI: 10.1103/PhysRevD.56.4302. arXiv: hep-ph/9705327.

[138] D. M. Asner et al. "Radiative decay modes of the D0 meson." In: *Phys. Rev. D* 58 (1998), p. 092001. DOI: 10.1103/PhysRevD.58.092001. arXiv: hep-ex/9803022.

[139] Bernard Aubert et al. "Measurement of the Branching Fractions of the Radiative Charm Decays D0 —> anti-K*0 gamma and D0 —> phi gamma." In: *Phys. Rev. D* 78 (2008), p. 071101. DOI: 10.1103/PhysRevD.78.071101. arXiv: 0808.1838 [hep-ex].

[140] F. E. Low. "Bremsstrahlung of Very Low-Energy Quanta in Elementary Particle Collisions." In: *Phys. Rev.* 110 (4 May 1958), pp. 974–977. DOI: 10.1103/PhysRev.110.974. URL: https://link.aps.org/doi/10.1103/PhysRev.110.974.

[141] Vittorio Del Duca. "High-energy bremsstrahlung theorems for soft photons." In: *Nuclear Physics B* 345.2 (1990), pp. 369–388. ISSN: 0550-3213. DOI: https://doi.org/10.1016/0550-3213(90)90392-Q. URL: https://www.sciencedirect.com/science/article/pii/055032139090392Q.

[142] Giancarlo D'Ambrosio and Gino Isidori. "K —> pi pi gamma decays: A Search for novel couplings in kaon decays." In: *Z. Phys. C* 65 (1995), pp. 649–656. DOI: 10.1007/BF01578672. arXiv: hep-ph/9408219.

[143] Mark B. Wise. "Chiral perturbation theory for hadrons containing a heavy quark." In: *Phys. Rev. D* 45 (7 Apr. 1992), R2188–R2191. DOI: 10.1103/PhysRevD.45.R2188. URL: https://link.aps.org/doi/10.1103/PhysRevD.45.R2188.

[144] Gustavo Burdman and John F. Donoghue. "Union of chiral and heavy quark symmetries." In: *Physics Letters B* 280.3 (1992), pp. 287–291. ISSN: 0370-2693. DOI: https://doi.org/10.1016/0370-2693(92)90068-F. URL: https://www.sciencedirect.com/science/article/pii/037026939290068F.

[145] Tung-Mow Yan et al. "Heavy-quark symmetry and chiral dynamics." In: *Phys. Rev. D* 46 (3 Aug. 1992), pp. 1148–1164. DOI: 10.1103/PhysRevD.46.1148. URL: https://link.aps.org/doi/10.1103/PhysRevD.46.1148.

[146] R. Casalbuoni et al. "Effective lagrangian for heavy and light mesons. Semileptonic decays." In: *Physics Letters B* 299.1 (1993), pp. 139–150. ISSN: 0370-2693. DOI: https://doi.org/10.1016/0370-2693(93)90895-O. URL: https://www.sciencedirect.com/science/article/pii/037026939390895O.

[147] R. Casalbuoni et al. "Phenomenology of heavy meson chiral lagrangians." In: *Physics Reports* 281.3 (1997), pp. 145–238. ISSN: 0370-1573. DOI: https://doi.org/10.1016/S0370-1573(96)00027-0. URL: https://www.sciencedirect.com/science/article/pii/S0370157396000270.

[148] M. Bando et al. "Is the ρ Meson a Dynamical Gauge Boson of Hidden Local Symmetry?" In: *Phys. Rev. Lett.* 54 (12 Mar. 1985), pp. 1215–1218. DOI: 10.1103/PhysRevLett.54.1215. URL: https://link.aps.org/doi/10.1103/PhysRevLett.54.1215.

[149] Masako Bando, Taichiro Kugo, and Koichi Yamawaki. "On the vector mesons as dynamical gauge bosons of hidden local symmetries." In: *Nuclear Physics B* 259.2 (1985), pp. 493–502. ISSN: 0550-3213. DOI: https://doi.org/10.1016/0550-3213(85)90647-9. URL: https://www.sciencedirect.com/science/article/pii/0550321385906479.

[150] Masako Bando, Taichiro Kugo, and Koichi Yamawaki. "Nonlinear realization and hidden local symmetries." In: *Physics Reports* 164.4 (1988), pp. 217–314. ISSN: 0370-1573. DOI: https://doi.org/10.1016/0370-1573(88)90019-1. URL: https://www.sciencedirect.com/science/article/pii/0370157388900191.

[151] Svjetlana Fajfer, Anita Prapotnik, and Paul Singer. "Cabibbo allowed D —> K pi gamma decays." In: *Phys. Rev. D* 66 (2002), p. 074002. DOI: 10.1103/PhysRevD.66.074002. arXiv: hep-ph/0204306.

[152] Svjetlana Fajfer, Anita Prapotnik, and Paul Singer. "Charm radiative decays with neutral mesons D0 —> anti-K0 pi0 gamma, D0 —> anti-K0 eta (eta-prime) gamma." In: *Phys. Lett. B* 550 (2002), pp. 77–84. DOI: 10.1016/S0370-2693(02)02964-7. arXiv: hep-ph/0210423.

[153] A. Bramon, A. Grau, and G. Pancheri. "Radiative vector-meson decays in SU (3) broken effective chiral lagrangians." In: *Physics Letters B* 344.1 (1995), pp. 240–244. ISSN: 0370-2693. DOI: https://doi.org/10.1016/0370-2693(94)01543-L. URL: https://www.sciencedirect.com/science/article/pii/037026939401543L.

[154] Paul Singer. "Radiative decays of heavy mesons and the determination of the strong g coupling." In: *Acta Phys. Polon. B* 30 (1999). Ed. by A. Bialas and M. Praszalowicz, pp. 3849–3859. arXiv: hep-ph/9910558.

[155] A. Anastassov et al. "First measurement of Gamma(D*+) and precision measurement of m(D*+) - m(D0)." In: *Phys. Rev. D* 65 (2002), p. 032003. DOI: 10.1103/PhysRevD.65.032003. arXiv: hep-ex/0108043.

[156] B. Bajc et al. "Nonleptonic two-body charmed meson decays in an effective model for their semileptonic decays." In: *Phys. Rev. D* 56 (1997), pp. 7207–7215. DOI: 10.1103/PhysRevD.56.7207. arXiv: hep-ph/9706223.

[157] B. Bajc, S. Fajfer, and Robert J. Oakes. "Vector and pseudoscalar charm meson radiative decays." In: *Physical Review D* 51.5 (Mar. 1995), pp. 2230–2236. DOI: 10.1103/physrevd.51.2230. URL: https://doi.org/10.1103/physrevd.51.2230.

[158] B. Bajc, S. Fajfer, and R. J. Oakes. "An Effective model for charmed meson semileptonic decays." In: *Phys. Rev. D* 53 (1996), pp. 4957–4963. DOI: 10.1103/PhysRevD.53.4957. arXiv: hep-ph/9511455.

[159] R. C. Verma. "Decay constants and form factors of s-wave and p-wave mesons in the covariant light-front quark model." In: *J. Phys. G* 39 (2012), p. 025005. DOI: 10.1088/0954-3899/39/2/025005. arXiv: 1103.2973 [hep-ph].

[160] R. Casalbuoni et al. "Effective Lagrangian for heavy and light mesons: Radiative B decays." In: *Phys. Lett. B* 312 (1993), pp. 315–326. DOI: 10.1016/0370-2693(93)91087-4. arXiv: hep-ph/9304302.

[161] M. Beneke et al. "QCD factorization for exclusive, nonleptonic B meson decays: General arguments and the case of heavy light final states." In: *Nucl. Phys. B* 591 (2000), pp. 313–418. DOI: 10.1016/S0550-3213(00)00559-9. arXiv: hep-ph/0006124.

[162] Stefan W. Bosch and Gerhard Buchalla. "The Radiative decays $B \to V\gamma$ at next-to-leading order in QCD." In: *Nucl. Phys. B* 621 (2002), pp. 459–478. DOI: 10.1016/S0550-3213(01)00580-6. arXiv: hep-ph/0106081.

[163] S. Descotes-Genon and C. T. Sachrajda. "Factorization, the light cone distribution amplitude of the B meson and the radiative decay B —> gamma l nu(l)." In: *Nucl. Phys. B* 650 (2003), pp. 356–390. DOI: 10.1016/S0550-3213(02)01066-0. arXiv: hep-ph/0209216.

[164] Martin Beneke et al. "QCD factorization of the four-lepton decay $B^- \to \ell\bar{\nu}_\ell\ell^{(\prime)}\bar{\ell}^{(\prime)}$." In: *Eur. Phys. J. C* 81 (2021), p. 638. DOI: 10.1140/epjc/s10052-021-09388-y. arXiv: 2102.10060 [hep-ph].

[165] Jing-Wu Li, Mao-Zhi Yang, and Dong-Sheng Du. "D —> PV decays with final state interactions." In: *HEPNP* 27 (2003), pp. 665–672. arXiv: hep-ph/0206154.

[166] Yue-Liang Wu, Ming Zhong, and Yue-Feng Zhou. "Exploring final state hadron structure and SU(3) flavor symmetry breaking effects in D —> PP and D —> PV decays." In: *Eur. Phys. J. C* 42 (2005), p. 391. DOI: 10.1140/epjc/s2005-02302-2. arXiv: hep-ph/0405080.

[167] Zhi-Tian Zou, Cheng Li, and Cai-Dian Lü. "Pure annihilation type $D \to PP(V)$ decays in the perturbative QCD approach." In: *Chin. Phys. C* 37 (2013), p. 093101. DOI: 10.1088/1674-1137/37/9/093101. arXiv: 1301.3444 [hep-ph].

[168] Mykhailo Lisovyi, Andrii Verbytskyi, and Oleksandr Zenaiev. "Combined analysis of charm-quark fragmentation-fraction measurements." In: *Eur. Phys. J. C* 76.7 (2016), p. 397. DOI: 10.1140/epjc/s10052-016-4246-y. arXiv: 1509.01061 [hep-ex].

[169] Michael Gronau et al. "Measuring the photon polarization in B —> K pi pi gamma." In: *Phys. Rev. Lett.* 88 (2002), p. 051802. DOI: 10.1103/PhysRevLett.88.051802. arXiv: hep-ph/0107254.

[170] Michael Gronau and Dan Pirjol. "Photon polarization in radiative B decays." In: *Phys. Rev. D* 66 (2002), p. 054008. DOI: 10.1103/PhysRevD.66.054008. arXiv: hep-ph/0205065.

[171] Benjamin Grinstein et al. "The Photon polarization in B —> X gamma in the standard model." In: *Phys. Rev. D* 71 (2005), p. 011504. DOI: 10.1103/PhysRevD.71.011504. arXiv: hep-ph/0412019.

[172] Joachim Brod et al. "A Consistent Picture for Large Penguins in D -> pi+ pi-, K+ K-." In: *JHEP* 10 (2012), p. 161. DOI: 10.1007/JHEP10(2012)161. arXiv: 1203.6659 [hep-ph].

[173] Gudrun Hiller, Martin Jung, and Stefan Schacht. "SU(3)-flavor anatomy of nonleptonic charm decays." In: *Phys. Rev. D* 87.1 (2013), p. 014024. DOI: 10.1103/PhysRevD.87.014024. arXiv: 1211.3734 [hep-ph].

[174] Sarah Müller, Ulrich Nierste, and Stefan Schacht. "Topological amplitudes in D decays to two pseudoscalars: A global analysis with linear $SU(3)_F$ breaking." In: *Phys. Rev. D* 92.1 (2015), p. 014004. DOI: 10.1103/PhysRevD.92.014004. arXiv: 1503.06759 [hep-ph].

[175] A. Tayduganov, E. Kou, and A. Le Yaouanc. "The strong decays of K1 resonances." In: *Phys. Rev. D* 85 (2012), p. 074011. DOI: 10.1103/PhysRevD.85.074011. arXiv: 1111.6307 [hep-ph].

[176] Emi Kou, Alain Le Yaouanc, and Andrey Tayduganov. "Determining the photon polarization of the b –> s gamma using the B –> K1(1270) gamma –> (K pi pi) gamma decay." In: *Phys. Rev. D* 83 (2011), p. 094007. DOI: 10.1103/PhysRevD.83.094007. arXiv: 1011.6593 [hep-ph].

[177] A. Le Yaouanc et al. ""Naive" Quark-Pair-Creation Model of Strong-Interaction Vertices." In: *Phys. Rev. D* 8 (7 Oct. 1973), pp. 2223–2234. DOI: 10.1103/PhysRevD.8.2223. URL: https://link.aps.org/doi/10.1103/PhysRevD.8.2223.

[178] H. Guler et al. "Study of the $K^+\pi^+\pi^-$ Final State in $B^+ \to J/\psi K^+\pi^+\pi^-$ and $B^+ \to \psi - primeK^+\pi^+\pi^-$." In: *Phys. Rev. D* 83 (2011), p. 032005. DOI: 10.1103/PhysRevD.83.032005. arXiv: 1009.5256 [hep-ex].

[179] Roel Aaij et al. "Observation of Photon Polarization in the b→sγ Transition." In: *Phys. Rev. Lett.* 112.16 (2014), p. 161801. DOI: 10.1103/PhysRevLett.112.161801. arXiv: 1402.6852 [hep-ex].

[180] P. del Amo Sanchez et al. "Time-dependent analysis of $B^0 \to K^0_S\pi^-\pi^+\gamma$ decays and studies of the $K^+\pi^-\pi^+$ system in $B^+ \to K^+\pi^-\pi^+\gamma$ decays." In: *Phys. Rev. D* 93.5 (2016), p. 052013. DOI: 10.1103/PhysRevD.93.052013. arXiv: 1512.03579 [hep-ex].

[181] C. Daum et al. "Diffractive production of strange mesons at 63 GeV." In: *Nuclear Physics B* 187.1 (1981), pp. 1–41. ISSN: 0550-3213. DOI: https://doi.org/10.1016/0550-3213(81)90114-0. URL: https://www.sciencedirect.com/science/article/pii/0550321381901140.

[182] Bernard Aubert et al. "Measurement of branching fractions of B decays to K(1)(1270)pi and K(1)(1400)pi and determination of the CKM angle alpha from B0 —> a(1)(1260)+- pi-+." In: *Phys. Rev. D* 81 (2010), p. 052009. DOI: 10.1103/PhysRevD.81.052009. arXiv: 0909.2171 [hep-ex].

[183] Taruni Uppal and R. C. Verma. "Weak electromagnetic decays of charm baryons." In: *Phys. Rev. D* 47 (7 Apr. 1993), pp. 2858–2864. DOI: 10.1103/PhysRevD.47.2858. URL: https://link.aps.org/doi/10.1103/PhysRevD.47.2858.

[184] Hai-Yang Cheng et al. "Effective Lagrangian approach to weak radiative decays of heavy hadrons." In: *Phys. Rev. D* 51 (1995), pp. 1199–1214. DOI: 10.1103/PhysRevD.51.1199. arXiv: hep-ph/9407303.

[185] A. N. Kamal. "Calculation of the branching ratio for $\Lambda_c^+ \to \Sigma^+\gamma$." In: *Phys. Rev. D* 28 (9 Nov. 1983), pp. 2176–2179. DOI: 10.1103/PhysRevD.28.2176. URL: https://link.aps.org/doi/10.1103/PhysRevD.28.2176.

[186] Hai-Yang Cheng. "Charmed Baryon Physics Circa 2021." In: (Sept. 2021). arXiv: 2109.01216 [hep-ph].

[187] Paul Singer and Da-Xin Zhang. "Two-body Cabibbo suppressed decays of charmed baryons into vector mesons and into photons." In: *Phys. Rev. D* 54 (1996), pp. 1225–1228. DOI: 10.1103/PhysRevD.54.1225. arXiv: hep-ph/9603426.

[188] N.G. Deshpande, Xiao-Gang He, and Josip Trampetic. "Long distance contributions to penguin processes b → s and b → d ." In: *Physics Letters B* 367.1 (1996), pp. 362–368. ISSN: 0370-2693. DOI: https://doi.org/10.1016/0370-2693(95)01364-4. URL: https://www.sciencedirect.com/science/article/pii/0370269395013644.

[189] Eugene Golowich and Sandip Pakvasa. "Uncertainties from long range effects in B→$K^*\gamma$." In: *Phys. Rev. D* 51 (3 Feb. 1995), pp. 1215–1223. DOI: 10.1103/PhysRevD.51.1215. URL: https://link.aps.org/doi/10.1103/PhysRevD.51.1215.

[190] Gudrun Hiller and Roman Zwicky. "Endpoint relations for baryons." In: *JHEP* 11 (2021), p. 073. DOI: 10.1007/JHEP11(2021)073. arXiv: 2107.12993 [hep-ph].

[191] Stefan Meinel. "$\Lambda_c \to N$ form factors from lattice QCD and phenomenology of $\Lambda_c \to n\ell^+\nu_\ell$ and $\Lambda_c \to p\mu^+\mu^-$ decays." In: *Phys. Rev. D* 97.3 (2018), p. 034511. DOI: 10.1103/PhysRevD.97.034511. arXiv: 1712.05783 [hep-lat].

[192] R. N. Faustov and V. O. Galkin. "Rare $\Lambda_c \to p\ell^+\ell^-$ decay in the relativistic quark model." In: *Eur. Phys. J. C* 78.6 (2018), p. 527. DOI: 10.1140/epjc/s10052-018-6010-y. arXiv: 1805.02516 [hep-ph].

[193] K. Azizi, Y. Sarac, and H. Sundu. "Light cone QCD sum rules study of the semileptonic heavy Ξ_Q and Ξ'_Q transitions to Ξ and Σ baryons." In: *Eur. Phys. J. A* 48 (2012), p. 2. DOI: 10.1140/epja/i2012-12002-1. arXiv: 1107.5925 [hep-ph].

[194] Thomas A. Kaeding. "Tables of SU(3) isoscalar factors." In: *Atom. Data Nucl. Data Tabl.* 61 (1995), pp. 233–288. DOI: 10.1006/adnd.1995.1011. arXiv: nucl-th/9502037.

[195] C. Q. Geng et al. "Antitriplet charmed baryon decays with SU(3) flavor symmetry." In: *Phys. Rev. D* 97.7 (2018), p. 073006. DOI: 10.1103/PhysRevD.97.073006. arXiv: 1801.03276 [hep-ph].

[196] Martin J. Savage and Roxanne P. Springer. "SU(3) predictions for charmed-baryon decays." In: *Phys. Rev. D* 42 (5 Sept. 1990), pp. 1527–1543. DOI: 10.1103/PhysRevD.42.1527. URL: https://link.aps.org/doi/10.1103/PhysRevD.42.1527.

[197] Wei Wang, Zhi-Peng Xing, and Ji Xu. "Weak Decays of Doubly Heavy Baryons: SU(3) Analysis." In: *Eur. Phys. J. C* 77.11 (2017), p. 800. DOI: 10.1140/epjc/s10052-017-5363-y. arXiv: 1707.06570 [hep-ph].

[198] Ru-Min Wang et al. "Studying radiative baryon decays with the SU(3) flavor symmetry." In: *J. Phys. G* 48.8 (2021), p. 085001. DOI: 10.1088/1361-6471/abffdd. arXiv: 2008.06624 [hep-ph].

[199] Marcel Golz, Gudrun Hiller, and Tom Magorsch. "Pinning down $|\Delta c| = |\Delta u| = 1$ couplings with rare charm baryon decays." In: (Feb. 2022). arXiv: 2202.02331 [hep-ph].

[200] Philipp Böer, Thorsten Feldmann, and Danny van Dyk. "Angular Analysis of the Decay $\Lambda_b \to \Lambda(\to N\pi)\ell^+\ell^-$." In: *JHEP* 01 (2015), p. 155. DOI: 10.1007/JHEP01(2015)155. arXiv: 1410.2115 [hep-ph].

[201] Howard E. Haber. "Spin formalism and applications to new physics searches." In: *21st Annual SLAC Summer Institute on Particle Physics: Spin Structure in High-energy Processes (School: 26 Jul - 3 Aug, Topical Conference: 4-6 Aug) (SSI 93)*. Apr. 1994, pp. 231–272. arXiv: hep-ph/9405376.

[202] Federica Legger and Thomas Schietinger. "Photon helicity in $\Lambda_b \to pK\gamma$ decays." In: *Phys. Lett. B* 645 (2007). [Erratum: Phys.Lett.B 647, 527–528 (2007)], pp. 204–212. DOI: 10.1016/j.physletb.2006.12.011. arXiv: hep-ph/0605245.

[203] Gudrun Hiller and Alex Kagan. "Probing for new physics in polarized Λ_b decays at the Z." In: *Phys. Rev. D* 65 (2002), p. 074038. DOI: 10.1103/PhysRevD.65.074038. arXiv: hep-ph/0108074.

[204] "First search for the weak radiative decays $\Lambda_c^+ \to \Sigma^+\gamma$ and $\Xi_c^0 \to \Xi^0\gamma$." In: (June 2022). arXiv: 2206.12517 [hep-ex].

[205] Susumu Okubo. "Note on Unitary Symmetry in Strong Interactions." In: *Progress of Theoretical Physics* 27.5 (May 1962), pp. 949–966. DOI: 10.1143/ptp.27.949. URL: https://doi.org/10.1143/ptp.27.949.

[206] S. Aoki et al. "Review of lattice results concerning low-energy particle physics." In: *Eur. Phys. J. C* 77.2 (2017), p. 112. DOI: 10.1140/epjc/s10052-016-4509-7. arXiv: 1607.00299 [hep-lat].

[207] Hisaki Hatanaka and Kwei-Chou Yang. "B —> K(1) gamma Decays in the Light-Cone QCD Sum Rules." In: *Phys. Rev. D* 77 (2008). [Erratum: Phys.Rev.D 78, 059902 (2008)], p. 094023. DOI: 10.1103/PhysRevD.77.094023. arXiv: 0804.3198 [hep-ph].

[208] H. Leutwyler. "On the 1/N expansion in chiral perturbation theory." In: *Nucl. Phys. B Proc. Suppl.* 64 (1998). Ed. by Stephan Narison, pp. 223–231. DOI: 10.1016/S0920-5632(97)01065-7. arXiv: hep-ph/9709408.

[209] T. Feldmann, P. Kroll, and B. Stech. "Mixing and decay constants of pseudoscalar mesons." In: *Phys. Rev. D* 58 (1998), p. 114006. DOI: 10.1103/PhysRevD.58.114006. arXiv: hep-ph/9802409.

[210] V. Bernard. "First determination of $f_+(0)|V_{us}|$ from a combined analysis of $\tau \to K\pi\nu_\tau$ decay and πK scattering with constraints from $K_{\ell 3}$ decays." In: *JHEP* 06 (2014), p. 082. DOI: 10.1007/JHEP06(2014)082. arXiv: 1311.2569 [hep-ph].

[211] Christine Bruch, Alexander Khodjamirian, and Johann H. Kuhn. "Modeling the pion and kaon form factors in the timelike region." In: *Eur. Phys. J. C* 39 (2005), pp. 41–54. DOI: 10.1140/epjc/s2004-02064-3. arXiv: hep-ph/0409080.

[212] Diogo R. Boito, Rafel Escribano, and Matthias Jamin. "K pi vector form-factor, dispersive constraints and tau —> nu(tau) K pi decays." In: *Eur. Phys. J. C* 59 (2009), pp. 821–829. DOI: 10.1140/epjc/s10052-008-0834-9. arXiv: 0807.4883 [hep-ph].

[213] Matthias Jamin, Antonio Pich, and Jorge Portoles. "Spectral distribution for the decay tau —> nu(tau) K pi." In: *Phys. Lett. B* 640 (2006), pp. 176–181. DOI: 10.1016/j.physletb.2006.06.058. arXiv: hep-ph/0605096.

[214] J. Gasser and H. Leutwyler. "Chiral perturbation theory: Expansions in the mass of the strange quark." In: *Nuclear Physics B* 250.1 (1985), pp. 465–516. ISSN: 0550-3213. DOI: https://doi.org/10.1016/0550-3213(85)90492-4. URL: https://www.sciencedirect.com/science/article/pii/0550321385904924.

[215] J. M. Flynn and Christopher T. Sachrajda. "Heavy quark physics from lattice QCD." In: *Adv. Ser. Direct. High Energy Phys.* 15 (1998). Ed. by A. J. Buras and M. Lindner, pp. 402–452. DOI: 10.1142/9789812812667_0006. arXiv: hep-lat/9710057.

[216] Yue-Liang Wu, Ming Zhong, and Ya-Bing Zuo. "B(s), D(s) —> pi, K, eta, rho, K*, omega, phi Transition Form Factors and Decay Rates with Extraction of the CKM parameters |V(ub)|, |V(cs)|, |V(cd)|." In: *Int. J. Mod. Phys. A* 21 (2006), pp. 6125–6172. DOI: 10.1142/S0217751X06033209. arXiv: hep-ph/0604007.

[217] Svjetlana Fajfer and Jernej Kamenik. "Charm meson resonances and $D \to V$ semileptonic form factors." In: *Phys. Rev. D* 72 (3 Aug. 2005), p. 034029. DOI: 10.1103/PhysRevD.72.034029. URL: https://link.aps.org/doi/10.1103/PhysRevD.72.034029.

[218] D. Melikhov and B. Stech. "Weak form factors for heavy meson decays: An update." In: *Phys. Rev. D* 62 (1 May 2000), p. 014006. DOI: 10.1103/PhysRevD.62.014006. URL: https://link.aps.org/doi/10.1103/PhysRevD.62.014006.

[219] Hai-Bing Fu et al. "The $D \to \rho$ semileptonic and radiative decays within the light-cone sum rules." In: *Eur. Phys. J. C* 80.3 (2020), p. 194. DOI: 10.1140/epjc/s10052-020-7758-4. arXiv: 1808.06412 [hep-ph].

[220] S. Dobbs et al. "First Measurement of the Form Factors in the Decays $D^0 \to \rho^- e^+ \nu_e$ and $D^+ \to \rho^0 e^+ \nu_e$." In: *Phys. Rev. Lett.* 110.13 (2013), p. 131802. DOI: 10.1103/PhysRevLett.110.131802. arXiv: 1112.2884 [hep-ex].

[221] M. Ablikim et al. "Measurement of the form factors in the decay $D^+ \to \omega e^+ \nu_e$ and search for the decay $D^+ \to \phi e^+ \nu_e$." In: *Phys. Rev. D* 92.7 (2015), p. 071101. DOI: 10.1103/PhysRevD.92.071101. arXiv: 1508.00151 [hep-ex].

[222] Richard Kokoski and Nathan Isgur. "Meson decays by flux-tube breaking." In: *Phys. Rev. D* 35 (3 Feb. 1987), pp. 907–933. DOI: 10.1103/PhysRevD.35.907. URL: https://link.aps.org/doi/10.1103/PhysRevD.35.907.

[223] Avital Dery et al. "$SU(3)_F$ analysis for beauty baryon decays." In: *JHEP* 03 (2020), p. 165. DOI: 10.1007/JHEP03(2020)165. arXiv: 2001.05397 [hep-ph].

Eidesstattliche Versicherung

Ich versichere hiermit an Eides statt, dass ich die vorliegende Abschlussarbeit mit dem Titel “Rare radiative charm decays in and beyond the standard model” selbstständig und ohne unzulässige fremde Hilfe erbracht habe. Ich habe keine anderen als die angegebenen Quellen und Hilfsmittel benutzt, sowie wörtliche und sinngemäße Zitate kenntlich gemacht. Die Arbeit hat in gleicher oder ähnlicher Form noch keiner Prüfungsbehörde vorgelegen.

Ort, Datum	Unterschrift

Belehrung

Wer vorsätzlich gegen eine die Täuschung über Prüfungsleistungen betreffende Regelung einer Hochschulprüfungsordnung verstößt, handelt ordnungswidrig. Die Ordnungswidrigkeit kann mit einer Geldbuße von bis zu 50 000 € geahndet werden. Zuständige Verwaltungsbehörde für die Verfolgung und Ahndung von Ordnungswidrigkeiten ist der Kanzler/die Kanzlerin der Technischen Universität Dortmund. Im Falle eines mehrfachen oder sonstigen schwerwiegenden Täuschungsversuches kann der Prüfling zudem exmatrikuliert werden (§ 63 Abs. 5 Hochschulgesetz –HG–).

Die Abgabe einer falschen Versicherung an Eides statt wird mit Freiheitsstrafe bis zu 3 Jahren oder mit Geldstrafe bestraft.

Die Technische Universität Dortmund wird ggf. elektronische Vergleichswerkzeuge (wie z. B. die Software “turnitin”) zur Überprüfung von Ordnungswidrigkeiten in Prüfungsverfahren nutzen.

Die oben stehende Belehrung habe ich zur Kenntnis genommen.

Ort, Datum	Unterschrift